Stellingen behorende bij het proefschrift

LOCAL POWER SPECTRA

AND

SEISMIC INTERPRETATION

van

Philippe Steeghs

Delft, 25 september 1997

1. De structurele geologische sequentie in drie-dimensionale seismische data wordt zichtbaar in de verandering van de twee-dimensionale laterale gradient met de diepte.
   Hoofdstuk 6 in dit proefschrift.

2. De in dit proefschrift ontwikkelde techniek voor lokale spectraal-analyse kan met vrucht gebruikt worden om de veranderingen in 4-D ('time-lapse') seismische data te analyseren.

3. Het resultaat van de *minimum-entropie* methode van Loughlin et al. (1994) voor het berekenen van een niet-negatieve tijd-frequentie representatie met correcte marginals is sterk afhankelijk van de beginschatting. Deze methode kan daarom niet beschouwd worden als de oplossing voor het fundamentele probleem hoe een fysisch correcte tijd-frequentie representatie te verkrijgen.
   Loughlin, P., Pitton, J., Atlas, L., 1994, Construction of Positive Time-Frequency Distributions, *IEEE Trans. on Signal Processing*, vol. 42(10).

4. De schaaleigenschappen van seismische data kunnen worden geanalyseerd met behulp van de in dit proefschrift voorgestelde technieken voor de analyse van de frequentie-eigenschappen. Deze schaalanalyse kan worden uitgevoerd door de in Hoofdstuk 2 van dit proefschift ingevoerde frequentie operator, volgens de theorie van Cohen (1996), te vervangen door een dilatatie operator.
   Cohen, L., 1996, A General Approach for Obtaining Joint Representations in Signal Analysis - Part I: Characteristic Function Operator Method, *IEEE Trans. on Signal Processing*, vol. 44(5).

5. De seismische attributen analyse met behulp van complex-trace parameters is geïntroduceerd door Taner en Sheriff in 1977. Als zij in hun publicatie niet het gebruik van kleur voor de weergave van deze signaalparameters hadden gepropageerd, dan was het al veel eerder duidelijk geworden dat er aan de signaal-ruis verhouding van de complex-trace attributen nog veel te verbeteren is.
   Taner, T.H. and Sheriff, R.E., 1977, Applications of Amplitude, Frequency and Other Attributes to Stratigraphic and Hydrocarbon Determination, in: AAPG Memoir; 26, ***Seismic Stratigraphy - applications to hydrocarbon exploration***, Payton, C.E. ed., American Association of Petroleum Geologists, Tulsa, Oklahoma.

6. De verbetering van de kwaliteit van seismische reflectie data heeft er toe geleid dat de huidige technieken voor het voorwaarts modelleren van golfpropagatie niet meer voldoen als een realistische nabootsing van het seismische experiment in complexe geologische media.

7. Het verdient de aanbeveling om de seismische interpretator niet alleen de informatie te tonen die is overgebleven na dataprocessing, maar ook wat er is verdwenen.

8. De grote hoeveelheid beschikbare drie-dimensionale seismische data, afkomstig uit de olieindustrie, wordt onvoldoende benut voor fundamenteel geologisch onderzoek.

9. Ook een poldermodel heeft regelmatig bemaling nodig.

LOCAL POWER SPECTRA

AND

SEISMIC INTERPRETATION

LOCAL POWER SPECTRA

AND

SEISMIC INTERPRETATION

PROEFSCHRIFT

ter verkrijging van de graad van doctor
aan de Technische Universiteit Delft,
op gezag van de Rector Magnificus Prof. dr. ir. J. Blauwendraad,
in het openbaar te verdedigen ten overstaan van een commissie,
door het College van Dekanen aangewezen,
op donderdag 25 september 1997 te 16.00 uur

door

Theo Philippe Hubert STEEGHS

doctorandus in de geofysica
geboren te Heerlen

Dit proefschrift is goedgekeurd door de promotor:
Prof. dr .ir. J.T. Fokkema

Samenstelling promotiecommissie:

Prof. dr. ir. J.T. Fokkema,	Technische Universiteit Delft, promotor
Prof. ir. K.J. Weber,	Technische Universiteit Delft
Prof. dr. ir. A.J. Berkhout,	Technische Universiteit Delft
Prof. dr. ir. H. Blok,	Technische Universiteit Delft
Prof. dr. W. Schlager,	Vrije Universiteit, Amsterdam
Prof. dr. R.G. Baraniuk,	Rice University, Houston
Drs. G. Diephuis,	Geophysical Consultant, Assen

Dr. ir. G.G. Drijkoningen heeft als begeleider in belangrijke mate aan de totstandkoming van dit proefschrift bijgedragen

ISBN 90-9010812-2

'A thousand-li-long road starts with the first step', as
the proverb goes. Pity the road home does
not depend on that same step. It exceeds ten times
a thousand li, especially counting from zeros.

Joseph Brodsky

aan mijn ouders en Marjolijn

Acknowledgement

The research reported in this thesis has been financially supported through Tweede Fase Opleiding Mariene Aardwetenschappen, a cooperation between marine earth science research groups in the Netherlands. This support is gratefully acknowledged.

The Nederlandse Aardolie Maatschappij and Geco-Prakla provided the 3-D seismic data sets and are gratefully acknowledged for their support. Especially, Drs. G. Diephuis (NAM) and Dr. ir. W. Rietveld (Amoco EPTG) are gratefully acknowledged for their kind offices. The Alboran Sea data set was made available through the support of Prof. dr. A. Maldonado of the University of Granada. We gratefully acknowledge his contribution to this thesis.

Contents

Chapter 1

Introduction

Seismic profiling has been by far the most successful method for imaging the subsurface over large areas in the depth range between a few tens of meters to several kilometers. In many cases seismic cross-sections are the only images we have of ancient sedimentary environments on a large scale. Few people will have doubts about the impact seismic data have had on our understanding of the earth's geological history. The increased use of seismic data in the sixties and seventies resulted in a greatly improved view on sedimentary basins. On the basis of observations in seismic cross-sections the method of seismic sequence stratigraphy was developed. Analysis of seismic data showed the possibility of inferring the environment of deposition of sedimentary rocks from the reflection patterns observed in seismic data. Seismic sequence stratigraphy is based on the recognition of cyclic patterns of sedimentation in seismic data and the association of these patterns with the mechanisms of basin in-fill. The proposition of seismic sequence stratigraphy that changes of sea-level control sedimentation and that the history of these sea-level changes can be inferred from seismic data, has been one of the major contributions to geological theory in the last decades.

However, seismic data are usually not acquired for reasons of scientific curiosity. Seismic data acquisition and the subsequent evaluation, i.e. interpre-

tation, of these data have become the most important tools in present-day exploration for hydro-carbons. The growing demand for hydro-carbons and the increased difficulty finding these has been the driving force behind a tremendous growth of the seismic industry in the last decades. Seismic technology has seen significant improvements in recent years. The first commercial three-dimensional surveys were acquired in the late seventies. Since then three-dimensional seismic surveys have become the standard exploration tool in mature hydro-carbon provinces, such as the Gulf of Mexico and the North Sea. Developments in acquisition and imaging technology have resulted in a significant improvement of data quality. The improved quality of the data has resulted in a shift from exploration oriented seismic surveys towards the application of seismic data as an aid in the appraisal and development of oil and gas fields. High-resolution three-dimensional seismic reflection data are nowadays not only used to identify potential reservoirs, but may in favourable circumstances also reveal the internal structure of the reservoir.

1.1 Statement of the problem and the method employed

Three-dimensional seismic technology resulted in a radical change in seismic data handling and interpretation. For two-dimensional seismic data interpretation, paper sections and a set of colour pencils are usually sufficient, whereas the densely sampled three-dimensional seismic data sets can only be handled using a powerful computer and the appropriate software to display the large number of different slices through the data volume. Three-dimensional seismic interpretation also requires a different attitude from the interpreter. In the first place, the geological model is no longer constructed on the basis two-dimensional vertical cross-sections but on a volume of data. The increased amount and dense spatial sampling of information in a three-dimensional seismic data set has facilitated the construction of a subsurface model from seismic data considerably. However, the potential of the three-dimensional view is not always fully exploited. The consequence of the increased amount of data, in combination with the limited dynamic range of the optical display, is that much of the extra information and resolution present in the data may be missed in the display.

With the demand for a more detailed description of hydro-carbon reservoirs the need for integration of data from different sources has become more ur-

gent. The integration of seismic data with well-log measurements requires ways to characterize seismic data in terms of signal attributes. In a statistical approach towards reservoir characterization the signal attributes are used to predict the petrophysical properties of the reservoir away from a well location on the basis of an observed correlation between a set of seismic attributes and the petrophysical property that is measured in the bore-hole (lateral prediction).

The problem at hand is how to extract the information present in the data and use it to its full potential. In order to address this problem we turn to the field of signal analysis and data representations. The Fourier transformation is at the heart of a wide range of techniques that are used in seismic data analysis and processing. Mapping the data into the temporal frequency domain is an effective way of re-ordering the data such that their global characteristics can be assessed. However, the *change* of frequency content with time is one of the main features we observe in seismic data. Because of this change of frequency content with time, seismic signals belong to the class of non-stationary signals. The analysis of non-stationary signals requires techniques that extend the notion of a global frequency spectrum to a local frequency description. The spectral energy density function that is obtained by means of a Fourier transformation - the power spectrum - shows the frequencies that are present in our data, but does not reveal where changes in the frequency content occur. Consequently, for the interpretation of seismic data in terms of a changing frequency content, we need a representation of our data as a function of both time and frequency. Only quite recently, the joint time-frequency representation of signals has become a major area of research in signal processing. Although in the geophysical community the wavelet transform has become widely known as the tool for local frequency analysis, techniques that are more closely related to the Fourier transformation have been developed and successfully applied in a wide variety of signal estimation and detection problems. These time-frequency representations are rooted in the statistical description of quantum mechanics. The problems that are associated with simultaneous measurement of the position and momentum of a particle have their counterpart in time-frequency analysis, where one tries to obtain a simultaneous measurement of time and frequency. The relation between quantum mechanics and signal theory has been acknowledged since

long; in 1946 it was shown by Gabor that the celebrated uncertainty principle of quantum mechanics could be applied to signal analysis as well. In the early eighties the increased power of computers made the numerical implementation of these simultaneous representations feasible, which in turn was the onset of further theoretical development of the field of time-frequency analysis. The power spectrum that is employed in frequency analysis of stationary signals, has its counterpart in the Wigner distribution function as the time varying power spectrum of a non-stationary signal. The Wigner distribution function is a member of a class of functions that can serve as a non-stationary power spectrum. It is this class of local power spectra that we will employ for the characterization of seismic signals by their local frequency content.

As was indicated in the previous, the analysis of non-stationary signals requires the formulation of a theory for a simultaneous time and frequency description. A complete and comprehensive theory for joint time-frequency analysis does not yet exist. There is no unique time-frequency representation of a signal that satisfies all the properties of a physically correct joint time-frequency energy density function. However, discarding the requirement that all properties must be satisfied in *one* time-frequency representation, a class of joint time-frequency representations can be derived that serves as a model of a local power spectrum.

In order to employ the concept of a local power spectrum in seismic signal analysis we need to decide which time-frequency representation to use. This choice cannot be made on the basis of a mathematical analysis alone. We should also take into account what we aim to achieve with a local frequency analysis. Our main area of application of the time-frequency representation is the analysis of seismic sequences and seismic attribute extraction. A study of the properties of the generalized class of time-frequency representations should provide a guideline to which representation to choose in these applications.

The theory of non-stationary signal analysis has mainly been applied to one-dimensional time series analysis. In seismic data interpretation, an analysis of the characteristics of the signal as a function of the spatial coordinates is equally important. Hence, we will address an extension of the theory to signals that depend on more than one variable and show how this extension

can be applied for seismic data analysis and characterization.

In the method employed in this thesis one important assumption is made. We assume that the seismic data represent a band-limited reflectivity function and that the data is free of artifacts that have their origin in the acquisition geometry and inadequacies in the data processing. Although we are fully aware that thorough understanding of wave propagation is a prerequisite for seismic interpretation, the quality of seismic data we have today justifies such an assumption. The following quotation sharply expresses the idea behind our approach: 'Consider everything to be geology until proved otherwise', *Milos Backus* (in: Brown 1997).

1.2 Outline of the thesis

In the two chapters following this introduction the joint time-frequency description of signals is addressed. In the first part of Chapter 2 some fundamental concepts and their interpretation are discussed. It will be shown how the Wigner distribution naturally emerges as the model of a non-stationary power spectrum and we will briefly discuss its relation to other methods for the description of non-stationary signals. In the last part of Chapter 2 the most important properties of the Wigner distribution function will be derived.

In Chapter 3, the general class of time-frequency representations will be introduced. The general class of time-frequency representations can be parameterized in terms of a time-frequency smoothing that is applied on the Wigner distribution. In the first part of this chapter we show how this parameterization can be employed in the derivation of time-frequency representations that satisfy certain desirable properties. In the second part of this chapter we will discuss some possible choices for this smoothing function and their associated time-frequency representations.

The applications of the time-frequency representations of the generalized class to seismic data analysis is the subject of Chapter 4. First, the subsurface model that is the basis of seismic sequence analysis is discussed in the context of signal analysis. A combination of the concepts of seismic sequence stratigraphy and signal analysis results in a method for the characterization and validation of seismic sequence models by means of a time-frequency representation of the seismic data. The second part of Chapter 4 addresses

the extraction of signal properties from the time-frequency representation for seismic attribute analysis. Significant improvements with regard to existing methods for seismic attribute analysis can be made if the attributes are extracted from a time-frequency representation rather than directly from the signal.

We extend the idea of combining time and frequency to the spatial directions in Chapter 5 and a general class of local power spectra of signals that depend on more than one variable is formulated. A new type of local slant-stack power spectrum is introduced in the second part of this chapter. The new representation, which has been coined the 'Wigner-Radon representation', is proposed as the local counterpart of the global Radon transformation.

Finally, in Chapter 6 the application of the Wigner-Radon representation to the analysis of three-dimensional seismic data is discussed. The measurement of local time dip and local azimuth in the generalized Wigner-Radon representation and displaying them in a time slice map is shown to be a very effective method to reveal the structural and stratigraphic information that is contained in the seismic data.

Chapter 2

Time-Frequency Analysis and the Wigner Distribution

2.1 Introduction

The Fourier transformation offers a tool for determining how the energy of a signal is distributed in the Fourier - frequency - domain. The information on where these frequencies are localized in time is contained in the phase spectrum of the Fourier transform of a signal. However, even for moderately complicated signals it is hardly possible to interpret a phase spectrum in terms of time localization of frequency components. Physical measurements in which the frequency content of a recorded signal changes with time are numerous. In many of those situations it is important to know when this change in the spectrum occurs. Clearly, a time or frequency description alone is not sufficient in such problems. An example is the problem of inferring stratigraphy from seismic data. The change of frequency content with time in seismic reflection data is an important indicator of stratigraphic changes. In a description of the frequency content for seismic interpretation purposes, time or depth localization is clearly essential, since the goal of such an interpretation is to infer geology as a function of seismic travel time or depth. In order to study the spectral changes of the signal with time, an approach is proposed that combines the information of the time and frequency domains

into a *time-frequency representation.* In a time-frequency representation the localization of the energy of a signal is considered as a joint function of time and frequency.

A number of ways exists to devise such a time-frequency representation. The most straightforward approach would be to divide the signal into short time segments and determine the local spectrum by means of a Fourier transformation of the segment. The result of this operation is a widely used time-frequency representation; the short-time or sliding-window Fourier transformation. The sliding-window Fourier transform of a signal inherently suffers from a trade-off between the length of the window and resolution of the representation.

Improvement of the resolution of the sliding-window Fourier transform was one of the motivations behind the development of other techniques for the analysis of non-stationary signals. However, the search for the physical significance of the time-varying spectrum has been the main impetus behind all efforts to formulate better ways to characterize the non-stationary behaviour of a signal.

Important contributions to the theory of time-frequency analysis were made by Gabor (1946) and Ville (1948). Their translation of some basic concepts from quantum theory into the signal analysis context proved to be fundamental for later developments. In the late seventies and early eighties a renewed interest in the application of these concepts developed. Some of the first applications were in seismic signal analysis (Morlet et al. 1982), but also applications in general signal analysis (Claasen and Mecklenbräuker 1980) and audio signal analysis (Janse and Kaizer 1980) were published. Since then the number of publications on the subject has been steadily growing. In recent years, the theory of time-frequency analysis appears to have reached a more mature stage. However, there are many gaps and flaws in the theory that need to be addressed and the field is still developing rapidly. A comprehensive overview of the present state of affairs is given in two books by Cohen (1995) and Flandrin (1993).

The question how to represent a signal as a joint function of time and frequency has been addressed by many researchers (Gabor 1946; Ville 1948; Page 1952; Priestley 1965; Rihaczeck 1968; Mark 1970). Most derivations

of a fundamental time-frequency representation start with the definition of a set of desirable properties that a time-frequency representation should have. This set of properties is then the starting point for the derivation of a representation that satisfies those properties. In many cases the derivation results in a different representation, depending on the properties one chooses to be satisfied. An important breakthrough came with the acknowledgement that many of the previously derived representations all belong to the same class: the class of quadratic shift-invariant representations, also known as Cohen's class (Cohen 1966). One of the best known time-frequency representations within the Cohen's class is the Wigner distribution. The Wigner distribution is considered to be representative for the Cohen's class. In that quality, it is the time-frequency representation that has been studied most extensively, apart from the sliding-window Fourier transformation. Originally, the Wigner distribution was derived by Wigner (1932) for the calculation of the quantum correction terms to the Boltzmann formula. In the early eighties Claasen and Mecklenbräuker developed a comprehensive approach for the application of the Wigner distribution to joint time-frequency analysis (Claasen and Mecklenbräuker 1980).

This thesis deals with the Wigner distribution and the other members of Cohen's class of time-frequency representations. Numerous other approaches to non-stationary signal analysis exist, of which the evolutionary spectrum (Priestley 1965), the Gabor logon approach (Gabor 1946) and the wavelet transform (Rioul and Vetterli 1991) have been particularly successful. We prefer the Wigner distribution as a starting point. Not only for its attractive mathematical properties in general, but also because there is a close relation between the complex-trace attributes (Taner et al. 1979) that are used in seismic interpretation and the Wigner distribution.

In this chapter the Wigner distribution and its Fourier dual, the ambiguity function will be discussed. The general class of time-frequency representations will be the subject of Chapter 3.

First, some of the concepts of joint time-frequency analysis and terminology will be introduced.

2.2 Time and Frequency Analysis

In the next sections some of the concepts that are essential to the theory of time-frequency analysis will be introduced. Through the years, the field of time-frequency analysis acquired its own terminology. Much of the terminology is influenced by the strong links with quantum mechanics and statistics. Moreover, many terms are borrowed from random signal theory, although the application of the concepts involves deterministic signals. We speak of a deterministic signal if we know its actual values. For instance, because the signal is the outcome of some measurement.

First, the use of the energy density function for the description of signals in the time and frequency domain will be demonstrated. We will then discuss on the possibility of an extension of these concepts to a joint time-frequency density function.

The signals we are studying are generally represented by the generic function $u(\boldsymbol{x}, t)$, depending on space via the location vector $\boldsymbol{x}$ and on time via the scalar coordinate t. This class of functions is representative for the seismic signal. The frequency representation of a signal is found by a Fourier transformation. The Fourier transformation with respect to the time variable t of a signal $u(\boldsymbol{x}, t)$ is defined as

$$\hat{u}(\boldsymbol{x}, f) = \mathcal{F}_t^-\{u(\boldsymbol{x}, t)\} = \int_{t \in \mathbb{R}} \exp(-\mathrm{j}2\pi f t) u(\boldsymbol{x}, t)\, \mathrm{d}t, \tag{2.1}$$

where f is the temporal frequency. The inverse Fourier transformation is defined as

$$u(\boldsymbol{x}, t) = \mathcal{F}_f^+\{\hat{u}(\boldsymbol{x}, f)\} = \int_{f \in \mathbb{R}} \exp(\mathrm{j}2\pi f t) \hat{u}(\boldsymbol{x}, f)\, \mathrm{d}f. \tag{2.2}$$

In this thesis we adopt the symbol $\mathcal{F}_t^-$ to denote the Fourier transform operator. The variable that is transformed is given by the subscript and the superscript denotes the sign of argument of the exponential function. Some properties the Fourier transformation are given in Appendix A.

In the next chapters we will confine ourselves to the time and frequency description of signals. The space and spatial frequency description will be incorporated in Chapter 5. However, most of the following is directly applicable to space-spatial frequency analysis. From now on the spatial dependence will be omitted and the signal $u(\boldsymbol{x}, t)$ will be denoted as $u(t)$.

The distribution of energy of a signal, $u(t)$, over frequency is given by its power spectrum, which is defined as

$$E(f) = |\hat{u}(f)|^2. \tag{2.3}$$

The power spectrum is a real and non-negative function by definition and hence it can be treated as a density function. The possibility of manipulating the power spectrum as a density function is advantageous, since in many cases we will attempt to characterize the power spectrum by a limited number of parameters. For instance, the average frequency of a signal can be measured as the mean frequency of the power spectrum, defined as

$$\langle f \rangle = \frac{\int_{f \in I\!R} \; f E(f)\,\mathrm{d}f}{\int_{f \in I\!R} \; E(f)\,\mathrm{d}f}, \tag{2.4}$$

where the brackets $\langle\rangle$ denote the average. For real-valued signals we have a two-sided power spectrum with $E(f) = E(-f)$. In that case the mean frequency is usually defined as the average of Eq.(2.4) for positive frequencies only, i.e. the integration is carried out for $f \in I\!R^+$, where $I\!R^+ = \{f \in I\!R, f \geq 0\}$.

A measure for the concentration of energy around this average can be found as the standard deviation of the power spectrum. The standard deviation, σ_f, of the power spectrum is also known as the bandwidth, B, and is given by

$$B^2 = \sigma_f^2 = \frac{\int_{f \in I\!R} \; (f - \langle f \rangle)^2 E(f)\,\mathrm{d}f}{\int_{f \in I\!R} \; E(f)\,\mathrm{d}f}. \tag{2.5}$$

For real-valued signals we once again replace $f \in I\!R$ by $f \in I\!R^+$. Another way to characterize a density function is through its moments. The moment of order n, denoted by $[f^n]$, of the power spectral density is given by

$$[f^n] = \int_{f \in I\!R} \; f^n E(f)\,\mathrm{d}f. \tag{2.6}$$

A density function is characterized through its moments. This can be seen if we take the Fourier transformation of the density. The inverse Fourier transform $M(\tau)$ of the power spectral density is given by

$$M(\tau) = \int_{f \in I\!R} \; \exp(\mathrm{j}2\pi f\tau) E(f)\,\mathrm{d}f. \tag{2.7}$$

By expanding the exponential we obtain

$$M(\tau) = \int_{f \in \mathbb{R}} \sum_{n=0}^{\infty} \frac{(\mathrm{j}2\pi f\tau)^n}{n!} E(f)\,\mathrm{d}f = \sum_{n=0}^{\infty} (\mathrm{j}2\pi)^n [f^n] \frac{\tau^n}{n!}. \tag{2.8}$$

From which we conclude that $M(\tau)$ is represented by a Taylor series with coefficients $(\mathrm{j}2\pi)^n [f^n]$. Since the Fourier transform pairs $M(\tau)$ and $E(f)$ are uniquely related, Eq.(2.8) implies that the density $E(f)$ is fully characterized by its moments. The Fourier transform of a density is therefore called the characteristic function of the density. The advantage of using the moments of the density instead of the density itself for the characterization of the frequency content of a signal is that for many densities a finite number of moments is sufficient to fully describe the density function. The coefficients of the Taylor series Eq.(2.8) are following from the nth derivative of $M(\tau)$ in $\tau = 0$, i.e.

$$[f^n] = \frac{1}{(\mathrm{j}2\pi)^n} \frac{\partial^n M(\tau)}{\partial \tau^n}\Big|_{\tau=0} \quad . \tag{2.9}$$

For a smooth density function, the derivative of its characteristic function will become insignificant after a certain order n. Consequently, for most power spectral densities only a limited number of moments is needed to characterize the frequency content of a signal. The characteristic function of the power spectral density can also be directly obtained from the signal itself,

$$M(\tau) = r\{u,u\}(\tau) = \int_{t \in \mathbb{R}} u(t+\tau)u^*(t)\,\mathrm{d}t. \tag{2.10}$$

The function $r\{u,u\}(\tau)$ is the auto-correlation function of the signal $u(t)$ (Eq.(A.7)).

For the time domain characteristics of a signal we define a similar set of parameters and relations. The energy distribution in the time domain is given by the squared modulus of the signal $u(t)$ itself,

$$E(t) = |u(t)|^2. \tag{2.11}$$

In a similar way as the mean frequency (cf. Eq.(2.4)), the mean time $\langle t \rangle$ is introduced as

$$\langle t \rangle = \frac{\int_{t \in \mathbb{R}} tE(t)\,\mathrm{d}t}{\int_{t \in \mathbb{R}} E(t)\,\mathrm{d}t}. \tag{2.12}$$

A measure for the duration of a signal, denoted by T, can be found as the standard deviation σ_t around the mean time,

$$T^2 = \sigma_t^2 = \frac{\int_{t\in I\!R} (t - \langle t \rangle)^2 E(t)\,\mathrm{d}t}{\int_{t\in I\!R} E(t)\,\mathrm{d}t}. \tag{2.13}$$

The characteristic function of the time density is the spectral auto-correlation function $r\{\hat{u},\hat{u}\}(\nu)$ and is given by

$$r\{\hat{u},\hat{u}\}(\nu) = \int_{t\in I\!R} \exp(-\mathrm{j}2\pi\nu t)|u(t)|^2\,\mathrm{d}t. \tag{2.14}$$

In terms of the Fourier transform $\hat{u}(f)$, the spectral correlation function can be expressed as

$$r\{\hat{u},\hat{u}\}(\nu) = \int_{f\in I\!R} \hat{u}(f+\nu)\hat{u}^*(f)\,\mathrm{d}f, \tag{2.15}$$

where ν is the frequency-shift variable.

2.2.1 Joint Time-Frequency Analysis

In seismic interpretation, the time and frequency representation alone is not sufficient. The main interest is not the frequency content of the signal as a whole, but how the frequency content changes with time and space. In the ideal situation we would have a joint time-frequency energy density $E(t;f)$. We could then treat this function as a bivariate density function and use the corresponding set of mathematical tools to manipulate and characterize the time-frequency density $E(t;f)$. For instance, the average frequency as a function of time can be measured from $E(t;f)$ by calculating the mean frequency for a fixed t:

$$\langle f \rangle_t = \frac{\int_{f\in I\!R} fE(t;f)\,\mathrm{d}f}{\int_{f\in I\!R} E(t;f)\,\mathrm{d}f}. \tag{2.16}$$

The fundamental problem in time-frequency analysis is that there is no such function of time and frequency that satisfies the following requirements that are imposed on a density function.

The first requirement is that the density function is a non-negative, real valued function, i.e.

$$E(t;f) \geq 0, \text{ for } t \in I\!R \text{ and } f \in I\!R \tag{2.17}$$

and

$$\mathrm{Im}\{E(t;f)\} = 0, \text{ for } t \in I\!R \text{ and } f \in I\!R. \tag{2.18}$$

The second requirement is that the density $E(t;f)$ satisfies the so-called marginals. A marginal density of a two dimensional density $E(t;f)$ is the density as a function of one of the two variables. The time marginal, $E(t)$, is found by integration of $E(t;f)$ over frequency,

$$E(t) = u(t)u^*(t) = \int_{f\in I\!R} E(t;f)\,\mathrm{d}f. \tag{2.19}$$

Similarly, the frequency marginal is given by

$$E(f) = \hat{u}(f)\hat{u}^*(f) = \int_{t\in I\!R} E(t;f)\,\mathrm{d}t. \tag{2.20}$$

The time and frequency marginal cannot be specified independently, as $u(t)$ and $\hat{u}(f)$ are connected through their Fourier transform relations. Because of this dependency, the non-negativity constraint (Eq.(2.17)) and marginal properties of Eqs.(2.19) and (2.20), cannot both be satisfied in one time-frequency representation of the signal $u(t)$. The proof for the contradiction of non-negativity and correct marginals has been given for the quantum mechanical joint distributions of coordinates and momentum by Wigner (1971). We will follow his argument here and translate it to the time-frequency case.

In order to show that it is impossible to satisfy both the non-negativity and marginal requirements for all $u(t)$, it is sufficient to consider the linear combination of two signals, $u(t) = au_1(t) + bu_2(t)$, such that $u_1(t)$ vanishes for all t, for which $u_2(t)$ non-vanishing. First, we impose the time marginal requirement on a non-negative time-frequency energy density function of u. We will show that the result is incompatible with the frequency marginal requirement. We start with the following lemma:

Lemma 1. If the signal $u(t)$ vanishes in some time interval T, and $\chi_T(t)$ is the characteristic function of this interval, we have for the non-negative function $E(t;f)$,

$$\int_{t\in I\!R} E(t;f)\chi_T(t)\,\mathrm{d}t = 0, \text{ for } f \in I\!R. \tag{2.21}$$

Here, we have used $\chi_T(t)$; the characteristic function of the set T. The set T is made up of the interval T, the boundaries ∂T and the complement in $\mathbb{R}$ of the union of T and ∂T, denoted by T'. We now define $\chi_T(t)$ as

$$\chi_T(t) = \{1, \tfrac{1}{2}, 0\} \text{ when } t \in \{T, \partial T, T'\}. \tag{2.22}$$

The result of Lemma 1 can be verified by considering the time marginal, Eq.(2.19), in Eq.(2.21),

$$\int_{f\in\mathbb{R}} \int_{t\in\mathbb{R}} E(t;f)\chi_T(t)\,\mathrm{d}t\,\mathrm{d}f = \int_{t\in\mathbb{R}} u(t)u^*(t)\chi_T(t)\,\mathrm{d}t = 0. \tag{2.23}$$

The integrand with respect to f is non-negative as long as Eq.(2.17) holds for $E(t;f)$. It follows that the integrand with respect to f must vanish, except for a set of f of measure zero.

As Eq.(2.21) is valid for all f and any $\chi_T(t)$, we can also conclude from Eq.(2.21) that if $u(t)$ vanishes in an interval T, the corresponding $E(t;f)$ vanishes for all values of t inside the interval T. This last result is illustrated in Fig. 2.1.

We now consider two functions $u_1(t)$ and $u_2(t)$ which vanish outside two non-overlapping intervals T_1 and T_2, respectively.

The time-frequency energy density of the sum of the two functions, $E_{u_1+u_2}(t;f)$, is zero outside the two time intervals T_1 and T_2. This is a consequence of the fact that we have taken $E_{u_1+u_2}(t;f)$ everywhere non-negative and we want to have the correct time marginal, i.e.

$$\int_{f\in\mathbb{R}} E_{u_1+u_2}(t;f)\chi_{T_1'}(t)\chi_{T_2'}(t)\,\mathrm{d}f = 0. \tag{2.24}$$

This result is illustrated in Fig. 2.2.

Consequently, we can express the non-negative time-frequency energy density function of $u(t) = au_1(t) + bu_2(t)$, with the correct time marginal as

$$E_{u_1+u_2}(t;f) = |a|^2 E_{u_1}(t;f) + |b|^2 E_{u_2}(t;f), \tag{2.25}$$

for all a and b. The result Eq.(2.25) is incompatible with the frequency marginal property Eq.(2.20). We can demonstrate this by considering the

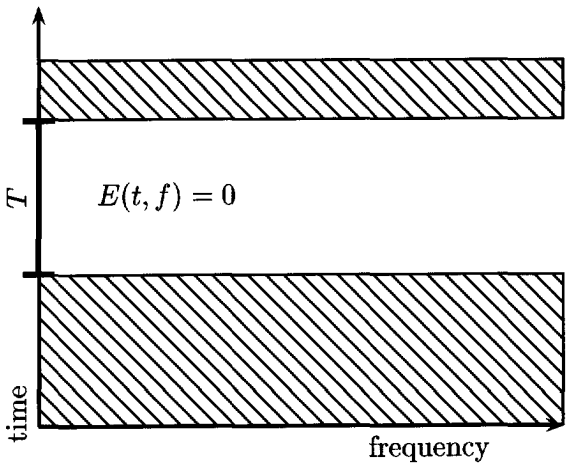

Figure 2.1: *Graphical illustration of the result of Lemma 1. If $u(t)$ vanishes in time interval T then the non-negative function $E(t;f)$ is zero for $f \in \mathbb{R}$ and $t \in T$.*

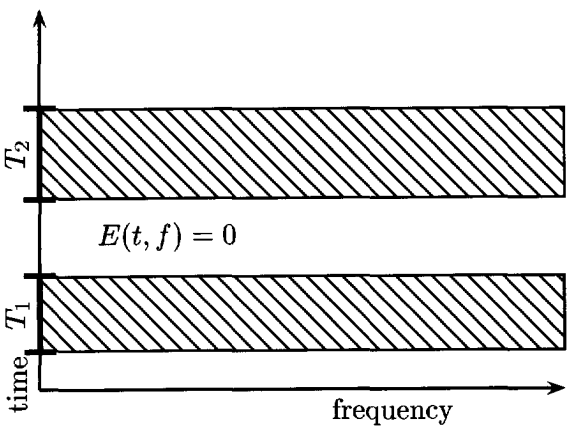

Figure 2.2: *The non-negative $E\{u,u\}(t;f)$ with correct time marginal, vanishes everywhere outside T_1 and T_2.*

frequency marginal of the non-negative density with correct time marginal, given by Eq.(2.25):

$$\int_{t\in I\!R} E_{u_1+u_2}(t;f)\,\mathrm{d}t = |a|^2 \int_{t\in I\!R} E_{u_1}(t;f)\,\mathrm{d}t + |b|^2 \int_{t\in I\!R} E_{u_2}(t;f)\,\mathrm{d}t. \tag{2.26}$$

The frequency marginal can also be found from the Fourier transform of $u(t) = au_1(t) + bu_2(t)$, i.e.

$$E(f) = |\mathcal{F}_t^-\{u(t)\}|^2 = |a|^2\hat{u}_1(f)^2 + |b|\hat{u}_2(f)^2 + 2\mathrm{Re}\{ab^*\hat{u}_1(f)\hat{u}_2^*(f)\}. \tag{2.27}$$

Since we want both Eq.(2.26) and Eq.(2.27) to be valid for all a and b, we must have

$$\hat{u}_1(f)\hat{u}_2^*(f) = 0. \tag{2.28}$$

This last identity cannot hold for the signals $u_1(t)$ and $u_2(t)$, as they vanish outside the intervals T_1 and T_2 respectively. The Fourier transform of a function that vanishes outside a restricted time interval will have an infinite support in the frequency domain and as a result both $\hat{u}_1(f)$ and $\hat{u}_2(f)$ will not vanish in any frequency interval. Consequently, Eq.(2.28) cannot hold for the signal $u(t)$, which completes our proof of the incompatibility of non-negativity and correct marginals.

For a long time the preceding argument has been used to demonstrate that time-frequency representations that are both non-negative and have correct marginals do not exist. In the proof it is assumed that the representation is bilinear, which implies that the representation is independent of the constants a and b. However, if the bilinearity condition is dropped and the marginals are treated as independent densities it is possible to construct non-negative time-frequency representations with the correct marginals.

Using the same methods that are used in statistical theory to construct a bivariate density function from its marginals, a time-frequency representation can be constructed from the instantaneous energy and power spectrum of a signal. For instance, one could propose a time-frequency representation, $P(t;f)$, of the form

$$P(t;f) = C(a(t),b(f))|u(t)|^2|\hat{u}(f)|^2, \tag{2.29}$$

where $C(a(t), b(f))$ is a functional that specifies the correlation between the marginals. If certain conditions are imposed on $C(a(t), b(f))$, one can construct non-negative densities with the correct time and frequency marginals. Time-frequency representations of this type have been proposed in Cohen and Posch (1985), where the authors give a parameterization of the function $C(a(t), b(f))$ that results in a non-negative density with the correct marginals. However, the problem with the representations of the type of Eq.(2.29) is that the representation depends on the signal and there is no satisfactory way to find the correlation between the marginals without taking into account their functional dependence. We will therefore not further consider the representations of the type of Eq.(2.29) and refer to Cohen (1995) and references therein for a more thorough discussion. At this point we only want to make clear that the marginals alone are not sufficient to construct a joint time-frequency density function, but we have to specify somehow the correlation between the variables t and f.

The functional dependence of the marginals sets the time-frequency energy density functions apart from the bivariate density functions in statistics. However, we have not yet clearly defined this functional dependence. There is no direct relation between the time energy density, $|u(t)|^2$, and the power spectrum, $|\hat{u}(f)|^2$, in the sense that if we know one marginal, we can find the other. What we have is the Fourier-transform relation between the time signal, $u(t)$, and its frequency-domain representation, $\hat{u}(f)$. Therefore, one cannot specify a signal in one domain, without at the same time fixing its representation in the other domain.

The basic consequence of this Fourier transform relation is that a narrow waveform in time has a broad spectrum and that a narrow spectrum yields a broad time signal. This last observation is known as the uncertainty principle of signal analysis. A graphical illustration of the uncertainty relation between the time and frequency representations of a signal is shown in Fig. 2.3. A measure for the duration and bandwidth of a signal was given by Eqs.(2.13) and (2.5). The standard deviations of the time and frequency density functions, σ_t and σ_f, were proposed as the parameters that describe the broadness of the signal in time and frequency domains respectively. With these two measures for the broadness of a signal, the uncertainty relation can be expressed

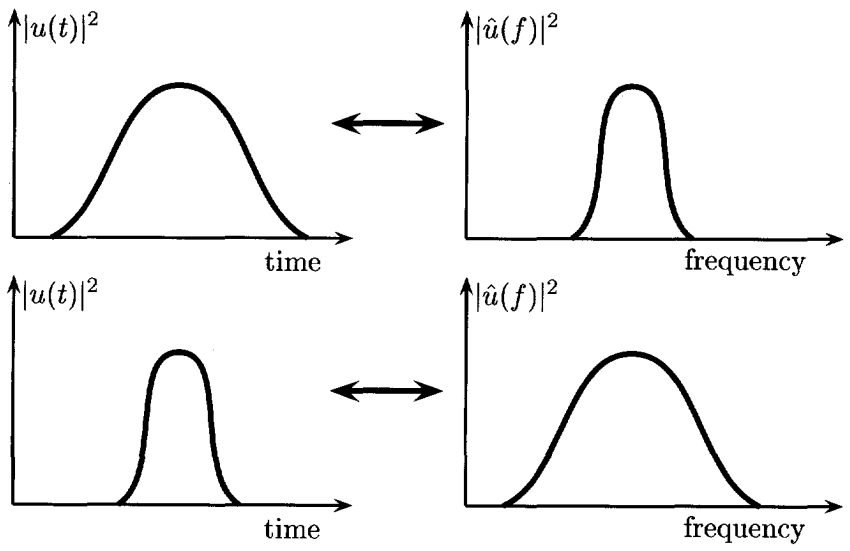

Figure 2.3: *The uncertainty relation for time and frequency marginals. A broad waveform in time gives a narrow frequency spectrum and vice versa.*

as (Gabor 1946)

$$\sigma_t \sigma_f \geq \frac{1}{4\pi}. \tag{2.30}$$

We will refer to the inequality Eq.(2.30) as Gabor's uncertainty relation, in order to distinguish it from Heisenberg's uncertainty relation of quantum mechanics. Although the two relations are the same in their mathematical expression, they relate to different physical concepts. In quantum mechanics the uncertainty relation emerges in a probabilistic context, while in signal analysis it is an expression of the simple fact that one cannot make B and T arbitrarily small. An excellent discussion of the uncertainty principle in signal analysis and its relation to quantum mechanical concepts can be found in Cohen (1995).

It should be noted that the uncertainty principle is a statement about the marginals. As such it puts only a mild restriction on the time-frequency representation itself. As long as the representation satisfies the marginals, the uncertainty principle is not violated. The uncertainty relation constraints the region of the time-frequency plane where energy is localized. The boundaries of this region are roughly given by the duration and bandwidth of the signal.

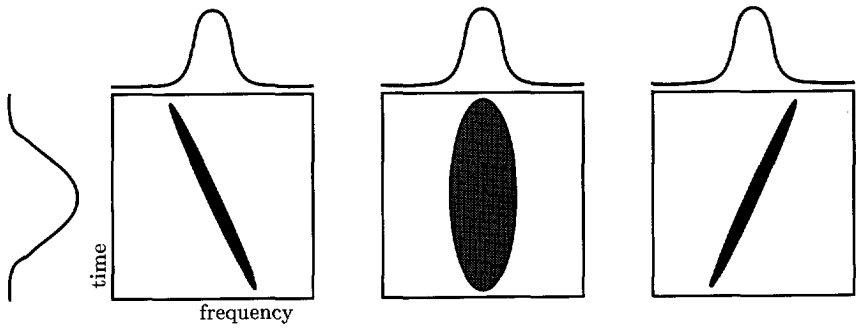

Figure 2.4: *Time-frequency representations that yield the same marginals can have a totally different time-frequency correlation structure.*

However, there is still an infinite number of ways to distribute the energy within this region. The wide variety of time-frequency representations that yield the same marginals is graphically indicated in Fig. 2.4. In the previous we have discussed some of the requirements that a joint time-frequency representation should satisfy. It was shown that the requirement of correct marginals is only a mild restriction on the representation. The non-negativity and marginal conditions can only be satisfied in one time-frequency representation by making the representation dependent on the signal. As we presently have no idea how this dependence can be introduced in the representation, the non-negativity condition is dropped. The remaining question is how the correlation is introduced into in the time-frequency representation.

The correlation between the marginals can be brought into the representation if the concept of the characteristic function of the densities of a single variable is extended to the bivariate case. The joint time-frequency characteristic function $M(\nu;\tau)$ of the time-frequency representation $P(t;f)$ is introduced as

$$M(\nu;\tau) = \int_{t\in I\!R} \int_{f\in I\!R} \exp(-\mathrm{j}2\pi(\nu t - f\tau))P(t;f)\,\mathrm{d}t\,\mathrm{d}f. \tag{2.31}$$

The characteristic function can be interpreted as the average value of $\exp(-\mathrm{j}2\pi(\nu t - f\tau))$ as a function of ν and τ. If we can derive the character-

istic function, the time-frequency representation $P(t;f)$ can be obtained as the two-dimensional Fourier transform of $M(\nu;\tau)$, given by

$$P(t;f) = \int_{\nu\in I\!R}\int_{\tau\in I\!R} \exp(\mathrm{j}2\pi(\nu t - f\tau)M(\nu;\tau)\,\mathrm{d}\nu\,\mathrm{d}\tau. \tag{2.32}$$

At present there is only one method with which the characteristic function $M(\nu;\tau)$ can be derived from first principles. It is known as the 'characteristic function operator method' (Cohen 1995). The association of variables with (Hermitian) operators is a concept that emerged in quantum physics and only recently has found its way to signal analysis. It is a particularly helpful concept if one wants to derive joint distributions other than of time and frequency (Cohen 1996a, 1996b). In time-frequency analysis, the operator method does not really have any practical implications. For that reason we will only briefly describe the method here. In the following, we will use the operator method to derive the prototype bilinear time-frequency representation; the Wigner distribution.

Time and frequency can be associated with the Hermitian operators $\mathcal{T}$ and $\mathcal{F}$. The time operator is defined as

$$\mathcal{T}\{u\}(t) = tu(t), \tag{2.33}$$

in the time domain, and in the frequency domain we have

$$\mathcal{T}\{\hat{u}\}(f) = \frac{\mathrm{j}}{2\pi}\frac{\mathrm{d}}{\mathrm{d}f}\hat{u}(f). \tag{2.34}$$

The frequency operator[1] is given by

$$\mathcal{F}\{\hat{u}\}(f) = f\hat{u}(f), \tag{2.35}$$

in the frequency domain. In the time domain the frequency operator is given by

$$\mathcal{F}\{u\}(t) = \frac{-\mathrm{j}}{2\pi}\frac{\mathrm{d}}{\mathrm{d}t}u(t). \tag{2.36}$$

[1]Note that here we use the symbol $\mathcal{F}$ for the frequency operator, It should not be confused with $\mathcal{F}_t^-$, which denotes the Fourier transformation over the variable t.

The fundamental commutation relation between the operators is

$$\mathcal{T}\mathcal{F} - \mathcal{F}\mathcal{T} = \frac{\mathrm{j}}{2\pi} \tag{2.37}$$

and follows directly by using Eqs.(2.33)-(2.36) on either u or $\hat{u}$. The crucial step in the derivation of the joint time-frequency characteristic function, $M(\nu;\tau)$, is that the average, $\langle \exp(-\mathrm{j}2\pi(\nu t - \tau f))\rangle$ can be obtained directly from the signal $u(t)$ as

$$M(\nu;\tau) = \int_{t\in I\!R} u^*(t)\mathcal{M}(\nu;\tau)\{u\}(t)\,\mathrm{d}t, \tag{2.38}$$

where $\mathcal{M}$ is the so-called characteristic function operator. An example of this operator is found by substituting the time and frequency operators for the time and frequency variables in the expression $\exp(-\mathrm{j}2\pi(\nu t - \tau f))$ (Ville 1948),

$$\mathcal{M}(\nu;\tau) = \exp(-\mathrm{j}2\pi(\nu\mathcal{T} - \tau\mathcal{F})). \tag{2.39}$$

We now find the characteristic function by substitution of this operator into Eq.(2.38),

$$M(\nu;\tau) = \int_{t\in I\!R} u^*(t)\ \exp(-\mathrm{j}2\pi(\nu\mathcal{T} - \tau\mathcal{F}))\{u\}(t)\,\mathrm{d}t. \tag{2.40}$$

The exponent can be broken up, using a special case of the Baker-Hausdorf theorem (Cohen 1995; Wilcox 1967), i.e.

$$\exp(-\mathrm{j}2\pi(\nu\mathcal{T} - \tau\mathcal{F})) = \exp(-\mathrm{j}2\pi\nu\tau/2)\exp(-\mathrm{j}2\pi\nu\mathcal{T})\exp(\mathrm{j}2\pi\tau\mathcal{F}). \tag{2.41}$$

Using Eq.(2.41) in Eq.(2.40), the characteristic function can now be expressed as

$$M(\nu;\tau) = \int_{t\in I\!R} u^*(t)\exp(-\mathrm{j}2\pi\nu\tau/2)\exp(-\mathrm{j}2\pi\nu\mathcal{T})\exp(\mathrm{j}2\pi\tau\mathcal{F})\{u\}(t)\,\mathrm{d}t. \tag{2.42}$$

The operator $\exp(\mathrm{j}2\pi\tau\mathcal{F})$ is the translation operator

$$\exp(\mathrm{j}2\pi\tau\mathcal{F})\{u\}(t) = u(t+\tau) \tag{2.43}$$

and as a result we find

$$M(\nu;\tau) = \int_{t\in I\!R} u^*(t)\exp(-\mathrm{j}2\pi\nu\tau/2)\exp(-\mathrm{j}2\pi\nu t)u(t+\tau)\,\mathrm{d}t. \qquad (2.44)$$

Finally, with the change of variables $s = t + \frac{1}{2}\tau$, $\mathrm{d}s = \mathrm{d}t$, we arrive at

$$M(\nu;\tau) = \int_{s\in I\!R} u^*(s-\tfrac{1}{2}\tau)\exp(-\mathrm{j}2\pi\nu s)u(s+\tfrac{1}{2}\tau)\,\mathrm{d}s. \qquad (2.45)$$

The characteristic function is bilinear in the signal $u(t)$, by which is meant that the signal enters twice in the representation. In this case the signal enters twice through the product of the signal with its reverse conjugate. We shall therefore from now on adopt the notation $M\{u,u\}(\nu;\tau)$ for the bilinear characteristic function. Since we have found the characteristic function of the representation, we can use Eq.(2.32) to obtain the bilinear time-frequency representation, $P\{u,u\}(t;f)$, as

$$P\{u,u\}(t;f) = \int_{\tau\in I\!R} \exp(-\mathrm{j}2\pi f\tau)u(t+\tfrac{1}{2}\tau)u^*(t-\tfrac{1}{2}\tau)\,\mathrm{d}\tau. \qquad (2.46)$$

This time-frequency representation is the Wigner distribution. The Wigner distribution was posed by Wigner (1932) in a quantum-mechanical context. The first derivation of the Wigner distribution as a time-frequency representation was made by Ville (1948). When used in the context of joint time-frequency analysis, it is also referred to as the Wigner-Ville distribution. From now on we will use the notation $W\{u,u\}(t;f)$ for the Wigner distribution.

The above derivation, which started from the time and frequency operators, suggests that the Wigner distribution is the fundamental time-frequency representation. There is however an ambiguity in the derivation, which has its origin in the commutation relation Eq.(2.37). The time and frequency operators do no commute, which means that changing their order changes the outcome of the operations. A consequence of the commutation relation is that there is an infinite number of ways to associate an operator with the function $\exp(-\mathrm{j}2\pi(\nu t - \tau f))$. In the derivation of the Wigner distribution the Weyl ordering was used, i.e.

$$\exp(-\mathrm{j}2\pi(\nu t - \tau f)) \longrightarrow \mathcal{M}_W = \exp(-\mathrm{j}2\pi(\nu\mathcal{T} - \tau\mathcal{F})). \qquad (2.47)$$

However, other correspondence rules can be used as well. For instance,

$$\exp(-\mathrm{j}2\pi(\nu t - \tau f)) \longrightarrow \mathcal{M}_N = \exp(\mathrm{j}2\pi\tau\mathcal{F})\exp(-\mathrm{j}2\pi\nu\mathcal{T}), \tag{2.48}$$

which is the called the normal correspondence. The normal correspondence leads to a different characteristic function (Cohen 1995), given by

$$M\{u,u\}(\nu;\tau) = \int_{t\in\mathbb{R}} u^*(t)\exp(-\mathrm{j}2\pi\nu t)u(t)\,\mathrm{d}t. \tag{2.49}$$

The corresponding time-frequency representation is the Margenau-Hill distribution,

$$P\{u,u\}(t;f) = u^*(t)\exp(-\mathrm{j}2\pi ft)\hat{u}(f). \tag{2.50}$$

Using all possible correspondence rules an infinite number of time-frequency representations is obtained. However, if we adopt the Weyl ordering, all other orderings $\mathcal{M}_i$, can be expressed as

$$\mathcal{M}_i \longrightarrow \Psi(\nu;\tau)\exp(-\mathrm{j}2\pi(\nu\mathcal{T} - \tau\mathcal{F})), \tag{2.51}$$

where $\Psi(\nu;\tau)$ is a kernel function (Cohen 1995). We shall use this relation between the correspondences to generate other time-frequency representations from the Wigner distribution in Chapter 3. In this thesis we will adopt the Weyl ordering and consequently the Wigner distribution will be our basic time-frequency representation. The reason for this is simply that the Wigner distribution has been extensively studied in the past. As we can obtain all other representations from the Wigner distribution through the relation given by Eq.(2.51), we will first study the Wigner distribution. The properties of the other time-frequency representations can then be derived by an evaluation of the associated kernel function $\Psi(\nu;\tau)$.

The properties of the Wigner distribution will be studied in more detail in the last part of this chapter. First, we will briefly discuss two classical methods for time-frequency analysis; the sliding-window Fourier transformation and complex-trace analysis. The purpose of discussing them here, is to establish their place in the framework of the bilinear time-frequency representations.

2.2.2 The sliding-window Fourier transformation

The spectrogram is the classic method for the estimation of the local frequency content of a signal. It is obtained as the squared modulus of the Fourier transform of a windowed portion of the signal. If we weight the data at each time t with a window function $w(t)$, a modified signal $u_t(\tau)$ is obtained as

$$u_t(\tau) = u(\tau)w(\tau - t). \tag{2.52}$$

We take a real-valued window function that is centered at $t = 0$. By changing the duration of the window, we change the time interval in which the signal $u_t(\tau)$ is localized. The sliding-window Fourier transform, the local spectrum $\hat{u}_t(f)$, is found by a Fourier transformation of the localized signal,

$$\hat{u}_t(f) = \mathcal{F}_\tau^- \{u_t(\tau)\}. \tag{2.53}$$

Repeating this procedure for each time t and taking the squared modulus of $\hat{u}_t(f)$, we obtain a time-frequency representation $P\{u,u\}(t;f)$ as

$$P\{u,u\}(t;f) = |\hat{u}_t(f)|^2, \tag{2.54}$$

which is called the spectrogram of $u(t)$.

A problem that is often associated with the sliding-window Fourier transformation, is that the result is strongly influenced by the choice of the window, $w(t)$. The windowed signal, $u_t(\tau)$, and the local spectrum are a Fourier transform pair. Consequently, their broadness in time and frequency is governed by the uncertainty principle. The duration of the windowed signal is determined by the window length. Improving time localization by using a shorter window, results in a broadening of the spectrum and consequently the frequency localization is diminished. Of course, the reverse will happen if we lengthen the window. In that case, frequency localization is improved, at the cost of time localization.

In the interpretation of a spectrogram one must always take the shape and size of the analysis window into account. The best results are usually achieved, if a window is used that is matched to the characteristics of the signal. The effect of the window on the local spectrum will be minimal if the characteristics of the signal are not altered by the application of the window. However,

in many cases it is difficult, or even impossible, to find this matched window. For instance, if the characteristics of the signal change rapidly as a function of time. In those cases one could try to find a time-dependent matched window. The simplest way to achieve this, is to use the signal itself as the window. For example by taking

$$\hat{u}_t(f) = \mathcal{F}_\tau^-\{u(\tau)u^*(\tau - t)\}. \tag{2.55}$$

The symmetric form Eq.(2.55) is given by

$$P\{u,u\}(t;f) = \mathcal{F}_\tau^-\{u(t + \tfrac{1}{2}\tau)u^*(t - \tfrac{1}{2}\tau)\}, \tag{2.56}$$

which is the Wigner distribution of the signal $u(t)$. One of the interpretations we can attach to the Wigner distribution is that of a Fourier transform of the signal after it has been windowed with the reverse of itself. With this interpretation we can anticipate a problem that will be encountered when using the Wigner distribution as a local spectrum. With a sliding-window Fourier transformation, the results depend strongly on the interaction of the window with the signal. Similarly, the Wigner distribution will be strongly influenced by the interaction of the signal with its reverse. The consequences of this interaction remain an important issue throughout this thesis. The relation between the spectrogram and Wigner distribution will be established in more detail in Chapter 3.

2.2.3 Polar representation of the spectrum and the complex time signal

Complex functions of a real variable, such as the Fourier transform of a function, can be given in their polar representation. The polar representation enables the decomposition of the Fourier transform of a function into a *spectral amplitude* function $a_f(f)$ and *spectral phase* function $\phi_f(f)$ by taking

$$\hat{u}(f) = a_f(f)\exp(\mathrm{j}\phi_f(f)). \tag{2.57}$$

Another parameter that is used to describe the Fourier spectrum is the *group delay*, $\tau_g(f)$, which is the scaled derivative of the spectral phase function with respect to frequency, and is defined as

$$\tau_g(f) = -\frac{1}{2\pi}\frac{\mathrm{d}\phi_f(f)}{\mathrm{d}f}. \tag{2.58}$$

The same representation can be adopted for complex time functions. A complex function $u(t)$ can be decomposed into an envelope function, $a_t(t)$, and phase function, $\phi_t(t)$, by taking

$$u(t) = a_t(t) \exp(\mathrm{j}\phi_t(t)). \tag{2.59}$$

Measured signals are real valued. The signal is made complex by adding an imaginary part to it. For obvious reasons, it is important that there is a unique relation between the complex signal and the original signal. There is a unique relation between real and imaginary part if the signal is analytic. In the context of signal analysis, an analytic signal is a complex-valued signal with a real and imaginary part that are their respective Hilbert transforms. The complex-trace attributes as used in seismic interpretation are closely related to the notion of the analytic signal (Taner et al. 1979). The imaginary part of the analytic seismic signal is found by a Hilbert transformation of the real signal $u(t)$:

$$\mathrm{Im}\{u^a\}(t) = \mathcal{H}_t\{u\}(t), \tag{2.60}$$

where the superscript a denotes analytic with respect to time and $\mathcal{H}_t\{u\}$ denotes the Hilbert transformation of u with respect to time. The Hilbert transformation can conveniently be expressed in the Fourier domain as

$$\widehat{\mathcal{H}_t\{u\}}(f) = -\mathrm{j}\ \mathrm{sign}(f)\hat{u}(f), \tag{2.61}$$

where $\mathrm{sign}(f)$ is the *sign* function, defined by

$$\mathrm{sign}(f) = \{-1, 0, 1\} \text{ when } \{f < 0, f = 0, f > 0\}. \tag{2.62}$$

Hence, we can find the imaginary part of the analytic signal by a Hilbert transformation of the real signal in the Fourier domain, followed by an inverse Fourier transformation. The full complex trace is found by summation of the real and imaginary signals in the Fourier domain:

$$\begin{aligned} \hat{u}^a(f) = \ \hat{u}(f) + \mathrm{j}\widehat{\mathcal{H}_t\{u\}}(f) &= (1 + \mathrm{sign}(f))\hat{u}(f) \\ &= 2\ \chi_{I\!R^+}(f)\hat{u}(f), \end{aligned} \tag{2.63}$$

where $\chi_{I\!R^+}(f)$ is the characteristic function on the domain $I\!R^+$ given by

$$\chi_{I\!R^+}(f) = \{0, \tfrac{1}{2}, 1\} \text{ when } \{f < 0, f = 0, f > 0\}. \tag{2.64}$$

As a result, we find the complex trace by setting the Fourier transform of the signal to zero for negative frequencies and taking twice the value for positive frequencies, while the zero frequency is left unchanged.

For the analytic signal the following nomenclature is widely used. Given the signal

$$u^a(t) = u(t) + \mathrm{j}\mathcal{H}_t\{u\}(t) = a_t(t)\exp(\mathrm{j}\phi_t(t)), \tag{2.65}$$

the following terms are used:

$u^a(t)$	$=$	$u(t) + \mathrm{j}\mathcal{H}_t\{u\}(t)$	is the *analytic* signal,
$u(t)$	$=$	$\mathrm{Re}\{u^a\}(t)$	is the *real* signal,
$\mathcal{H}_t\{u\}(t)$	$=$	$\mathrm{Im}\{u^a\}(t)$	is the *imaginary* signal,
$a_t(t)$	$=$	$\sqrt{u(t)^2 + \mathcal{H}_t\{u\}(t)^2}$	is the *modulus* or *envelope*,
$\phi_t(t)$	$=$	$\tan^{-1}\left\{\frac{\mathcal{H}_t\{u\}(t)}{u(t)}\right\}$	is the *argument* or *phase*.

Because the envelope and phase of the analytic signal are functions of time - as opposed to the spectral amplitude and phase functions - they are often called *instantaneous* amplitude and *instantaneous* phase. An important parameter is the derivative of the phase with time

$$f_t^i(t) = \frac{1}{2\pi}\frac{\mathrm{d}\phi_t(t)}{\mathrm{d}t}, \tag{2.66}$$

where $f_t^i(t)$ is the *instantaneous frequency.*

In seismic signal analysis the instantaneous amplitude, instantaneous phase and instantaneous frequency are called the *complex-trace attributes.*

The physical interpretation of the complex-trace attributes has been a controversial subject. Especially, the interpretation of the instantaneous frequency has been continuously under discussion (White 1991; Barnes 1993). Many of the misunderstandings and misinterpretations can be brought back to the fact that one tries to enforce some relationship between the instantaneous frequency and Fourier frequencies. It is tempting to interpret instantaneous frequency as a measure for the frequency as a function of time. However, some properties of the instantaneous frequency are difficult to reconcile with this interpretation. One of the contradictions is that for most seismic signals

the instantaneous frequency attains negative values. However, there is no energy at negative frequencies in the spectrum of an analytic signal. If the instantaneous frequency is to be regarded as a measure for the distribution of Fourier frequencies over time, it is at least remarkable to find values that are outside the bandwidth of the Fourier spectrum.

Much of the controversy about the complex-trace attributes can be clarified by considering their relation with the bilinear time-frequency representations. The time marginal of the Wigner distribution of the complex trace is the instantaneous energy. The instantaneous frequency can be found by calculating the average frequency for a fixed time, of the Wigner distribution, i.e.

$$f_t^i(t) = \langle f \rangle_t = \frac{\int_{f \in I\!R} \; fW\{u,u\}(t;f)\,\mathrm{d}f}{\int_{f \in I\!R} \; W\{u,u\}(t;f)\,\mathrm{d}f}. \tag{2.67}$$

In the same way the group delay can be found as the average time for a fixed frequency of the Wigner distribution.

This type of relation is not only of theoretical interest. The extraction of attributes via the time-frequency representation of the signal, instead of directly from the signal, leads to significant improvements in signal to noise ratio of the attributes. Moreover, the average frequency is just one characteristic of the time-frequency representation. Other measures, such as local bandwidth of higher order relative moments, are potentially useful attributes as well. Complex-trace attribute analysis is one of the few methods the seismic interpreter has for a quantitative description of the characteristics of the seismic trace. When discussing the properties of the time-frequency representations, we will therefore also take the relation with the complex-trace attributes into account.

2.3 The Wigner distribution function

In this section we will discuss the Wigner distribution as a candidate for the non-stationary power spectrum in more detail. In the previous section it was shown that the Wigner distribution can be derived by determining the characteristic function of a joint time-frequency density function through the Weyl ordering of the time and frequency operators. Here, our starting point in the derivation of the Wigner distribution will be a generalization of the auto-correlation function to the non-stationary case. The Wigner

distribution has a large number of mathematical properties that make it a good candidate for the basic time-frequency representation. It is for those attractive mathematical properties that we adopt it as the starting point of all time-frequency analysis methods that are discussed in this thesis. The generalization of the auto-correlation function (Eq.A.7) to the non-stationary case is given by the instantaneous auto-correlation function $R\{u,u\}(t;\tau)$. The instantaneous auto-correlation of a signal $u(t)$ is obtained by considering the symmetric auto-correlation of a signal around fixed time t, i.e.

$$R\{u,u\}(t;\tau) = u(t+\tfrac{1}{2}\tau)u^*(t-\tfrac{1}{2}\tau). \tag{2.68}$$

The Wigner distribution of a function $u(t)$ is defined as the non-stationary power spectrum that is associated with the instantaneous auto-correlation function

$$W\{u,u\}(t;f) = \mathcal{F}_\tau^- \left\{R\{u,u\}(t;\tau)\right\}. \tag{2.69}$$

It is the Fourier transformation of the instantaneous auto-correlation over the time-shift variable τ.

The Wigner distribution can also be expressed in terms of the Fourier spectrum $\hat{u}(f)$. To that end, we consider the Fourier transformation with respect to time of Eq.(2.69),

$$\mathcal{F}_t^- \left\{W\{u,u\}(t;f)\right\} = \mathcal{F}_t^- \mathcal{F}_\tau^- \left\{u(t+\tfrac{1}{2}\tau)u^*(t-\tfrac{1}{2}\tau)\right\}. \tag{2.70}$$

Next, we replace the variables of integration t and τ in Eq.(2.70) by t' and τ', through

$$\begin{aligned} \tau' &= t - \tfrac{1}{2}\tau, \\ t' &= t + \tfrac{1}{2}\tau, \end{aligned} \tag{2.71}$$

which entails that $\mathrm{d}t\mathrm{d}\tau = \mathrm{d}t'\mathrm{d}\tau'$. Hence, Eq.(2.70) is replaced by

$$\begin{aligned} &\mathcal{F}_t^- \left\{W\{u,u\}(t;f)\right\} = \\ &\int_{t'\in I\!R} \exp(-\mathrm{j}2\pi(f+\tfrac{1}{2}\nu)t')u(t')\mathrm{d}t' \left(\int_{\tau'\in I\!R} \exp(-\mathrm{j}2\pi(f-\tfrac{1}{2}\nu)\tau')u(\tau')\mathrm{d}\tau'\right)^* \\ &= \hat{u}(f+\tfrac{1}{2}\nu)\hat{u}^*(f-\tfrac{1}{2}\nu). \end{aligned} \tag{2.72}$$

As a result, by considering the inverse Fourier transformation with respect to ν of both the left-hand side and right-hand side of Eq.(2.72), we obtain

$$W\{u,u\}(t;f) = \mathcal{F}_{\nu}^{+}\left\{R\{\hat{u},\hat{u}\}(\nu;f)\right\}, \tag{2.73}$$

where,

$$R\{\hat{u},\hat{u}\}(\nu;f) = \hat{u}(f+\tfrac{1}{2}\nu)\hat{u}^{*}(f-\tfrac{1}{2}\nu), \tag{2.74}$$

which is the local spectral auto-correlation function with frequency-shift variable ν.

The Wigner distribution has many interesting mathematical properties. Those properties that are important in the present context are given below. A comprehensive list of properties of the Wigner distribution is given in Hlawatsch and Boudreaux-Bartels (1992).

2.3.1 Properties of the Wigner distribution

Property 1: Realness. The Wigner distribution is real. To verify this property, we consider the complex conjugate of Eq.(2.69).

$$\begin{aligned} W^{*}\{u,u\}(t;f) &= \int_{\tau\in\mathbb{R}} \exp(\mathrm{j}2\pi f\tau)u^{*}(t+\tfrac{1}{2}\tau)u(t-\tfrac{1}{2}\tau)\,\mathrm{d}\tau \\ &= \int_{\tau\in\mathbb{R}} \exp(-\mathrm{j}2\pi f\tau)u^{*}(t-\tfrac{1}{2}\tau)u(t+\tfrac{1}{2}\tau)\,\mathrm{d}\tau \\ &= W\{u,u\}(t;f), \end{aligned} \tag{2.75}$$

from which we conclude that $W\{u,u\}(t;f)$ is a real-valued function.

Since the Wigner distribution is a real-valued function, it has no phase. However, the phase information of the signal is preserved in the Wigner distribution. This can be concluded from the inversion property of the Wigner distribution:

Property 2: Inversion. The signal can be recovered from its Wigner distribution up to a constant phase factor. Taking the inverse Fourier transformation of the Wigner distribution with respect to the frequency we obtain the instantaneous auto-correlation function

$$u(t+\tfrac{1}{2}\tau)u^{*}(t-\tfrac{1}{2}\tau) = \mathcal{F}_{f}^{+}\left\{W\{u,u\}(t;f)\right\}. \tag{2.76}$$

If we now consider the value, $t = \frac{1}{2}\tau$, and replace τ by t, we obtain

$$u(t) = \frac{1}{u^*(0)} \mathcal{F}_f^+ \left\{ W\{u,u\}(\tfrac{1}{2}t; f) \right\}. \tag{2.77}$$

Consequently the signal can be recovered from its Wigner distribution up to a constant $1/u^*(0)$. The constant arises because to obtain the Wigner distribution we have multiplied the signal with its complex conjugate. In this multiplication a constant phase factor drops out and can therefore not be recovered from the Wigner distribution.

Property 3: Marginals. Integration of the Wigner distribution over time yields the spectral energy density spectrum, $E(f)$, of the signal, i.e.

$$E(f) = \int_{t \in \mathbb{R}} W\{u,u\}(t; f)\, \mathrm{d}t = |\hat{u}(f)|^2, \tag{2.78}$$

which follows from Eq.(2.69) and the identity

$$\int_{t \in \mathbb{R}} \exp(\mathrm{j}2\pi\nu t) = \delta(\nu), \tag{2.79}$$

where $\delta(\nu)$ is the delta function of Dirac.

In the same fashion, integration of the Wigner distribution over frequency yields the instantaneous energy, $E(t)$, of the signal, i.e.

$$E(t) = \int_{f \in \mathbb{R}} W\{u,u\}(t; f)\, \mathrm{d}f = |u(t)|^2, \tag{2.80}$$

which follows from Eq.(2.73). Equations (2.78) and (2.80) are called the *frequency marginal* and *time marginal* of the Wigner distribution, respectively (cf. Eqs.(2.19)) and (2.20)).

The total energy, E_u, of a signal $u(t)$ is given by

$$E_u = \int_{t \in \mathbb{R}} u(t)u^*(t)\, \mathrm{d}t = \int_{f \in \mathbb{R}} \hat{u}(f)\hat{u}^*(f)\, \mathrm{d}f, \tag{2.81}$$

where Parseval's theorem has been used (Eq.(A.9)). Consequently, the combination of time and frequency marginal properties leads to the total energy condition

$$E_u = \int_{t \in \mathbb{R}} \int_{f \in \mathbb{R}} W\{u,u\}(t; f)\, \mathrm{d}t\mathrm{d}f. \tag{2.82}$$

Property 4: Local averages. The relative first-order moment of the Wigner distribution with respect to frequency is given by

$$\langle f \rangle_t = \frac{1}{E(t)} \int_{f \in I\!R} f\, W\{u,u\}(t;f)\, \mathrm{d}f, \tag{2.83}$$

where the brackets denote the average and the underscore t that this average is taken for every time t. The average frequency of the Wigner distribution can also be obtained directly from the signal. Equation (2.83) can also be written as an inverse Fourier transformation:

$$\langle f \rangle_t = \frac{1}{E(t)} \mathcal{F}_f^+ \left\{ f W\{u,u\}(t;f) \right\} (t;\tau = 0). \tag{2.84}$$

Then, using the definition of $W\{u,u\}(t;f)$ of Eq.(2.69) and the transformation of a time derivative of a function as given in Eq.(A.12), we obtain

$$f W\{u,u\}(t;f) = \frac{1}{\mathrm{j}2\pi} \mathcal{F}_\tau^- \left\{ \partial_\tau R\{u,u\}(t;\tau) \right\}. \tag{2.85}$$

Substitution of Eq.(2.85) in the right hand side of Eq.(2.84) leads to

$$\langle f \rangle_t = \frac{1}{\mathrm{j}2\pi E(t)} \partial_\tau R\{u,u\}(t;\tau)|_{\tau=0}\,. \tag{2.86}$$

We now substitute the definition of $R\{u,u\}(t;\tau)$ of Eq.(2.68) and perform the differentiation. An expression of the average frequency in terms of the signal $u(t)$ is then found as

$$\langle f \rangle_t = \frac{\mathrm{j}}{4\pi E(t)} \left[u(t) \partial_t u^*(t) - u^*(t) \partial_t u(t) \right]. \tag{2.87}$$

Using the relation $E(t) = u(t)u^*(t)$, we can further simplify this result and arrive at

$$\langle f \rangle_t = \frac{1}{2\pi} \mathrm{Im} \left\{ \frac{\partial_t u(t)}{u(t)} \right\} = \frac{1}{2\pi} \mathrm{Im} \left\{ \partial_t \ln u(t) \right\}. \tag{2.88}$$

In the case that $u(t)$ is an analytic signal (Eq.2.65) we have

$$\langle f \rangle_t = \frac{1}{2\pi} \mathrm{Im} \left\{ \partial_t \ln \left[a_t(t) \exp(\mathrm{j}\phi_t(t)) \right] \right\} = \frac{1}{2\pi} \partial_t \phi_t(t) = f_t^i(t), \tag{2.89}$$

where $\phi_t(t)$ is the *instantaneous phase* and $f_t^i(t)$ is the *instantaneous frequency* of the analytic signal. Hence, we can obtain the instantaneous frequency of a signal as the average frequency as a function of time of the Wigner distribution of the signal.

The first order moment of the Wigner distribution with respect to time is given by

$$\langle t \rangle_f = \frac{1}{E(f)} \int_{t \in \mathbb{R}} tW\{u,u\}(t;f)\,\mathrm{d}t = -\frac{1}{2\pi}\partial_f \phi_f(f) = \tau_g(f), \qquad (2.90)$$

where $\phi_f(f)$ is the *spectral phase* (Eq.(2.57)) and $\tau_g(f)$ is the *group delay* (Eq.(2.58)). This result can be verified in a similar way as the derivation of the relation between the average frequency of the Wigner distribution and the instantaneous frequency.

Property 5: Time and frequency shifts. An important feature of the Wigner distribution is that it is covariant to time and frequency shifts. If a signal is shifted over a time t_0 or a frequency f_0, according to

$$u'(t) = \exp(\mathrm{j}2\pi f_0 t)u(t-t_0), \qquad (2.91)$$

then the Wigner distribution of the time and frequency shifted signal, $u'(t)$, is given by

$$\begin{aligned} W\{u',u'\}(t;f) &= \mathcal{F}_\tau^- \left\{ \exp(\mathrm{j}2\pi(t+\tfrac{1}{2}\tau)f_0)\; u(t-t_0+\tfrac{1}{2}\tau) \right. \\ &\qquad \left. \exp(-\mathrm{j}2\pi(t-\tfrac{1}{2}\tau)f_0)\; u^*(t-t_0-\tfrac{1}{2}\tau) \right\} \\ &= \int_{\tau \in \mathbb{R}} \exp(-\mathrm{j}2\pi(f-f_0)\tau)\; u(t-t_0+\tfrac{1}{2}\tau)u^*(t-t_0-\tfrac{1}{2}\tau)\,\mathrm{d}\tau \\ &= W\{u,u\}(t-t_0;f-f_0). \end{aligned} \qquad (2.92)$$

The joint time-frequency domain shift properties of the Wigner distribution are similar to the time and frequency domain shift properties of the Fourier transformation (cf. Eqs.(A.10) and (A.11)).

Property 6: Convolution in time and frequency. The Wigner distribution of a product of two Fourier transformed signals can be expressed in terms of the Wigner distributions of each of the signals, which can be derived from the convolution property of the Fourier transformation (cf. Eqs.(A.3) and (Eq.A.4)). In order to demonstrate this property, we consider a signal

$\hat{u}(f)$ that is the product of two Fourier transforms. Let the signal be given by

$$\hat{u}(f) = \hat{u}_1(f)\hat{u}_2(f), \tag{2.93}$$

then the local spectral auto-correlation function of this signal is found as

$$\begin{aligned} R\{\hat{u},\hat{u}\}(\nu;f) &= \hat{u}_1(f+\tfrac{1}{2}\nu)\hat{u}_2(f+\tfrac{1}{2}\nu)\hat{u}_1^*(f-\tfrac{1}{2}\nu)\hat{u}_2^*(f-\tfrac{1}{2}\nu) \\ &= R\{\hat{u}_1,\hat{u}_1\}(\nu;f)R\{\hat{u}_2,\hat{u}_2\}(\nu;f). \end{aligned} \tag{2.94}$$

The Wigner distribution of this signal can be obtained by taking the inverse Fourier transformation of $R\{\hat{u},\hat{u}\}(\nu;f)$ with respect the frequency-shift variable ν. Using Eq.(A.3), we find for the Wigner distribution of the product of two Fourier transforms

$$\begin{aligned} W\{u,u\}(t;f) &= \mathcal{F}_\nu^+ \{R\{\hat{u}_1,\hat{u}_1\}(\nu;f)R\{\hat{u}_2,\hat{u}_2\}(\nu;f)\} \\ &= \int_{t'\in I\!R} W\{u_1,u_1\}(t';f)W\{u_2,u_2\}(t-t';f)\mathrm{d}t'. \end{aligned} \tag{2.95}$$

A similar relation exists for the Wigner distribution of the product of two time signals. Let the time signal be given by

$$u(t) = u_1(t)u_2(t), \tag{2.96}$$

then instantaneous auto-correlation function of this signal is found as

$$R\{u,u\}(t;\tau) = R\{u_1,u_1\}(t;\tau)R\{u_2,u_2\}(t;\tau). \tag{2.97}$$

Taking the Fourier transformation of the instantaneous auto-correlation function with respect to the time-shift τ and using Eq.(A.4), the Wigner distribution of the product of two time signal can be expressed as

$$W\{u,u\}(t;f) = \int_{f'\in I\!R} W\{u_1,u_1\}(t;f')W\{u_2,u_2\}(t;f-f')\mathrm{d}f'. \tag{2.98}$$

2.4 Fourier transform relations

In the previous we saw that the generalized time and frequency auto-correlation functions $R\{u,u\}(t;\tau)$ and $R\{\hat{u},\hat{u}\}(\nu;f)$ are related to the Wigner distribution by a Fourier transformation with respect to the time and frequency *shift*

variables τ and ν (see Eqs.(2.69) and (2.73)). The Fourier dual of the Wigner distribution is obtained by a double Fourier transformation with respect to time and frequency.

$$A\{u,u\}(\nu;\tau) = \mathcal{F}_t^- \mathcal{F}_f^+ \{W\{u,u\}(t;f)\}\,. \tag{2.99}$$

The Fourier dual, $A\{u,u\}(\nu;\tau)$, of the Wigner distribution is known as the ambiguity function. If we consider the Wigner distribution as a joint time-frequency energy density function, the ambiguity function can be seen as its associated joint time-frequency correlation function. It is therefore also known as the *correlative dual* or *characteristic function* of the Wigner distribution. The ambiguity function plays an important role in the theory of radar detection and matched filtering (Woodward 1953). Its relation with the Wigner distribution has been acknowledged since long, but has only quite recently been fully exploited for studying the properties of the Wigner distribution and the design of new time-frequency representations. It is straightforward to derive some properties of the ambiguity function by considering the properties of the Wigner distribution in the Fourier transformed domain. For instance, the time-frequency shift covariance of the Wigner distribution (Eq.(2.92)) corresponds to time-frequency shift invariance of the ambiguity function. A comprehensive list of properties of the ambiguity function is given by Hlawatsch and Boudreaux-Bartels (1992). The relation between ambiguity function and Wigner distribution will be the starting point for the derivation of other time-frequency representations in Chapter 3.

To summarize, we present an overview of the Fourier transform duality between the Wigner distribution, ambiguity function, instantaneous auto-correlation and local spectral correlation.

Instantaneous auto-correlation

$$R\{u,u\}(t;\tau) = u(t+\tfrac{1}{2}\tau)u^*(t-\tfrac{1}{2}\tau). \tag{2.100a}$$

Local spectral auto-correlation.

$$R\{\hat{u},\hat{u}\}(\nu;f) = \hat{u}(f+\tfrac{1}{2}\nu)\hat{u}^*(f-\tfrac{1}{2}\nu) \tag{2.100b}$$

and

$$R\{\hat{u},\hat{u}\}(\nu;f) = \mathcal{F}_t^- \mathcal{F}_\tau^- \{R\{u,u\}(t;\tau)\}\,. \tag{2.100c}$$

Wigner distribution

$$W\{u,u\}(t;f) = \mathcal{F}_{\tau}^{-}\left\{R\{u,u\}(t;\tau)\right\} \tag{2.100d}$$

and

$$W\{u,u\}(t;f) = \mathcal{F}_{\nu}^{+}\left\{R\{\hat{u},\hat{u}\}(\nu;f)\right\}. \tag{2.100e}$$

Ambiguity function

$$A\{u,u\}(\nu;\tau) = \mathcal{F}_{t}^{-}\left\{R\{u,u\}(t;\tau)\right\}, \tag{2.100f}$$

$$A\{u,u\}(\nu;\tau) = \mathcal{F}_{f}^{+}\left\{R\{\hat{u},\hat{u}\}(\nu;f)\right\} \tag{2.100g}$$

and

$$A\{u,u\}(\nu;\tau) = \mathcal{F}_{t}^{-}\mathcal{F}_{f}^{+}\left\{W\{u,u\}(t;f)\right\}. \tag{2.100h}$$

A graphical illustration of the Fourier transform relations is shown in Fig. 2.5.

2.5 Examples of Wigner distributions and ambiguity functions

In order to gain some insight in the properties of the Wigner distribution, we derive the Wigner distribution and ambiguity function of two basic signals for which the analysis can be carried out analytically. The point of departure is the definition of the instantaneous auto-correlation function of Eq.(2.68), followed by the definition of the Wigner distribution Eq.(2.69). To obtain the ambiguity function we use Eq.(2.100e).

Chirp signal

A complex signal with a purely linear frequency modulation (chirp) is represented by the function

$$u(t) = \exp(\mathrm{j}2\pi\tfrac{1}{2}ct^2), \tag{2.101}$$

where c is a real-valued constant. The real part of this signal is shown in Fig. 2.6. The instantaneous auto-correlation function of this signal is given by

$$\begin{aligned} R\{u,u\}(t;\tau) &= \exp\left(\mathrm{j}2\pi\tfrac{1}{2}c(t+\tfrac{1}{2}\tau)^2\right)\exp\left(-\mathrm{j}2\pi\tfrac{1}{2}c(t-\tfrac{1}{2}\tau)^2\right) \\ &= \exp(\mathrm{j}2\pi ct\tau). \end{aligned} \tag{2.102}$$

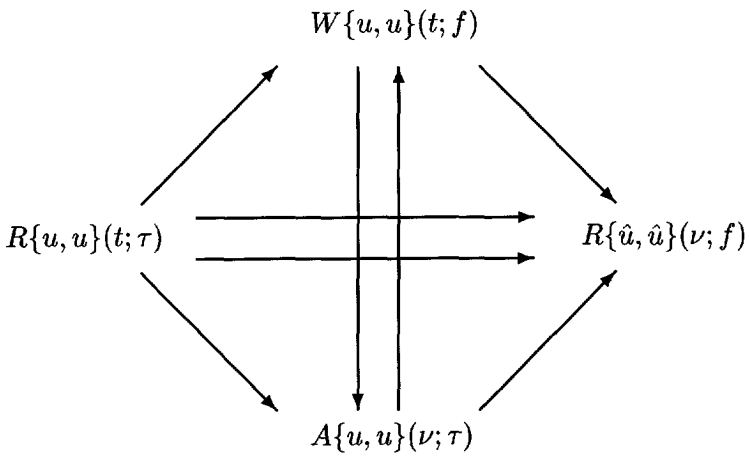

Figure 2.5: *Graphical illustration of the Fourier transform relations between the Wigner distribution, $W\{u,u\}(t;f)$; ambiguity function, $A\{u,u\}(\nu;\tau)$; instantaneous auto-correlation function, $R\{u,u\}(t;\tau)$; and the local frequency correlation, $R\{\hat{u},\hat{u}\}(\nu;f)$. The arrows indicate a Fourier transformation with a minus sign in the exponential function, in the direction of the arrow.*

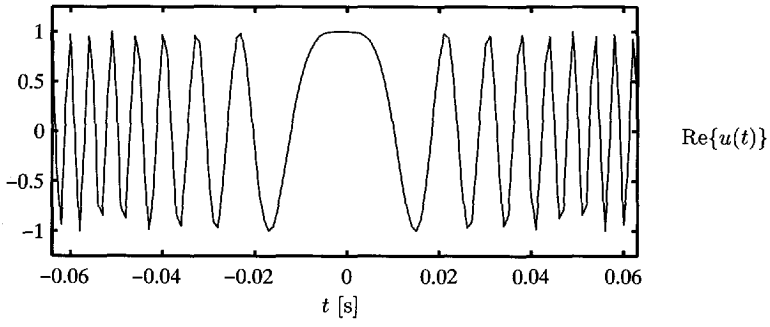

Figure 2.6: *Real part of the chirp signal.*

The Wigner distribution of the chirp signal is now found as

$$W\{u,u\}(t;f) = \mathcal{F}_\tau^- \{\exp(\mathrm{j}2\pi ct\tau)\} = \delta(f-ct). \tag{2.103}$$

The ambiguity function of the chirp signal is given by

$$A\{u,u\}(\nu;\tau) = \mathcal{F}_t^- \{\exp(\mathrm{j}2\pi ct\tau)\} = \delta(\nu-c\tau). \tag{2.104}$$

The Wigner distribution and the ambiguity function of this signal are shown in Fig. 2.7, for $c = 4000$.

Gaussian signal

Consider a signal given by a Gaussian function:

$$u(t) = \sqrt{\sigma}\exp\left[-\pi\sigma^2 t^2\right], \tag{2.105}$$

where σ is a real-valued constant. The signal is shown in Fig. 2.8. The instantaneous auto-correlation of the Gaussian signal is given by

$$R\{u,u\}(t;\tau) = \sigma\exp\left[-2\pi\sigma^2 t^2\right]\exp\left[-\frac{\pi}{2}\sigma^2\tau^2\right]. \tag{2.106}$$

The Wigner distribution is given by

$$\begin{aligned} W\{u,u\}(t;f) &= \sigma\exp\left[-2\pi\sigma^2 t^2\right]\mathcal{F}_\tau^-\left\{\exp\left[-\frac{\pi}{2}\sigma^2\tau^2\right]\right\} \\ &= \sqrt{2}\exp\left[-2\pi\sigma^2 t^2 - 2\pi\frac{f^2}{\sigma^2}\right], \end{aligned} \tag{2.107}$$

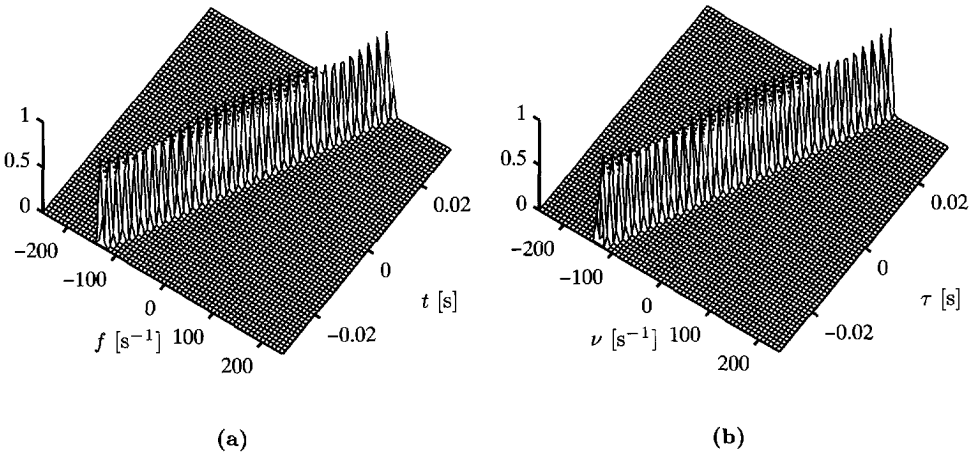

Figure 2.7: *(a) Wigner distribution and (b) ambiguity function of the chirp signal.*

where we have used the known result of the Fourier transform of the Gaussian function (Bracewell 1978).

The ambiguity function of the Gaussian signal is found by a Fourier transformation of Eq.(2.106) with respect to time,

$$A\{u,u\}(\nu;\tau) = \frac{1}{\sqrt{2}} \exp\left[-\frac{\pi}{2}\left(\sigma^2\tau^2 + \frac{\nu^2}{\sigma^2}\right)\right]. \tag{2.108}$$

Both functions are shown in Fig. 2.9.

For the signals shown here the localization of energy by the Wigner distribution, closely matches our expectation of what the local power spectrum of these signal should be like. These signals are called mono-component because their Wigner distribution is well delineated in a region of the time-frequency plane. However, for many other signals the Wigner distribution is often difficult to interpret as a time-frequency energy density function. This is the result of the property that the Wigner distribution of the sum of two mono-component signals is not simply the sum of their respective Wigner distributions. The Wigner distribution maps also values to regions of the time-frequency plane where the Wigner distributions of both the original sig-

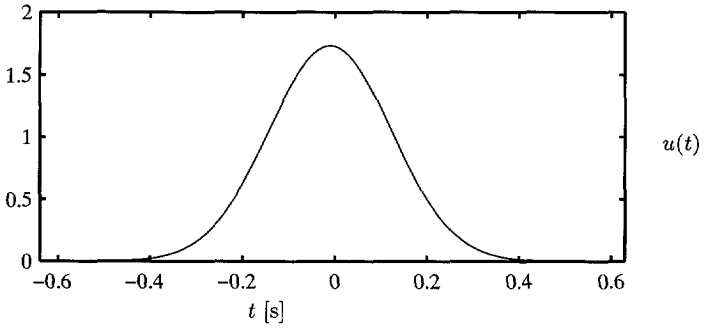

Figure 2.8: *Gaussian signal.*

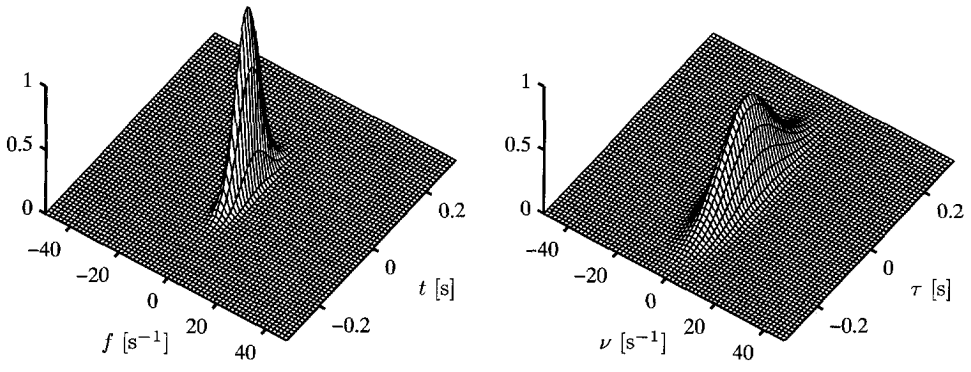

(a) **(b)**

Figure 2.9: *(a) Wigner distribution of the Gaussian signal and (b) ambiguity function of the Gaussian signal.*

consist of more than one component are called multi-component. The origin and nature of the cross terms that arise in the Wigner distribution and ambiguity function of a multi-component signal is the subject of the next section.

2.6 Cross terms in the Wigner distribution

The cross terms in the Wigner distribution of a multi-component signal find their origin in the quadratic superposition principle. Consider the signal $u(t)$ that is sum of two signals; $u(t) = u_k(t) + u_l(t)$. The instantaneous auto-correlation function (Eq.(2.68)) of this sum is given by

$$\begin{aligned} R\{u,u\}(t;\tau) = {} & u_k(t+\tfrac{1}{2}\tau){u_k}^*(t-\tfrac{1}{2}\tau) + u_l(t+\tfrac{1}{2}\tau){u_l}^*(t-\tfrac{1}{2}\tau) \\ & + u_k(t+\tfrac{1}{2}\tau){u_l}^*(t-\tfrac{1}{2}\tau) + u_l(t+\tfrac{1}{2}\tau){u_k}^*(t-\tfrac{1}{2}\tau). \end{aligned} \tag{2.109}$$

We define the *instantaneous cross-correlation* function of two functions $u_k(t)$ and $u_l(t)$ as

$$R\{u_k,u_l\}(t;\tau) = u_k(t+\tfrac{1}{2}\tau){u_l}^*(t-\tfrac{1}{2}\tau), \tag{2.110}$$

The following property of the instantaneous cross-correlation is readily obtained:

$$R\{u_l,u_k\}(t;\tau) = R\{u_k,u_l\}(t;-\tau). \tag{2.111}$$

The instantaneous auto-correlation of the sum of two signals can now be written as

$$\begin{aligned} R\{u,u\}(t;\tau) = {} & R\{u_k,u_k\}(t;\tau) + R\{u_l,u_l\}(t;\tau) \\ & + R\{u_k,u_l\}(t;\tau) + R\{u_l,u_k\}(t;\tau). \end{aligned} \tag{2.112}$$

We now find for the Wigner distribution of the sum of two signals,

$$\begin{aligned} W\{u,u\}(t;f) = {} & W\{u_k,u_k\}(t;f) + W\{u_l,u_l\}(t;f) \\ & + 2\mathrm{Re}\{W\{u_k,u_l\}\}(t;f), \end{aligned} \tag{2.113}$$

where we have used the property Eq.(2.111) $W\{u_k,u_l\}(t;f)$ is the *cross-Wigner distribution* of $u_k(t)$ and $u_l(t)$, defined by

$$W\{u_k,u_l\}(t;f) = \mathcal{F}_\tau^- \left\{R\{u_k,u_l\}(t;\tau)\right\}. \tag{2.114}$$

As a result of Eq.(2.113), we can now study the cross terms by considering the cross-Wigner distribution of the individual components. In order to derive some of the properties of the cross terms, we consider the special case where the multi-component signal is the sum of two time and frequency-shifted versions of an elementary signal $u(t)$. The multi-component signal $u'(t)$ is then given by

$$u'(t) = u_k(t) + u_l(t) = \exp(\mathrm{j}2\pi f_k t)u(t - t_k) + \exp(\mathrm{j}2\pi f_l t)u(t - t_l), \tag{2.115}$$

where the t_k, t_l and f_k, f_l are the time-shifts and frequency-shifts respectively, with the subscript indicating the component under consideration. Using the shift property of the Wigner distribution Eq.(2.92), the cross-Wigner distribution of two time-frequency shifted signal components is found as

$$W\{u_1, u_2\}(t; f) = \exp(\mathrm{j}2\pi(f_d t - (f - f_m)t_d))\, W\{u, u\}(t - t_m; f - f_m). \tag{2.116}$$

where we have introduced the difference frequency $f_d = f_k - f_l$, the difference time $t_d = t_k - t_l$ and the mid-time and mid-frequency, $f_m = (f_k + f_l)/2$ and $t_m = (t_k + t_l)/2$. The two auto terms are given by

$$\begin{aligned} W\{u_k, u_k\} &= W\{u, u\}(t - t_k; f - f_k), \\ W\{u_l, u_l\} &= W\{u, u\}(t - t_l; f - f_l). \end{aligned} \tag{2.117}$$

Thus, the cross-Wigner distribution of the time-frequency shifted signals is equal to the Wigner distribution of the elementary signal $u(t)$, translated by the average or mid-time shift t_m and the mid-frequency f_m. Further the cross term shows an oscillatory behaviour determined by t_d and f_d. In general, the cross terms in the Wigner distribution of a multi-component signal have the following properties (Kadambe and Boudreaux-Bartels 1992):

- They occur mid-time mid-frequency on the line connecting the auto components in the time-frequency plane and
- oscillate at frequencies proportional to the difference time and difference frequency of the auto terms.
- The direction of the oscillation is orthogonal with respect to the line connecting the auto components.

- The amplitude of the auto terms can be twice as large as the product of the magnitudes of the Wigner distributions of the two signals under consideration.

For a signal $u(t) = \sum_{k=1}^{N} u_k(t)$, consisting of N components the Wigner distribution can be written as a combination of auto- and cross-Wigner distributions of the individual components in the following way (Hlawatsch and Boudreaux-Bartels 1992):

$$W\{u,u\}(t;f) = \sum_{k=1}^{N} W\{u_k,u_k\}(t;f) + \sum_{k=1}^{N}\sum_{l=1,l\neq k}^{N} 2\mathrm{Re}\{W\{u_k,u_l\}\}(t;f). \tag{2.118}$$

As a result, the Wigner distribution of an N component signal comprises N auto terms and $\binom{N}{2} = N(N-1)/2$ cross terms.

In order to illustrate the relation between auto terms and cross terms in the Wigner distribution we derive the Wigner distribution of the sum of two time-shifted and frequency-shifted Gaussians. A Gaussian signal shifted over time t_k and frequency f_k is given by

$$u(t) = \sqrt{\sigma}\exp\left[-\pi\left(\sigma(t-t_k)\right)^2\right]\exp(\mathrm{j}2\pi f_k t). \tag{2.119}$$

The Wigner distribution of this signal is the Wigner distribution of the Gaussian (Eq.(2.107)), shifted by time t_k and frequency f_k:

$$W\{u,u\}(t;f) = \sqrt{2}\exp\left[-2\pi\left((\sigma(t-t_k))^2 + \left(\frac{f-f_k}{\sigma}\right)^2\right)\right], \tag{2.120}$$

where we have used of the time and frequency shift covariance property of the Wigner distribution (Eq.(2.92)). The cross-Wigner distribution of the sum of two Gaussians, each shifted over different times and frequencies t_k, f_k and t_l, f_l is given by

$$\begin{aligned} W\{u_k,u_l\}(t;f) =& \sqrt{2}\exp\left(\mathrm{j}2\pi(f_d t - (f-f_m)t_d)\right) \\ & \exp\left[-2\pi\left((\sigma(t-t_m))^2 + \left(\frac{f-f_m}{\sigma}\right)^2\right)\right], \end{aligned} \tag{2.121}$$

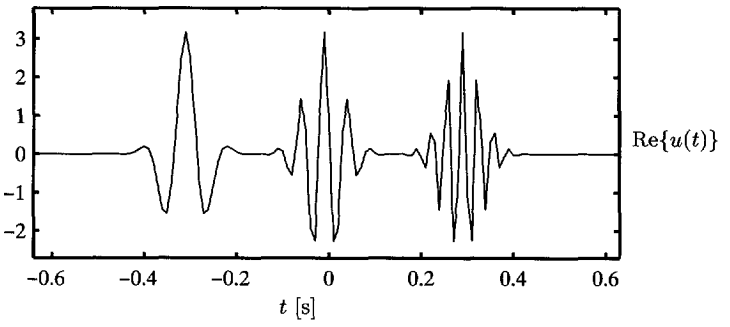

Figure 2.10: *Real part of a signal composed of three time-shifted modulated Gaussians.*

where f_d and t_d are the difference frequency and time and f_m and t_m are the mid-frequency and time (cf. Eq.(2.116)).

As an example we show the decomposition of the Wigner distribution into its auto terms and cross terms for a three-component signal. The signal consists of three time-frequency shifted Gaussians, where each of the components is given by Eq.(2.119). The real part of the signal is shown in Fig. 2.10. In Fig. 2.11 the Wigner distribution and the decomposition into auto terms and cross terms of this signal is shown. The auto terms are given by the sum of the Wigner distribution of the components, the cross terms can be found by taking twice the sum of the real parts of the cross-Wigner distributions of the components.

The example shows that the auto terms give an easily interpretable picture of the time-frequency structure of the signal. The more complicated structure of the cross terms will seriously hamper the interpretation of the Wigner distribution of a multi-component signal. In particular where the cross terms interfere with the auto terms, as in this example is the case for the component located midway between two other components in the $t - f$ plane. In this example we could easily separate the auto terms and cross terms because we know how the signal can be decomposed into elementary signals. However, in most practical situations we do not know the individual components of the signal. It is therefore not always possible to distinguish between auto terms and cross terms in the Wigner distribution. Moreover, for a signal with many components, the cross terms and auto terms will always have

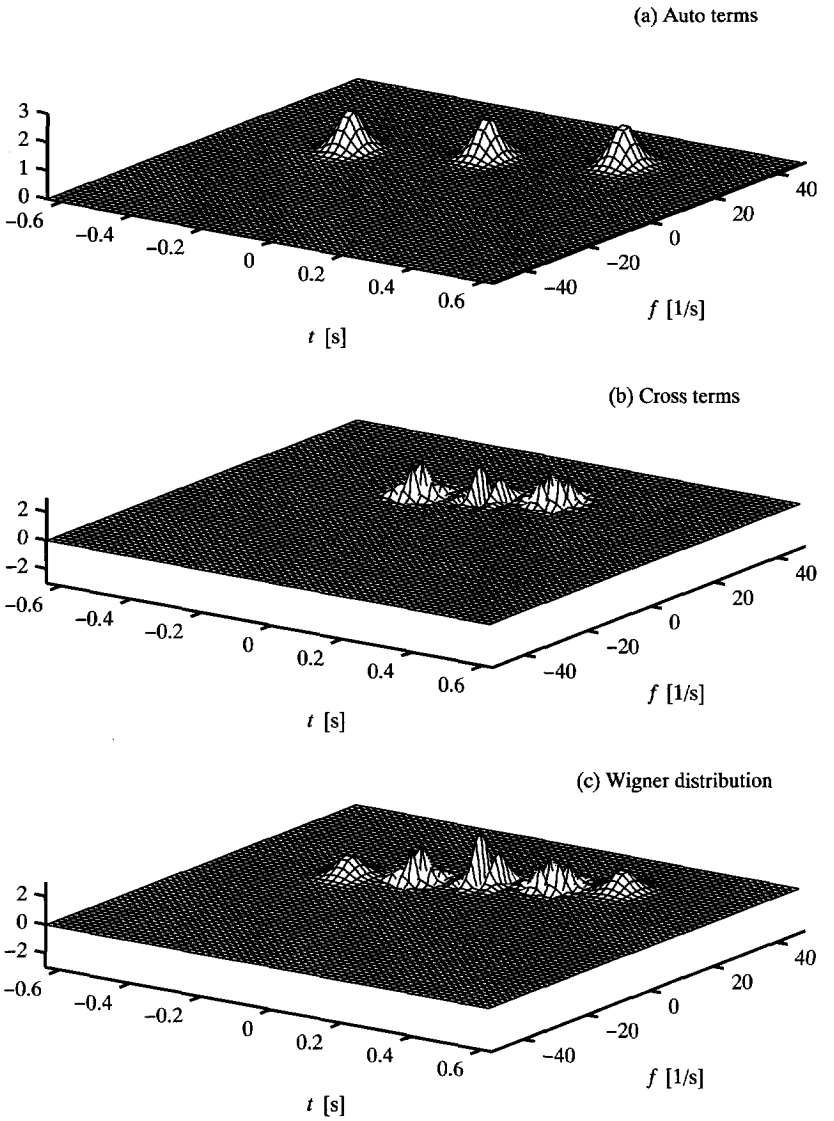

Figure 2.11: *Wigner distribution of three time-shifted and modulated Gaussians; (a) Wigner distribution, (b) auto terms and (c) cross terms.*

significant overlap. In order to suppress the cross terms we first have to find a way to distinguish auto terms from cross terms. For that reason we will study the relation between auto terms and cross terms in the ambiguity function in the next section.

2.7 Cross terms in the ambiguity function

The ambiguity function of the sum $u(t)$ of two signals $u_k(t)$ and $u_l(t)$ is given by the Fourier transform with respect to time t of the instantaneous auto-correlation function of the signal (Eq.(2.112)),

$$\begin{aligned} A\{u_k + u_l, u_k + u_l\}(\nu;\tau) = A\{u_k, u_k\}(\nu;\tau) + A\{u_l, u_l\}(\nu;\tau) \\ + A\{u_k, u_l\}(\nu;\tau) + A\{u_l, u_k\}(\nu;\tau). \end{aligned} \tag{2.122}$$

Using the property Eq.(2.111), we can also write

$$\begin{aligned} A\{u_k + u_l, u_k + u_l\}(\nu;\tau) = A\{u_k, u_k\}(\nu;\tau) + A\{u_l, u_l\}(\nu;\tau) \\ + A\{u_k, u_l\}(\nu;\tau) + A^*\{u_k, u_l\}(-\nu;-\tau). \end{aligned} \tag{2.123}$$

where $A\{u_k, u_l\}(\nu;\tau)$ is the *cross-ambiguity function* of $u_k(t)$ and $u_l(t)$, defined as

$$A\{u_k, u_l\}(\nu;\tau) = \mathcal{F}_t^- \left\{R\{u_k, u_l\}(t;\tau)\right\}. \tag{2.124}$$

For the ambiguity function of a linear combination of mono-component signals the derivation of the domain allocation is similar to that for the Wigner distribution. Consider a combination of two elementary signals that are shifted in time and frequency:

$$u'(t) = u_k(t) + u_l(t) = \exp(\mathrm{j}2\pi f_k t)u(t - t_k) + \exp(\mathrm{j}2\pi f_l t)u(t - t_l). \tag{2.125}$$

The ambiguity function of one time-frequency shifted elementary signal is

$$A\{u_k, u_k\}(\nu;\tau) = \exp(\mathrm{j}2\pi(f_k\tau - t_k\nu))\, A\{u, u\}(\nu;\tau), \tag{2.126}$$

which is the ambiguity function of the original signal modulated proportionally to the time-shift and frequency-shift. Hence, the auto terms of a signal u consisting of N time-frequency shifted components are given by:

$$A\{u, u\}(\nu;\tau) = \sum_{k=1}^{N} A\{u_k, u_k\}(\nu;\tau) \exp(\mathrm{j}2\pi(f_k\tau - t_k\nu)). \tag{2.127}$$

The cross terms in the ambiguity function of the signal are given by the last term of Eq.(2.123), which is the cross-ambiguity function of the two components. The cross-ambiguity function of two time-frequency shifted signals is given by

$$A\{u_k, u_l\}(\nu;\tau) = \exp(\mathrm{j}2\pi(f_m\tau - (\nu - f_d)t_m)\, A\{u,u\}(\nu - f_d;\tau - t_d). \tag{2.128}$$

where we have introduced the difference frequency $f_d = f_k - f_l$, the difference time $t_d = t_k - t_l$ and the mid-frequency and mid-time $f_m = (f_k + f_l)/2$ and $t_m = (t_k + t_l)/2$.

The cross terms in the ambiguity function of a signal that is the sum of time-frequency shifted elementary signals are given by the ambiguity function of the elementary signal, shifted over the distance in time, t_d and frequency, f_d, between the components and modulated by the mean time, t_m and mean frequency, f_m. As a result the ambiguity function of a signal consisting of N time-frequency shifted components is given by

$$\begin{aligned} A\{u,u\}(\nu;\tau) &= \sum_{k=1}^{N} A\{u_k,u_k\}(\nu;\tau)\exp(\mathrm{j}2\pi(f_k\tau - t_k\nu)) \\ &+ \sum_{k=1}^{N}\sum_{l=1,k\neq l}^{N} A\{u_k,u_l\}(\nu - f_d^{kl},\tau - t_d^{kl})\exp(\mathrm{j}2\pi(f_m^{kl}\tau - (\nu - f_d^{kl})t_m^{kl})) \\ &+ \sum_{k=1}^{N}\sum_{l=1,k\neq l}^{N} A\{u_l,u_k\}(\nu - f_d^{lk},\tau - t_d^{lk})\exp(\mathrm{j}2\pi(f_m^{lk}\tau - (\nu - f_d^{lk})t_m^{lk})), \end{aligned} \tag{2.129}$$

where the superscripts denote the components under consideration, e.g. $f_d^{kl} = f_k - f_l$. From Eq.(2.129), we conclude that the auto terms of in the Wigner distribution transform to a region around the origin, while cross terms will be located further away from the origin than auto terms. The distance between the auto terms and the cross terms in the ambiguity plane is proportional to the (t,f)-distance of the components that generate the cross term. In order to demonstrate this, we show the ambiguity function of the same signal that was used to illustrate the cross term relations in the Wigner distribution (Fig. 2.10). This signal is the sum of three time-shifted modulated Gaussians

(Eq.(2.119)). The ambiguity function of a (t, f)-shifted Gaussian signal, $u_k(t)$ is the ambiguity function of a Gaussian (Eq.(2.108)), modulated by the time-shift t_k and frequency-shift f_k:

$$A\{u_k, u_k\}(\nu;\tau) = \frac{1}{\sqrt{2}} \exp(\mathrm{j}2\pi(f_k\tau - t_k\nu)) \exp\left[-\frac{\pi}{2}\left((\sigma\tau)^2 + \left(\frac{\nu}{\sigma}\right)^2\right)\right]. \tag{2.130}$$

Using Eq.(2.128), we have for the cross-ambiguity function of two time-frequency shifted Gaussians $u_k(t)$ and $u_l(t)$

$$\begin{aligned} A\{u_k, u_l\}(\nu;\tau) =& \frac{1}{\sqrt{2}} \exp(\mathrm{j}2\pi(f_m\tau - (\nu - f_d)t_m)) \\ & \exp\left[-\frac{\pi}{2}\left((\sigma(\tau - t_d))^2 + \left(\frac{\nu - f_d}{\sigma}\right)^2\right)\right], \end{aligned} \tag{2.131}$$

where t_m is the mean time-shift, f_m is the mean frequency-shift and t_d and f_d are the difference in time-delay and frequency-shift of the Gaussians. The ambiguity function of a signal consisting of three modulated Gaussians is shown in Fig. 2.12, together with the sum of the ambiguity function of the components and the sum of their cross-ambiguity functions. Because the ambiguity function is a complex-valued function we show its absolute value, $|A\{u, u\}(\nu;\tau)|$, also referred to as the *ambiguity surface*.

The property that in the ambiguity function a cross term will always be shifted away from the auto terms of the components generating the cross term, can be exploited for suppression of the cross terms. The cross terms in the Wigner distribution can be suppressed by zeroing the portion of the ambiguity function that contains cross term energy. This is essentially the application of a two-dimensional low-pass window on the ambiguity function. The time-frequency representation with reduced cross terms is then found by a two-dimensional Fourier transformation of the windowed ambiguity function. However, this windowing operation will have its effects on the properties of the resulting time-frequency representation. The choice of a window in the ambiguity domain and how the window affects the properties of the time-frequency representation is the subject of the next chapter.

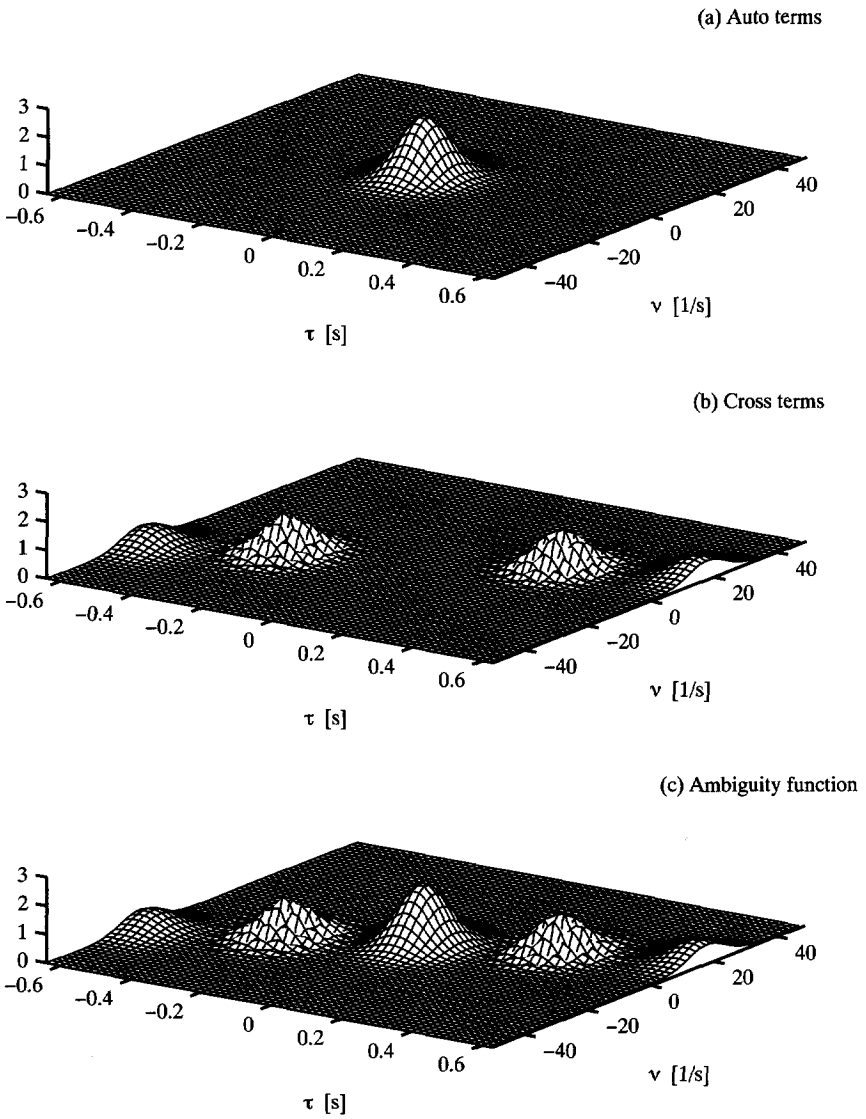

Figure 2.12: *Modulus of the ambiguity function of three time-shifted and modulated Gaussian; (a) ambiguity function, (b) auto terms and (c) cross terms.*

Chapter 3

General Class of joint Time-Frequency Representations

3.1 Introduction

The mathematical properties of the Wigner distribution make it an attractive function for the time-frequency representation of a signal. However, the Wigner distribution often peaks in regions of the time-frequency plane that do not correspond to our intuitive notion of the time-frequency structure of the signal under analysis. These regions were identified as the cross terms. In case we have a multi-component signal, such as a seismic recording, the interference by the cross terms may seriously hamper the interpretation of the Wigner distribution as a time-frequency energy density function. In this chapter an approach for the suppression of these cross terms will be developed. The main application of time-frequency analysis in this thesis will be the extraction of seismic attributes from the time-frequency representation of the signal. For that reason we may want to retain some of the mathematical properties of the Wigner distribution, such as the marginals and local averages, in the time-frequency representation.

First, a general class of time-frequency representations will be defined. The parameterization of this general class allows an effective approach to deter-

mine the properties of a time-frequency representation. The properties of the time-frequency representations in the general class will be discussed in relation to the properties that were derived for the Wigner distribution in Chapter 2.

In the second part of this chapter we will discuss some time-frequency representations from the general class in more detail. Most of these time-frequency representations have been proposed because they combine the property of reduced cross term interference for certain types of signals and a number of other desirable properties. The formulation of the cross term suppression as an optimization problem has proven to be very effective (Baraniuk and Jones 1993a, 1993b). In the last part of this chapter we will discuss this approach.

3.2 The general class of joint time-frequency representations

In the previous chapter it was shown that in order to reduce the interference by cross terms in the Wigner distribution, the application of a low pass window to the ambiguity function may be an effective approach.

A time-frequency representation, $P\{u,u\}(t;f)$, is related to its characteristic function, $M(\nu;\tau)$, by a Fourier transformation with respect to the correlation variables ν and τ (cf. Section 2.2.1). The characteristic function of the Wigner distribution is the ambiguity function (Eq.(2.100h)). The application of a filter on the ambiguity function results in a new time-frequency representation, given by

$$P\{u,u\}(t;f) = \mathcal{F}_{\nu}^{+}\mathcal{F}_{\tau}^{-}\left\{M(\nu;\tau)\right\}, \tag{3.1}$$

where $M(\nu;\tau)$ is the weighted ambiguity function, i.e.

$$M(\nu;\tau) = \Psi^{\nu\tau}(\nu;\tau)A\{u,u\}(\nu;\tau). \tag{3.2}$$

We conclude that for $\Psi^{\nu\tau}(\nu;\tau)$ equal to the identity operator, $P\{u,u\}(t;f)$ is equal to the Wigner distribution. This follows from the inverse of the Fourier transformation defined in Eq.(2.100h). Since the ambiguity function is Fourier transform related to the instantaneous auto-correlation $R\{u,u\}(t;\tau)$; the local spectral correlation $R\{\hat{u},\hat{u}\}(\nu;f)$; and the Wigner distribution $W\{u,u\}(t;f)$, the transform equivalents of $\Psi^{\nu\tau}$ act as convolutional filters on the Fourier duals. The representation of these filters follow from the set

of Fourier transformations in Eqs.(2.100f)-(2.100h) and are given by

$$\Psi^{t\tau}(t;\tau) = \mathcal{F}_{\nu}^{+}\left\{\Psi^{\nu\tau}(\nu;\tau)\right\}, \tag{3.3}$$

$$\Psi^{\nu f}(\nu;f) = \mathcal{F}_{\tau}^{-}\left\{\Psi^{\nu\tau}(\nu;\tau)\right\}, \tag{3.4}$$

and

$$\Psi^{tf}(t;f) = \mathcal{F}_{\nu}^{+}\mathcal{F}_{\tau}^{-}\left\{\Psi^{\nu\tau}(\nu;\tau)\right\}. \tag{3.5}$$

In addition, we can deduce from the Fourier transformations of the Wigner distribution, defined in Eqs.(2.100d) and (2.100e), the relations

$$\Psi^{t\tau}(t;\tau) = \mathcal{F}_{f}^{+}\left\{\Psi^{tf}(t;f)\right\} \tag{3.6}$$

and

$$\Psi^{\nu f}(\nu;f) = \mathcal{F}_{t}^{-}\left\{\Psi^{tf}(t;f)\right\}. \tag{3.7}$$

A graphical illustration of the Fourier transform relations is given in Fig. 3.1.

From these relations we deduce the following convolutional operations in the different domains leading to the same representation $P\{u,u\}(t;f)$. Starting in the time and frequency auto-correlation domain we have

$$P\{u,u\}(t;f) = \mathcal{F}_{\tau}^{-}\left\{\int_{t'\in I\!R} \Psi^{t\tau}(t-t';\tau)R\{u,u\}(t';\tau)\mathrm{d}t'\right\} \tag{3.8}$$

and

$$P\{u,u\}(t;f) = \mathcal{F}_{\nu}^{+}\left\{\int_{f'\in I\!R} \Psi^{\nu f}(\nu;f-f')R\{\hat{u},\hat{u}\}(\nu;)\mathrm{d}f'\right\}. \tag{3.9}$$

In the time-frequency domain we have

$$P\{u,u\}(t;f) = \int_{t'\in I\!R}\int_{f'\in I\!R} \Psi^{tf}(t-t';f-f')W\{u,u\}(t';f')\mathrm{d}t'\mathrm{d}f'. \tag{3.10}$$

The general class of time-frequency representations was first formulated by Cohen (1966) in a quantum-mechanical context. It is also referred to as Cohen's class of time-frequency representations. In time-frequency analysis

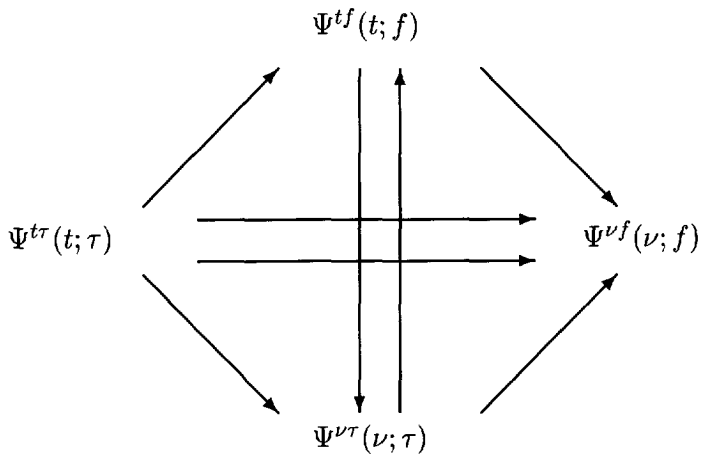

Figure 3.1: *Graphical illustration of the Fourier transform relations between the weight function Ψ in the various domains. The arrows indicate a Fourier transformation with a negative sign in the exponential, in the direction of the the arrow. (cf. Fig. 2.5).*

literature, the filter $\Psi^{\nu\tau}$, is referred to as the *kernel* of the time-frequency representation (Claasen and Mecklenbräuker 1980).

Evaluation of the kernel function $\Psi^{\nu\tau}$ is an effective way to derive the properties of time-frequency representation that is associated with a particular kernel. In Chapter 2 some of the properties of the Wigner distribution were derived. Whether a time-frequency representation from the general class satisfies one of these properties depends on the kernel. An effective way to obtain a time-frequency representation with a certain property is to constrain the kernel function in such a way that the property is satisfied. The properties of the time-frequency representations are therefore expressed in terms of constraints on the kernel. In the next section we will discuss some properties in the light of the corresponding kernel constraints.

3.3 Constraints on the kernel

The properties of a Cohen's class time-frequency representation can be expressed as a set of constraints on the kernel function. In this section we will derive these constraints for some of the properties of the Wigner distribution that were derived in Chapter 2.

Property 1. Realness. From the representation of the $A\{u,u\}(\nu;\tau)$ as shown in Eq.(2.100h) and the property that $W\{u,u\}(t;f)$ is real, it follows that

$$A^*\{u,u\}(-\nu;-\tau) = A\{u,u\}(\nu;\tau). \tag{3.11}$$

If we require that $M\{u,u\}(\nu;\tau)$ conserves this property, i.e.

$$M^*\{u,u\}(-\nu;-\tau) = M\{u,u\}(\nu;\tau), \tag{3.12}$$

the kernel function $\Psi^{\nu\tau}$ is constrained in the same way,

$$(\Psi^{\nu\tau}(-\nu;-\tau))^* = \Psi^{\nu\tau}(\nu;\tau). \tag{3.13}$$

Property 2. Energy and marginals. The total energy of the time-frequency representation $P\{u,u\}(t;f)$ is given by

$$\begin{aligned}\int_{t\in\mathbb{R}} \int_{f\in\mathbb{R}} P\{u,u\}(t;f)\mathrm{d}t\mathrm{d}f &= M\{u,u\}(0,0) \\ &= \Psi^{\nu\tau}(0,0)A\{u,u\}(0,0).\end{aligned} \tag{3.14}$$

If we want the total energy to be equal to the energy of the signal, then we require

$$\Psi^{\nu\tau}(0,0) = 1, \tag{3.15}$$

where we have used the property Eq.(2.82) of the Wigner distribution.

Integration of the Wigner distribution over frequency yields the instantaneous energy (cf. Eq.(2.80)). This property is referred to as the time marginal property.

If we want to retain this property in a representation from the general class, we require that

$$\int_{f\in\mathbb{R}} P\{u,u\}(t;f)\mathrm{d}f = |u(t)|^2. \tag{3.16}$$

On the other hand, using the representation of Eq.(3.1), for $P\{u,u\}(t;f)$, we can write

$$\int_{f\in I\!R} P\{u,u\}(t;f)\mathrm{d}f = \mathcal{F}_{\nu}^{+}\left\{\Psi^{\nu\tau}(\nu;0)A\{u,u\}(\nu;0)\mathrm{d}\nu\right\}. \tag{3.17}$$

Next, using the expression of Eq.(2.100f) for $A\{u,u\}(\nu;0)$ in Eq.(3.17) we arrive at

$$\int_{f\in I\!R} P\{u,u\}(t;f)\mathrm{d}f = \mathcal{F}_{\nu}^{+}\left\{\int_{t'\in I\!R} \Psi^{\nu\tau}(\nu;0)R\{u,u\}(t';0)\mathrm{d}t'\right\}. \tag{3.18}$$

From Eq.(3.18) we conclude that if

$$\Psi^{\nu\tau}(\nu;0) = 1, \text{ for } \nu \in I\!R, \tag{3.19}$$

then Eq.(3.18) reduces to

$$\int_{f\in I\!R} P\{u,u\}(t;f) = R\{u,u\}(t;0) = |u(t)|^2. \tag{3.20}$$

Consequently, the marginal property of Eq.(3.16) is satisfied.

In a similar way, requiring the frequency marginal property

$$\int_{t\in I\!R} P\{u,u\}(t;f)\mathrm{d}t = |u(f)|^2, \tag{3.21}$$

leads to the condition

$$\Psi^{\nu\tau}(0,\tau) = 1, \text{ for } \tau \in I\!R. \tag{3.22}$$

Note that if either the time marginal and frequency marginal properties are satisfied, then we have also preserved the total energy, since $\Psi^{\nu\tau}(0,0) = 1$.

Further, we conclude from the expression for $\Psi^{t\tau}(t;\tau)$ that is given by Eq.(3.3), using the result of Eq.(3.19), that

$$\lim_{\nu\to 0} \Psi^{t\tau}(t;\tau) = \int_{\nu\in I\!R} \exp(\mathrm{j}2\pi\nu t)\mathrm{d}\nu = \delta(t) \tag{3.23}$$

and by the same line of reasoning, using the expression for $\Psi^{\nu f}(\nu;f)$ of Eq.(3.4) and the result of Eq.(3.22), we obtain

$$\lim_{\nu\to 0} \Psi^{\nu f}(\nu;f) = \int_{\tau\in I\!R} \exp(-\mathrm{j}2\pi f\tau)\mathrm{d}\tau = \delta(f). \tag{3.24}$$

From Eqs.(3.23) and (3.24) and Eqs.(3.6) and (3.7) we derive the integral constraints for $\Psi^{tf}(t;f)$, also recognized by Janssen (1984),

$$\int_{f\in I\!R} \Psi^{tf}(t;f)\mathrm{d}f = \delta(t) \tag{3.25}$$

and

$$\int_{t\in I\!R} \Psi^{tf}(t;f)\mathrm{d}f = \delta(f). \tag{3.26}$$

From these we can conclude that the marginal preserving filter $\Psi^{tf}(t;f)$ cannot be the Wigner distribution of any function, say $v(t)$, because in that case we would have $|v(t)|^2 = \delta(t)$ and $|\hat{v}(f)|^2 = \delta(f)$. These conditions are mutually exclusive and hence the result.

In case the marginal properties are to be satisfied, kernel functions of the product type,

$$\Psi^{\nu\tau}(\nu;\tau) = \Phi^{\nu\tau}(\nu\tau), \tag{3.27}$$

are of interest, because they also preserve many other desirable properties of the Wigner distribution. The marginal property is preserved with the constraint

$$\lim_{\tau\to 0} \Phi^{\nu\tau}(\nu\tau) = 1, \tag{3.28}$$

from which also follows that

$$\lim_{\nu\to 0} \Phi^{\nu\tau}(\nu\tau) = 1. \tag{3.29}$$

From the condition on realness of the time-frequency representation, i.e. $(\Psi^{\nu\tau}(\nu;\tau))^* = \Psi^{\nu\tau}(-\nu;-\tau)$, it follows directly that the product kernel $\Phi(\nu\tau)$ is real-valued.

In the local auto-correlation domain, the marginal preserving product kernel takes the form

$$\Psi^{t\tau}(t;\tau) = \frac{1}{\tau}\Phi^{t\tau}\left(\frac{t}{\tau}\right), \tag{3.30}$$

with the condition that

$$\lim_{\tau \to 0} \frac{1}{\tau} \Phi^{t\tau} \left(\frac{t}{\tau} \right) = \delta(t), \tag{3.31}$$

which is recognized as the generating sequence of generalized functions for the Dirac function, provided that

$$\lim_{\tau \to 0} \Phi^{t\tau} \left(\frac{t}{\tau} \right) = 0, \text{ for } t \in I\!R \tag{3.32}$$

and

$$\lim_{t \to 0} \Phi^{t\tau} \left(\frac{t}{\tau} \right) = 0, \text{ for } \tau \in I\!R. \tag{3.33}$$

Property 3. Local averages. The average frequency as a function of time of the Wigner distribution is the derivative of the temporal phase of the signal. For an analytic signal the derivative of the temporal phase is the instantaneous frequency. The average frequency with time, $\langle f \rangle_t$, of the time-frequency representation, $P\{u,u\}(t;f)$, is given by

$$\langle f \rangle_t = \frac{[f^1]_t}{[f^0]_t} = \frac{\int_{f \in I\!R} f\, P\{u,u\}(t;f)\, \mathrm{d}f}{\int_{f \in I\!R} P\{u,u\}(t;f) \mathrm{d}f}. \tag{3.34}$$

Using Eq.(3.8) and the differentiation property (A.12) of the Fourier transformation, we can write

$$\begin{aligned} [f^1]_t =& \frac{1}{\mathrm{j}2\pi} \lim_{\tau \to 0} \partial_\tau \int_{t' \in I\!R} \Psi^{t\tau}(t-t';\tau) R\{u,u\}(t';\tau) \mathrm{d}t' \\ =& \frac{1}{\mathrm{j}2\pi} \lim_{\tau \to 0} \int_{t' \in I\!R} \Psi^{t\tau}(t-t';\tau) \partial_\tau R\{u,u\}(t';\tau) \mathrm{d}t' \\ &+ \frac{1}{\mathrm{j}2\pi} \lim_{\tau \to 0} \int_{t' \in I\!R} R\{u,u\}(t';\tau) \partial_\tau \Psi^{t\tau}(t-t';\tau) \mathrm{d}t'. \end{aligned} \tag{3.35}$$

For $[f^0]_t$, which is the time marginal of $P\{u,u\}(t;f)$, we have in the local auto-correlation domain

$$[f^0]_t = \lim_{\tau \to 0} \int_{t' \in I\!R} \Psi^{t\tau}(t-t';\tau) R\{u,u\}(t';\tau) \mathrm{d}t'. \tag{3.36}$$

With Eqs.(3.2) and (3.3) we write for Eq.(3.35) in terms of the characteristic function as

$$\begin{aligned}\left[f^1\right]_t =& \frac{1}{\mathrm{j}2\pi} \lim_{\tau\to 0} \mathcal{F}_\nu^+ \left\{\Psi^{\nu\tau}(\nu;\tau)\partial_\tau A\{u,u\}(\nu;\tau)\right\} \\ &+ \frac{1}{\mathrm{j}2\pi} \lim_{\tau\to 0} \mathcal{F}_\nu^+ \left\{A\{u,u\}(\nu;\tau)\partial_\tau \Psi^{\nu\tau}(\nu;\tau)\right\}.\end{aligned} \tag{3.37}$$

We see that if we want to retain the local average frequency of the Wigner distribution (cf. Eqs.(2.83)-(2.89)), we must require that

$$\lim_{\tau\to 0} \Psi^{\nu\tau}(\nu;\tau) = 1 \text{ for } \nu \in I\!R, \tag{3.38}$$

which is the constraint for the frequency marginal property, and also

$$\lim_{\tau\to 0} \partial_\tau \Psi^{\nu\tau}(\nu;\tau) = 0 \text{ for } \nu \in I\!R. \tag{3.39}$$

Note that for the product kernel $\Psi^{\nu\tau}(\nu;\tau) = \Phi^{\nu\tau}(\nu\tau)$ this is always the case.

The average time as a function of frequency, $\langle t\rangle_f$, can be found by a similar derivation. For the Wigner distribution, $\langle t\rangle_f$ is equal to the group delay $\tau_g(f)$ of the signal (see Eq.(2.90)). In case we want to obtain the group delay as the average time of the time-frequency representation, i.e.

$$\langle t\rangle_f = \frac{\left[t^1\right]_f}{\left[t^0\right]_f} = \tau_g(f), \tag{3.40}$$

we require the time marginal property

$$\lim_{\nu\to 0} \Psi^{\nu\tau}(\nu;\tau) = 1, \text{ for } \tau \in I\!R, \tag{3.41}$$

in combination with the constraint

$$\lim_{\nu\to 0} \partial_\nu \Psi^{\nu\tau}(\nu;\tau) = 0, \text{ for } \nu \in I\!R. \tag{3.42}$$

Property 4. Non-negativity. It is tempting to interpret a time-frequency representation as a time-frequency energy density function. However a proper energy density should be strictly non-negative and real-valued as there is no physical interpretation for negative or complex-valued energy. The constraint that results in a real valued time-frequency representation was discussed previously (see Eq.(3.13)). The Wigner distribution attains negative values for

most signals. The only signal, other than the time and frequency delta functions, with a non-negative Wigner distribution is given by (Hudson 1974)

$$u(t) = \exp\left(\mathrm{j}2\pi(\tfrac{1}{2}ct^2 + f_1 t)\right)\sqrt{\sigma}\exp\left[-\pi\left(\frac{t-t_0}{\sigma}\right)^2\right]. \tag{3.43}$$

The signal of Eq.(3.43) can be characterized as a modulated Gaussian chirp signal, where f_0, c, and σ are real valued constants that represent the modulation frequency, chirp rate and standard deviation of the Gaussian respectively. This type of signal is nowadays often denoted as a 'chirplet'. In Chapter 2 the Wigner distributions of a Gaussian (Eq.(2.107)) and chirp signal (Eq.(2.103)) were given. These Wigner distributions were both non-negative and as a result the Wigner distribution of their product will also be a non-negative function, as can be derived from the product property Eq.(2.93). Since these are the only signals with a non-negative Wigner distribution, the question arises if there is a subclass of time-frequency representations that are non-negative for every signal. Equation (3.2) expresses the Cohen's class time-frequency representation as an averaging of the Wigner distribution over the time-frequency plane. This results in a non-negative representation, if the kernel $\Psi^{tf}(t;f)$ is also Wigner distribution. Note that in that case the marginal property cannot be satisfied, as we concluded from Eqs.(3.25) and (3.26) that the marginal preserving kernel can never be a Wigner distribution. If we take for the kernel $\Psi^{tf}(t;f)$ the Wigner distribution of a function $v(t)$, the smoothing can be expressed as

$$\begin{aligned} P\{u,u\}(t;f) = \int_{t'\in\mathbb{R}}\int_{f'\in\mathbb{R}} & W\{v,v\}(t-t';f-f') \\ & W\{u,u\}(t';f')\,\mathrm{d}t'\,\mathrm{d}f' \;\geq 0, \text{ for } (t,f)\in\mathbb{R}^2. \end{aligned} \tag{3.44}$$

Although this may seem a remarkable result, it is less so. This can be understood if we substitute the definition of the Wigner distribution into Eq.(3.44). We then express the averaging in terms of the instantaneous auto-correlation function $R\{u,u\}(t;\tau)$ as

$$P\{u,u\}(t;f) = \mathcal{F}_\tau^- \left\{ \int_{t'\in\mathbb{R}} R\{v,v\}(t-t';\tau) R\{u,u\}(t';\tau)\mathrm{d}t' \right\}. \tag{3.45}$$

We now define, $t'' = t' + \frac{1}{2}\tau$ and $\tau' = t' - \frac{1}{2}\tau$, which entails that $\mathrm{d}t''\mathrm{d}\tau' = \mathrm{d}t'\mathrm{d}\tau$. Inserting these new variables and with the definition of the instantaneous

auto-correlation function (Eq.(2.68)) we find

$$\begin{aligned} P\{u,u\}(t;f) =& \mathcal{F}^{-}_{\tau'}\left\{v(t-\tau')u^*(\tau')\right\}\mathcal{F}^{-}_{t''}\left\{v^*(t-t'')u(t'')\mathrm{d}t''\right\} \\ =& \left|\mathcal{F}^{-}_{\tau}\left\{v^*(t-\tau)u(\tau)\mathrm{d}\tau\right\}\right|^2. \end{aligned} \tag{3.46}$$

This result shows that smoothing the Wigner distribution of u with the Wigner distribution $W\{v,v\}(t;f)$ is equivalent to the spectrogram (the squared modulus of the sliding-window Fourier transformation) of the function u, evaluated with a window function, $w(t) = v^*(-t)$ (see Eqs.(2.52)-(2.54)). Since the spectrogram is a non-negative function by definition, smoothing a Wigner distribution with another Wigner distribution will always yield a non-negative time-frequency representation. The kernel that generates a positive time-frequency is then the ambiguity function of the smoothing function v,

$$\Psi^{\nu\tau}(\nu;\tau) = A\{v,v\}(\nu;\tau). \tag{3.47}$$

If we consider Eq.(3.46) in relation to a spectrogram with window function $w(t)$, we conclude that the kernel that generates the spectrogram is given by

$$\Psi^{\nu\tau}(\nu;\tau) = A\{w,w\}(-\nu;\tau), \tag{3.48}$$

which is the ambiguity function of $w^*(-t)$. We also conclude that the spectrogram cannot satisfy the marginal property for any window function $w(t)$, which is once again a consequence of the result that a kernel that preserves the marginals can never be a Wigner distribution (see Eqs.(3.25) and (3.26)).

Although we can obtain non-negative time-frequency representations through a suitable average of the Wigner distribution, we are not able to define a general class time-frequency representation that is a proper energy density function. A proper energy density is not only real-valued and positive but satisfies the time marginal and frequency marginal property as well, which is impossible for any window function $v(t)$. How to obtain a non-negative time-frequency representation with correct marginals is still largely an unanswered question. In Section 2.2.1 that non-negativity of the time-frequency representation can be only be guaranteed if the representation depends on the signal. However, in that case we do not know how this signal dependence should be brought into the representation.

Property 5. Reduced cross term interference. An important reason for deriving time-frequency representations that are different from the Wigner distribution is that we want less, and ideally no, cross term energy in the representation.

The maximum energy of the ambiguity function is found at the origin, which can be derived as follows. Using Eq.(2.100e), we can write

$$|A\{u,u\}(\nu;\tau)|^2 = \left|\mathcal{F}_t^- \{R\{u,u\}(t;\tau)\}\right|^2. \tag{3.49}$$

For the right-hand side of Eq.(3.49), we have the following inequality:

$$\begin{aligned}\left|\mathcal{F}_t^- \{R\{u,u\}(t;\tau)\}\right| &\leq \int_{t\in I\!R} \left|\exp(-\mathrm{j}2\pi\nu t) R\{u,u\}(t;\tau)\right| \mathrm{d}t \\ &= \int_{t\in I\!R} \left|R\{u,u\}(t;\tau)\right| \mathrm{d}t.\end{aligned} \tag{3.50}$$

Now we insert the definition of the instantaneous auto-correlation function, Eq.(2.68), into the right-hand side of Eq.(3.50) and obtain

$$\begin{aligned}\int_{t\in I\!R} \left|R\{u,u\}(t;\tau)\right| \mathrm{d}t &= \int_{t\in I\!R} \left|u(t+\tfrac{1}{2}\tau)u^*(t-\tfrac{1}{2}\tau)\right| \mathrm{d}t \\ &\leq \left[\int_{t\in I\!R} \left|u(t+\tfrac{1}{2}\tau)\right|^2 \mathrm{d}t\right]^{\frac{1}{2}} \left[\int_{t\in I\!R} \left|u(t-\tfrac{1}{2}\tau)\right|^2 \mathrm{d}t\right]^{\frac{1}{2}},\end{aligned} \tag{3.51}$$

where we have used Hölders inequality. Hence, by changing variables we have

$$\left|\mathcal{F}_t^- \{R\{u,u\}(t;\tau)\}\right| \leq \int_{t\in I\!R} |u(t)|^2 \mathrm{d}t, \tag{3.52}$$

which results in the inequality

$$|A\{u,u\}(\nu;\tau)| \leq E_u = A\{u,u\}(0,0), \text{ for } (\nu,\tau) \in I\!R^2. \tag{3.53}$$

The analysis of auto terms and cross terms in the ambiguity function showed that the auto terms will be concentrated near the origin of the (ν,τ)-plane and the cross terms will generally be located away from the origin (see Section 2.7). Consequently, the sum of the auto terms of a signal will always have its maximum energy at the origin. To preserve the auto term energy in the time-frequency representation, we should choose a kernel that is peaked at

the origin. The properties of the cross terms are determined by the signal components that generate them. As such, their location in the ambiguity function strongly depends on the signal under analysis. However, a cross term is always located away from the two auto terms that generated the cross term. From the analysis in Sections 2.6 and 2.7 it was concluded that amount of shift is approximately the time-frequency distance (t_d, f_d) between the location of the two auto terms in the time-frequency plane. Hence, we will reduce the cross term energy in the time-frequency representation if

$$\Psi^{\nu\tau}(\nu;\tau) << 1, \text{ for } (\nu,\tau) \approx (f_d, t_d). \tag{3.54}$$

Because the exact location of auto terms and cross terms in the ambiguity function depends on the signal, it is not possible to achieve a strong reduction of cross terms for different signal types, using one type of kernel. An optimal suppression of the cross terms for a wide variety of signals can only be achieved by adapting the kernel to the signal. A kernel that does not depend on the signal is called a fixed kernel. Most time-frequency representations that have been proposed are fixed kernel representations. Their main advantage over a signal dependent kernel is that numerical implementation is rather straightforward. Furthermore, a kernel does not explicitly depend on the signal results in the same time-frequency representation for each signal that is analyzed. This greatly facilitates the comparison between signals and further calculations with the time-frequency representations.

First, we will give some examples of fixed kernel representations in the next section. In the last part of this chapter we will discuss a signal-dependent time-frequency representation. The signal dependent kernel is found by formulating the reduction of cross terms as an optimization problem.

3.4 Examples of time-frequency representations with a fixed kernel

In the previous sections we saw that the kernel formulation is an effective way to find a time-frequency representation that satisfies certain properties. However, none of the representations of the general class satisfies all these properties. If we consider all properties equally important, then the Wigner distribution comes close to the ideal time-frequency representation. A major drawback of the Wigner distribution is that it is often difficult to interpret

because of the cross terms at locations in the time-frequency plane where no energy is expected. Furthermore, the Wigner distribution is manifestly negative for most signals, which prohibits the interpretation of the Wigner distribution as a proper energy density function. This negativity is closely related to the marginal property. Non-negativity and correct marginals are mutually exclusive properties for a time-frequency representation of the bi-linear type. Consequently, if we require a certain property to be satisfied by a time-frequency representation, this usually results in discarding another property. The fixed kernel representations discussed here, all suffer from this trade-off. They do, however, perform very well in many situations, which is the reason why they were proposed in the first place and why they are discussed here. In this section we will introduce the kernels and show an example of their numerical implementation. In Chapter 4, their merits for the analysis of seismic data will be evaluated.

For the numerical examples, a signal consisting of two modulated Gaussian signals will be used. The signal, $u(t) = u_1(t) + u_2(t)$, is given by

$$u(t) = \exp\left[-\pi\left(\frac{(t-t_1)}{\sigma_1}\right)^2\right]\exp\left(\mathrm{j}2\pi(f_1+\alpha t)t\right) + \exp\left[-\pi\left(\frac{(t-t_2)}{\sigma_2}\right)^2\right]\exp(\mathrm{j}2\pi f_2 t). \tag{3.55}$$

The real and imaginary parts of this signal are shown in Fig. 3.2. In the example, $u_1(t)$ has been given the constants $t_1 = 0.5$ [s], $f_1 = 5$ [s^{-1}], $\alpha = 30$ [s^{-2}], $\sigma_1 = 1.0$ and for $u_2(t)$ we have taken $t_2 = 0.75$ [s], $f_2 = 10$ [s^{-1}] and $\sigma_2 = 0.33$. The signal has been discretized for a time length of 1 [s], using 128 samples.

The signal of Eq.(3.55) is an analytic signal. In the sense of the definition of an analytic signal that was given in Section 2.2.3, the spectrum of an analytic signal is zero for negative frequencies. Because there is no energy at negative frequencies, no cross terms will be generated between negative and positive frequency part of the spectrum of the signal.

3.4.1 Pseudo Wigner distribution

The pseudo Wigner distribution is the Wigner distribution, evaluated over a finite time-shift window $w(\tau)$ (Claasen and Mecklenbräuker 1980). In terms

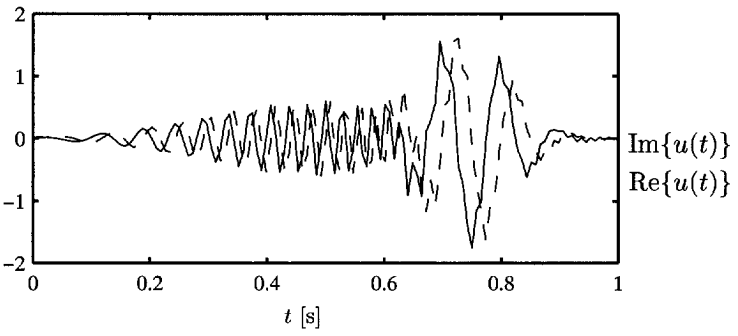

Figure 3.2: *Signal composed of two modulated Gaussians (Eq.(3.55))*

of the instantaneous auto-correlation the pseudo Wigner distribution is given by

$$P\{u,u\}(t;f) = \mathcal{F}_\tau^- \{w(\tau)R\{u,u\}(t;\tau)\}\,, \tag{3.56}$$

where $w(\tau)$ is a real and symmetric window function. In terms of the general class of time-frequency representations, the pseudo Wigner distribution is obtained by taking

$$\Psi^{t\tau}(t;\tau) = w(\tau), \text{ for } t \in I\!R. \tag{3.57}$$

Since the window function is real-valued and symmetric, we have $w(\tau) = w(-\tau)$ and the pseudo Wigner distribution is real-valued as well. If we also take, $w(0) = 1$ and $\lim_{\tau\to 0} \partial_\tau w(\tau) = 0$, we see that the pseudo Wigner distribution satisfies the time marginal property and that the mean time $\langle t\rangle_f$ is the group delay of the signal.

In a numerical implementation, the closest approximation to the Wigner distribution is a pseudo Wigner distribution with $w(\tau)$ a box-car window of the same duration as the signal. In Fig. 3.3a the pseudo Wigner distribution of the signal of Eq.(3.55) is shown. The window that was used is a box-car window given by

$$w(\tau) = \begin{cases} 1 & \text{for } |\tau| \le t_0 \\ 0 & \text{for } |\tau| > t_0 \end{cases}, \tag{3.58}$$

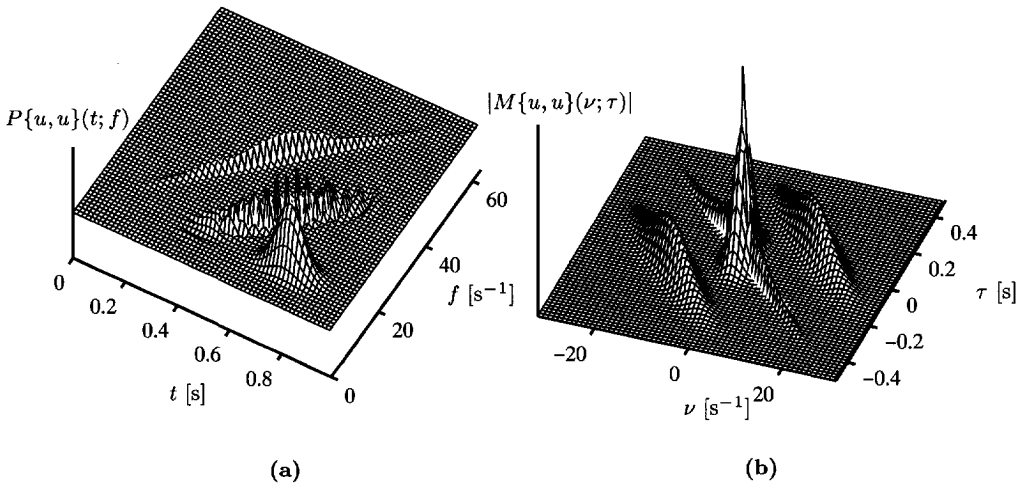

Figure 3.3: *(a) Pseudo Wigner distribution of the signal given by Eq.(3.55) obtained with the box-car window Eq.(3.58); (b) modulus of the characteristic function (ambiguity function).*

where $t_0 = 1$ [s]; the time length of the discrete signal. For this window, the time-frequency representation is a numerical approximation of a Wigner distribution that is discrete in time and continuous in frequency. The frequency marginal and instantaneous frequency properties of the Wigner distribution will therefore be satisfied. However, these properties should be considered in the context of the discretization of the time signal and the associated numerical approximation.

The characteristic function that corresponds to the time-frequency representation is shown in Fig. 3.3b. For this window choice, the characteristic function is the ambiguity function of the signal, as we have $\Psi^{\nu\tau}(\nu;\tau) = 1$ (cf. Eq.(3.2)). The figure illustrates the domain allocation of cross terms and auto terms. In the time-frequency representation the cross terms are located between the auto terms. In the characteristic function the auto terms are located near the origin, where they overlap. The cross terms are located away from the origin. The window $w(\tau)$ can be used for the suppression of cross terms between components of the signal that are separated in time. A

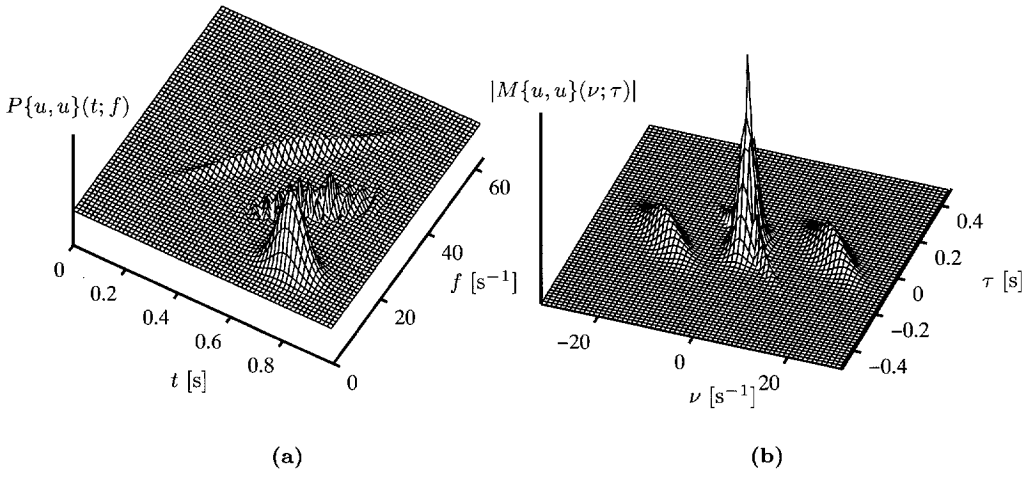

Figure 3.4: *(a) Pseudo Wigner distribution of the signal given by Eq.(3.55) obtained with a Gaussian shaped window, (b) characteristic function.*

window that emphasizes the auto-correlation for small time shifts, effectively removes the cross terms between signal components that are spaced further apart that the length of the window. Figure 3.4a shows the pseudo Wigner evaluated with the Gaussian shaped window; $w(\tau) = \exp(-2\pi\tau^2)$. In the characteristic function (Fig. 3.4b) we see that the filter $\Psi^{\nu\tau}(\nu;\tau)$ weights the ambiguity function in the time-shift (τ) direction. Consequently, cross term energy that results from the time separation of the components will be suppressed. However, the cross terms between the frequency locations of the two components remains largely unaffected. The use of a window different from the box-car given by Eq.(3.58), implies a smoothing in the frequency direction of the time-frequency representation. Hence, the frequency marginal and instantaneous frequency properties will not be satisfied for this window.

3.4.2 Choi-Williams distribution

The ambiguity domain kernel of the exponential distribution is given by

$$\Psi^{\nu\tau}(\nu;\tau) = \exp\left[-\left(\frac{\nu\tau}{\sigma}\right)^2\right]. \tag{3.59}$$

This kernel was introduced by Choi and Williams (Choi and Williams 1989) and the associated time-frequency representation is therefore nowadays known as the Choi-Williams representation. The Choi-Williams kernel is a product kernel, and it has all the properties of the general form of product kernel that was given in Eqs.(3.27)-(3.29). Consequently, the Choi-Williams representation satisfies the marginal properties and its local time and frequency averages are the group delay instantaneous frequency of the signal.

With Eq.(3.3), the Choi-Williams kernel in the instantaneous autocorrelation domain is found as

$$\Psi^{t\tau}(t;\tau) = \frac{\sigma\sqrt{\pi}}{|\tau|} \exp\left[-\left(\frac{\pi\sigma t}{\tau}\right)^2\right] \tag{3.60}$$

and using Eq.(3.3), we find the expression of the Choi-Williams time-frequency representation

$$P\{u,u\}(t;f) = \mathcal{F}_\tau^- \left\{ \int_{t'\in I\!R} \frac{\sigma\sqrt{\pi}}{|\tau|} \exp\left[-\left(\frac{\pi\sigma(t-t')}{\tau}\right)^2\right] R\{u,u\}(t';\tau)\,\mathrm{d}t' \right\}. \tag{3.61}$$

The general shape of the Choi-Williams kernel in the ambiguity domain and (t,τ)-domain, is shown in Fig. 3.5. The shape of the kernel in the ambiguity domain suppresses energy that is located away from the $\nu = 0$ and $\tau = 0$ axes, with the parameter σ determining the degree of suppression. This shape makes it an effective kernel for the cross term suppression for signals with auto term energy that is localized parallel and close to the zero axes in the (ν,τ)-domain, such as sinusoidal and impulse-like signals. For $\sigma \to \infty$, the Choi-Williams distribution becomes the Wigner distribution. The Choi-Williams distribution of the signal according to Eq.(3.55) is shown in Fig. 3.6.

The representation has considerably less cross term energy compared to the pseudo Wigner distribution (Fig. 3.4). However, the auto term energy of the first component ($u_1(t)$ in Eq.(3.55)) is smeared out over the (t,f)-plane. Since this component is located away from the axes in the (ν,τ)-domain, the kernel also suppresses auto term energy that belongs to this component.

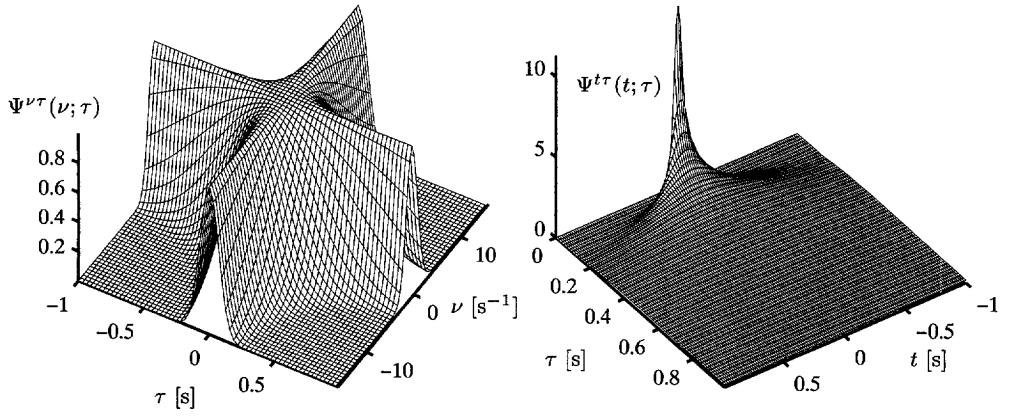

Figure 3.5: *General shape of the Choi-Williams kernel (Eq.3.59)); (a) (ν,τ)-domain, (b) (t,τ)-domain.*

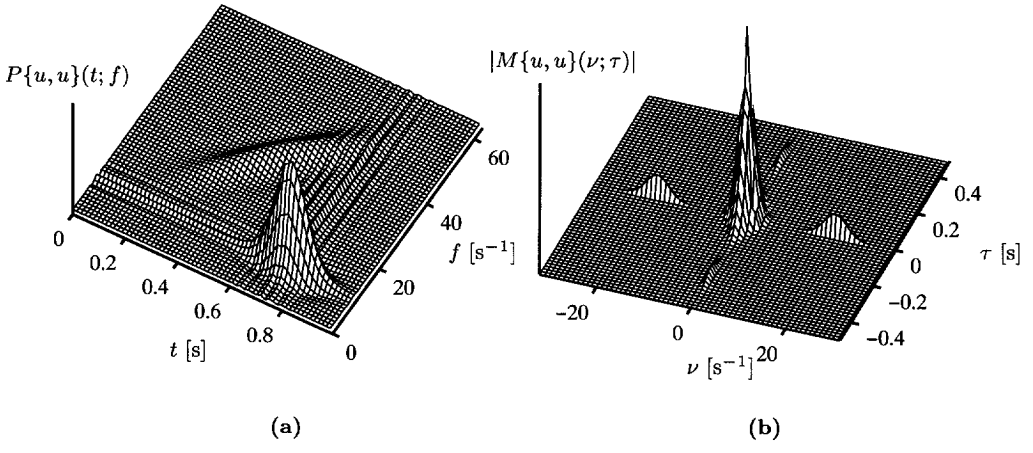

Figure 3.6: *(a) Choi-Williams representation of the signal given by Eq.(3.55), (b) characteristic function.*

3.4.3 Cone-kernel representation

The cone kernel was first introduced by Zhao, Atlas, and Marks (Zhao et al. 1990) and the associated time-frequency representation is also known as the Zhao, Atlas, Marks (ZAM) time-frequency representation. The cone kernel in the (ν, τ)-domain is given by

$$\Psi(\nu;\tau) = w(\tau)|\tau|\frac{\sin(2\pi a\nu\tau)}{2\pi a\nu\tau}, \tag{3.62}$$

where $w(\tau)$ is a real and symmetric window function and a is a dimension-less constant. Using Eq.(3.3), we find for the cone kernel in the instantaneous auto-correlation domain

$$\Psi^{t\tau}(t;\tau) = w(\tau)\mathcal{F}_{\nu}^{+}\left\{\frac{\sin(2\pi a\nu\tau)}{2\pi a\nu\tau}\right\} = w(\tau)\frac{\Pi(t/2a|\tau|)}{2a}, \tag{3.63}$$

where $\Pi(t/2a|\tau|)$ is a box-car function, given by

$$\Pi(t/2a|\tau|) = \begin{cases} 1 & \text{for } |t| < a|\tau| \\ 0 & \text{for } |t| > a|\tau| \end{cases}. \tag{3.64}$$

Hence, following the previous definitions (Eqs.(3.8) and (3.64)), we can express the cone kernel time-frequency representation as

$$P\{u,u\}(t;f) = \mathcal{F}_{\tau}^{-}\left\{\frac{w(\tau)}{2a}\int_{t-\frac{|\tau|}{a}}^{t+\frac{|\tau|}{a}} R\{u,u\}(t';\tau)\,\mathrm{d}t'\right\}. \tag{3.65}$$

Generally, $a = 1/2$ is chosen, because in that case the time-frequency representation the time-frequency representation has no energy outside the time support of the signal, i.e. if $u(t) = 0$ for $t > t_0$, then we also have $P\{u,u\}(t;f) = 0$ for $t > t_0$. The general shape of this kernel in the ambiguity and instantaneous auto-correlation domain is shown in Fig. 3.7. For the window function $w(\tau)$ a Gaussian has been used. An important feature of this kernel is that $\Psi^{\nu\tau}(\nu;0) = 0$. As a result impulse like signal components will be suppressed in the time-frequency representation. An analysis of the properties of the cone kernel is given by Oh and Marks (1992). Figure 3.8 shows the cone-kernel time-frequency representation for the signal Eq.(3.55). The cross terms are greatly reduced. However, the component with a linearly increasing frequency is smeared out over time and frequency, as it is not parallel to the time axis.

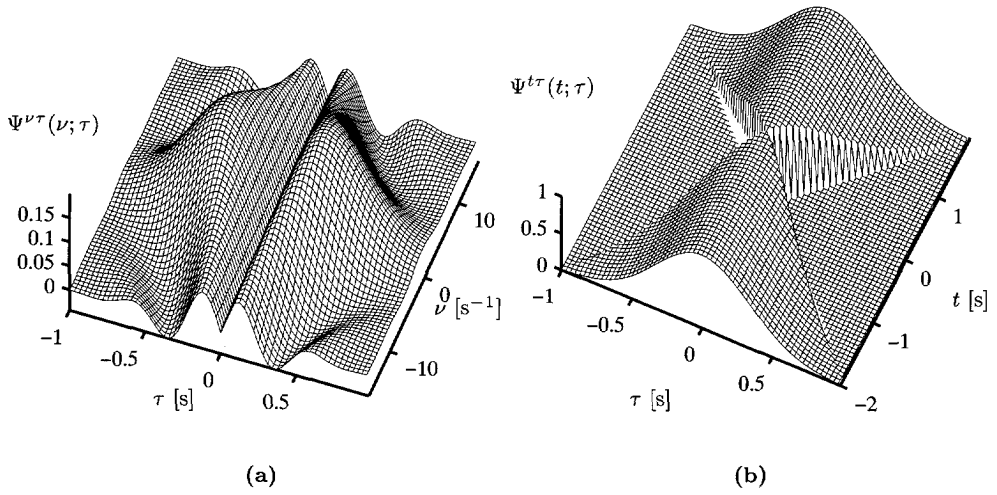

Figure 3.7: *General shape of the cone kernel (Eq.3.59); (a) (ν,τ)-domain, (b) (t,τ)-domain.*

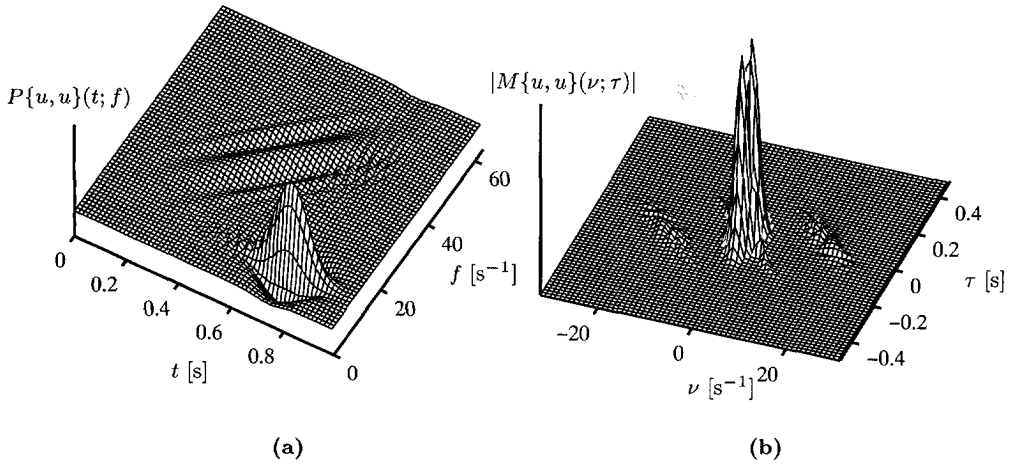

Figure 3.8: *Cone-kernel (t,f)-representation of the signal given by Eq.(3.55), (b) characteristic function.*

3.4.4 Spectrogram

The spectrogram is the quadratic form of the sliding-window Fourier transform of a signal. The sliding-window Fourier transformation and spectrogram were previously discussed in Section (2.2.2) and in the previous section in the context of the general class of time-frequency representations. If we apply a short window around every time t and take the Fourier transformation of the windowed portion of data we obtain an estimate of the Fourier spectrum for every time t (see Eqs.(2.52)-(2.54)). We can estimate a local energy density spectrum as the square of the short time Fourier transform for every time t. The result is a time-frequency representation, known as the spectrogram,

$$P\{u,u\}(t;f) = \left|\mathcal{F}_{\tau}^{-}\left\{u(\tau)w(\tau-t)\right\}\right|^2 . \tag{3.66}$$

The kernel of the spectrogram was given by Eq.(3.48). Using Eq.(3.48) for the spectrogram kernel in the ambiguity domain, an expression for the spectrogram in terms of the general class of time-frequency representations is found as

$$P\{u,u\}(t;f) = \mathcal{F}_{\nu}^{+}\mathcal{F}_{\tau}^{-}\left\{A\{w,w\}(-\nu;\tau)A\{u,u\}(\nu;\tau)\right\} , \tag{3.67}$$

where $A\{w,w\}(\nu;\tau)$ is the ambiguity function of the window. The spectrogram satisfies the total energy condition if the energy of the window is taken to one, because in that case we have $\Psi^{\nu\tau}(0;0) = 1$. The spectrogram kernel never satisfies both marginal constraints, as was shown in the previous section. The resolution of the spectrogram strongly depends on the size of the window. If a short window is chosen, the Fourier transform is taken over a signal of short duration and the result will contain little information on the spectral properties of the signal. For longer windows we will have less time information in our representation. The relation between window size and resolution properties of the spectrogram is an expression of the uncertainty principle, that states that the duration and bandwidth of a window $w(t)$ cannot be chosen independently. The uncertainty principle was discussed in Section 2.2.1 and is this trade-off between window size and resolution was one of the motivations to search for other representations than the spectrogram. As we saw in our previous discussion, the choice of time window $w(t)$ in the spectrogram fixes the degree of smoothing in the frequency direction. Consequently, the frequency resolution depends on the time resolution and

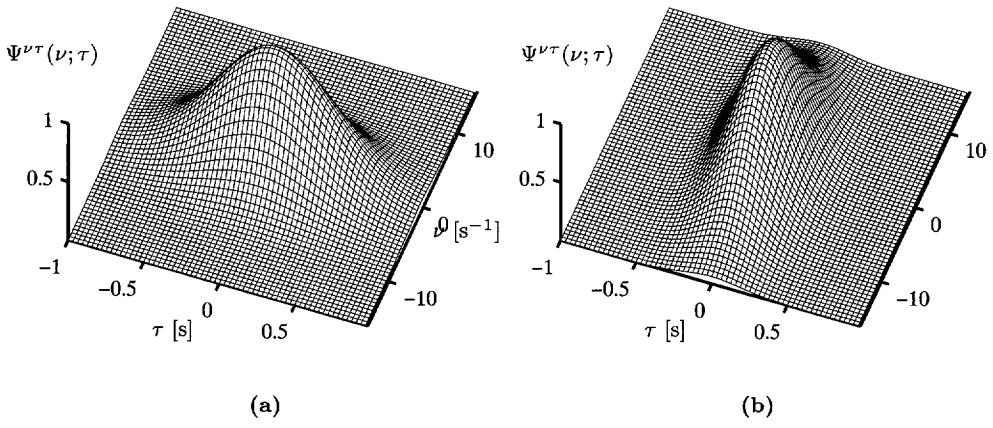

Figure 3.9: *General shape of the spectrogram kernel $\Psi^{\nu\tau}(\nu;\tau)$ (Eq.3.48), with (a) a long duration window and (b) a short duration window.*

vice versa. One of the major advantages of the kernel approach is that time and frequency smoothing can be specified independently. The smoothing is handled by choosing a kernel function $\Psi^{tf}(t;f)$, for which time and frequency smoothing are not necessarily related.

The general shapes of a short and a long duration Gaussian window in the ambiguity domain are shown in Fig. 3.9. The spectrograms of the signal Eq.(3.55), obtained with a short, intermediate and long Gaussian window are shown in Fig. 3.10.

The best results can be obtained with a window that is *matched* to the components of the signal. A matched window is a window that has the same characteristics as the signal components, such as general shape and duration. In this case, the signal consists of modulated Gaussians and we used a Gaussian shaped window. Application of a window with a shape and duration that is similar to the shape and duration of the components is effectively a decomposition into the components. The resulting spectrogram will then approximately be the sum of the spectrograms of the components, without much distortion caused by the window. In some respects this is an

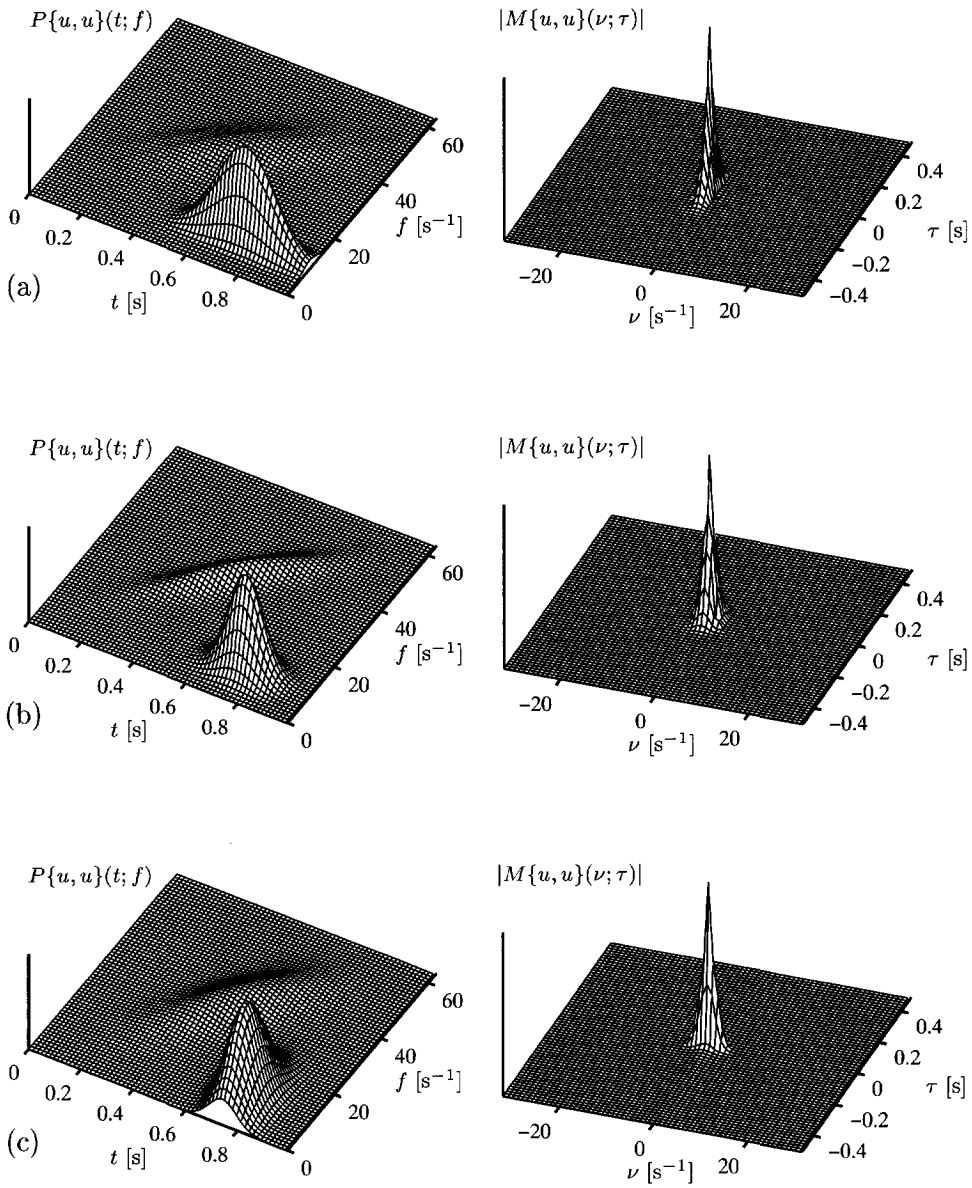

Figure 3.10: *(left) Spectrograms and (right) characteristic functions of the signal given by Eq.(3.55); (a) long window, (b) intermediate window, and (c) short window.*

ideal time-frequency representation as it will contain hardly any cross terms. It should be noted however that for many signals it will be very difficult to find this matched time window, either because the characteristics of the signal vary rapidly with time or because there is significant time overlap of components that have very different characteristics. We will take an approach that is similar to the matched time window spectrogram in the next section. With the optimal kernel method, a kernel is obtained that is matched to the ambiguity function of the auto terms. The matched filter spectrogram is a special case of this *signal-dependent* kernel. One of the advantages of the optimal kernel approach is that we can impose constraints on the matched kernel and consequently obtain a time-frequency representation with desired properties, such as correct marginals and local averages.

3.5 Signal dependent kernel optimization

Cross term suppression can be achieved for a variety of signals by adapting the kernel to the signal in such a way that auto term energy is passed and the cross terms are rejected in the ambiguity function of the signal. The maximum energy of the auto terms of a multi-component signal is at the origin of the ambiguity function (see Eq.(3.53)) and in Section 2.7 it was shown that the cross terms are located away from the auto terms. An optimum kernel with regard to cross term suppression leaves the auto terms unaltered and rejects the cross terms in the ambiguity domain. The drawback of using a fixed kernel for cross term reduction is that the shape of the ambiguity function of the auto terms is signal dependent. Furthermore, the domain allocation of auto terms and cross terms is also strongly signal dependent. A fixed kernel is capable of separating the auto terms from cross terms for only limited number of signal types. To illustrate this, we show the modulus of the ambiguity function, $|A\{u,u\}(\nu;\tau)|^2$, of the signal consisting of two Gaussian components, given by Eq.(3.55). Because we have, $A^*\{u,u\}(-\nu;-\tau) = A\{u,u\}(\nu;\tau)$, only the half of the ambiguity plane with positive frequency shift, $\nu \in I\!R^+$, is shown. Although the auto terms and cross terms are well separated for this signal we saw that the shape of the auto terms will be difficult to match by any of the fixed kernels that were discussed in the previous sections. For that reason we will attempt to find a kernel that is adapted to the correlation structure of a signal. In order to do this we can exploit the knowledge we have about the domain allocation

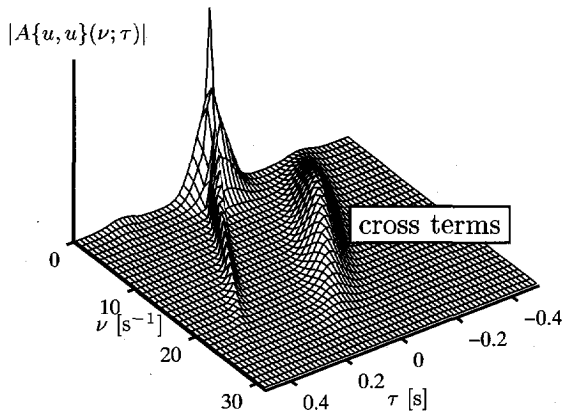

Figure 3.11: *Ambiguity surface of the signal given by Eq.(3.55).*

of the cross terms in the ambiguity function.

3.5.1 Optimal kernel design

The property that the auto term energy of a multi-component signal is concentrated in one particular region of the ambiguity plane, while the cross term energy is distributed over another, larger, region can be used in the search for a kernel that suppresses cross terms. With help of this property we can formulate the cross term suppression as an optimization problem (Baraniuk and Jones 1993a). First we specify the volume under the pass-band of the kernel as a fixed parameter, α, that is real and positive. The second constraint we impose is that the kernel is one at the origin, to preserve the total energy property (see Eq.(3.14)), and is *radially non-increasing.* The last constraint forces the kernel to be essentially a low-pass filter with a pass-band that occupies an area connected to the origin. We now specify a functional $\mathcal{E}[\Psi^{\nu\tau}]$ of the kernel as

$$\mathcal{E}[\Psi^{\nu\tau}] = \int_{\tau\in\mathbb{R}} \int_{\nu\in\mathbb{R}} |\Psi^{\nu\tau}(\nu;\tau)|^2 \, A\{u,u\}(\nu;\tau)\,\mathrm{d}\tau\,\mathrm{d}\nu, \tag{3.68}$$

with as a special case $\Psi^{\nu\tau}(\nu;\tau) = 1$ for $(\nu,\tau) \in I\!R^2$,

$$\mathcal{E}(1) = E_u^2, \tag{3.69}$$

where E_u is the energy of the signal. To get a feeling for the upper bound of $\mathcal{E}[\Psi^{\nu\tau}]$ and using Eq.(3.53)

$$|A\{u,u\}(\nu;\tau)| \leq A\{u,u\}(0;0) = E_u, \text{ for } (\nu,\tau) \in I\!R^2, \tag{3.70}$$

we arrive at

$$\mathcal{E}[\Psi^{\nu\tau}(\nu;\tau)] \leq E_u^2 \int_{\tau\in I\!R} \int_{\nu\in I\!R} |\Psi^{\nu\tau}(\nu;\tau)|^2 \,\mathrm{d}\nu\mathrm{d}\tau. \tag{3.71}$$

Further we condition $\Psi^{\nu\tau}$ such that

$$\Psi^{\nu\tau}(0;0) = 1. \tag{3.72}$$

The goal of the optimization is to separate auto term from cross term energy, while by maximizing the auto term energy that is passed by a kernel that has a limited size. The first step is to constrain the volume under the kernel by the constraint

$$\int_{\tau\in I\!R} \int_{\nu\in I\!R} |\Psi(\nu;\tau)|^2 \,\mathrm{d}\tau\mathrm{d}\nu \leq \alpha, \tag{3.73}$$

where α is a real and positive parameter and $0 < \alpha \leq 1$. The last constraint we add is that the kernel is non-increasing in any radial direction away from the origin. By this constraint the performance on cross term suppression of the kernel is determined. If it would not be imposed, the kernel would be large, wherever $|A\{u,u\}(\nu;\tau)|^2$ is large, regardless whether a cross term or auto term is passed. With the non-increasing constraint, cross terms can only be passed if the relatively low-energy region of the ambiguity function between the cross terms and auto terms is incorporated into the kernel. If the cross terms and auto terms are well separated this region contributes little to the performance measure Eq.(3.68). In this way the formulation of the optimization problem implies a penalty for crossing the region between auto terms and cross terms. Consequently, the optimal kernel will be constrained to the region of the auto terms. The constraint that the kernel is radially non-increasing is best implemented using polar coordinates. It is straightforward to formulate the performance measure and other constraints in polar

coordinates, and doing so, we define the following optimization problem. The energy functional is given by, using the symmetry relations Eqs.(3.11)-(3.13) due to the realness,

$$\mathcal{E}\left[\Psi^{\nu\tau}\right] = 2\int_0^\infty \int_0^\pi \left|\bar{A}\{u,u\}(r,\theta)\bar{\Psi}^{r\theta}(r,\theta)\right|^2 r\mathrm{d}r\mathrm{d}\theta, \tag{3.74}$$

with

$$\begin{aligned}
&\bar{A}\{u,u\}(r,\theta) = A\{u,u\}(r\cos(\theta), r\sin(\theta)),\\
&\bar{\Psi}^{r\theta}(r,\theta) = \Psi^{\nu\tau}(r\cos(\theta), r\sin(\theta)),\\
&r = (\nu^2+\tau^2)^{1/2} \geq 0.
\end{aligned}$$

Then the optimization problem consists of maximizing $\mathcal{E}\left[\Psi\right]$, subject to the following conditions:

$$\bar{\Psi}^{r\theta}(0,\theta) = 1, \tag{3.75}$$

the kernel volume constraint

$$2\int_0^\infty \int_0^\pi \left|\bar{\Psi}^{r\theta}(r,\theta)\right|^2 r\mathrm{d}r\mathrm{d}\theta \leq \alpha, \tag{3.76}$$

and the radially non-increasing constraint

$$\bar{\Psi}^{r\theta}(r_2,\theta) \leq \bar{\Psi}^{r\theta}(r_1,\theta), \text{ for } r_2 > r_1 \text{ and for } 0 \leq \theta \leq \pi. \tag{3.77}$$

Additional constraints can be imposed in order to extend the cross term reduction property of the optimal kernel representation with other properties. For instance, to obtain a representation that satisfies the marginal properties Eqs.(3.17) and (3.21), it is sufficient to add the constraints

$$\begin{aligned}
&\bar{\Psi}^{r\theta}(r,0) = 1, \text{ for } 0 \leq r \leq \infty\\
&\qquad \text{and}\\
&\bar{\Psi}^{r\theta}(r,\frac{\pi}{2}) = 1, \text{ for } 0 \leq r \leq \infty.
\end{aligned} \tag{3.78}$$

Two algorithms have been implemented for the numerical computation of the optimum kernel time-frequency representation. The first algorithm a radially Gaussian shaped kernel to the ambiguity function of the signal (Baraniuk

and Jones 1993a). The Gaussian shaped kernel can be expressed in polar coordinates as

$$\bar{\Psi}(r,\theta) = \exp\left(\frac{r^2}{2\sigma^2(\theta)}\right). \tag{3.79}$$

The spread σ of the kernel is taken to be dependent on the angle θ and the optimization problem is solved with a gradient ascent algorithm. For the numerical computation, the squared ambiguity function in polar coordinates is interpolated from the rectangularly sampled squared ambiguity function with a bilinear interpolation. The bilinear interpolation is implemented as a sequence of two linear interpolations. The four rectangular sample points that surround a polar sample point are first used to interpolate in the ν direction along the sides of the rectangle, followed by interpolation in the τ direction.

In order to solve the optimization problem by a linear method, the kernel can only take on the values one or zero (Baraniuk and Jones 1993b). A smooth shape of the kernel is often desirable to reduce artifacts in the representation caused by the sharp cut-off at the edges of the kernel. Tapering the kernel yields formally a sub-optimal kernel. However, the linear optimization problem can be solved with considerably less computational effort than is required for a non-linear optimization technique. Moreover, if there is overlap of cross terms and auto terms, the sub-optimal kernel will not perform significantly less than an optimal one. This can be seen as a consequence of the degree of freedom that is introduced by enabling an application dependent choice of the kernel volume parameter α. A fast algorithm that solves the linear optimization problem is described in Baraniuk and Jones (1994). The algorithm is based on an iterative expansion of the kernel from the origin. In every iteration the contribution to the energy performance measure is maximized, by expanding the kernel with the sample point that has the maximum energy. By taking locally optimal steps a globally optimal solution is obtained.

An important feature of the algorithm is the discretization of the squared ambiguity function and kernel on a tree structure. The tree structure enables an efficient implementation of the non-increasing constraint (Eq.(3.77)), which was formulated in polar coordinates, on a rectangular grid. The kernel is discretized on a tree structure in the (ν,τ)-plane and the radius r is approximated as the length of the path along a branch of the tree. An example of the

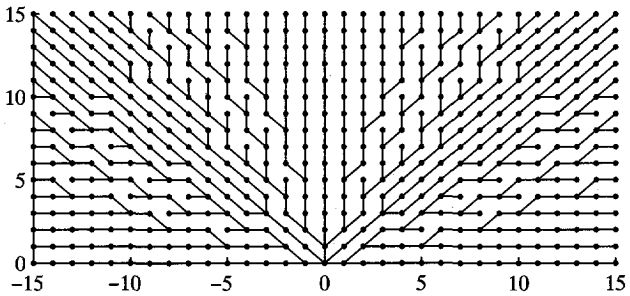

Figure 3.12: *Tree structure consisting of 31 by 16 tree nodes. The tree shown here is a minimum norm tree, which implies that the branches are chosen such that the path from a rectangular grid-node to the origin has a minimum deviation from a straight line connecting the grid-node and the origin.*

tree structure is shown in Fig. 3.12. Here, we give an example of the result of the linear optimization procedure, that has been implemented according to the Condensing Sort and Select Algorithm (CSSA) of Baraniuk and Jones (1994).

The optimal kernel for the two-component Gaussian signal of Eq.(3.55) is shown in Fig. 3.13, together with the ambiguity surface of the optimal kernel time-frequency representation. The optimal kernel time-frequency representation of the signal Eq.(3.55) is shown in Fig. 3.14. The cross terms have been suppressed without any significant loss of energy localization in the time-frequency representation.

In the next chapter the application of time-frequency analysis to the interpretation of seismic reflection data will be discussed.

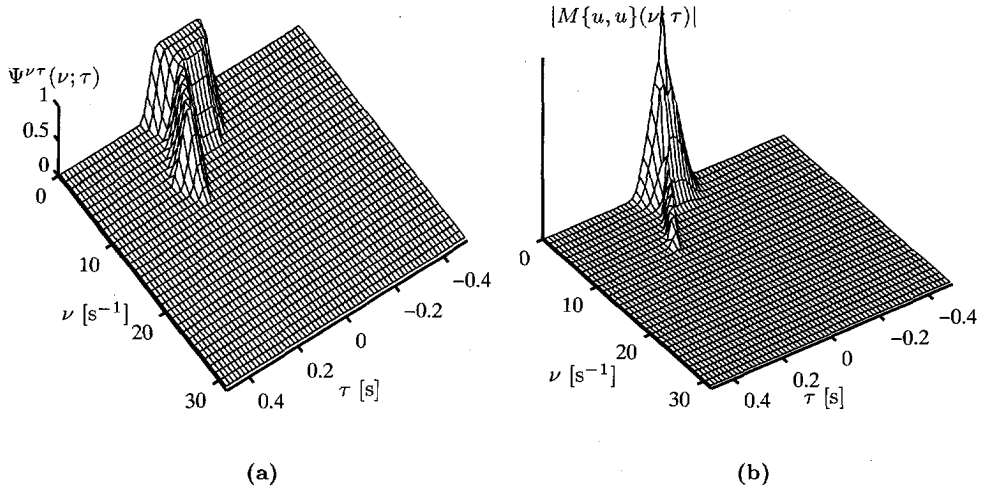

Figure 3.13: *(a) Optimal kernel and (b) modulus of the optimally weighted ambiguity function of the signal given by Eq.(3.55).*

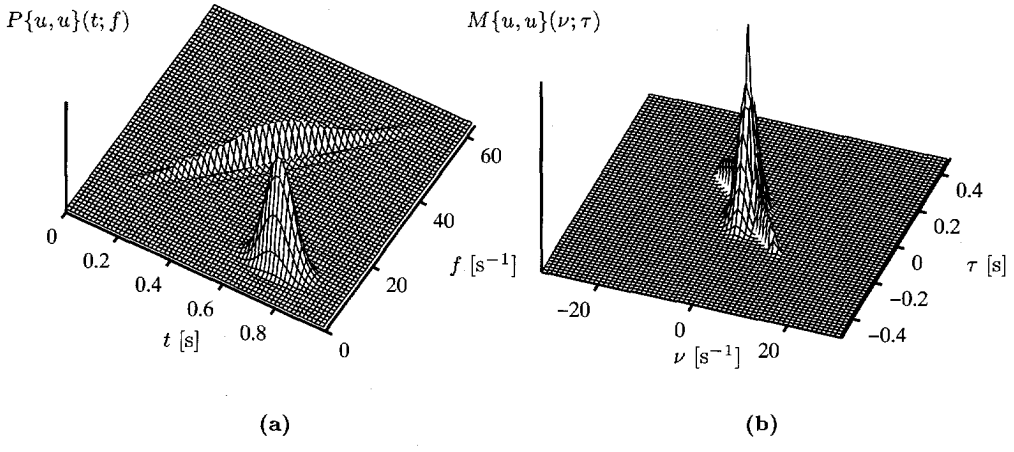

Figure 3.14: *(a) Optimal kernel time-frequency representation of the signal given by Eq.(3.55) and (b) characteristic function.*

Chapter 4

Time-Frequency Analysis and Seismic Interpretation

4.1 Introduction

In this chapter the time-frequency representation is introduced as an aid for seismic attribute extraction and seismo-stratigraphic analysis. In the first part of this chapter, it will be shown how time-frequency analysis can help in the identification and classification of seismic sequences. The second part of this chapter addresses the use of the time-frequency representation for seismic attribute extraction.

The concept of a seismic sequence is closely related to the stratification of the subsurface. This notion has been the basis for one of the most important developments in geology of the last decades: sequence stratigraphy. The development of sequence stratigraphy started as a systematic approach for the interpretation of large scale seismic profiles. In the late sixties and early seventies the use of seismic data by the oil-industry had grown considerably. With the acquisition of large quantities of good quality data, a systematic approach towards seismic interpretation had to be developed. In 1977 AAPG memoir 26 was published, in which the concepts and techniques of what is now known as seismic sequence stratigraphy were laid down. This publica-

tion had great impact in the geological community because of the relation that was proposed between seismic stratigraphy and global changes of sea-level. Nowadays, sequence stratigraphy is a method that is applied to the interpretation of a wide variety of geological data. Seismic interpretation is no longer the main field of application and the focus has shifted away to interpretation of outcrop, core and well-log data.

In this chapter we will return to the initial field of application: seismic stratigraphy. The fundamental concept behind seismic stratigraphy is that basic patterns that are observed on seismic sections can be related to sequences of geological events. Seismo-stratigraphic interpretation starts with the identification of these basic patterns in a seismic section, which results in a subdivision of the section into seismic units. The visual appearance of such a seismic unit is called seismic facies. Once these seismic units have been identified in the seismic section, the seismic facies of each unit is described on the basis of the signatures of the seismic events within the unit. These properties may concern the general character of the events, such as continuity and amplitude. However, local features, such as reflection truncations or lap-outs are important in a seismic facies description as well.

In Section 4.4 the time-frequency representation of the signal is proposed as a method for seismic facies analysis. In a time-frequency display the two major parameters that characterize the seismic facies - amplitude and frequency - are combined into one display. This combined display is particularly useful for bringing forward the characteristics of the reflection pattern and how they change within the unit.

In Section 4.6 the time-frequency is taken as the point of departure for seismic attribute analysis. It will be shown that existing methods, such as complex-trace attribute analysis (Taner et al. 1979), can be greatly improved upon by considering the attribute extraction in the context of joint time-frequency analysis.

We will start with a brief discussion of the subsurface model that is the basis of seismic sequence stratigraphy.

4.2 The subsurface model for seismic stratigraphy

Through the years, the analysis of large quantities of seismic data has resulted in detailed sequence models for a variety of depositional environments.

Many detailed descriptions of the methods that can be applied to infer depositional environments from seismic data have been published. Overviews of the seismic stratigraphic principles and methods are given in Vail et al. (1977), Sheriff (1980) and Hardage (1987). In the following, we will address some aspects of seismic stratigraphy that are relevant in the context of time-frequency analysis of seismic data.

At the basis of seismic sequence analysis is a model of a stratified subsurface. The nature of this stratification and the presence of appreciable contrasts in acoustic impedance are the link between the seismic unit and its associated depositional system. Frequency analysis of seismic data is a way to extract information about the cyclicity in the succession of seismic events. With the proposition that seismic events can be related to the depositional surfaces, the frequency information present in the data can be related to subsurface stratification. Hence, if certain assumptions about the nature of seismic reflection data are made (see Section 4.3), we expect to be able to infer how the stratification changes as a function of seismic travel time by means of a local frequency analysis.

The stratigraphic model for seismic analysis is one of time-stratigraphic units and the proposition is made that the section can be broken into such units based on seismic observations. A time-stratigraphic unit is a three-dimensional set of facies deposited contemporaneously as parts of the same system. The different facies within the unit genetically linked by depositional processes and environments. Different portions of the depositional unit are made of different mixes of grain sizes and lithology. This is caused by the fact that the unit may be the product of several sedimentary processes. A time-stratigraphic unit may also be called a depositional sequence.

Because it is determined by a single criterion, i.e. the physical relation of the strata themselves, the depositional sequence is useful in establishing a stratigraphic framework. The depositional sequence is not primarily dependent rock types, fossils, depositional processes or other criteria that may vary within a given sequence. A depositional sequence is time-stratigraphic significant because it was deposited during a given interval of geologic time limited by the ages of the sequence boundaries, in case these boundaries are conformities. However, if the boundaries are unconformities, the age range of the strata between the sequence boundaries may differ from place to place.

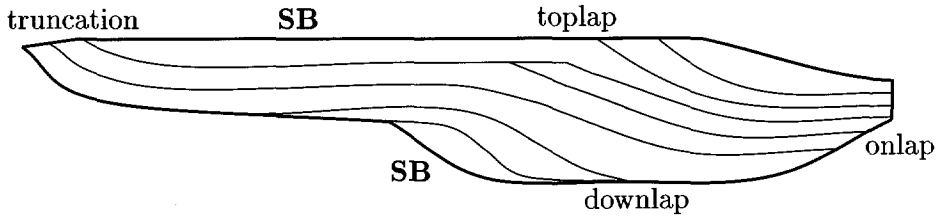

Figure 4.1: *The basic seismic sequence and seismic reflection terminations within the idealized sequence (from Mitchum et al. (1977)). SB denotes the sequence boundary.*

The type of boundary that qualifies as a sequence boundary has been continuously under discussion (see Schlager 1991). This discussion is not relevant in the present context, but it should be noted that the term seismic sequence is used in the sense of the original definition that was given by Mitchum et al. (1977). In the original definition, a seismic sequence is a depositional sequence identified on a seismic section. It is a relatively conformable succession of reflections, interpreted as genetically related strata. This succession is bounded at its top and base by surfaces of discontinuity marked by reflection terminations and interpreted as unconformities or their correlative conformities.

Figure 4.1 shows the prototype of a seismic sequence. The sequence boundary, denoted by **SB**, is an unconformity or its correlative conformity. Within the sequence there are stratal bedding surfaces that can be characterized by the nature of their reflection terminations. Some possible types of reflection terminations are given in the figure. Seismic sequences have all the properties of depositional sequences, provided that these properties may be recognized and interpreted from the seismic reflection data.

A reflection sequence can be described with properties such as the configuration, continuity, amplitude and frequency of the events. Reflection configuration reveals the gross stratification pattern, from which depositional processes, erosion, and paleo-topography can be inferred. Reflection continuity is closely associated with the continuity of strata; continuous reflections suggest widespread, uniformly stratified deposits. Reflection amplitude contains

information on the impedance contrasts of individual interfaces and their spacing. It is used to predict lithologies and occasionally pore-fill properties.

The frequency content is primarily determined by the bandwidth of the outgoing seismic pulse and the absorption characteristics of the subsurface. However, the variations within this band are primarily the result of the spacing of reflectors or a strong lateral change in interval velocity. This variation of frequency content due to the stratification pattern will be the main object of study in the following section. First, we will discuss how the description of seismic facies may be incorporated in a signal analysis framework. In order to do so, we first discuss the relation between the subsurface model and the observations that can be made in a migrated seismic section.

4.3 A signal analysis view on seismic facies

In the following sections we will focus on those aspects of the seismic facies that can be related to the time-varying spectral content of the seismic signal. In this chapter we will confine ourselves to a one-dimensional description. The two-dimensional local spectrum analysis is the subject of Chapters 5 and 6. Table 4.1 gives a summary of the reflection parameters that are used in a seismic facies description. The first and third column are taken from Mitchum et al. (1977, Table 2). The parameters given in the first column are widely used as the point of departure in seismo-stratigraphic interpretation. The second column gives the signal parameters that are proposed to quantify these seismic facies parameters. The signal parameters mentioned here are by no means the only measures that can be used for a quantitative analysis. We only give those signal attributes that can be extracted from a local power spectrum of the data. Other, perhaps even more significant parameters, such as velocity, density and amplitude versus offset behaviour, have to be extracted from the data by an inversion process, which is beyond the goal of the signal analysis techniques discussed in this thesis.

In order to connect the parameters that can be extracted by signal analysis to the subsurface model some assumptions and simplifications have to be made with regard to the physics involved in a seismic experiment.
The first corollary is related to the physical model that links the seismic sequence to stratification. It is assumed that the seismic reflection data represent a band-limited reflection coefficient sequence. This is a strong as-

Seismic facies parameters	**Signal attributes**	**Geologic interpretation**
Reflection configuration	*Temporal frequency*	Stratification pattern
	Dip angle	Depositional process
		Erosion and paleo-topography
		Fluid contacts
Reflection continuity	*Change of temporal frequency and phase*	Bedding Continuity
	Dip bandwidth	Depositional process
Reflection amplitude	*Amplitude*	Impedance contrast
		Bed spacing
		Fluid content
Reflection frequency	*Temporal frequency*	Bed thickness
	Temporal bandwidth	Fluid content
Interval velocity	*N.A.*	Estimation of lithology
		Estimation of porosity
		Fluid content
External form and areal association of seismic facies units	*Dip angle*	Gross depositional environment
	Dip bandwidth	sediment source
		Geologic setting

Table 4.1: *Seismic facies parameters, signal attributes and their geological significance (columns 1 and 3 from Mitchum et al. (1977, Table 2)).*

sumption, as we know that seismic data we measure at the surface is generally quite remote from a primary-only, acoustic, reflection response. Many other wave phenomena are present in our data, such as multiple reflections, energy conversions from longitudinal to shear waves and an-elastic effects giving rise to attenuation and dispersion. The goal of seismic pre-processing and migration is to remove all wave phenomena, other than the specular reflections from impedance contrasts. Hence, the assumption can be phrased differently by saying that it is assumed that the seismic processing did its work and the time-frequency representation of our data is a good approximation of the time-frequency representation of the subsurface reflection response. As there is a one to one time-depth relation between the time and depth reflectivity functions, we assume that an event that is localized in time in the time-frequency representation of the data is an expression of the stratification of impedance at the corresponding depth.

The second corollary pertains to the method that is used for modelling of the seismic response. The synthetic examples in the section were generated using a plane-wave modelling scheme based on the reflectivity method (Fuchs and Müller 1971; Fokkema and Ziolkowski 1987). The input model is that of a layered earth, where the layers are bounded by impedance discontinuities. Gradual changes in impedance are therefore approximated by replacing them by thin layers with small reflection coefficients between them. Although this is not a trivial step, it will be shown that in the cases presented here the assumption of a layered earth leads to synthetic seismic data that can closely match the measured data. The examples all represent the vertical incidence response, which precludes the presence of angle dependent effects and longitudinal to shear wave energy conversion. However, internal multiple reflections have been included in the modelling.

4.4 Topology of the time-frequency representation of a seismic sequence

In this section we will discuss the observations that can be made from a time-frequency representation of a seismic section that has been migrated. First, the time-frequency representations that were introduced in Chapter 3, will be discussed in the context of seismic sequence analysis. In the second part of this section, some types of seismic sequences are discussed and how time-frequency analysis can help to identify them in seismic data. In order

to facilitate our discussion we first make some remarks about the domain allocation of signal components in the time-frequency representation and its Fourier transformation: the characteristic function. Figure 4.2 illustrates the distinction we make between four types of signal components. The characteristic function is shown only for positive frequency-shifts, as the domain allocation for the other half of the (ν, τ)-plane can be derived from the symmetry with respect to the origin.

The first type are impulse-like signals, denoted with ❶ in the figure. In the time-frequency representation the energy of this type of component is well localized in time, but extends over a large range of frequencies. In the characteristic function, the energy is located near the frequency-shift axis, extending over a large range of frequency-shifts.

The second type of component is a sinusoid or a purely harmonic component, denoted by ❷. The energy of a sinusoidal component is localized at a single frequency in the time-frequency plane. In the characteristic function these components are found parallel to the time-shift axis and extend over a large range of time-shifts.

The frequencies of the third and fourth type of component, denoted by ❸ and ❹, change with time. Although they extend over a large time and frequency range, their energy is well localized near a ridge in the time-frequency plane. The component of type 3 has an increasing frequency as a function of time. In the characteristic function the energy of these components is found in the area occupied by positive time-shifts. The components of type 4, with a frequency that decreases as a function, can be found in the area that is occupied by negative time-shifts. In the following we will we show how these types of components can be related to the signal structure of a seismic sequence.

Our model of a seismic sequence is based on the observation that a seismic reflection profile on the scale of several hundreds of meters consists of a limited number of strong reflections. Between these major boundaries one usually observes a seismic reflection pattern that result from closely spaced impedance contrasts that cannot be resolved individually. The strong reflections are associated with sequence boundaries and the interference composites determine the seismic facies. An idealized model of this type of impedance distribution is shown in Fig. 4.3, together with the seismic reflection response

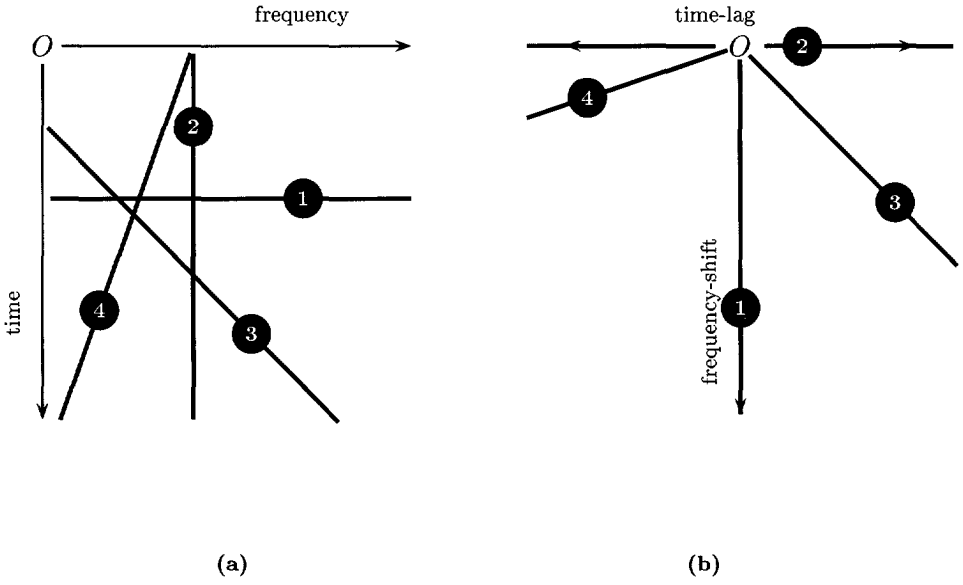

Figure 4.2: *Classification of signal components in the time-frequency plane. (a) time-frequency domain (b) characteristic function, the numbers are explained in the text.*

to the model. The model is that of a layered sequence in between two homogeneous layers. The mean velocity of the sequence is 2000 [m/s]. The velocity fluctuation consists of two components. The first type of component of the velocity function consists of two harmonic with an amplitude of 50 [m/s] and a spatial frequency of 0.1 [m^{-1}]and 0.125 [m^{-1}]. The second component has an amplitude of 50 [m/s] and a spatial frequency that increases with depth at a rate of 0.0003 [m^{-2}]. In the depth model the density has been kept constant at 1000 [kg/m^3]. Note that the time image of the reflection pattern does not reveal the nature of the stratification. In Fig. 4.4 the amplitude spectrum of the source signal and the seismic reflection response are shown. The spectrum of the seismic response shows two peaks at frequencies 100 [s^{-1}]and 125 [s^{-1}], related to the harmonic components of the stratification. Apart from these two peaks, the shape of the amplitude spectrum of the seismic reflection response follows that of the source pulse.

The Wigner distribution of the reflection pattern is shown in Fig. 4.5. The three components of the stratification and the boundaries of the sequence show up as separate entities in the time-frequency plane. The strong reflec-

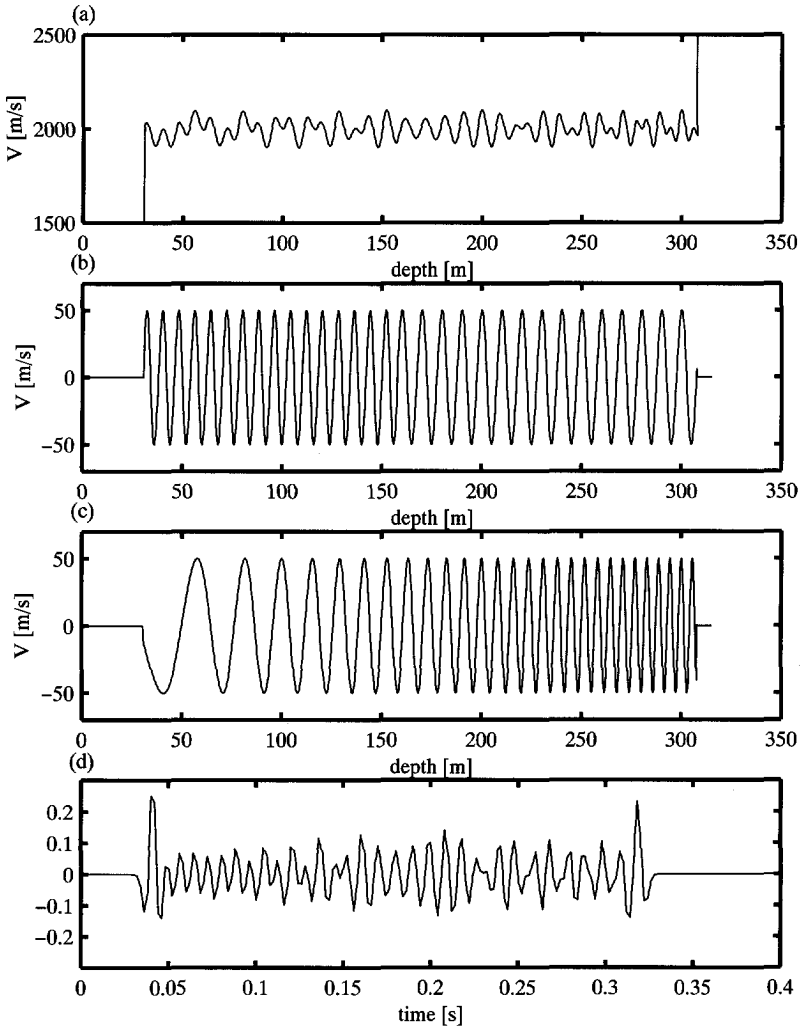

Figure 4.3: *(a) Velocity model (b) first component of the velocity fluctuation (c) second component of the velocity fluctuation (d) seismic reflection response.*

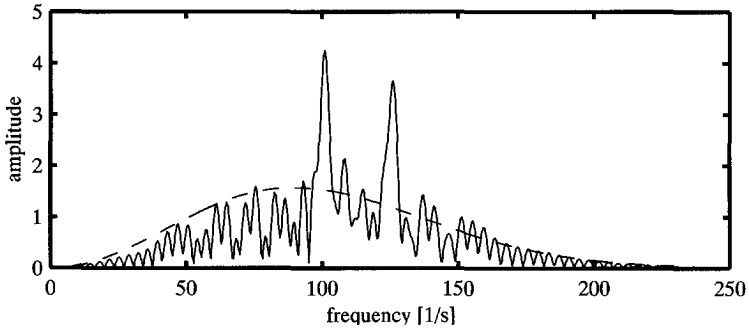

Figure 4.4: *Amplitude spectrum of the seismic reflection response of Fig. 4.3d (solid line) and amplitude spectrum of the source wavelet (dashed line).*

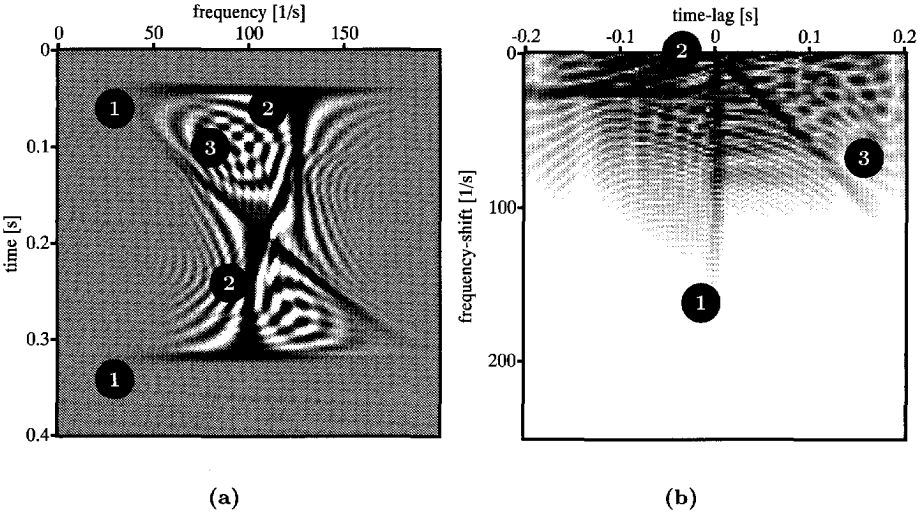

Figure 4.5: *Wigner distribution and ambiguity function of the reflection pattern.*

tions from the top and base of the sequence are visible as two impulse type components (denoted by a 1 in the figure). The energy that is reflected on two harmonic components (2) is located on a ridge at frequencies 100 $[s^{-1}]$ and 125 $[s^{-1}]$. The linear increase of frequency with depth of component (3) results from the increase of spatial frequency with depth of the third component of the velocity fluctuation.

For more complicated signals it will be hard to distinguish cross term energy between the components from the energy that can be attributed to the components themselves. Consequently, it may not be feasible to interpret a Wigner distribution in terms of individual signal components. Since it is our aim to interpret seismic facies in terms of the localization properties of seismic reflection patterns in the time-frequency plane, cross term suppression will be an important property when considering other kernels for the time-frequency representation.

Using a particular kernel does not only result in cross term suppression, but implies the enhancement of certain signal components at the cost of suppressing others as well. Depending on the goal of the analysis, a certain type of time-frequency representation will perform best. For instance, the extraction of cyclic events from the seismic data can be improved by suppression of impulse type signals from the time-frequency representation. A kernel that suppresses energy around the frequency-shift axis in the characteristic function, will favour type 2 and type 3 components in the signal, at the cost of the impulse-like components. The following examples illustrate the type of information that is brought forward by different choices for the kernel. The time-frequency representations we show here were discussed in the context of the general class of time-frequency representations Sections 3.4 and 3.5.

The kernel of the spectrogram (Section 3.4.4) has a fixed size in the ambiguity domain. This size is determined by the time length of the window (Fig. 4.6b). Using a short time-window and implicitly high time resolution is equivalent to a kernel that is concentrated around the ν-axis in the characteristic function. Increasing the frequency resolution by lengthening the time window goes to the expense of time resolution. The window used here is a compromise between time and frequency resolution. The result is a time-frequency representation in which all components are clearly visible but with considerable less time and frequency resolution than in the Wigner distribu-

tion. For more complicated signals the absence of cross terms will be a clear advantage of the spectrogram. However, the smoothing that is performed by the spectrogram kernel will make it difficult to make a distinction between the signal components for more complicated signals. For the signal model that we adopted here, a kernel that preserves the resolution of the Wigner distribution while at the same time suppresses the cross terms would provide us with an ideal time-frequency representation.

The cone-kernel time-frequency representation is shown in (Section 3.4.3) Fig. 4.6b. Since its kernel is zero along the frequency-shift axis and consequently suppresses impulse-like components, the cone-kernel representation is very well suited for extracting the harmonic components from the signal. The fact that it does not smooth impulses, as the spectrogram does, but suppresses them makes it a very effective time-frequency representation to localize rapid transitions in frequency. This can be clearly observed in the time-frequency representation of the synthetic sequence, where the transition between the two harmonics can be very well localized in time.

The Choi-Williams kernel (Section 3.4.2) suppresses energy that is located away from the ν and τ axes (Fig. 4.6c). Consequently, both impulses and sinusoids are enhanced while the energy of a component whose frequency changes with time will be reduced. However, in the Choi-Williams representation the cross terms between the components are greatly suppressed, since the energy of the cross terms is located away from origin in the characteristic function domain. This property, together with the fact that it satisfies the marginal property makes it an attractive alternative for the Wigner distribution. The Choi-Williams representation has the advantage that the time that is needed for its computation is much less than for a signal adaptive kernel, which we will discuss next.

Superior results are achieved by adapting the kernel of the representation to the signal (Section 3.5). Figure 4.6d shows the time-frequency representation that results if we use a Gaussian shaped kernel that is adapted to the signal. The kernel is adapted for each time sample, which results in a time-dependent optimum kernel time-frequency representation. The characteristic function clearly shows that the optimum kernel time-frequency representation effectively suppresses cross terms, while retaining excellent time-frequency resolution. However, the transition between the two harmonic components can

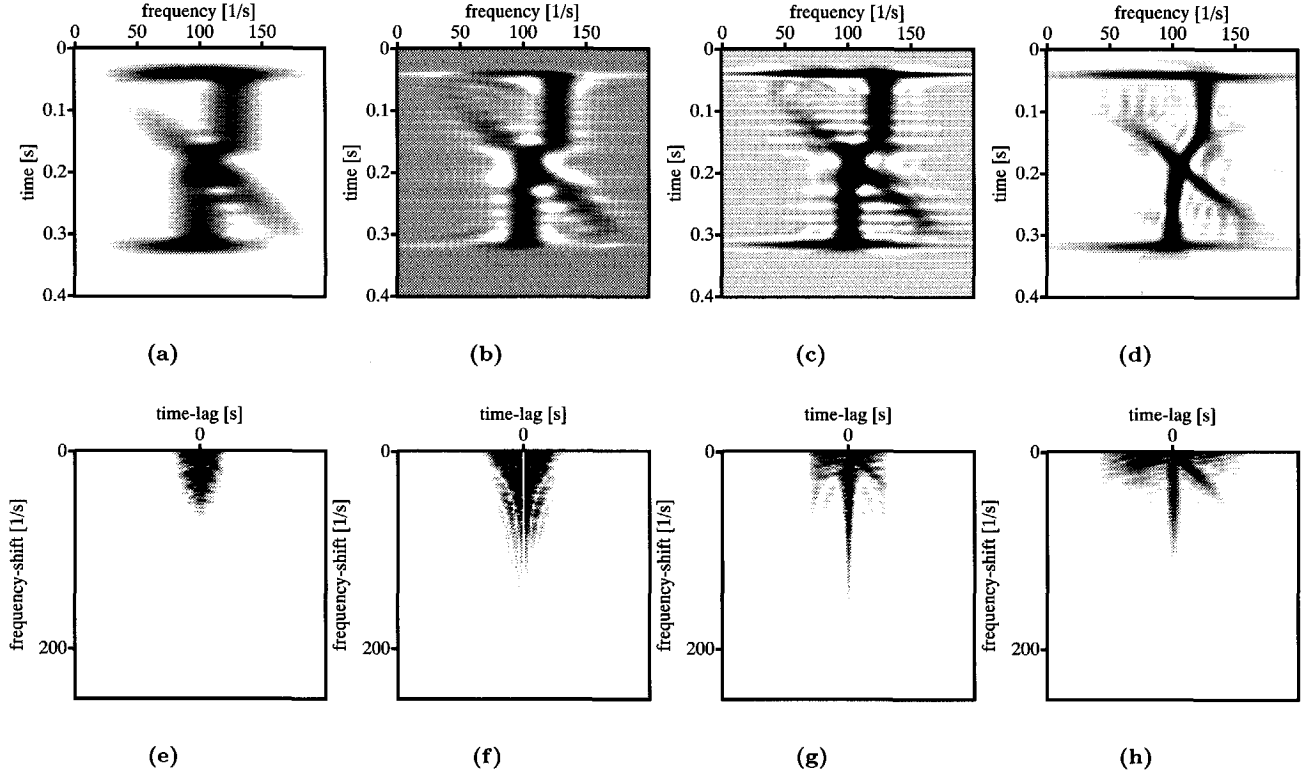

Figure 4.6: *Time-frequency representations of the seismic reflection pattern and (below) their associated characteristic function; (a) and (e) spectrogram ; (b) and (f) Cone kernel; (c) and (g) Choi-Williams representation; (d) and (h) Optimum kernel time-frequency representation.*

be less well localized in time than in the cone-kernel representation.

The examples given above serve as a handle for the interpretation of a time-frequency representation of a seismic sequence. The purpose of the discussion was to illustrate that the choice of a particular kernel depends on the type of information one wants to extract from the signal. When interpreting a time-frequency representation one must keep in mind that the kernel function is reflected in the type of information that is observed. To illustrate the main point of the previous discussion, we show three time-frequency representations of a trace from a marine seismic data set (Fig. 4.7). The properties of the kernels have been chosen such that their characteristics are brought forward in an extreme way. Choosing the kernel sizes the same for each time-frequency representation would lead to a closer resemblance of the results.

We observe in all three time-frequency representations that there is a general decrease of frequency as a function of time. The spectrogram which was obtained using a short time window, shows the signal as a succession of distinct reflections. Some frequency variation is visible between the reflectors, but the general appearance is that of well time-localized events that extend over a broad range of frequencies. The cone-kernel representation shows a completely different signal structure. The energy is now localized on narrow frequency bands with a broad time extent. Hence, we observe that the cone kernel brings forward the cyclicities that are present in the signal. The time-adaptive optimum kernel representation effectively brings forward a wide variety of signal components. Several of the basic signal components that were observed in the synthetic sequence model can also be recognized in the real data. The results show that adapting the kernel to the signal in contrast to enforcing a fixed kernel on the signal, leads to what appears an unbiased view of the time-frequency structure of the signal. For that reason, an adaptive kernel time-frequency representation is preferred in the analysis of seismic sequences.

4.4.1 Seismic sequences

Figure 4.7 shows that we can clearly distinguish separate basic signal components in the time-frequency representation of a real seismic signal. The synthetic example of the previous section showed that we can generate these components in the seismic response introducing the same type of components

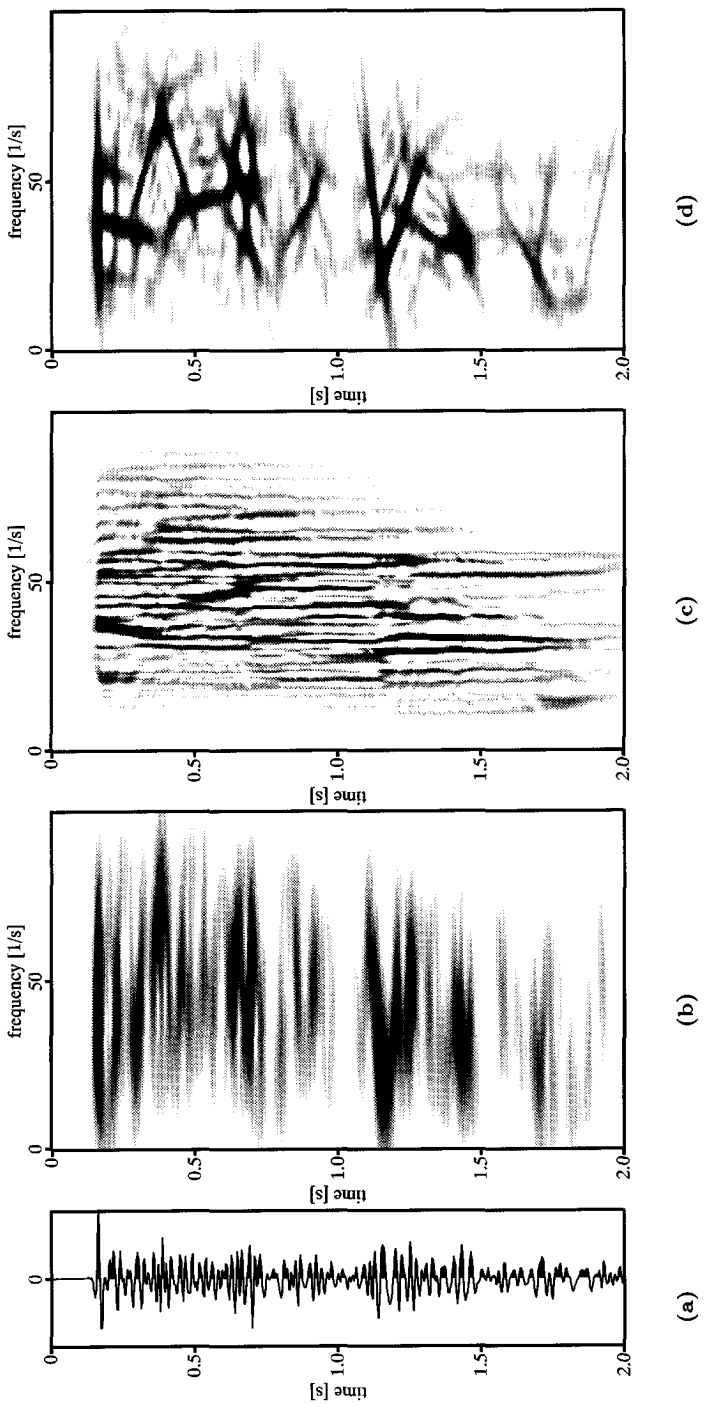

Figure 4.7: *A seismic trace from a marine seismic section (Alboran Sea), spectrogram with window length 0.064 [s], cone-kernel representation with cone length 1 [s] and time adaptive optimal Gaussian kernel representation. Only the positive values of (b) and (c) are shown.*

into the depth model as building blocks of the impedance stratification. Some additional modelling results are presented here with the purpose to illustrate the use of the time-frequency representation as a template for the interpretation and validation of seismic sequence interpretation. In stratigraphic modelling it is hardly ever possible to obtain synthetic seismic data that closely match real data. As was shown in the previous section, the time-frequency representation provides a good tool to extract information on the gross pattern of stratification.

In Fig. 4.8 four one-dimensional impedance models are shown together with their vertical incidence seismic response and their optimum kernel time-frequency representation.

The response to the reflectivity was modelled in the frequency domain and then band-limited with a 70 [s^{-1}] Ricker wavelet. Internal multiples were taken into account in the modelling. Each of the models has a first layer with a thickness of 200 [m] on top. Velocity and density in the first layer of the model are 1500 [m/s] and 1000 [kg/m^3].

The first sequence has layers of constant thickness of 6 [m]. The velocity of the layers alternates between 1625 [m/s] and 1675 [m/s]. This type of sequence is also known as a binary sequence. A set of two layers is called a motif. The reflected signal from this type of sequence is narrow-band around the frequency of the response to one motif and integer multiples of this frequency. In this case the temporal frequency of one motif is around 68 [s^{-1}]. Higher frequency bands are not observed because they are outside the frequency band of the source pulse. Although this is not immediately apparent in the time-frequency representation shown here, the transfer of energy from primary to multiple reflections results in an attenuation of the primary pulse and delay of the arrival of energy. An elaborate discussion of the seismic response to this type of sequence can be found in Morlet et al. (1982).

The second sequence consists of 50 layers with randomly distributed thicknesses and velocities. The mean thickness is 3 [m] and the maximum deviation of the (uniform) random component of the thickness is 2 [m]. The velocity is 1650 [m/s] with a maximum deviation of 130 [m/s]. Density was taken proportionally to the velocity. The random thicknesses and velocities

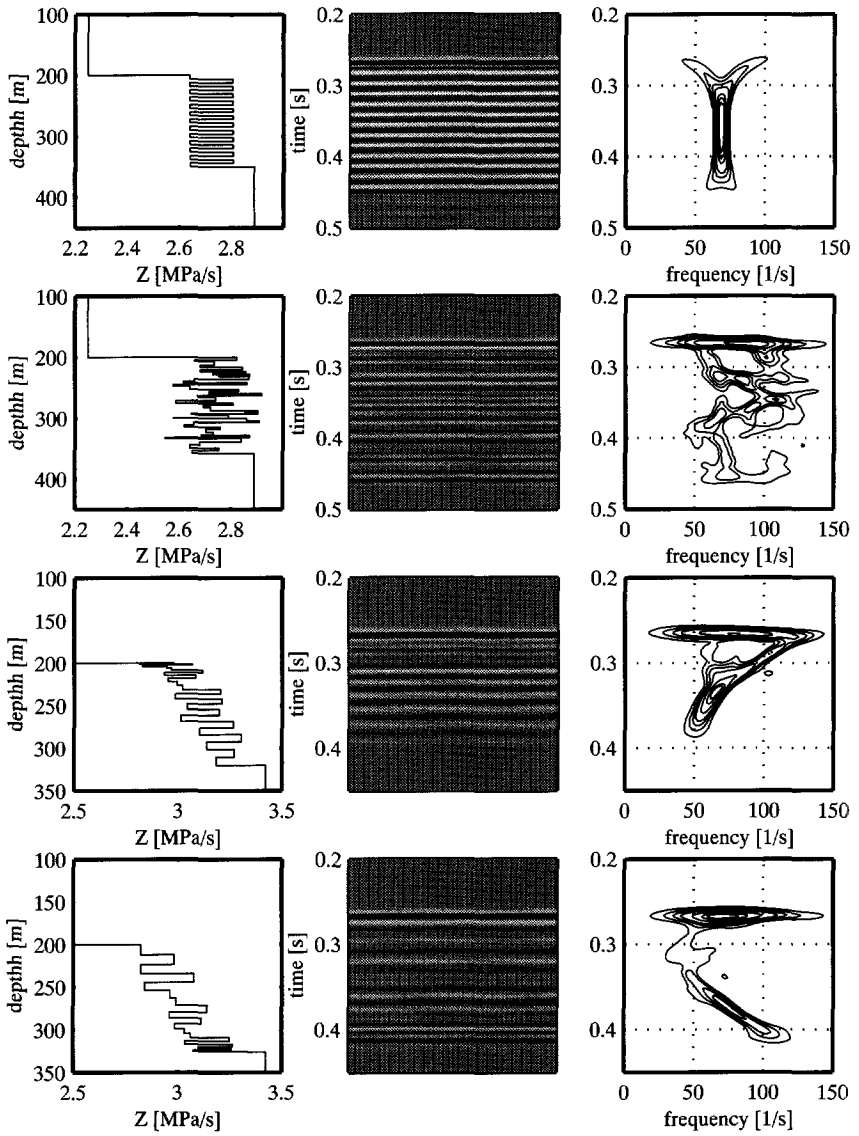

Figure 4.8: *(left) Seismic sequence models, (middle) their seismic reflection response and (right) time-frequency representations of the seismic response (time adaptive Gaussian kernel).*

result in a time-frequency representation of the reflection pattern with no evident relation between time and frequency localization of the energy.

The third and fourth sequences are a combination of Gaussian distributed, alternating velocities, superposed on a linear velocity gradient. Their main feature is an increase of layer thickness with depth for the third sequence and a decrease of layer thickness with depth for the fourth sequence. Both models consist of 25 layers with thicknesses ranging between 0.5 [m] and 12 [m]. In sequence 3 the thickness of the layers increases with depth and this model may serve as a model for a depositional sequence in which the rate of sedimentation decreases with geologic time. The thickness of layers in the fourth sequence decreases with depth, as would happen in the case sediment input increases as a function of geologic time.
The change of layer thickness gives rise to frequency tuning of the response towards the frequency of the (time) thickness of the layering. As a result, these gradual changes in layer thicknesses can be recognized in the time-frequency representation of the seismic signal as a change of frequency content as a function of seismic travel time.

We observed in the synthetic examples that the contribution of the stratification of the impedance to the frequency content of a reflected signal is elicited by the time-frequency representation of the data. The time-frequency representation effectively maps the reflection response into an time-frequency pattern from which the reflection configuration can be interpreted more easily than from the time image.

Figure 4.10 shows the time section from 0 - 1 [s] of a part of a seismic profile from the Alboran Sea. A standard marine seismic data-processing sequence was applied to the data, followed by FK migration. In figure 4.9 the time frequency representations of the first and last trace of this section are shown. In the upper 0.5 [s] we can distinguish three components in both time-frequency representations. The resemblance of the upper part of the two time-frequency representations indicates that the properties of the signal remain fairly constant over a large spatial range. In a seismic facies interpretation we can infer from the time-frequency representation that the upper 0.5 [s] of the section can be characterized by continuous events with little change of reflector spacing as a function of lateral distance. The first component is the reflection from the strong sea bottom, which shows up

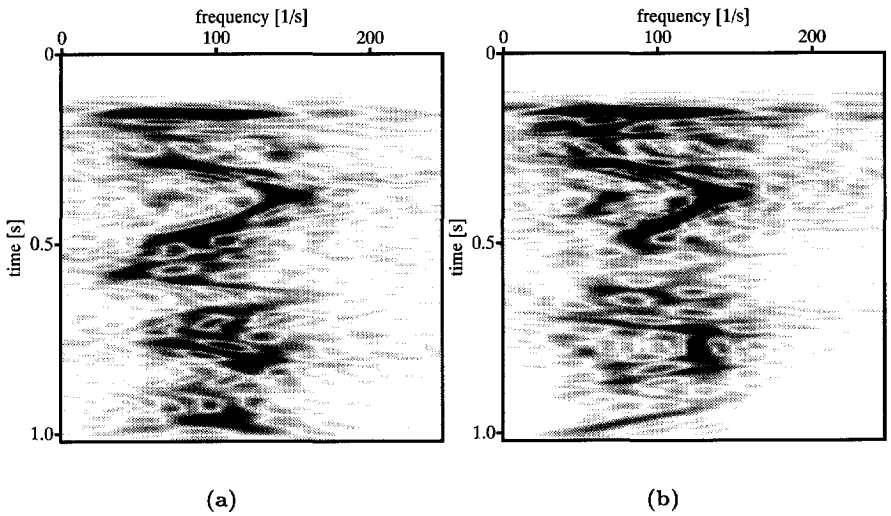

Figure 4.9: *(a) Time-frequency representation of the first trace of the seismic section of Fig. 4.10 and (b) time-frequency representation of the last trace (time adaptive CSSA kernel).*

as an impulse-like event in the time-frequency plane. Below the sea-bottom reflector we observe an increase of frequency with time until about 0.35 [s]. At 0.35 [s] there is an abrupt change and a decrease of frequency time occurs until 0.5 [s]. Below 0.5 [s], the energy is less well localized in the time-frequency representation indicating a more random stratification. The localization of energy in the lower part of the first trace is clearly different than in the last trace. This difference can be attributed to a change of bed spacing with offset. Hence, an evaluation of time-frequency representation results in a division of the seismic section into two seismic units. In the upper unit we can distinguish three separate components, which results in a further division of the upper unit into three sub-units.

Although the time-frequency representation itself provides a clear display of seismic facies characteristics, it will be difficult to use in a routine seismic facies analysis. Computing the time-frequency representation for each trace in a seismic section results in a three-dimensional data volume. The size of this data volume will clearly complicate the interpretation of the time-frequency representation. However, we can attempt to reduce the amount of data by describing the time-frequency representation with a limited number

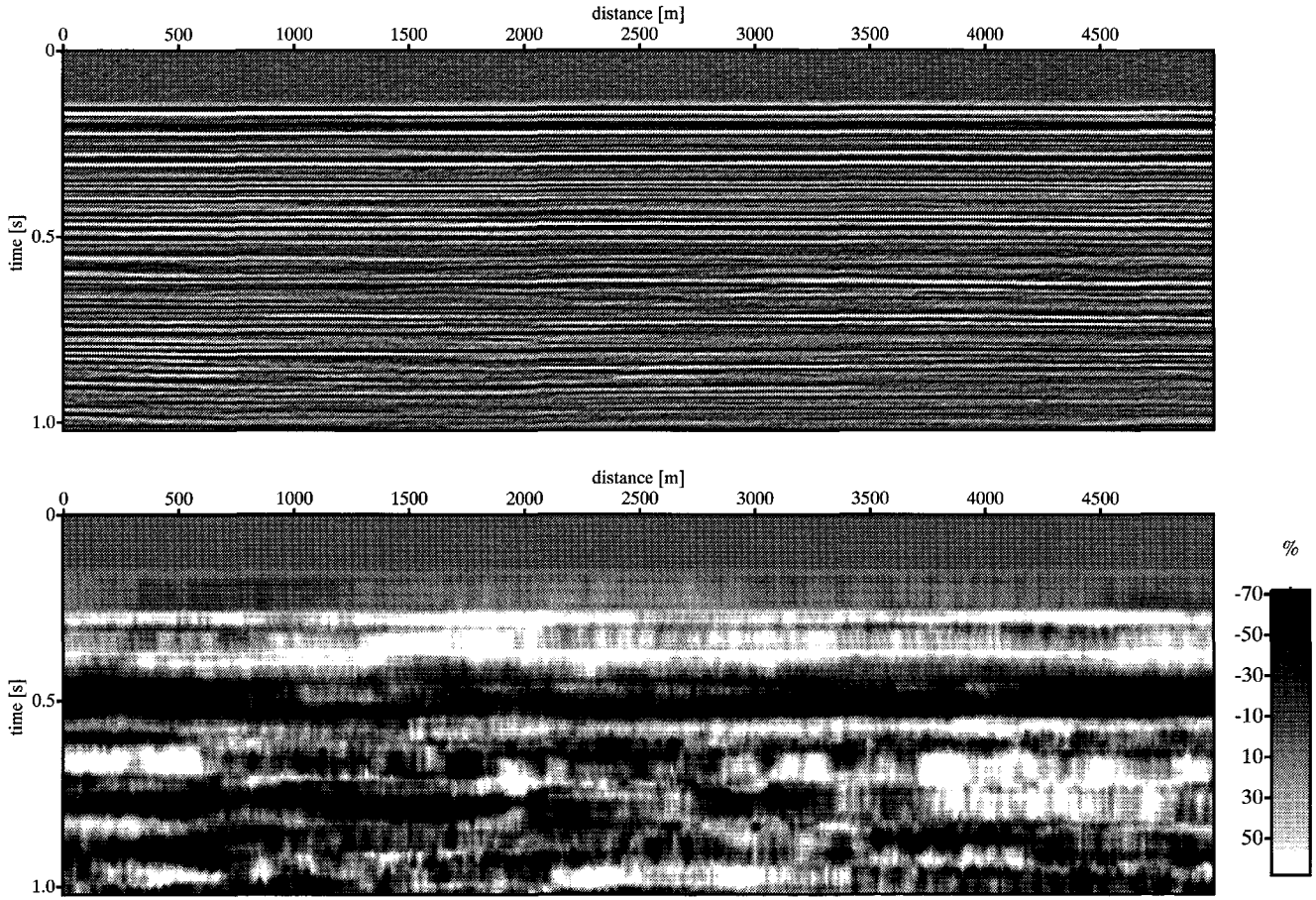

Figure 4.10: *(top) Migrated seismic section Alboran Sea and (bottom) relative amounts of energy with increasing frequency as a function of time (70 % = white) and decreasing as a function of time (70 % = black).*

of parameters. For example, we can attempt to divide the time-frequency representation into components with an increasing frequency as a function of seismic travel time and components that show a decrease of frequency as a function of time. We can separate these components in the characteristic function of the time-frequency representation, since these two types of components occupy different half-planes in the (ν, τ)-domain (cf. Fig. 4.2). Once we have separated the two types of components, we can map them into a one-dimensional parameter, that gives the relative contribution of each component type as a function of time and offset. The result is plotted below the seismic section in Fig. 4.10. The darker the color, the more energy is found in components that have a decreasing frequency as a function of travel time. We can now clearly distinguish the two units. The upper unit shows little spatial variation and the three sub-units can be clearly distinguished. The frequency remains fairly constant in the first 0.15 [s], there is an overall increase in frequency between 0.15 [s] and 0.35 [s] and decrease between 0.35 [s] and 0.5 [s]. The lower unit shows large variation as a function of offset and time, indicating a less pronounced stratification pattern.

Jarado and Comas (1992) consider the seismo-stratigraphic interpretation of seismic reflection data from the same region. The part of the section shown here coincides with their facies unit I, consisting of sediments of Pliocene to recent age. They divide the unit into two sub-units that are separated by an unconformity. The result of the time-frequency analysis confirms this division and adds a further refinement by the subdivision of the upper unit.

4.5 Synthesis of time-frequency components from the Wigner distribution

The previous analysis of seismic data in terms of time-frequency components is an effective way for studying seismic facies characteristics. Seismic sequences can be identified and interpreted by evaluation of the localization of energy in a time-frequency representation of the data. In this section we will take a closer look at the decomposition of a signal into its time-frequency components. We will discuss the synthesis of a time signal from a time-frequency component in the Wigner distribution. The ability to reconstruct the time signal form its time-frequency representation is not a prerequisite for the interpretation of the signal in terms of time-frequency localization of

energy. However, reconstruction of the time signal can be used as a check on interpretation of a time-frequency representation.

The bilinearity of the Wigner distribution and other time-frequency representations from Cohen's class is a major drawback if one considers using the time-frequency representation for time-variant filtering and time-frequency decomposition. However, the high resolution of the bilinear time-frequency representations gives them an advantage above linear time-frequency representations, such as the wavelet transform or sliding-window Fourier transforms.

The Wigner distribution in itself is invertible (see Section 2.3). With an inverse Fourier transformation of the Wigner distribution the local auto-correlation function is obtained. A signal can be reconstructed from the local auto-correlation function up to a constant phase (Eq.(2.77)). The problem arises, if one wants to synthesize signals from a region of the time-frequency plane. For instance, to apply a time-variant frequency filter, the Wigner distribution $W\{u,u\}(t;f)$ is masked by a time-frequency window $w(t,f)$, i.e.

$$\bar{W}(t;f) = w(t,f)W\{u,u\}(t;f). \tag{4.1}$$

By the weighting operation a time-frequency function $\bar{W}(t;f)$ of the modified signal $v(t)$ is obtained. This time-frequency function usually is not a Wigner distribution. The reconstruction of the modified signal, $v(t)$, can be formulated as an optimization problem, which results in an orthogonal projection (Hlawatsch and Krattenthaler 1992). The orthogonal projection results in an approximation of $\bar{W}(t;f)$ by a time-frequency function, $W\{v,v\}(t;f)$, that is a valid Wigner distribution.

The projection method is discussed by Hlawatsch and Krattenthaler (1992) for continuous signals. An algorithm to solve the projection for discrete signals has been derived by Boudreaux-Bartels and Parks (1986). The discrete algorithm is similar to algorithms that are used for the synthesis of a signal from its ambiguity function (Sussman 1962). The goal of the projection method is to minimize the approximation error. The approximation error is defined as the energetic difference between the time-frequency function $\bar{W}\{v,v\}(t;f)$ and a valid Wigner distribution $W\{v,v\}(t;f)$, given by

$$\epsilon_v^2 = \int_{t\in I\!R} \int_{f\in I\!R} \left|\bar{W}(t;f) - W\{v,v\}(t;f)\right|^2 \mathrm{d}t\mathrm{d}f. \tag{4.2}$$

The minimization of this error takes place in the local auto-correlation domain. The problem is then given as the synthesis of a signal from a function $\bar{R}(t;\tau)$ that is closest to a valid local auto-correlation $R\{u,u\}(t;\tau)$. The modified auto-correlation function found by an inverse Fourier transformation of the function $\bar{W}(t;f)$, i.e.

$$\bar{R}(t;\tau) = \mathcal{F}_f^+ \left\{ \bar{W}(t;f) \right\}. \tag{4.3}$$

In order to find the signal that has an local auto-correlation that is closest to $\bar{R}(t;\tau)$, the modified auto-correlation function is first expressed as the local auto-correlation of a sum of orthonormal eigenfunctions, (Hlawatsch an Krattenthaler 1992), i.e.

$$\bar{R}(t;\tau) = \sum_{k=1}^{\infty} \lambda_k R\{u_k,u_k\}(t;\tau), \tag{4.4}$$

with λ_k the eigenvalues and u_k the associated eigenfunctions. The signal that has a Wigner distribution that is closest to $\bar{W}(t;f)$ is now given by

$$v(t) = \exp(\mathrm{j}\phi)\sqrt{\lambda_1}u_1(t), \tag{4.5}$$

where λ_1 the largest eigenvalue and $u_1(t)$ its associated eigenfunction The approximation error equals

$$\epsilon_v^2 = \sum_{k=2}^{\infty} \lambda_k^2. \tag{4.6}$$

The synthesis of a signal component from the Winger distribution is performed with a five step procedure:

1. first, the component is isolated in the (t,f)-plane by applying a mask function $w(t,f)$.
2. The next step is an inverse Fourier transformation of the (t,f)-component over the frequency in order to obtain the (t,τ)-domain representation of the component.
3. This is followed by an eigenvalue decomposition of the (t,τ)-representation.

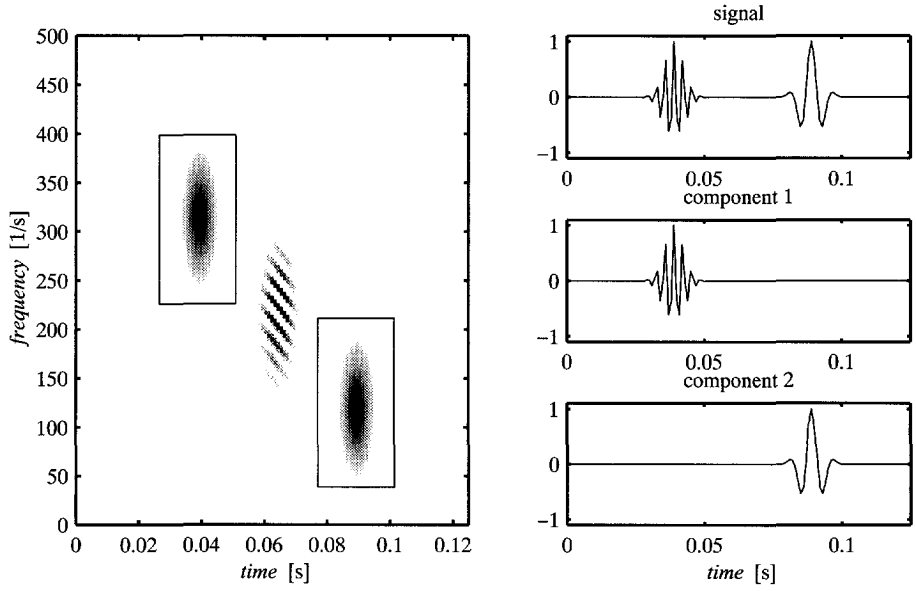

Figure 4.11: *Reconstruction of a two component signal. The boxes outline the time-frequency mask function.*

4. Next, the component is synthesized by taking the largest eigenvalue multiplied by its corresponding eigenfunction.

5. Finally, we are left with a constant phase factor that cannot be determined by the reconstruction. In case we have the original signal, which we usually do, this factor can be estimated by matching the phase of the synthesized components to the phase of the original signal. Algorithms for phase matching can be found in Boudreaux-Bartels and Parks (1986) and Tobback (1996).

An example of the decomposition is given in Fig. 4.11. The signal is a two-component signal, composed of two modulated Gaussians. In the Wigner distribution of this signal the two components and the cross terms between the components are well separated. The signal can be perfectly synthesized from the Wigner distribution by isolating the two auto terms, followed by the reconstruction from the separate auto terms. In Section 2.6 it was shown that the Wigner distribution of this signal can be decomposed into three

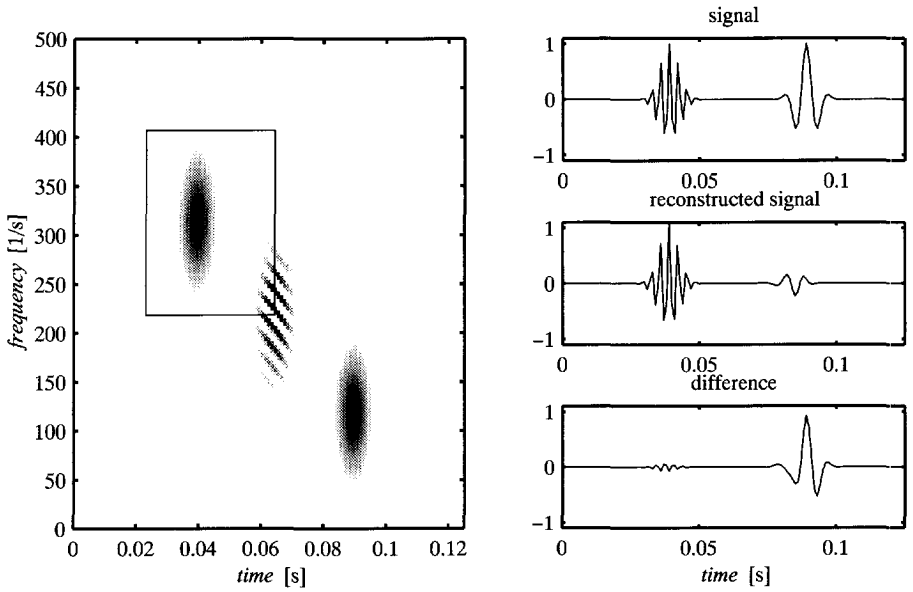

Figure 4.12: *Reconstruction when cross-term energy is included.*

terms. Two terms are auto terms, which are the Wigner distributions of the individual components. The third term is the cross-term between the two components. The reconstruction works well in this case, because the (t, f)-components that were isolated in the (t, f)-plane, are Wigner distributions. As a result, the projection reduces to the inversion of a Wigner distribution. That this is perfectly possible can be derived from the inversion property of the Wigner distribution that was given in Section 2.3 (Eq.(2.77)).

Problems arise in case cross-term energy is incorporated in the (t, f)-masked Wigner distribution. This is illustrated in Fig. 4.12. In that case the algorithm reconstructs a signal that has a Wigner distribution that is closest to the (t, f)-masked function with cross term energy. As a consequence, also the second component that generates the cross term will be partly reconstructed.

In case we want to synthesize more components from a Wigner distribution, incorporating cross terms will give rise to cumulative errors in the reconstructed signal. In order to avoid cumulative errors, a hierarchical decomposition is proposed. In the hierarchical decomposition a synthesized compo-

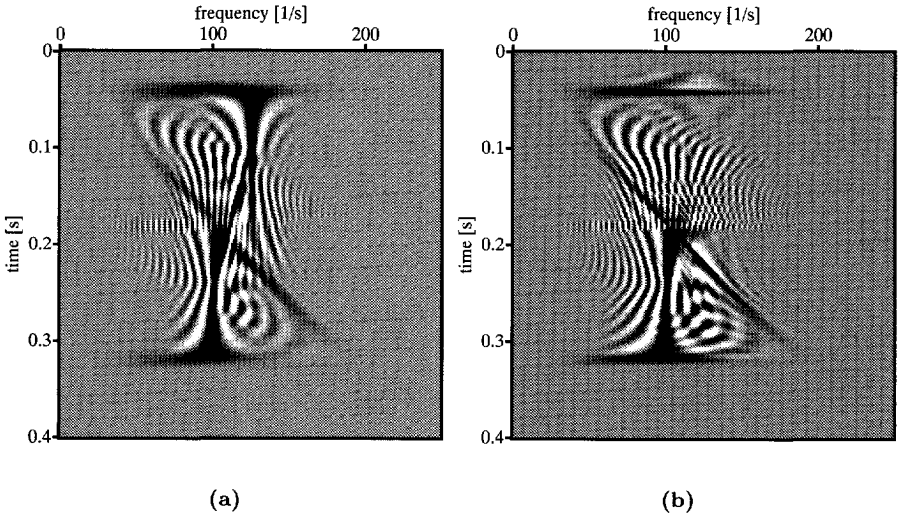

Figure 4.13: *(a) Wigner distribution of the signal, (b) Wigner distribution of the signal minus the first extracted component*

nent is subtracted from the signal. In the next step of the decomposition, the Wigner distribution of the signal minus the component is computed. Then, the next component is synthesized from the modified Wigner distribution and the process can be repeated until all desired components have been extracted from the signal.

The hierarchical decomposition is illustrated in Figs. 4.14 and 4.15. The signal is the same signal that was used as a model for a reflection pattern in Section 4.4. The Wigner distribution of the signal after subtraction of the first component is shown in Fig. 4.15b.

The synthesis error is quite large. This is partly due to the fact that the components were selected on the basis of prior knowledge about the signal structure. The signal was decomposed into five components. At those locations were the components have overlap the reconstruction performs poorly, because energy that belongs to another component than the component under consideration is brought into the synthesis. It is interesting to compare the sum of the Wigner distributions of the synthesized components with the time-frequency representation of the signal (Fig. 4.15). In the sum of the

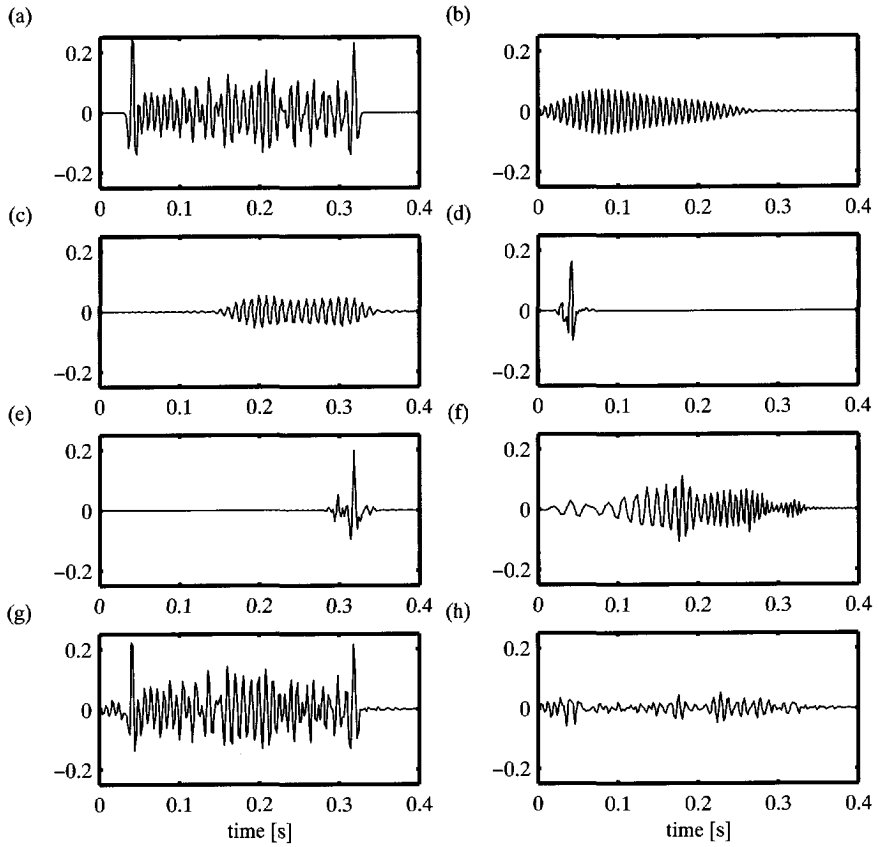

Figure 4.14: *(a) signal, (b)-(f) reconstructed components, (g) sum of the components and (h) difference between the sum of the components and original signal.*

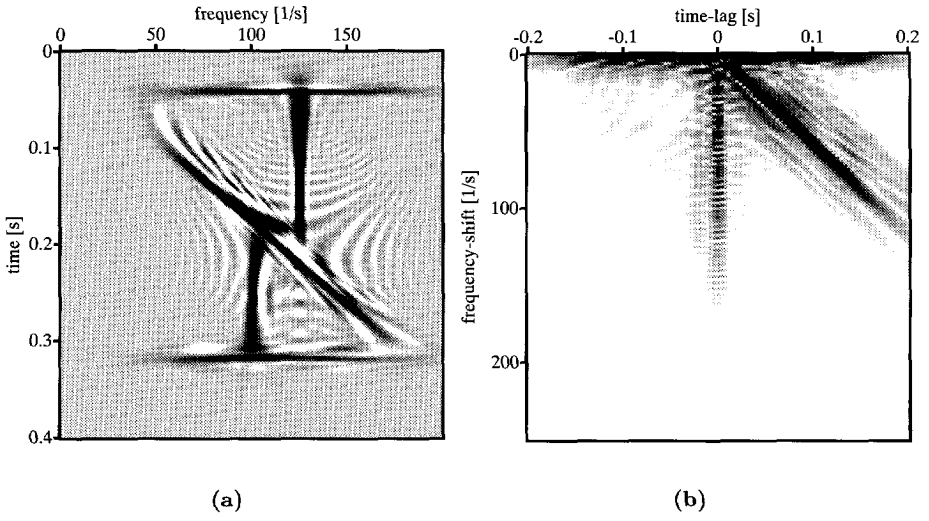

Figure 4.15: *(a) sum of the Wigner distributions of the components, (b) characteristic function of the sum of the Wigner distributions.*

Wigner distributions, cross term energy between components is absent and the result is a time-frequency representation with high time-frequency resolution. In the (ν, τ)-plane the components are very well separated and cross term energy between the components has been removed. Note however that there still is cross term energy present in the Wigner distributions of the individual components.

Figures 4.16 and 4.17 show the decomposition of a seismic trace from a migrated seismic section. It is the same trace as the one shown in Fig. 4.7. Nine components were synthesized through hierarchical decomposition. In this case, the reconstruction error is nearly zero. The total error is about 1 % of the total energy of the signal. The Wigner distribution of the signal and the sum of the Wigner distributions of the components is shown in Fig. 4.17.

4.6 Seismic attribute analysis

Seismic attribute analysis is a widely used method for detailed interpretation of seismic reflection data. Almost any study that attempts to predict reservoir properties from seismic data involves in one way or another the extraction of attributes from the seismic trace. At the base of geo-statistical integration

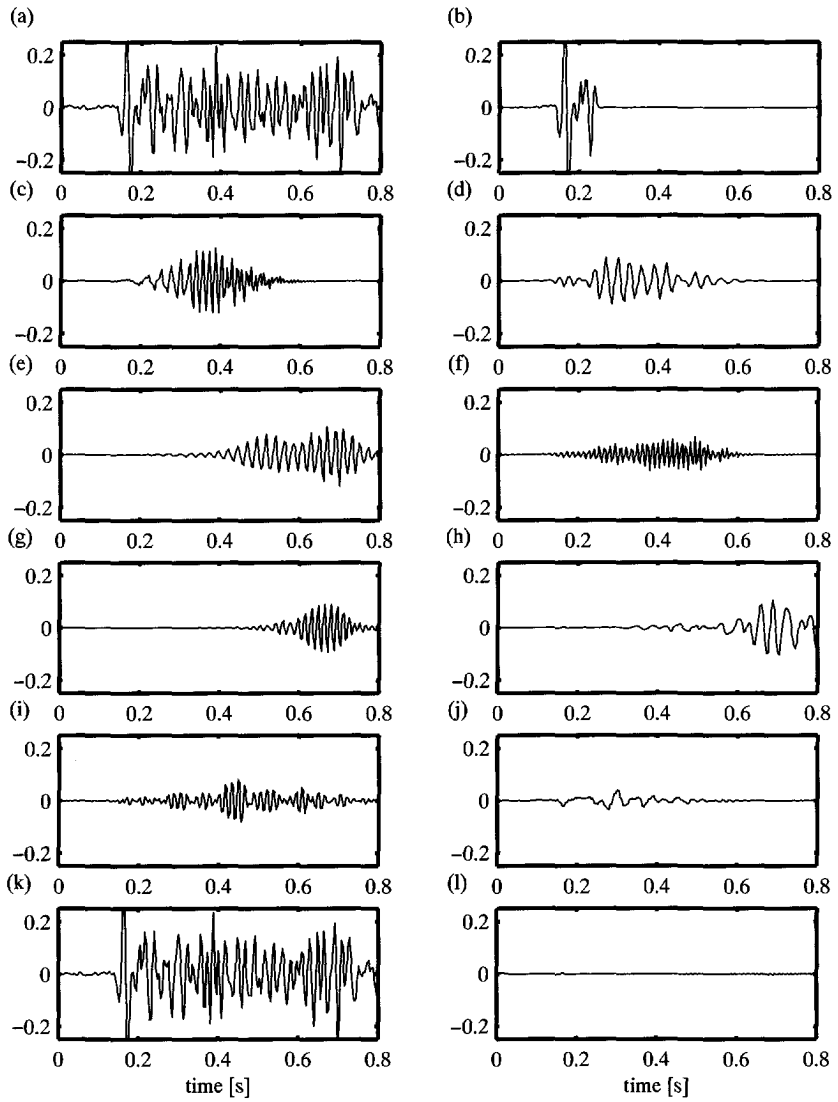

Figure 4.16: *(a) Signal, (b)-(j) reconstructed components, (k) sum of the components and (l) difference between summed components and original signal.*

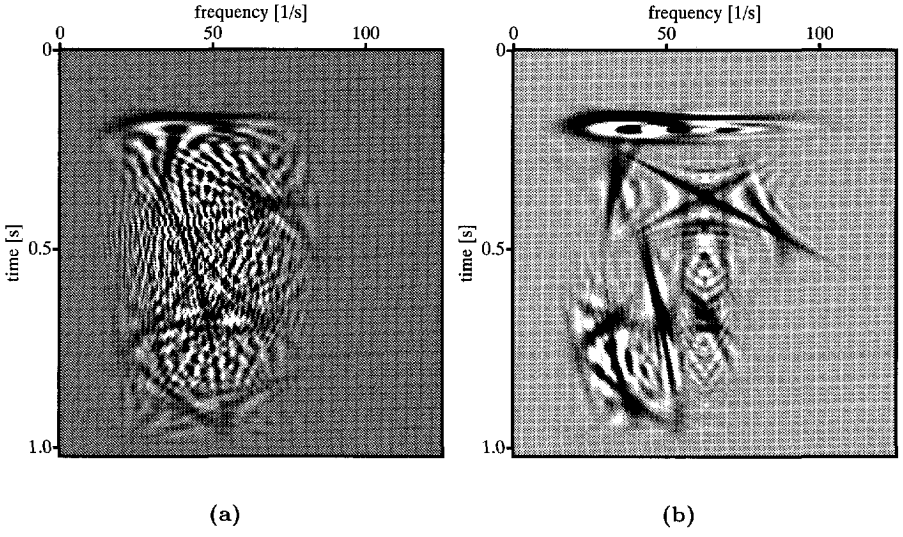

Figure 4.17: *Wigner distributions, (a) original trace, (b) sum of Wigner distributions of components.*

of seismic and well data is the correlation between the seismic trace attributes and the petrophysical properties measured in the bore-hole. This correlation determines the relation that is used to predict reservoir properties away from the well. After attribute extraction and correlation, the prediction is performed with multivariate statistical methods (see e.g. Fournier and Derain 1996) or neural networks.

It is remarkable that in most seismic attribute studies little attention is paid to the extraction of the attributes, that after all form the basic input. In many cases the set of attributes that is used is in the orders of tens or even hundreds (Kalkomey 1996). In one way or another most seismic attributes can be categorized into two types: measures for the amplitude and measures for frequency. The attributes are either extracted from the time characteristics of the trace, for instance amplitude, loop width, peak to through width, number of zero crossings, or as frequency characteristics, such as instantaneous frequency, local bandwidth and spectral ratios.

The examples given here immediately show that this type of analysis has its dangerous side. Clearly, loop width, the number of zero crossings and local frequency characteristics will be highly correlated measures. Using these at-

tributes can lead to grossly over- or under-estimating the degree of correlation between seismic data and reservoir properties.

The complex-trace attributes, first introduced to seismic interpretation by Taner and Sheriff in 1977, are still widely used for the characterization of waveforms. In Chapters 2 and 3 it was shown that the complex-trace description and the general class time-frequency representation are intimately related. This was first pointed out in the geophysical literature by Bodine (1986), whho shows that the complex-trace attributes can be obtained as the relative moments of a time-frequency energy density function. In his paper he argues that a local frequency measurement from this energy density is best obtained at a location where the energy is largest. He proposes the measurement of frequency and phase at peaks of the trace envelopes and coins these attributes response phase and response frequency.
From a time-frequency analysis perspective, it is immediately clear why these measures perform better for waveform classification of seismic signal than the complex-trace attributes for all samples of the trace. Several theoretical explanations can be given, based on the relation between the rate of change of the envelope and the variance of instantaneous frequency (see e.g Cohen 1995). A more intuitive explanation is given by the observation that strong cross terms in the time-frequency representation will be located between two envelope peaks. These cross terms do not contain information about the signal at that particular location but are generated by the interaction of the two neighbouring peaks. The observation that the instantaneous frequency attains negative values can also be attributed to the cross terms. As the cross terms attain negative values and will dominate the time-frequency representation between two strong components the mean frequency at this location may also attain a negative value.
An alternative way to solve this problem is to suppress the cross terms in the time-frequency representation and then extract the attributes. This method has a significant advantage over the response attributes. Since the characteristics of the trace are extracted on a sample by sample basis, instead of only at envelope peaks, more detailed time information will be incorporated in the attribute analysis.

In conclusion, the time-frequency representation is proposed as the basic characterization method for seismic traces for two reasons. The errors that

result from introducing highly dependent data into a statistical analysis can be avoided by first inspecting the time-frequency representation to obtain confidence about significance of a particular set of seismic attributes. As almost any attribute can be extracted from the time-frequency representation, the extraction of two attributes that describe the same time-frequency characteristic of the trace can be avoided. Second, the sensitivity to noise and cross terms of the attributes can be greatly reduced, if they are extracted from a smoothed time-frequency representation. In the previous section it was shown that careful smoothing can greatly reduce the cross terms, while retaining resolution and detectability of certain time-frequency characteristics of the data.

The following examples illustrate the relation between the type of kernel that is used to obtain a time-frequency representation and the attributes that are extracted from the representation. Here, we will only discuss the extraction of the mean frequency as a function of time in detail. Next to the amplitude, which can be extracted from the data without any problems, it is regarded as the most important feature of the data.

4.6.1 Extraction of the mean frequency

Instantaneous frequency estimation is extensively treated in signal processing literature; a wide variety of methods is discussed by Boashash (1992a, 1992b). A direct estimate of the instantaneous frequency is obtained by differentiation of the phase, $\phi(t)$ of the analytic signal (see Section 2.2.3).

$$\langle f \rangle_t = \frac{\mathrm{d}\phi(t)}{\mathrm{d}t}. \tag{4.7}$$

The mean frequency as a function of time is extracted from the time-frequency representation by calculating the relative first-order moment with frequency for each time sample, i.e.

$$\langle f \rangle_t = \frac{[f^1]_t}{[f^0]_t}, \tag{4.8}$$

where $[f^n]_t$ stands for taking the n^{th} moment for fixed time t, as introduced in Section 2.2.

In case the kernel of the time-frequency representation satisfies the constraints given in Eqs.(3.38) and (3.39), the direct estimate and the estimate

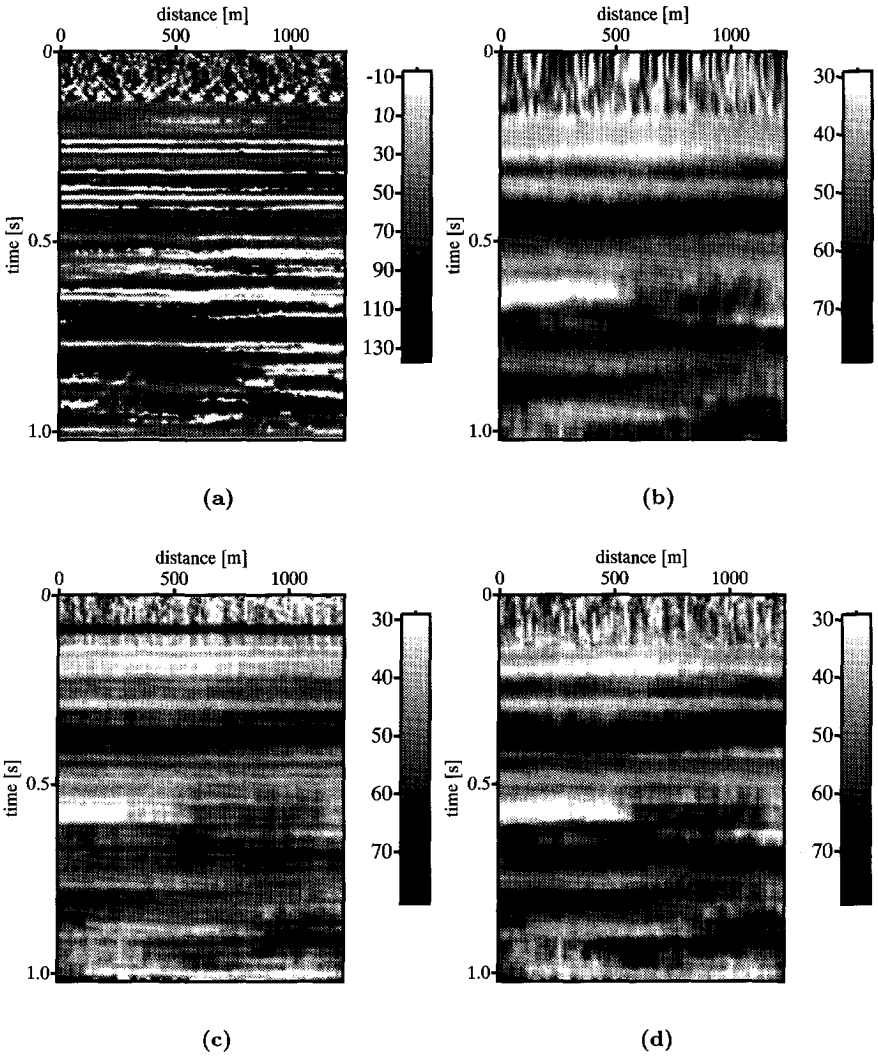

Figure 4.18: *Mean frequency; (a) Instantaneous frequency (Wigner distribution), (b) spectrogram, (c) modulus of the Choi-Williams representation, (d) positive part cone-kernel representation.*

from the time-frequency representations are equivalent. The time-frequency representation of the analytic signal is used and consequently the calculation is performed for positive frequencies only. In order to avoid spurious values in case the time-frequency representation attains negative values, either the modulus of the time-frequency representation, or the positive part of the representation is used in the calculations.

Fixed kernel time-frequency representations

For time-frequency representations with a fixed kernel, the properties of the average frequency that is extracted can be derived by an evaluation of the smoothing kernel. Figure 4.18 shows the instantaneous frequency that was extracted from a pseudo Wigner distribution of the first 100 traces of the seismic section that is shown in Fig. 4.10. It is comparable to the instantaneous frequency that is extracted from the complex trace. Cross terms and noise give rise to spurious peaks that obscure the actual local frequency content of the section.

Next to the instantaneous frequency the mean frequency that is extracted from the spectrogram is shown. The smoothness and non-negativity of the spectrogram lead to a robust estimation of the frequency content. However, the time localization is poor which makes the correlation of frequency with separate events in the seismic section difficult.

The Choi-Williams and cone-kernel representations result in a better time-localization of the mean frequency. In the Choi-Williams representation this better localization is achieved by the fact that the kernel enhances both impulse-like signals (the separate events) and harmonic components (between strong events), at the expense of cross terms. The mean frequency that is extracted from the cone-kernel representation illustrates the capability of this representation to sharply localize frequency transitions. Impulse type events are suppressed by the cone kernel, but changes of frequency between strong events are sharply localized in time and frequency. For the Choi-Williams representation the best results are obtained by extracting the mean frequency from the modulus of the time-frequency representation. The best result for a cone kernel is achieved by considering the positive values only.

Adaptive methods

Instantaneous frequency measurement of noisy signals can be improved by adapting the time-frequency representation to the signal under analysis. This can be done by signal adaptive cross-term suppression or an iterative method. The iterative method is based on peak detection in the cross-Wigner distribution of a signal and an initial estimate of the signal (Boashash and O'Shea 1993). Although the method is designed for instantaneous frequency estimation of mono-component signals, good results are also obtained for seismic signals.

The iterative estimation is applied according to the following scheme:

- Initialization: a first estimate of the instantaneous frequency is obtained and a (unit amplitude) reference signal is formed from it.
- Estimation: the current signal estimate is is used as reference and the cross-Wigner distribution of the reference signal and current estimate is computed. The instantaneous frequency is estimated as the peak of the cross-Wigner distribution.
- Recursion: the procedure is repeated until the estimate differs from the previous one by less than a specified amount.

To obtain the initial estimate, the peak of a spectrogram of the signal is extracted. If for the initial estimate the instantaneous frequency based on the direct definition (Eq.(4.7)) is used, the reference signal becomes the observed signal. In that case the cross-Wigner distribution estimation is equivalent to extraction of the location of the maximum energy (the peak value) from a Wigner distribution. The iterative method is illustrated in Figs. 4.19 and 4.20. The signal is a quadratic frequency modulated signal, contaminated by random noise. Figure 4.19 shows the signal and the instantaneous frequency that is obtained by direct estimation. The estimate that is obtained by peak extraction from the cross-Wigner distribution is shown in Fig. 4.20. The example shows that for random noise the adaptive method is quite well capable of estimating the instantaneous frequency of the noise-free signal.

The results of the cross-Wigner distribution estimation on the seismic data are shown in Fig. 4.21. The result that is obtained from the peak estima-

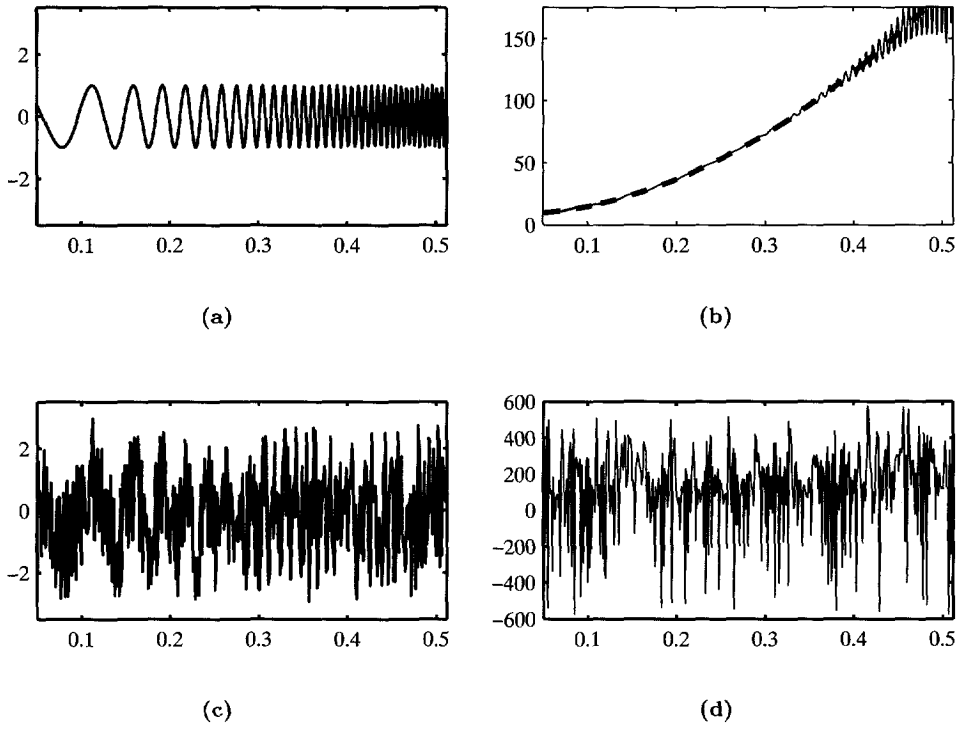

Figure 4.19: *(a) Real part of the quadratic frequency modulated signal, (b) instantaneous frequency obtained from phase differencing and true instantaneous frequency (dashed line), (c) real part of the signal plus random noise (-10 [dB]), (d) instantaneous frequency of the signal (c).*

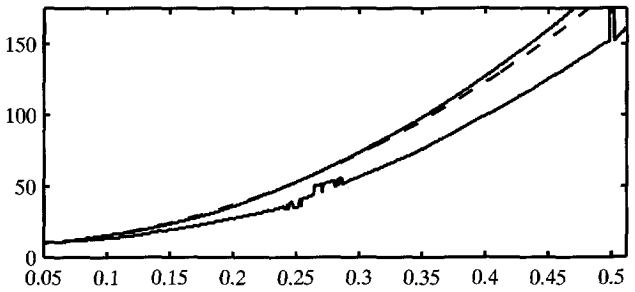

Figure 4.20: *Instantaneous frequency obtained from cross-Wigner distribution peak of the noisy signal (lower solid curve) and noise-free signal (upper solid curve). The dashed curve is the true instantaneous frequency.*

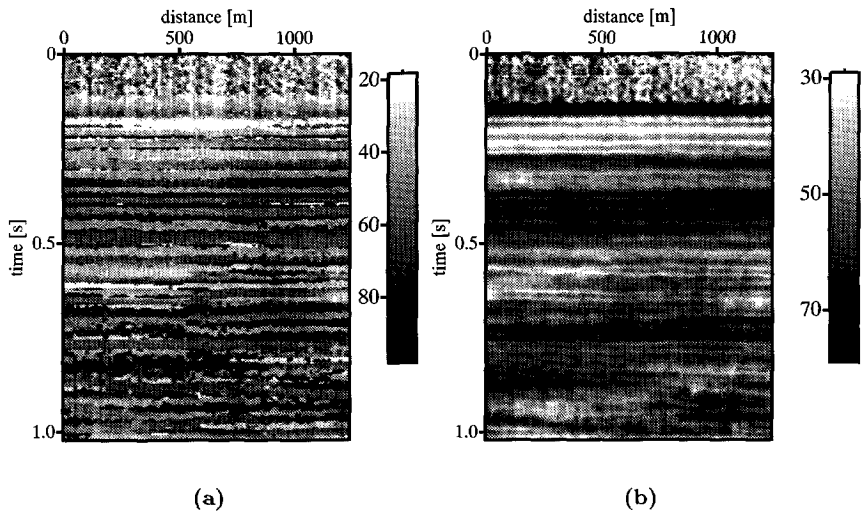

Figure 4.21: *Mean frequency cross-Wigner estimation (a) peak, (b) mean.*

tion has a blocky appearance, which may not always be desirable for visual interpretation. However, the scheme can also be adapted for estimation of the mean frequency from the cross-Wigner distribution. The result is for the mean frequency estimation is shown in Fig 4.21b.

The result that is the visually most appealing is obtained by estimation from an optimal kernel time-frequency representation. Figure 4.22 shows a part of a migrated seismic section from the Alboran Sea and the local mean frequency of the data, extracted from an optimum kernel time-frequency representation. Fine detail that is difficult to observe in the original section is brought out by the mean frequency display. The high frequency event at about 0.35 [s] was also observed in the time-frequency representations of Fig. 4.9. The event marks the lower boundary of the upper sub-unit that was observed in the seismic facies analysis of the same seismic section (cf. Fig. 4.10 and the discussion in the text).

In the mean frequency display the boundary shows up as a highly correlative event, which is not easily recognized in the original section. Note also that reflection terminations can be much better identified in the mean frequency display than in the original section.

4.6.2 Attributes derived from higher-order moments of the time-frequency representation

Besides the amplitude and frequency many other attributes can be extracted from a time-frequency representation. A logical step is to introduce the local higher-order moments to characterize the representation.

The local bandwidth σ_t, which can be found by calculating the variance around the mean frequency, $\langle f \rangle_t$, is given by

$$\sigma_t^2 = \frac{\left[(f - \langle f \rangle_t)^2\right]_t}{[f^0]_t}. \tag{4.9}$$

Other measures that are used in statistics to characterize density functions are the skewness and kurtosis (Press et al. 1992). Skewness is a measure for the deviation of the density function from a normal (Gaussian) distribution and is related to the third moment around the mean. A skewness measure is

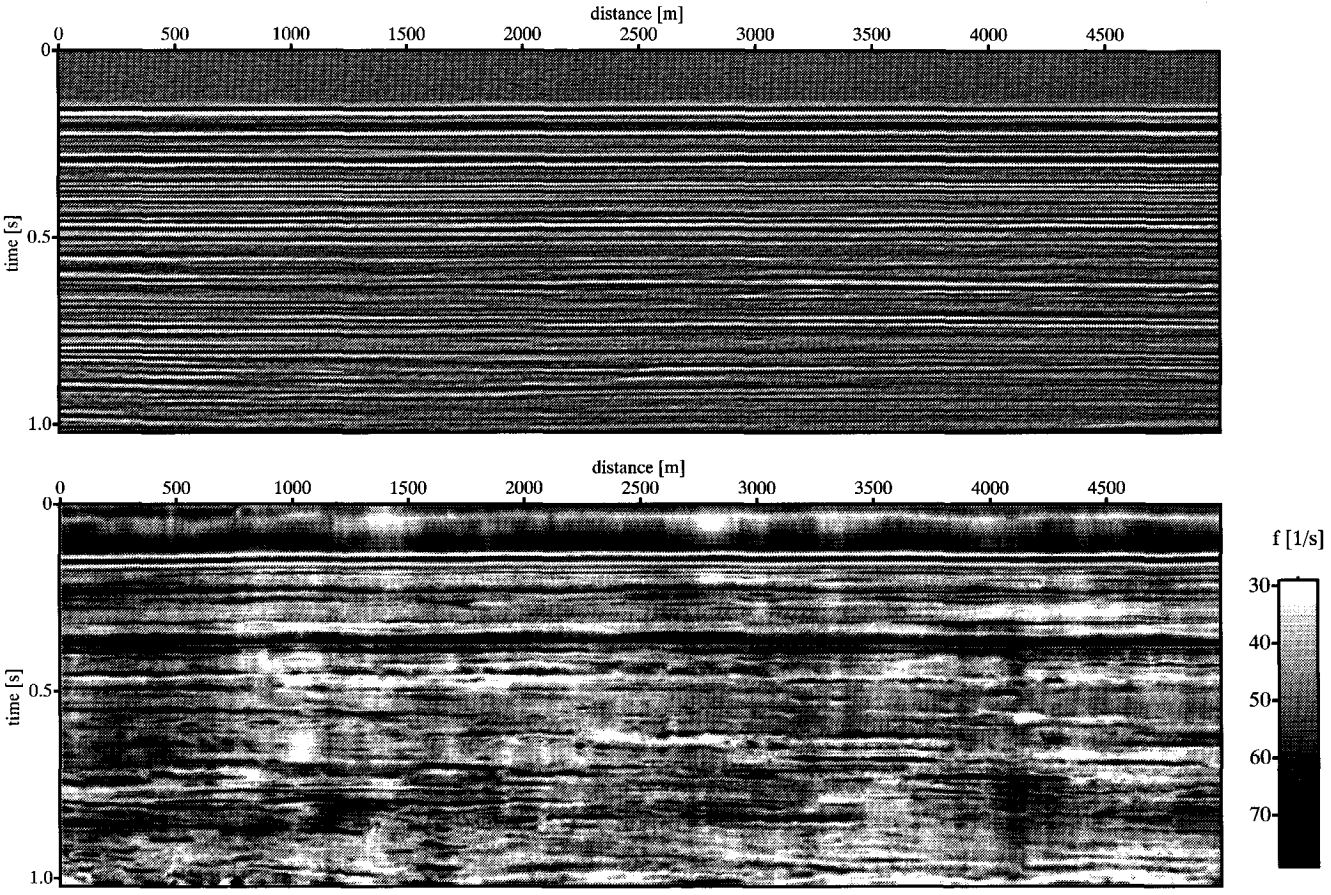

Figure 4.22: *(top) Migrated seismic section Alboran Sea and (bottom) mean frequency extracted from an optimum kernel time-frequency representation.*

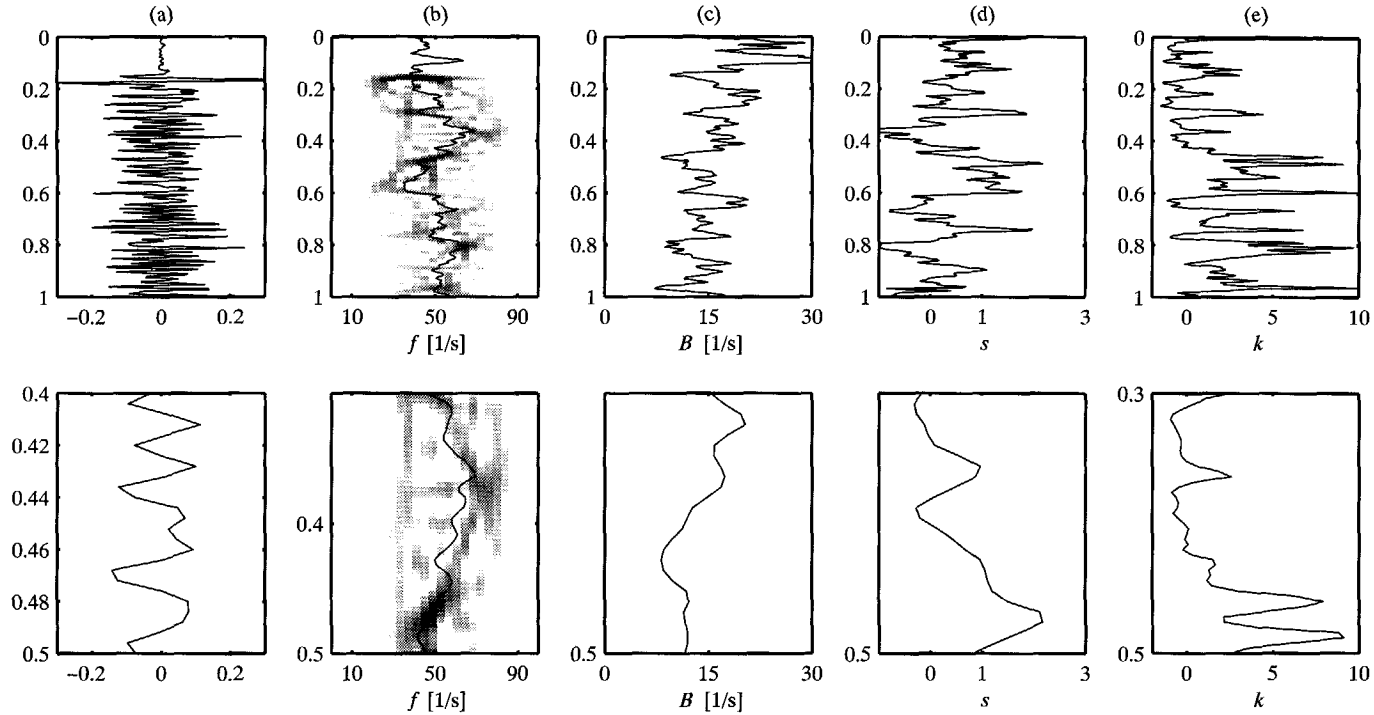

Figure 4.23: *Attributes derived from higher order moments of the the time-frequency representation: (a) seismic trace, (b) time-frequency representation (Choi-Williams representation) and mean frequency (line), (c) bandwidth, (d) skewness, and (e) kurtosis.*

given by

$$s_t = \frac{\left[(f - \langle f \rangle_t)^3\right]_t}{\left(\sigma_t \left[f^0\right]_t\right)^3}. \tag{4.10}$$

A positive skewness signifies an asymmetric distribution with a tail extending out towards positive frequencies. A normal distribution has skewness zero. Kurtosis is used as a measure for the peakedness of the distribution. Using the usual definition, the kurtosis of a time-frequency representation as a function of time is given by

$$k_t = \frac{\left[(f - \langle f \rangle_t)^4\right]_t}{\left(\sigma_t \left[f^0\right]_t\right)^4} - 3, \tag{4.11}$$

where the term -3 makes the value zero for a normal distribution. Density functions with a positive kurtosis have a more sharply peaked shape than a Gaussian and are called leptokurtic. Negative kurtosis signifies a distribution that is flatter than a normal distribution. These distributions are called platykurtic.

Figure 4.23 shows a seismic trace, its time-frequency representation (Choi-Williams representation) and the higher-order relative moments as a function of time. A part of a seismic section and the attributes extracted from its time-frequency representation is shown in Fig. 4.24. The seismic data are the first 100 traces of the section shown in Fig. 4.22. Skewness values vary between 2 and -1, kurtosis varies between 10 and -1. Interpretation of these attributes is not straightforward. Their usefulness for seismic interpretation should be assessed in terms of the significance that can be attached to the width, symmetry and peakedness of the local spectrum as a function of time. However, from the figure some tentative conclusions can be drawn.

The local bandwidth (Fig. 4.24a) appears to be related to the uniformity of reflection spacing. Uniformly spaced events tend to show up as regions relatively low bandwidth. In the figure this is most clearly observed for the events around 0.5 [s] travel time.

We cannot derive an interpretation in terms of event characteristics of the skewness from the figure. However, a high skewness value appears to indicate a facies change. In section 4.4 we could make a subdivision of this section into two facies units (Figs. 4.9 and 4.10). The upper unit (0.16 [s] - 0.5 [s]) was

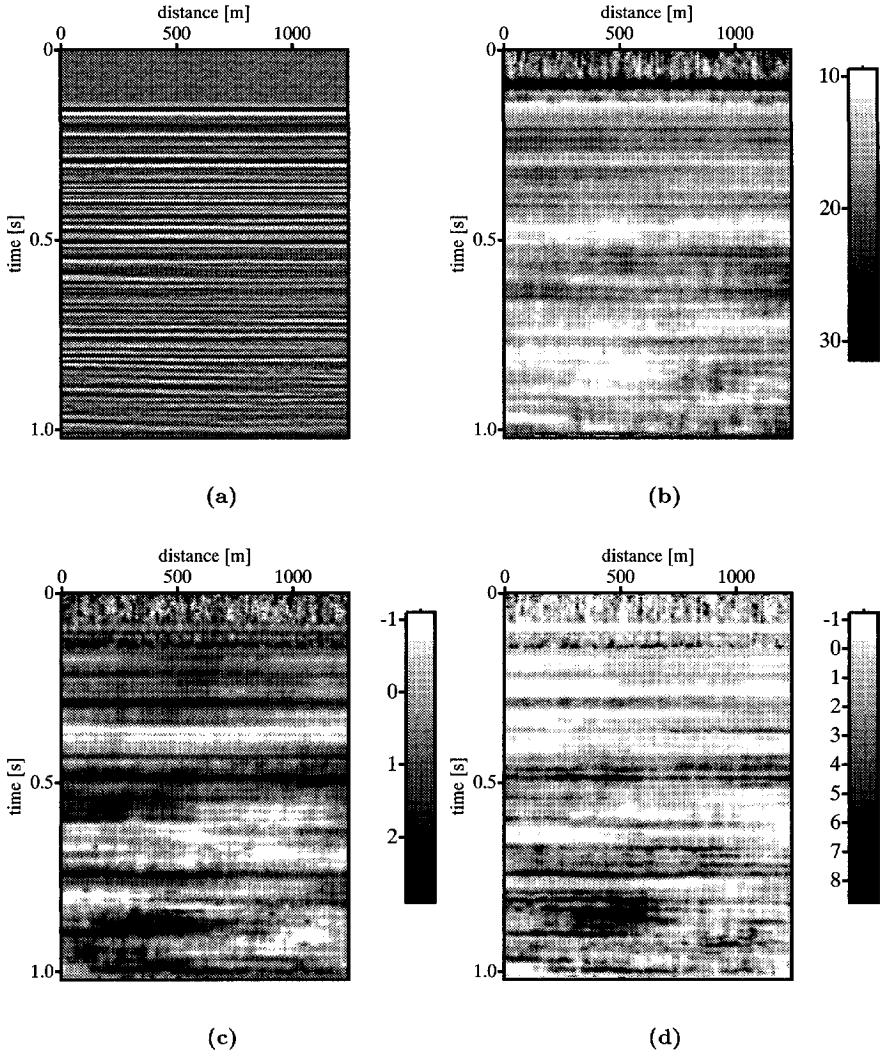

Figure 4.24: *(a) Seismic section, (b) local bandwidth, (c) local skewness, (d) local kurtosis. The attributes were extracted from the modulus of the Choi-Williams representation.*

further divided into two subunits. The boundary between the two subunits is clearly visible at 0.35 [s] travel time. We also observe the boundary between the upper and lower unit.

In the image of the kurtosis we observe relatively high kurtosis values below 0.5 [s]. Below the 0.5 [s] the events are less continuous and less regularly spaced that in the upper unit. The higher degree of disorder in the lower section is expressed in a more peaked character of the local spectrum. This relation is also known in other areas of seismic data analysis. In minimum entropy wavelet deconvolution kurtosis is used as a heuristic measure for entropy (Wiggins 1985).

There are of course many other attributes that could be defined. Here we have chosen to illustrate only those that appear relevant in the context of a statistical description. Other measures that may be defined are cumulative energies, peak counts or spectral fall-off rates.

Chapter 5

Multi-dimensional Local Power Spectra

5.1 Joint Representations of more than two variables

Seismic reflection data are not only recorded in time but are also sampled in space. In seismic interpretation, the spatial characteristics of seismic events are often more significant than features that are associated with the temporal behaviour of the signal. The lateral continuity of an event in a seismic section is the key to its interpretation. Continuous events are identified as important geological surfaces and a discontinuity of the signal in a lateral direction is often associated with a geological discontinuity, such as a fault, a pinch-out or an erosional truncation. Seismic signal analysis should therefore not be limited to time domain analysis, but comprise the spatial behaviour of the signal as well.

In this chapter we will define the multi-dimensional local power spectrum of a signal that depends not only on time, but also on one or more spatial coordinates. This definition is for the greater part a straightforward extension of the theory of time-frequency analysis that was discussed in Chapters 2 and 3.

In the second half of this chapter a local Radon power spectrum is defined.

The global Radon transformation is an important transformation in seismic data analysis. The Radon transformation is used in a wide range of seismic processing and analysis applications. The main reason for its popularity is that it can be used for decomposition of the data into its plane-wave components. (Stoffa et al. 1981; Phinney et al. 1981; Treitel et al. 1982).

For seismic interpretation purposes, a local Radon transformation would be preferred. Ideally, a local Radon representation results in a decomposition of the signals energy into a spectrum of its dip content in every point in space and time. The dip angle and dip direction (azimuth) of a surface are essential parameters for the visualization of three dimensional features on a two-dimensional map. For that reason, a local space-time-dip angle representation will be considered the point of departure for multi-trace seismic attribute analysis, in the same manner as the time-frequency representation was shown to be fundamental in single trace attribute analysis. The Wigner-Radon representation that we will introduce later in this chapter as a candidate for the local slant-stack power spectrum, naturally emerges from the definition of the local wavenumber-frequency power spectrum.

First, we will discuss the bilinear joint representation of more than two variables. Not surprisingly, a general class of space-time-frequency shift-covariant local spectra can be defined. In analogy with the one-dimensional case, the properties of the local spectra from this class are determined by a kernel function. Once the generalized multi-dimensional local spectrum has been defined, we will concentrate on the local wavenumber-frequency representation of two-dimensional functions of space and time. The kernel functions that are commonly used in time-frequency analysis can be easily extended to two-dimensional functions. The general class leads to an infinite number of choices for a local spectrum. In this chapter we shall investigate three possible kernel choices in more detail; the pseudo Wigner distribution, the spectrogram, and the generalized Wigner distribution (Jacobson and Wechsler 1988; Stankovič et al. 1995). Once the properties of the local two-dimensional spectrum are known, the extension to higher dimensions is straightforward.

5.2 Multi-dimensional Wigner distribution and general class

In this section the Wigner distribution of a function that depends on three spatial dimensions and time is defined. Time and space variables will be

treated separately, because of the opposite sign in the exponent in the spatial and temporal Fourier transformations. First, we introduce the three-dimensional spatial Fourier transform operator of a function $u(\boldsymbol{a}), \boldsymbol{a} \in I\!R^3$, as

$$\mathcal{F}_{\boldsymbol{a}}^{\pm}\{u(\boldsymbol{a})\}(\boldsymbol{b}) = \int_{\boldsymbol{a}\in I\!R^3} \exp(\pm \mathrm{j}2\pi \boldsymbol{a}\cdot\boldsymbol{b}) u(\boldsymbol{a})\mathrm{d}\boldsymbol{a}. \tag{5.1}$$

The spatial Fourier transform representation of $u(\boldsymbol{a})$ will be denoted by $\tilde{u}(\boldsymbol{b})$. In situations where the transform variable can be unambiguously derived by considering the functional dependence of the result of the transformation, e.g. $\tilde{u}(\boldsymbol{b})$, we will use a short-hand for Eq.(5.1), i.e.

$$\tilde{u}(\boldsymbol{b}) = \mathcal{F}_{\boldsymbol{a}}^{\pm}\{u(\boldsymbol{a})\}, \tag{5.2}$$

where we have dropped the functional dependence $(\boldsymbol{b})$ on the right-hand side. The signals we consider will be represented by the generic function $u(\boldsymbol{x}, t)$, where $\boldsymbol{x} \in I\!R^3$ denotes the spatial dependence and $t \in I\!R$ is the time variable. Although the value of the function $u(\boldsymbol{x}, t)$ at a point in the $(\boldsymbol{x}, t)$ space is a scalar, it is common practice to refer to these signals as multi-dimensional signals, because of their functional dependence on more than one independent variable (Priestley 1989).

Given a signal, $u(\boldsymbol{x}, t)$, defined for $\boldsymbol{x} = \{x_1, x_2, x_3\}$, $-\infty < x_i < \infty, i = 1, 2, 3$ the local space-time auto-correlation function is given by

$$R\{u,u\}(\boldsymbol{x}, t; \boldsymbol{\xi}, \tau) = u(\boldsymbol{x} + \tfrac{1}{2}\boldsymbol{\xi}, t + \tfrac{1}{2}\tau) u^*(\boldsymbol{x} - \tfrac{1}{2}\boldsymbol{\xi}, t - \tfrac{1}{2}\tau), \tag{5.3}$$

where $\boldsymbol{\xi} = \{\xi_1, \xi_2, \xi_3\}$ is a point in the space of spatial shift variables and τ is the temporal shift variable.
The Wigner distribution of the signal $u(\boldsymbol{x}, t)$ is the Fourier transform of the local auto-correlation function with respect to the space-shift and time-shift variables, i.e.

$$W\{u,u\}(\boldsymbol{x}, t; \boldsymbol{k}, f) = \mathcal{F}_{\boldsymbol{\xi}}^{+}\mathcal{F}_{\tau}^{-}\{R\{u,u\}(\boldsymbol{x}, t; \boldsymbol{\xi}, \tau)\}, \tag{5.4}$$

where $\boldsymbol{k} = \{k_1, k_2, k_3\}$ is a point in the spatial frequency or wavenumber space and f is the temporal frequency.
Let $\tilde{u}(\boldsymbol{k}, f)$ be the Fourier transform of $u(\boldsymbol{x}, t)$. A local spectral correlation function, $R\{\tilde{u}, \tilde{u}\}(\boldsymbol{\kappa}, \nu; \boldsymbol{k}, f)$, can then be defined as

$$R\{\tilde{u}, \tilde{u}\}(\boldsymbol{\kappa}, \nu; \boldsymbol{k}, f) = \tilde{u}(\boldsymbol{k} + \tfrac{1}{2}\boldsymbol{\kappa}, f + \tfrac{1}{2}\nu) \tilde{u}^*(\boldsymbol{k} - \tfrac{1}{2}\boldsymbol{\kappa}, f - \tfrac{1}{2}\nu), \tag{5.5}$$

where $\boldsymbol{\kappa} = \{\kappa_1, \kappa_2, \kappa_3\}$ is a point in the space of wavenumber-shift variables. The Wigner distribution in terms of the local spectral auto-correlation function can now be found as an inverse Fourier transformation of the spectral auto-correlation function over the frequency shift variables,

$$W\{u,u\}(\boldsymbol{x},t;\boldsymbol{k},f) = \mathcal{F}_{\boldsymbol{\kappa}}^{-}\mathcal{F}_{\nu}^{+}\left\{R\{\tilde{u},\tilde{u}\}(\boldsymbol{\kappa},\nu;\boldsymbol{k},f)\right\}. \tag{5.6}$$

The joint space-time-wavenumber-frequency correlation function or ambiguity function of the multi-dimensional signal $u(\boldsymbol{x},t)$, can be expressed as the Fourier transform of the space-time correlation function over the space and time variables. The ambiguity function in terms of the local space-time auto-correlation function is given by

$$A\{u,u\}(\boldsymbol{\kappa},\nu;\boldsymbol{\xi},\tau) = \mathcal{F}_{\boldsymbol{x}}^{+}\mathcal{F}_{t}^{-}\left\{R\{u,u\}(\boldsymbol{x},t;\boldsymbol{\xi},\tau)\right\}. \tag{5.7}$$

Starting from the frequency representation of the data, $\tilde{u}(\boldsymbol{k},f)$, the ambiguity function is found by Fourier transformation of the frequency correlation function over the wavenumber and frequency variables,

$$A\{u,u\}(\boldsymbol{\kappa},\nu;\boldsymbol{\xi},\tau) = \mathcal{F}_{\nu}^{+}\mathcal{F}_{\boldsymbol{k}}^{-}\left\{R\{\tilde{u},\tilde{u}\}(\boldsymbol{\kappa},\nu;\boldsymbol{k},f)\right\}. \tag{5.8}$$

From Eq.(5.7) it follows that

$$R\{u,u\}(\boldsymbol{x},t;\boldsymbol{\xi},\tau) = \mathcal{F}_{\boldsymbol{\kappa}}^{-}\mathcal{F}_{\nu}^{+}\left\{A\{u,u\}(\boldsymbol{\kappa},\nu;\boldsymbol{\xi},\tau)\right\}. \tag{5.9}$$

Substituting Eq.(5.9) into Eq.(5.4), we observe the multi-dimensional ambiguity function and the Wigner distribution are Fourier duals. The relation between the ambiguity function and Wigner distribution function is given by

$$W\{u,u\}(\boldsymbol{x},t;\boldsymbol{k},f) = \mathcal{F}_{\boldsymbol{\kappa}}^{-}\mathcal{F}_{\nu}^{+}\mathcal{F}_{\boldsymbol{\xi}}^{+}\mathcal{F}_{\tau}^{-}\left\{A\{u,u\}(\boldsymbol{\kappa},\nu;\boldsymbol{\xi},\tau)\right\}. \tag{5.10}$$

Equation (5.10) suggests that in the multi-dimensional case a general class of local power spectra can be defined, along the lines of the general class of Cohen for one-dimensional functions (Cohen 1966, 1989). The generalized multi-dimensional local power spectrum, $P\{u,u\}(\boldsymbol{x},t;\boldsymbol{k},f)$, can be found by a Fourier transformation of the characteristic function,

$$P\{u,u\}(\boldsymbol{x},t;\boldsymbol{k},f) = \mathcal{F}_{\boldsymbol{\kappa}}^{-}\mathcal{F}_{\nu}^{+}\mathcal{F}_{\boldsymbol{\xi}}^{+}\mathcal{F}_{\tau}^{-}\left\{M\{u,u\}(\boldsymbol{\kappa},\nu;\boldsymbol{\xi},\tau)\right\}, \tag{5.11}$$

where $M\{u,u\}(\boldsymbol{\kappa},\nu;\boldsymbol{\xi},\tau)$ is the characteristic function, given by

$$M\{u,u\}(\boldsymbol{\kappa},\nu;\boldsymbol{\xi},\tau) = \Psi(\boldsymbol{\kappa},\nu;\boldsymbol{\xi},\tau)A\{u,u\}(\boldsymbol{\kappa},\nu;\boldsymbol{\xi},\tau). \tag{5.12}$$

The properties of the local frequency representation $P\{u,u\}(\boldsymbol{x},t;\boldsymbol{k},f)$ are determined by the associated kernel function $\Psi(\boldsymbol{\kappa},\boldsymbol{\xi};\nu,\tau)$. The derivation of expressions for the generalized representation in terms of the Fourier transforms of the ambiguity function follows the analysis for the generalized time-frequency representation in Chapter 3. The Wigner distribution, local space-time auto-correlation function, local wavenumber-frequency auto-correlation function, and ambiguity function are related through their Fourier transforms. Consequently, the transform equivalents of the kernel function act as a convolutional filter on the Fourier duals. The representations of these filters follow the set of Fourier transformations between ambiguity function and the other representations (see Eqs.(5.7), (5.8), and (5.10)). This set of Fourier transformations now becomes quite large, because we now have a four-dimensional ambiguity function, and the corresponding number of possible combinations of Fourier pairs is sixteen. However, with a view on the practical applications there are only four filters that will be relevant. Apart from the ambiguity domain filter $\Psi(\boldsymbol{\kappa},\nu;\boldsymbol{\xi},\tau)$, we have

$$\Psi(\boldsymbol{x},t;\boldsymbol{\xi},\tau) = \mathcal{F}^{-}_{\boldsymbol{\kappa}}\mathcal{F}^{+}_{\nu}\left\{\Psi(\boldsymbol{\kappa},\nu;\boldsymbol{\xi},\tau\right\}, \tag{5.13}$$

in the space-time domain,

$$\Psi(\boldsymbol{\kappa},\nu;\boldsymbol{k},f) = \mathcal{F}^{+}_{\boldsymbol{\xi}}\mathcal{F}^{-}_{\tau}\left\{\Psi(\boldsymbol{\kappa},\nu;\boldsymbol{\xi},\tau\right\}, \tag{5.14}$$

in the wavenumber-frequency domain, and in the joint space-time-wavenumber-frequency domain we have

$$\Psi(\boldsymbol{x},t;\boldsymbol{k},f) = \mathcal{F}^{-}_{\boldsymbol{\kappa}}\mathcal{F}^{+}_{\nu}\mathcal{F}^{+}_{\boldsymbol{\xi}}\mathcal{F}^{-}_{\tau}\left\{\Psi(\boldsymbol{\kappa},\nu;\boldsymbol{\xi},\tau)\right\}. \tag{5.15}$$

In the next section the properties of the Wigner distribution of a multi-dimensional signal will be discussed. Once again, it is possible to retain the properties in the generalized local power spectrum by posing certain constraints on the kernel.

5.3 Properties of the Wigner distribution of a multi-dimensional function and associated kernel constraints

Derivation of the properties of the Wigner distribution of a function that depends on more than one independent variable is completely analogous to the one-variable case. As a result, the kernel constraints that need to be imposed to retain these properties in a representation from the generalized class can be easily extrapolated from the constraints that were derived for the one-dimensional general class. We will therefore confine ourselves here to some important properties and refer to Chapters 2 and 3 for a more thorough discussion.

Property 1: Realness. From Eq.(5.4) and the definition of the local space-time auto-correlation function Eq.(5.3), it follows that

$$\begin{aligned} W^*\{u,u\}(\boldsymbol{x},t;\boldsymbol{k},f) =& \mathcal{F}_{\boldsymbol{\xi}}^{+}\mathcal{F}_{\tau}^{-}\left\{R^*\{u,u\}(\boldsymbol{x},t;-\boldsymbol{\xi},-\tau)\right\} \\ =& \mathcal{F}_{\boldsymbol{\xi}}^{+}\mathcal{F}_{\tau}^{-}\left\{R\{u,u\}(\boldsymbol{x},t;\boldsymbol{\xi},\tau)\right\} \\ =& W\{u,u\}(\boldsymbol{x},t;\boldsymbol{k},f). \end{aligned} \tag{5.16}$$

Hence, $W\{u,u\}(\boldsymbol{x},t;\boldsymbol{k},f)$ is real. We can conclude with Eq.(5.10) that

$$A^*\{u,u\}(-\boldsymbol{\kappa},-\nu;-\boldsymbol{\xi},-\tau) = A\{u,u\}(\boldsymbol{\kappa},\nu,\boldsymbol{\xi},\tau). \tag{5.17}$$

From the definition of the generalized representation Eq.(5.11) it follows that this quality of Eq.(5.16) is preserved, provided that

$$\Psi^*(-\boldsymbol{\kappa},-\nu;-\boldsymbol{\xi},-\tau) = \Psi(\boldsymbol{\kappa},\nu;\boldsymbol{\xi},\tau). \tag{5.18}$$

Property 2: Energy and marginals. From Eq.(5.7) it follows that

$$\begin{aligned} A\{u,u\}(\mathbf{0},0;\mathbf{0},0) =& \mathcal{F}_{\boldsymbol{x}}^{+}\mathcal{F}_{t}^{-}\left\{R\{u,u\}(\boldsymbol{x},t;\mathbf{0},0)\right\} \\ =& \int_{\boldsymbol{x}\in I\!R^3}\int_{t\in I\!R}|u(\boldsymbol{x},t)|^2\mathrm{d}\boldsymbol{x}\mathrm{d}t \\ =& E_u, \end{aligned} \tag{5.19}$$

where E_u defines the total energy of the signal $u(\boldsymbol{x}, t)$.
In a similar way, starting from Eq.(5.8), we arrive at

$$\begin{aligned} A\{u,u\}(\mathbf{0},0;\mathbf{0},0) =& \mathcal{F}_{\boldsymbol{k}}^{-}\mathcal{F}_{f}^{+}\left\{R\{\tilde{u},\tilde{u}\}(\mathbf{0},0;\boldsymbol{k},f)\right\} \\ =& \int_{\boldsymbol{k}\in I\!R^3}\int_{f\in I\!R}|\tilde{u}(\boldsymbol{k},f)|^2\mathrm{d}\boldsymbol{k}\mathrm{d}f \\ =& E_u. \end{aligned} \tag{5.20}$$

Considering the inverse transformation of Eq.(5.10), we conclude

$$A\{u,u\}(\mathbf{0},0;\mathbf{0},0) = \mathcal{F}_{\boldsymbol{x}}^{+}\mathcal{F}_{t}^{-}\mathcal{F}_{\boldsymbol{k}}^{-}\mathcal{F}_{f}^{+}\left\{W\{u,u\}(\boldsymbol{x},t;\boldsymbol{k},f)\right\}(\mathbf{0},0;\mathbf{0},0) = E_u. \tag{5.21}$$

Retaining this property for the generalized representation yields the condition

$$\Psi(\mathbf{0},0;\mathbf{0},0) = 1. \tag{5.22}$$

The wavenumber-frequency power spectrum $E(\boldsymbol{k}, f)$ is found by

$$E(\boldsymbol{k},f) = \mathcal{F}_{\boldsymbol{x}}^{+}\mathcal{F}_{t}^{-}\left\{W\{u,u\}(\boldsymbol{x},t;\boldsymbol{k},f)\right\}(\boldsymbol{\kappa}=0,\nu=0;\boldsymbol{k},f). \tag{5.23}$$

Then substituting Eq.(5.6) into Eq.(5.23) we obtain

$$E(\boldsymbol{k},f) = R\{\tilde{u},\tilde{u}\}(\mathbf{0},0;\boldsymbol{k},f) = |\tilde{u}(\boldsymbol{k},f)|^2. \tag{5.24}$$

On the other hand, substituting Eq.(5.10) into Eq.(5.19) gives

$$E(\boldsymbol{k},f) = \mathcal{F}_{\boldsymbol{\xi}}^{+}\mathcal{F}_{\tau}^{-}\left\{A\{u,u\}(\mathbf{0},0;\boldsymbol{\xi},\tau)\right\}. \tag{5.25}$$

The preservation of this quality in the generalized representation forces the kernel to be constraint according to

$$\Psi(\mathbf{0},0;\boldsymbol{\xi},\tau) = 1, \text{ for } \boldsymbol{\xi}\in I\!R^3 \text{ and } \tau\in I\!R. \tag{5.26}$$

By the same token the instantaneous energy in the space-time domain is given by

$$E(\boldsymbol{x},t) = \mathcal{F}_{\boldsymbol{k}}^{-}\mathcal{F}_{f}^{+}\left\{W\{u,u\}(\boldsymbol{x},t;\boldsymbol{k},f)\right\}(\boldsymbol{x},t;\boldsymbol{\xi}=0,\tau=0). \tag{5.27}$$

When we substitute Eq.(5.4) into Eq.(5.27) we obtain

$$E(\boldsymbol{x},t;\mathbf{0},0) = |u(\boldsymbol{x},t)|^2, \tag{5.28}$$

while substitution of Eq.(5.10) leads to

$$E(\boldsymbol{x},t) = \mathcal{F}_{\boldsymbol{\kappa}}^{-}\mathcal{F}_{\nu}^{+}\left\{A\{u,u\}(\boldsymbol{\kappa},\nu;\mathbf{0},0)\right\}. \tag{5.29}$$

To retain this property in the generalized representation constraints the kernel according to

$$\Psi(\boldsymbol{\kappa},\nu;\mathbf{0},0) = 1, \text{ for } \boldsymbol{\kappa} \in I\!R^3 \text{ and } \nu \in I\!R. \tag{5.30}$$

Note that the constraint of Eq.(5.22) is contained in those of Eq.(5.23) and Eq.(5.30).

Property 3: Space-time and wavenumber-frequency shifts. If a function $u(\boldsymbol{x},t)$ is translated over a distance $\boldsymbol{x_0}$ and time t_0, its Wigner distribution is shifted accordingly, i.e. if we have

$$u(\boldsymbol{x},t) = u_0(\boldsymbol{x}-\boldsymbol{x_0}, t-t_0), \tag{5.31}$$

then the Wigner distribution is given by

$$W\{u,u\}(\boldsymbol{x},t;\boldsymbol{k},f) = W\{u_0,u_0\}(\boldsymbol{x}-\boldsymbol{x_0}, t-t_0;\boldsymbol{k},f). \tag{5.32}$$

If a function $u(\boldsymbol{x},t)$ is modulated in space and time with frequencies $\boldsymbol{k_0}$ and f_0, its Wigner distribution is shifted proportionally in wavenumber and frequency , i.e. if we have

$$u(\boldsymbol{x},t) = u_0(\boldsymbol{x},t)\exp(-\mathrm{j}2\pi(\boldsymbol{k_0}x - f_0 t)), \tag{5.33}$$

then the Wigner distribution is given by

$$W\{u,u\}(\boldsymbol{x},t;\boldsymbol{k},f) = W\{u_0,u_0\}(\boldsymbol{x},t;\boldsymbol{k}-\boldsymbol{k_0}, f-f_0). \tag{5.34}$$

From the definition of the generalized representation Eq.(5.12) and the Fourier transform relation between characteristic function and local power spectrum Eq.(5.11) it directly follows that these shift properties are retained for any kernel function $\Psi(\boldsymbol{\kappa},\nu;\boldsymbol{\xi},\tau)$.

Property 4: Convolutions and products. The Wigner distribution of the convolution or product of two signals is given by respectively the space-time and wavenumber frequency convolution the Wigner distribution of the

separate signals. Let the signal $u(\boldsymbol{x}, t)$ be the convolution of two signals given by

$$u(\boldsymbol{x}, t) = \int_{\boldsymbol{x}' \in I\!R^3} \int_{t' \in I\!R} u_1(\boldsymbol{x} - \boldsymbol{x}', t - t') u_2(\boldsymbol{x}', t') \mathrm{d}\boldsymbol{x}' \mathrm{d}t, \tag{5.35}$$

then the Wigner distribution of $u(\boldsymbol{x}, t)$ is given by

$$W\{u,u\}(\boldsymbol{x}, t; \boldsymbol{k}, f) = \int_{\boldsymbol{x}' \in I\!R^3} \int_{t' \in I\!R} W\{u_1, u_1\}(\boldsymbol{x} - \boldsymbol{x}', t - t'; \boldsymbol{k}, f) \\ W\{u_2, u_2\}(\boldsymbol{x}', t'; \boldsymbol{k}, f) \mathrm{d}\boldsymbol{x}' \mathrm{d}t'. \tag{5.36}$$

If a function is the product of two signals in the space-time domain, i.e.

$$u(\boldsymbol{x}, t) = u_1(\boldsymbol{x}, t) u_2(\boldsymbol{x}, t), \tag{5.37}$$

the Wigner distribution is given by

$$W\{u,u\}(\boldsymbol{x}, t; \boldsymbol{k}, f) = \int_{\boldsymbol{k}' \in I\!R^3} \int_{f' \in I\!R} W\{u_1, u_1\}(\boldsymbol{x}, t; \boldsymbol{k} - \boldsymbol{k}', f - f') \\ W\{u_2, u_2\}(\boldsymbol{x}, t; \boldsymbol{k}', f') \, \mathrm{d}\boldsymbol{k}' \, \mathrm{d}f'. \tag{5.38}$$

These convolution and product properties hold for all representations in the general class.

5.4 Examples of the Wigner distribution of a two-dimensional signal

In the remainder of this chapter we will concentrate on signals that can be represented by a function of two independent variables. As was shown in the previous section, the extension to more than one spatial dimension can be readily made as the general properties do not depend on the spatial dimension. For a two-dimensional signal that is a function of spatial variable x_1 and time t we will have a four-dimensional Wigner distribution function, $W\{u,u\}(x_1, t; k_1, f)$, with k_1 representing the spatial frequency in the direction x_1. In the following, the subscript of the spatial coordinate will be dropped, as the analysis will be limited to a single spatial coordinate. The whole analysis of the previous section applies.

For some basic multi-dimensional signals the Wigner distribution can be calculated analytically. We will do this for two basic signals; a signal that is the sum of two exponentials and a two-dimensional Gaussian signal.

Sum of two exponentials

Consider a signal that is composed of two exponential signals, given by

$$u(x,t) = \exp(-\mathrm{j}2\pi k_1 x) + \exp(\mathrm{j}2\pi f_1 t). \tag{5.39}$$

The local space-time auto-correlation function of this signal is given by

$$\begin{aligned} R\{u,u\}(x,t;\xi,\tau) = &\exp(-\mathrm{j}2\pi k_1\xi) + \exp(\mathrm{j}2\pi f_1\tau) + \\ &2\cos\left[2\pi(k_1 x - f_1 t)\right]\exp\left[-\mathrm{j}\pi(k_1\xi - f_1\tau)\right]. \end{aligned} \tag{5.40}$$

According to Eq.(5.4) the Wigner distribution of the signal is found as

$$\begin{aligned} W\{u,u\}(x,t;k,f) = &\mathcal{F}_\xi^+\mathcal{F}_\tau^-\left\{R\{u,u\}(x,t;\xi,\tau)\right\} = \\ &\delta(k-k_1) + \delta(f-f_1) + \\ &2\cos\left[2\pi(k_1 x - f_1 t)\right]\delta(k - \tfrac{1}{2}k_1, f - \tfrac{1}{2}f_1). \end{aligned} \tag{5.41}$$

The space-time modulating component is a cross term between the spatial and temporal frequency of the signal, which reflects the modulation of the signal envelope, and hence its energy with changing position in x and t. The non-modulating components reflect the constant energy at the frequencies k_1 and f_1. Figure 5.1 shows an example of this signal with $k_1 = 3$ [m^{-1}] and $f_1 = 18$ [s^{-1}] and a (k,f)-slice through its Wigner distribution.

Two-dimensional Gaussian signal

The Wigner distribution of the two-dimensional Gaussian signal

$$u(x,t) = \exp\left[-\pi\left(\sigma_x^2 x^2 + \sigma_t^2 t^2\right)\right], \tag{5.42}$$

is given by

$$\begin{aligned} W\{u,u\}(x,t;k,f) = \frac{2}{\sigma_x\sigma_t}\exp\left[-2\pi\left(\sigma_x^2 x^2 + \frac{k^2}{\sigma_x^2}\right)\right] \\ \exp\left[-2\pi\left(\sigma_t^2 t^2 + \frac{f^2}{\sigma_t^2}\right)\right]. \end{aligned} \tag{5.43}$$

This expression can be obtained by using the result for the one-dimensional Gaussian signal (Eq.2.107) and the fact that the integral defining the Wigner distribution is separable (Jacobson and Wechsler 1988).

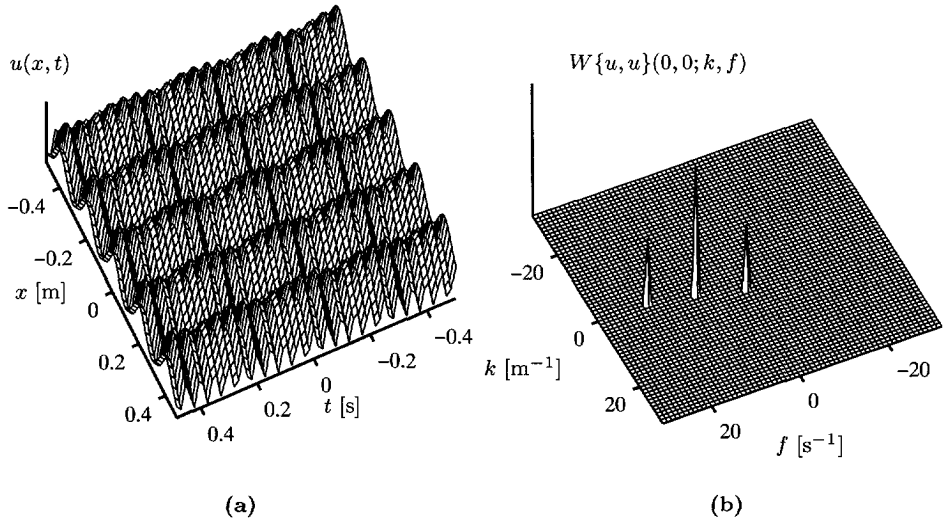

Figure 5.1: *Wigner distribution of the sum of two complex exponentials; (a) real part of the signal, (b)* $W\{u,u\}(0,0;k,f)$.

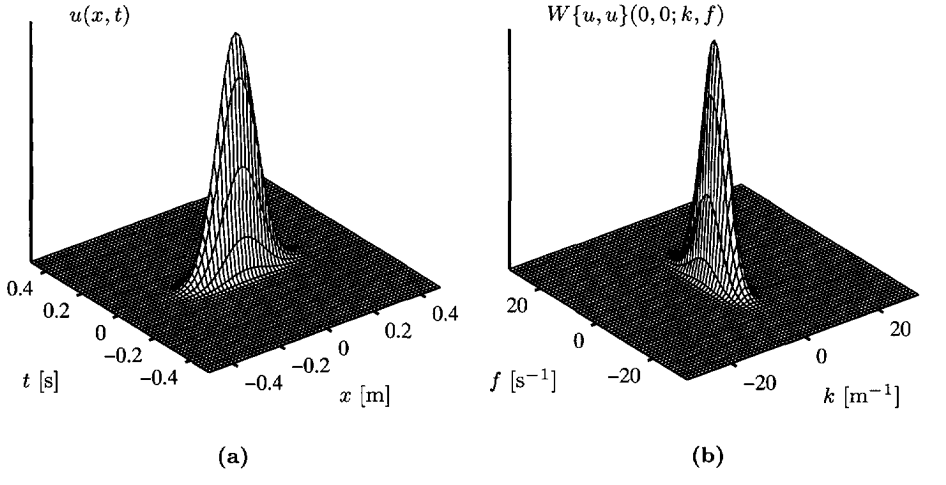

Figure 5.2: *Wigner distribution of a two-dimensional Gaussian signal; (a) signal, (b)* $W\{u,u\}(0,0;k,f)$.

5.5 Kernels for two-dimensional local power spectra

The evaluation of the Wigner distribution of a two-dimensional signal requires a local auto-correlation and Fourier transformation over an infinite two-dimensional window. In a practical implementation the evaluation will always take place over a finite window. This finite space-shift and time-shift window is the simplest form of kernel function. The resulting representation is called a pseudo Wigner distribution. Analogous to the one-dimensional time-frequency analysis, there is an infinite number of other kernel functions to be chosen from. An important aspect of a kernel is its capacity for cross term suppression. In the one-dimensional case it was shown that optimum cross term suppression can be achieved by the application of a low-pass weighting function on the ambiguity function. In order to do the same for a (sliding-window) two-dimensional analysis would require the computation of a four-dimensional ambiguity function and a two-dimensional Fourier transformation for every space-time point. The computation time involved in this optimization process would exceed the limit that is acceptable for a practical implementation on seismic data. Therefore, we have limited the implementation to fixed kernels.

We will consider two initial domains for the analysis. First, the straightforward approach in the space-time domain is taken. Here, the local power spectrum is obtained after three basic operations on the local space-time auto-correlation function (Eq.(5.3)) of a windowed portion of the signal. The first step is a convolution over the space-time variables with the space-time kernel function given by Eq.(5.13). The convolution is combined with a weighting over the correlation variables by the kernel. Finally, the local power spectrum is obtained by a Fourier transformation over the correlation variables of the modified space-time correlation function. The local power spectrum $P\{u,u\}(x,t;k,f)$ can be expressed in terms of the space-time auto-correlation function and space-time kernel function as

$$P\{u,u\}(x,t;k,f) = \mathcal{F}_{\xi}^{+}\mathcal{F}_{\tau}^{-}\left\{\int_{x'\in I\!R}\int_{t'\in I\!R}\Psi(x-x',t-t',\xi,\tau)R\{u,u\}(x',t';\xi,\tau)\mathrm{d}x'\mathrm{d}t'\right\}. \tag{5.44}$$

A flow chart illustrating the implementation through a smoothed local auto-

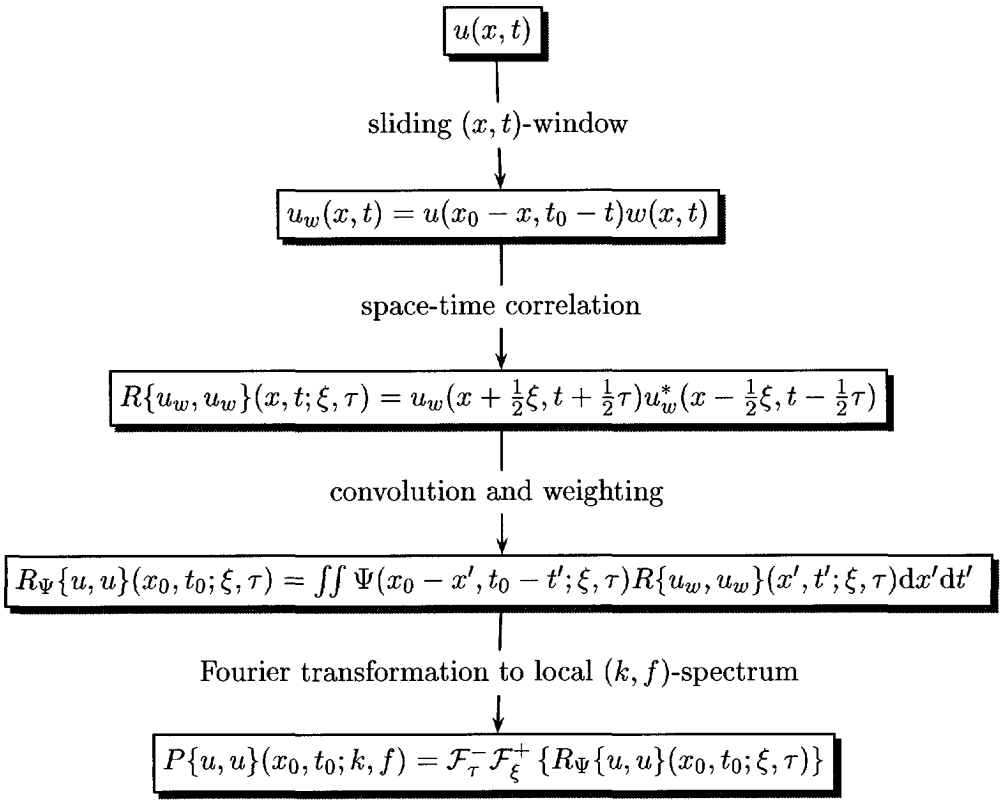

Figure 5.3: *Flow chart of the implementation of the multi-dimensional local power spectrum through a local space-time domain auto-correlation function.*

correlation function is shown in Fig. 5.3. In a numerical implementation the first three steps can be combined into the computation of a smoothed correlation over a finite number of shifts for each point in the (x,t)-domain to be analyzed.

Another Wigner type representation can be obtained by a windowed correlation of a sliding-window wavenumber-frequency spectrum. In this case, the kernel is introduced in the local spectral auto-correlation domain (Eq.(5.5)) by convolution with respect to the frequency variables. The local power spectrum is then obtained by an inverse Fourier transformation over the frequency-shift variables. The smoothing in the space-time domain is introduced by weighting the frequency-domain correlation function with respect to the frequency-shift variables. The local power spectrum can be expressed as

$$P\{u,u\}(x,t;k,f) = \mathcal{F}_\kappa^- \mathcal{F}_\nu^+ \left\{ \int_{k' \in I\!R} \int_{f' \in I\!R} \Psi(\kappa,\nu;k-k',f-f') R\{\tilde{u},\tilde{u}\}(k',f';\kappa,\nu) \mathrm{d}k' \mathrm{d}f' \right\}. \tag{5.45}$$

In the implementation of Eq.(5.45), the kernel $\Psi(\kappa,\nu;k,f)$ is brought into the computation through two window functions. The smoothing over frequency is determined by the window $w(x,t)$ of the sliding-window Fourier transformation,

$$\Psi(x=x_0,t=t_0;k,f) = \mathcal{F}_x^+ \mathcal{F}_t^- \{w(x,t)\}. \tag{5.46}$$

The smoothing over x and t is controlled by the size and shape of the window $w(\kappa,\nu)$ that is applied on the frequency correlation function, i.e.

$$\Psi(x,t;k=k_0,f=f_0) = \mathcal{F}_\kappa^- \mathcal{F}_\nu^+ \{w(\kappa,\nu)\}. \tag{5.47}$$

A flow chart illustrating a numerical implementation of the local wavenumber-frequency representation through a sliding window Fourier transformation is given in Fig. 5.4. Generally, window functions will be used that are independent of space, time, wavenumber and frequency. In that case the smoothing kernel in the joint space-time-wavenumber-frequency domain is given by

$$\Psi(x,t;k,f) = \Psi(x=x_0,t=t_0;k,f)\Psi(x,t;k=k_0,f=f_0). \tag{5.48}$$

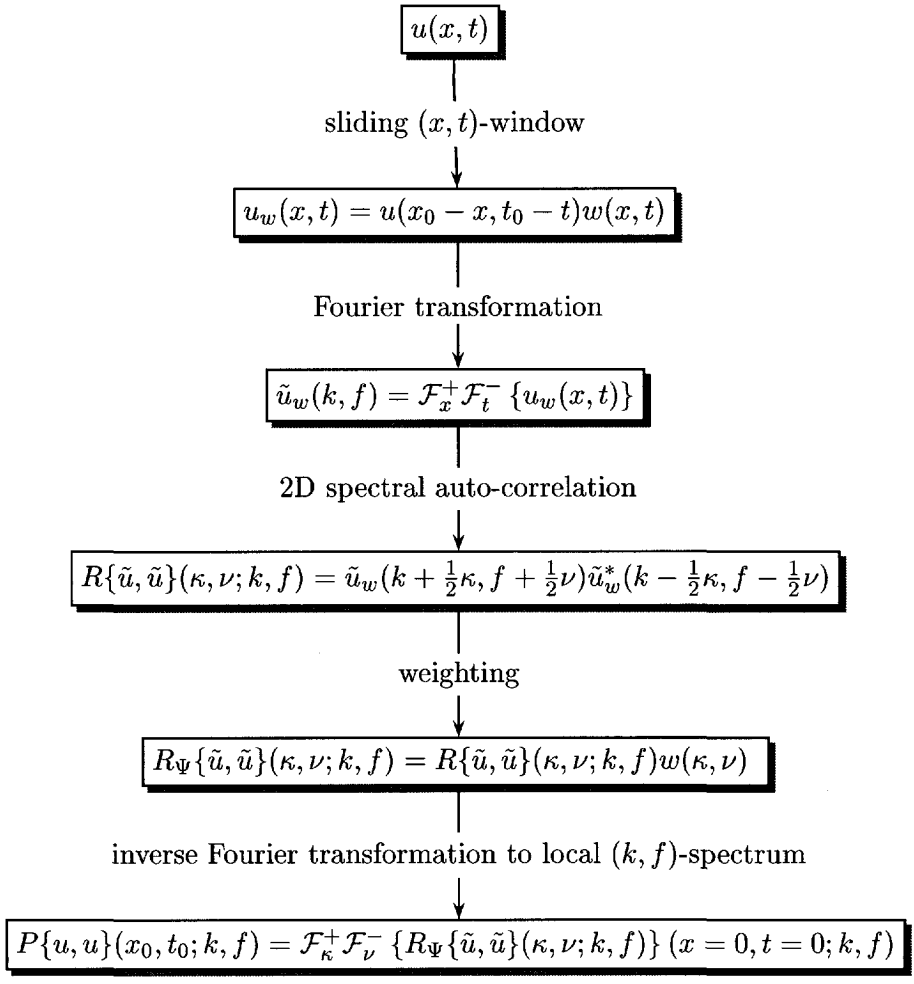

Figure 5.4: *Flow chart of the implementation of the multi-dimensional local power spectrum through a wavenumber-frequency domain correlation function.*

In the next sections some choices for the kernel function and their properties will be discussed and illustrated with numerical examples. The kernels are all separable in the space and time coordinates, i.e. they are products of two mutually independent kernels, given by

$$\Psi(\kappa, \nu; \xi, \tau) = \Psi(\kappa; \xi)\Psi(\nu; \tau). \tag{5.49}$$

5.5.1 Pseudo Wigner distribution

The closest computable approximation to the Wigner distribution is the pseudo Wigner distribution. It is the Wigner distribution computed over a finite window of space-shifts and time-shifts

$$P\{u,u\}(x,t;k,f) = \mathcal{F}_{\xi}^{+}\mathcal{F}_{\tau}^{-}\{\Psi(\xi,\tau)R\{u,u\}(x,t;\xi,\tau)\}. \tag{5.50}$$

The kernel $\Psi(\xi, \tau)$ is a symmetrical real-valued window function. The properties of the two-dimensional pseudo Wigner distribution are essentially the same as those of the one-dimensional pseudo Wigner distribution.

In Fig. 5.5 slices through the pseudo-Wigner distribution of an annular space-time shape is shown. The annular amplitude profile is given by

$$u(x,t) = \exp\left[-2\pi \frac{\left|\left((x-x_0)^2 + (t-t_0)^2 - r^2\right)\right|}{\sigma^2}\right], \tag{5.51}$$

where r is the radius. In the example the signal was discretized on a grid of 128 by 128 samples and the kernel was implemented on a 32 by 32 sliding window of data. The pseudo Wigner distribution provides an image of the frequency content that is sharply localized in both the space-time and frequency domains. However, as was to be expected, the pseudo Wigner distribution of a multi-component signal contains cross terms between the components. The analysis of the domain allocation of the cross terms of section 2.6 also applies for the multi-dimensional case.

The cross terms are located midway between the auto terms in joint space-time-wavenumber-frequency domain. For a signal that is composed of two components

$$u(x,t) = u_1(x,t) + u_2(x,t), \tag{5.52}$$

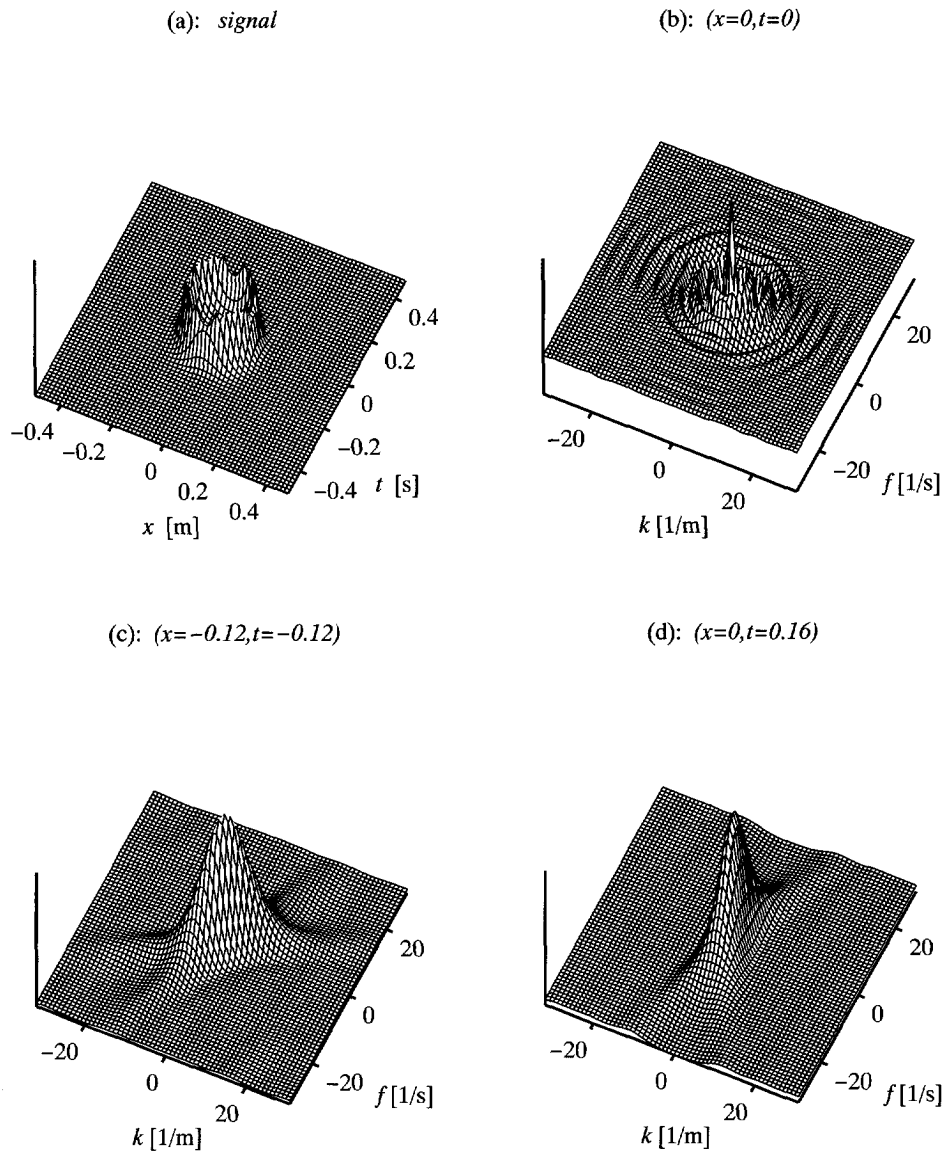

Figure 5.5: *Pseudo Wigner distribution of an annular region; (a) signal, (b)* $W\{u,u\}(0,0;k,f)$*, (c)* $W\{u,u\}(-0.12,-0.12;k,f)$*, and (d)* $W\{u,u\}(0,0.16;k,f)$.

the Wigner distribution is the sum of the Wigner distributions of the components and a cross term

$$\begin{aligned} W\{u,u\}(x,t;k,f) =& W\{u_1,u_1\}(x,t;k,f) + W\{u_2,u_2\}(x,t;k,f) \\ &+ 2\mathrm{Re}\{W\{u_1,u_2\}(x,t;k,f)\}. \end{aligned} \tag{5.53}$$

This cross term, $W\{u_1,u_2)(x,t;k,f)$, is the cross-Wigner distribution of the two components, given by

$$W\{u_1,u_2\}(x,t;k,f) = \mathcal{F}_\xi^+ \mathcal{F}_\tau^- \{R\{u_1,u_2\}(x,t;\xi,\tau)\}, \tag{5.54}$$

where $R\{u_1,u_2\}(x,t;\xi,\tau)$ is the local space-time cross-correlation function, defined as

$$R\{u_1,u_2\}(x,t;\xi,\tau) = u_1(x+\tfrac{1}{2}\xi, t-\tfrac{1}{2}\tau)u_2^*(x-\tfrac{1}{2}\xi, t-\tfrac{1}{2}\tau). \tag{5.55}$$

For a signal that is composed of two exponentials

$$u(x,t) = \exp\left[-\mathrm{j}2\pi(k_1x - f_1t)\right] + \exp\left[-\mathrm{j}2\pi(k_2x - f_2t)\right], \tag{5.56}$$

the cross-Wigner distribution between the two components is given by

$$\begin{aligned} W\{u_1,u_2\}(x,t;k,f) =& 2\cos\left[2\pi((k_2-k_1)x - (f_2-f_1)t)\right] \\ & \delta\left(k - \tfrac{1}{2}(k_1+k_2), f - \tfrac{1}{2}(f_1+f_2)\right). \end{aligned} \tag{5.57}$$

Equation (5.57) shows that the cross terms appear midway between the (x,t,k,f)-locations of the components and are modulated proportionally to the distance in the (k,f)-plane between the components. Figure 5.6 shows three (k,f)-slices through the pseudo Wigner distribution of a signal that is composed of two cosines,

$$u(x,t) = \cos\left[-2\pi(4x - 10t)\right] + \cos\left[-2\pi(10x - 20t)\right]. \tag{5.58}$$

The signal was discretized on 128 by 128 grid. The kernel was implemented on a 32 by 32 sliding window of data. Note that there are also a cross terms between the positive and negative frequencies of the signal.

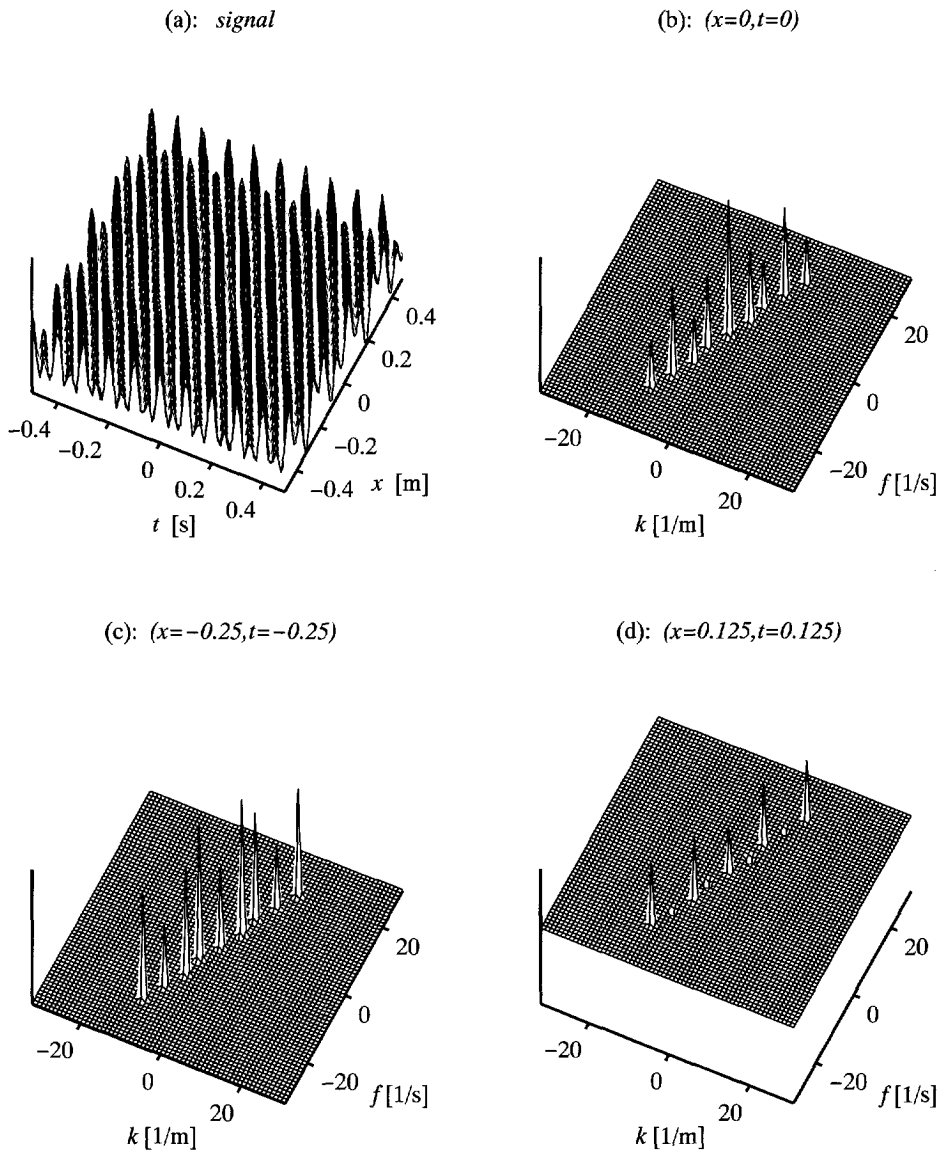

Figure 5.6: *Pseudo Wigner distribution of the sum of two cosines (Eq.(5.58)); (a) signal, (b)* $W\{u,u\}(0,0;k,f)$*, (c)* $W\{u,u\}(-0.25,-0.25;k,f)$*, and (d)* $W\{u,u\}(0.125,0.125;k,f)$*.*

5.5.2 Spectrogram

The two-dimensional spectrogram is the squared modulus of a Fourier transformation over a sliding window of data

$$P\{u,u\}(x,t;k,f) = \left|\mathcal{F}^{+}_{x'}\mathcal{F}^{-}_{t'}\left\{u(x',t')w(x'-x,t'-t)\right\}\right|^2. \tag{5.59}$$

In terms of the generalized class (Eqs.(5.11) and (5.12)), the kernel that generates the spectrogram is given by

$$\Psi(\kappa,\nu;\xi,\tau) = A\{w,w\}(-\kappa,-\nu;\xi,\tau), \tag{5.60}$$

where $A\{w,w\}(\kappa,\nu;\xi,\tau)$ is the ambiguity function of the window function $w(x,t)$. The spectrogram can therefore also be considered as a smoothed version of the Wigner distribution. In case the window function is real valued and symmetric, the smoothing kernel is the Wigner distribution of the window function $w(x,t)$. The smoothing can then be expressed in the (x,t,k,f)-domain as

$$\begin{aligned} &P\{u,u\}(x,t;k,f) = \\ &\int_{x'\in\mathbb{R}}\int_{t'\in\mathbb{R}}\int_{k'\in\mathbb{R}}\int_{f'\in\mathbb{R}} W\{w,w\}(x-x',t-t';k-k',f-f') \\ &\qquad W\{u,u\}(x',t';k',f')\mathrm{d}x'\mathrm{d}t'\mathrm{d}k'\mathrm{d}f'. \end{aligned} \tag{5.61}$$

Figures 5.7 and 5.8 show spectrogram slices for the annular region and the two-component cosine signal. The spectrogram was computed with a Gaussian shaped window of 32 by 32 samples. The localization of energy in the joint space-time-wavenumber-frequency domain is governed by the size of window. Rapid variations in either domain cannot be resolved by the spectrogram. This is clearly illustrated by the spectrogram of the two-component cosine signal, where the space-time behaviour of the signal is not reflected in the representation. However, the absence of cross term interference gives the spectrogram an important advantage over other representations. In the multi-dimensional case this property is even more important than in the representations of one-dimensional signals as visual separation of cross terms and auto terms will be very difficult in a four-dimensional representation.

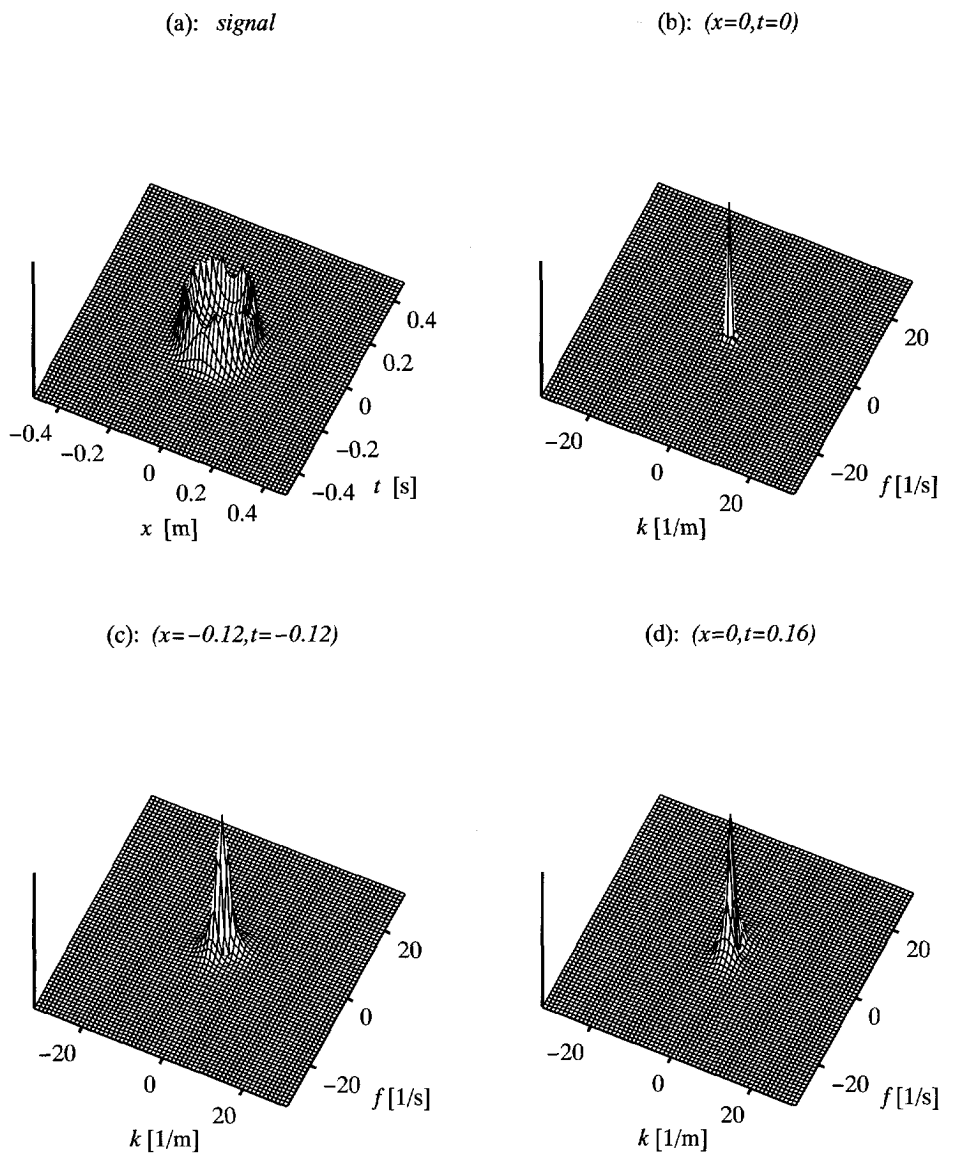

Figure 5.7: *Spectrogram of the annular region (Eq.(5.51)); (a) signal, (b)* $P\{u,u\}(0,0;k,f)$*, (c)* $P\{u,u\}(-0.12,-0.12;k,f)$*, and (d)* $P\{u,u\}(0,0.16;k,f)$.

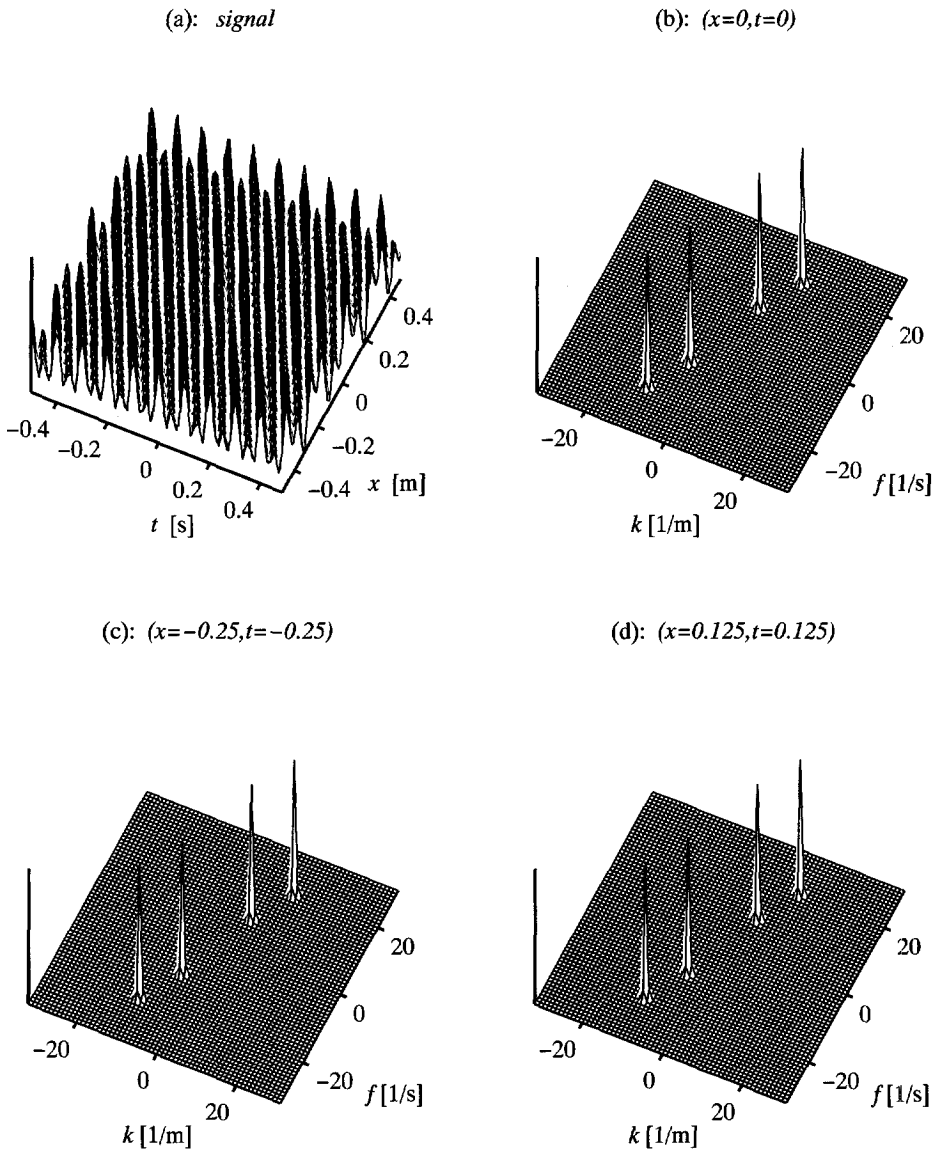

Figure 5.8: *Spectrogram of the sum of two cosines (Eq.(5.58)); (a) signal, (b)* $P\{u,u\}(0,0;k,f)$*, (c)* $P\{u,u\}(-0.25,-0.25;k,f)$*, and (d)* $P\{u,u\}(0.125,0.125;k,f)$.

5.5.3 Generalized Wigner distribution

The generalized Wigner distribution is found by independently smoothing the Wigner distribution along the space-time and wavenumber-frequency axes. The kernel function of the generalized Wigner distribution (Jacobson and Wechsler 1988) can be represented as

$$\Psi(x,t;k,f) = \Psi(x,t)\Psi(k,f). \tag{5.62}$$

The kernel is usually implemented in the space-time correlation domain (Eq.(5.44)). The generalized Wigner distribution is therefore also known as smoothed pseudo Wigner distribution. Independent smoothing in the space-time and wavenumber-frequency domains provides optimal control over the trade-off between energy localization and cross term interference in the representation. Figure 5.9 shows slices through the smoothed pseudo Wigner distribution of the two-component cosine signal. The smoothing suppresses nearly all cross-term interference in the wavenumber-frequency domain. However, removing the cross terms implies that the phase information is lost in the representation. As a result, the local wavenumber-frequency power spectrum slices are nearly identical for the three different space-time locations.

A different Wigner-type representation is obtained by correlation of the sliding-window Fourier transformation of the signal (Stankovič et al. 1995). If $\tilde{u}_w(k,f)$ is the Fourier transform of a windowed portion of the data, i.e. $u_w(x,t) = u(x',t')w(x'-x,t'-t)$, then the Wigner distribution of $u_w(x,t)$ is given by

$$P\{u_w,u_w\}(x,t;k,f) = \mathcal{F}_\kappa^- \mathcal{F}_\nu^+ \left\{\tilde{u}_w(k+\tfrac{1}{2}\kappa, f+\tfrac{1}{2}\nu)\tilde{u}_w^*(k-\tfrac{1}{2}\kappa, f-\tfrac{1}{2}\nu)\right\}. \tag{5.63}$$

In the centre of the window, at $(x=0,t=0)$, the local wavenumber frequency spectrum is found as

$$P\{u_w,u_w\}(0,0,k,f) = \mathcal{F}_\kappa^- \mathcal{F}_\nu^+ \left\{\tilde{u}_w(k+\tfrac{1}{2}\kappa, f+\tfrac{1}{2}\nu)\tilde{u}_w^*(k-\tfrac{1}{2}\kappa, f-\tfrac{1}{2}\nu)\right\}(x=0,t=0;k,f), \tag{5.64}$$

which implies that in a discrete implementation the inverse Fourier transformation over the wavenumber and frequency shift variables can be replaced

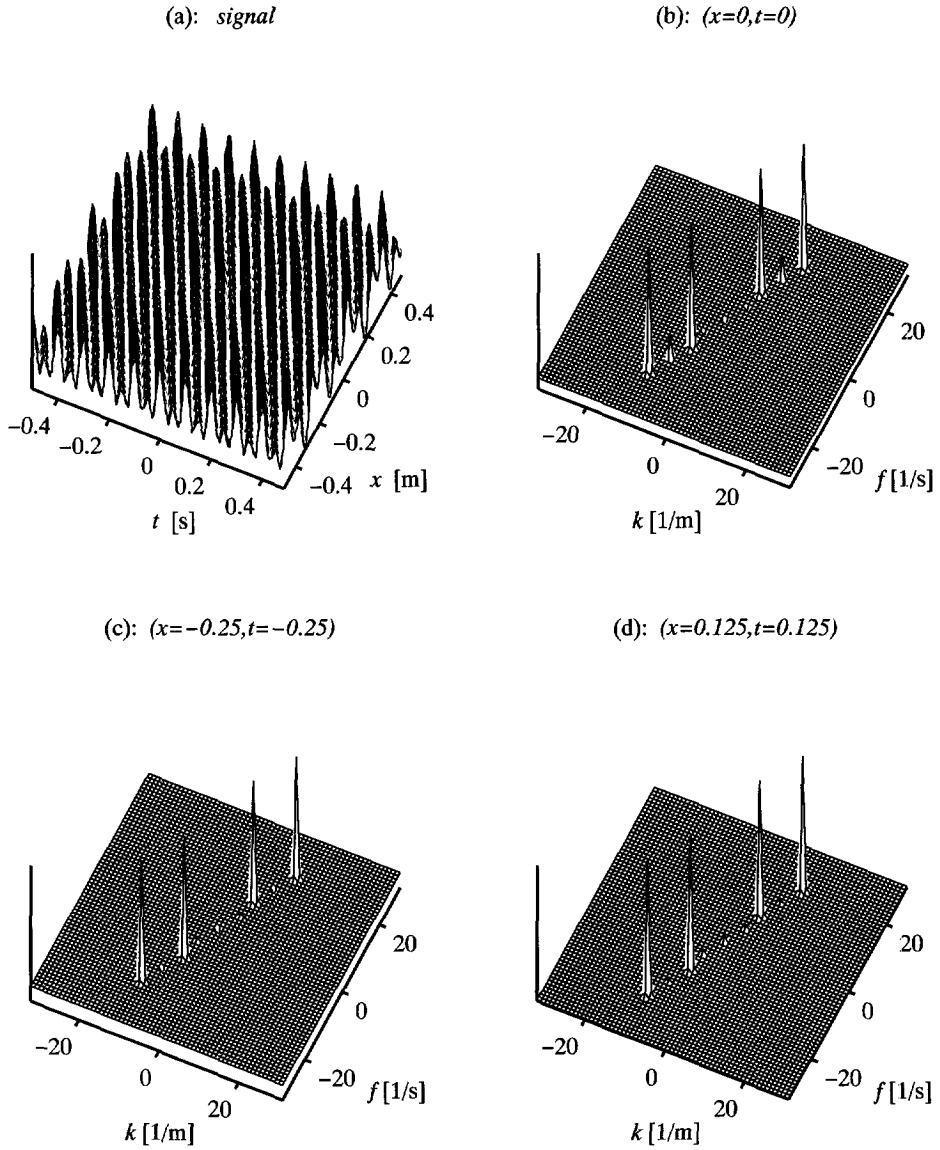

Figure 5.9: *Smoothed pseudo Wigner distribution of the sum of two cosines (Eq.(5.58)); (a) signal, (b)* $P\{u,u\}(0,0;k,f)$*, (c)* $P\{u,u\}(-0.25,-0.25;k,f)$*, and (d)* $P\{u,u\}(0.125,0.125;k,f)$*.*

by a summation over κ and ν. Eq.(5.64) can be applied to every space-time sample of an image, and the result will be a Wigner type representation with better localization properties, when compared to the spectrogram. However, the correlation in the wavenumber-frequency domain will also result in cross terms. A judicious choice of the windows $w(\nu)$ and $w(\kappa)$, can however minimize cross-term interference. Slices through modified sliding-window Fourier transformation of the annular shaped profile are shown in Fig. 5.10. The localization of energy is marginally sharper than in the spectrogram (Fig. 5.7).

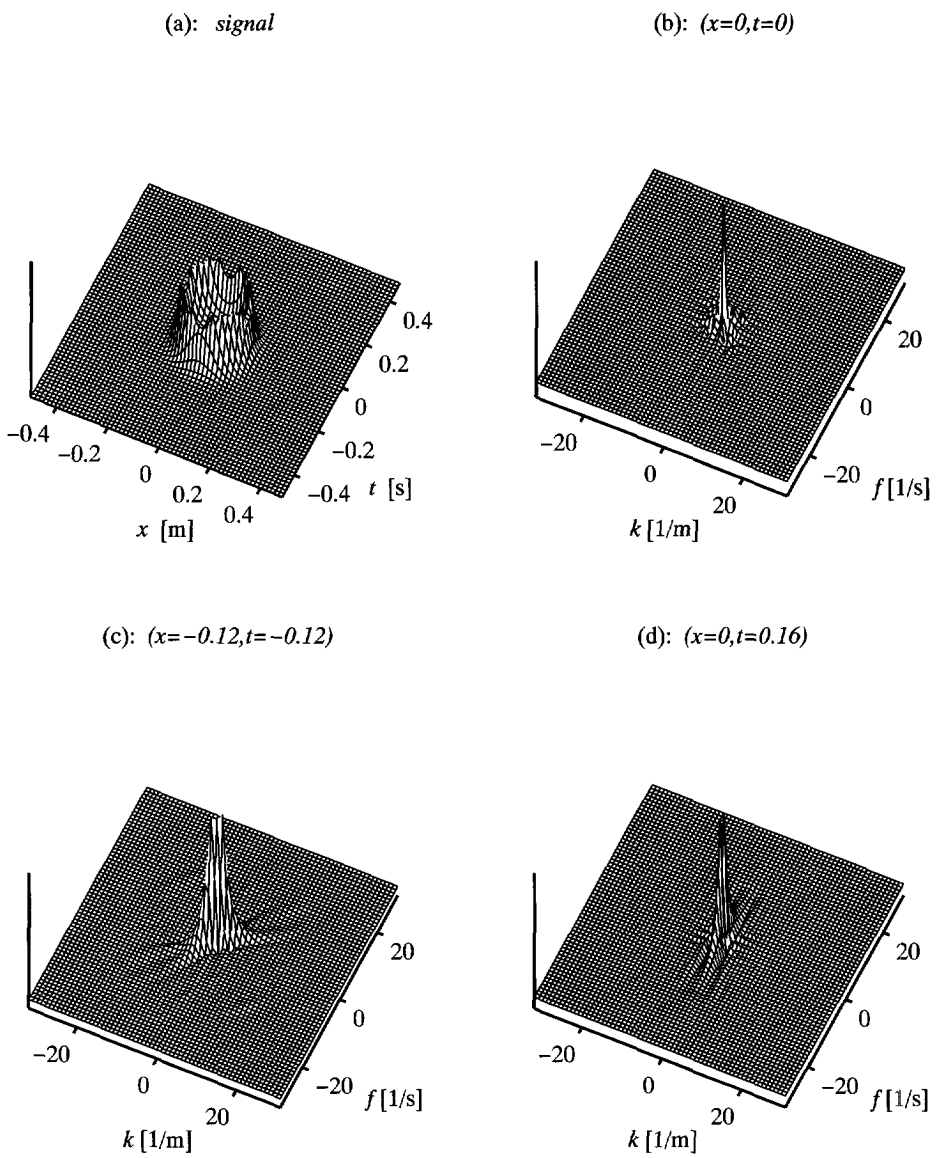

Figure 5.10: *Generalized Wigner representation of the annular region (Eq.(5.51)) obtained by correlation in the sliding-window Fourier transformation.; (a) signal, (b)* $P\{u,u\}(0,0;k,f)$*, (c)* $P\{u,u\}(-0.12,-0.12;k,f)$*, and (d)* $P\{u,u\}(0,0.16;k,f)$*.*

5.6 The local slant-stack power spectrum

The single Radon transform, or slant stack is a widely used data representation in exploration seismology. The Radon transformation plays a prominent role in the analysis of acoustic wave-fields, because it essentially performs a decomposition of the data into its plane-wave components. The application of the Radon transformation in geophysics was pioneered by Chapman (1978). He did not only recognize it as a method that can be used for synthesizing depth models from seismograms, but also contributed much to that is known today about the general properties and computational aspects of the Radon transformation (Chapman 1979, 1980). Nowadays, the Radon transformation is applied in a broad range of applications that are concerned with the intrinsic coupling of space and time in seismic data.

In certain applications the global Radon transform is not the ideal analysis tool. Sometimes it is not sufficient to know which plane wave components or dips are present in the data, but also where they occur. For instance, using a Radon transformation for the analysis of a stacked and migrated seismic section only makes sense if the locations of the dipping events are known. In this type of applications a localized Radon transformation would be required. Localized Radon transformations have been defined and applied for different purposes (McMechan 1983; Milkereit 1987; Copeland et al. 1995). These local Radon representations are all based on the application of the classical slant stack on windowed portions of the data. In the same way as the sliding-window power spectrum is a member of a very large class of possible local power spectra, the sliding-window Radon transformation is just one choice from an infinite number of possible localized Radon transformations. This class of localized Radon representations will be defined in terms of the general class of multi-dimensional local power spectra that was introduced earlier.

5.6.1 The Radon transformation

The Radon transform of a function $u(\boldsymbol{x}, t)$ in a three-dimensional geometry, where $\boldsymbol{x} = \{x_1, x_2, x_3\}$, can be expressed as

$$\mathcal{R}\{u\} = \breve{u}(\boldsymbol{p}, \tau) = \int_{\boldsymbol{x} \in I\!R^3} u(\boldsymbol{x}, \tau + p_i x_i) \mathrm{d}\boldsymbol{x}, \tag{5.65}$$

where $\boldsymbol{p}$ is the three-dimensional ray-parameter or slowness vector, given by $\boldsymbol{p} = \{p_1, p_2, p_3\}$ and τ is the intercept time. The Radon transformation in

the formulation of Eq.(5.65), is also known as $\tau - p$ transformation or slant stack. Taking the Fourier transformation with respect to the intercept time τ, Eq.(5.65) transforms into

$$\hat{\check{u}}(\boldsymbol{p}, f) = \int_{\boldsymbol{x} \in I\!R^3} \exp(\mathrm{j}2\pi f \boldsymbol{p} \cdot \boldsymbol{x}) \hat{u}(\boldsymbol{x}, f) \mathrm{d}\boldsymbol{x}, \quad f \in I\!R^+. \tag{5.66}$$

Equation (5.65) is a Fourier transformation of the function $\hat{u}(\boldsymbol{x}, f)$ over the spatial coordinates $\{x_1, x_2, x_3\}$. The relation between wavenumber vector $\boldsymbol{k} = \{k_1, k_2, k_3\}$ and slowness vector $\boldsymbol{p}$ is given by

$$\boldsymbol{k} = f\boldsymbol{p}, \tag{5.67}$$

and reveals the intimate relation between the temporal Fourier transformation of the slant stack, $\hat{\check{u}}(\boldsymbol{p}, f)$, and the wavenumber-frequency spectrum $\tilde{u}(\boldsymbol{k}, f)$:

$$\tilde{u}(\boldsymbol{k}, f) = \tilde{u}(f\boldsymbol{p}, f) = \hat{\check{u}}(\boldsymbol{p}, f), \ f \in I\!R^+. \tag{5.68}$$

In the next section we will propose a local Radon transformation, that is based on a relation between the multi-dimensional Wigner distribution and the local slowness-frequency power spectrum, similar to the relation of Eq.(5.68).

5.6.2 The Wigner-Radon representation and general class

In the previous sections the framework for local wavenumber-frequency analysis was derived. With the relations between the global Fourier transformations and the Radon transform in mind (Eqs.(5.65)-(5.68)), a local slant stack can be defined within the general class of local frequency representations. In view of our later definition of the local slant stack we want to restrict the frequency parameter f to positive values only. The domain occupied with positive frequencies is introduced as

$$I\!R^+ = \{f \in I\!R, \ f \geq 0\}. \tag{5.69}$$

We leave the frequency-shift parameter $\nu \in I\!R$. In Appendix B it is shown how this restriction is accommodated in the Fourier transform relations between Wigner distribution, instantaneous auto-correlation, local spectral auto-correlation and ambiguity function, without loss of generality of the

analysis of Chapters 2, 3, and the previous section. The restriction to positive f can only be made for signals that are real-valued or analytic. However, in all practical cases these are the only signals that we are interested in. Hence, we can distinguish two cases in our analysis: $u(\boldsymbol{x},t)$ is real valued and $u^a(\boldsymbol{x},t)$, which is the analytic function associated with the real valued function $u(\boldsymbol{x},t)$. First, we deal with $u(t)$ is real. We have

$$R\{u,u\}(\boldsymbol{x},t;\boldsymbol{\xi},\tau) = u(\boldsymbol{x}+\tfrac{1}{2}\boldsymbol{\xi},t+\tfrac{1}{2}\tau)u(\boldsymbol{x}-\tfrac{1}{2}\boldsymbol{\xi},t-\tfrac{1}{2}\tau) \tag{5.70}$$

and we have (cf. Eq.(B.13))

$$\begin{aligned} W\{u,u\}(\boldsymbol{x},t;\boldsymbol{k},f) &= \mathcal{F}^+_{\boldsymbol{\xi}}\mathcal{F}^-_{\tau}\left\{R\{u,u\}(\boldsymbol{x},t;\boldsymbol{\xi},\tau)\right\},\ f\in I\!R^+,\\ R\{u,u\}(\boldsymbol{x},t;\boldsymbol{\xi},t) &= 2\mathrm{Re}\mathcal{F}^-_{\boldsymbol{k}}\mathcal{F}^+_{f}\left\{\chi_{I\!R^+}(f)W\{u,u\}(\boldsymbol{x},t;\boldsymbol{k},f)\right\}, \end{aligned} \tag{5.71}$$

where $\chi_{I\!R^+}$ is the characteristic function of the domain $I\!R^+$ and is given by

$$\chi_{I\!R^+} = \left\{1,\tfrac{1}{2},0\right\} \text{ when } \{f>0, f=0, f<0\}. \tag{5.72}$$

The relation between the Wigner distribution and local wavenumber-frequency auto-correlation function is given by

$$\begin{aligned} W\{u,u\}(\boldsymbol{x},t;\boldsymbol{k},f) &= \mathcal{F}^-_{\boldsymbol{\kappa}}\mathcal{F}^+_{\nu}\left\{R\{\tilde{u},\tilde{u}\}(\boldsymbol{\kappa},\nu;\boldsymbol{k},f\right\},\ f\in I\!R^+,\\ R\{\tilde{u},\tilde{u}\}(\boldsymbol{\kappa},\nu;\boldsymbol{k},f) &= \mathcal{F}^+_{\boldsymbol{x}}\mathcal{F}^-_{t}\left\{W\{u,u\}(\boldsymbol{x},t;\boldsymbol{k},f)\right\},\ f\in I\!R^+. \end{aligned} \tag{5.73}$$

Next we introduce, using $\boldsymbol{k}=f\boldsymbol{p}$,

$$S\{u,u\}(\boldsymbol{x},t;\boldsymbol{p},f) = W\{u,u\}(\boldsymbol{x},t;f\boldsymbol{p},f),\ f\in I\!R^+ \tag{5.74}$$

and its time domain equivalent as

$$\check{S}\{u,u\}(\boldsymbol{x},t;\boldsymbol{p},\tau) = 2\mathrm{Re}\left\{\mathcal{F}^+_f\left\{\chi_{I\!R^+}(f)S\{u,u\}(\boldsymbol{x},t;p,f)\right\}\right\}. \tag{5.75}$$

Using Eq.(5.73) and the transformations of Eq.(5.70), we arrive at

$$\check{S}\{u,u\}(\boldsymbol{x},t;\boldsymbol{p},\tau) = \int_{\boldsymbol{\xi}\in I\!R^3} R\{u,u\}(\boldsymbol{x},t;\boldsymbol{\xi},\tau+\boldsymbol{p}\cdot\boldsymbol{\xi})\mathrm{d}\boldsymbol{\xi}. \tag{5.76}$$

Note that $\check{S}$ is real-valued. We will refer to Eq.(5.75) as the Wigner-Radon representation. Comparison of Eq.(5.76) with the expression of the global slant stack Eq.(5.65) shows that the Wigner-Radon representation can be

interpreted as a slant stack of the local space-time auto-correlation function over the space-time shift variables.

Next, we consider the case that we are dealing with $u^a(\boldsymbol{x},t)$. The analytic signal is most easily introduced in the frequency domain (see Section 2.2.3), hence,

$$\hat{u}^a(\boldsymbol{x},f) = 2\chi_{I\!R^+}(f)\hat{u}(\boldsymbol{x},f), \tag{5.77}$$

from which it follows that (cf. Eq.(B.17))

$$R\{\tilde{u}^a,\tilde{u}^a\}(\boldsymbol{\kappa},\nu;\boldsymbol{k},f) = 4\chi_{I\!R^+}(f)\Pi(\nu/4|f|)R\{\tilde{u},\tilde{u}\}(\boldsymbol{\kappa},\nu;\boldsymbol{k},f), \tag{5.78}$$

with Π, the box-car function defined by Eq.(B.18). Now we can write

$$\begin{aligned} W\{u^a,u^a\}(\boldsymbol{x},t;\boldsymbol{k},f) &= \mathcal{F}^-_{\boldsymbol{\kappa}}\mathcal{F}^+_{\nu}\left\{R\{\tilde{u}^a,\tilde{u}^a\}(\boldsymbol{\kappa},\nu;\boldsymbol{k},f)\right\}, \\ R\{\tilde{u}^a,\tilde{u}^a\} &= \mathcal{F}^-_{\boldsymbol{x}}\mathcal{F}^-_{t}\left\{W\{u^a,u^a\}(\boldsymbol{x},t;\boldsymbol{k},f)\right\}. \end{aligned} \tag{5.79}$$

In the same way we have

$$\begin{aligned} W\{u^a,u^a\}(\boldsymbol{x},t;\boldsymbol{k},f) &= \mathcal{F}^+_{\boldsymbol{\xi}}\mathcal{F}^-_{\tau}\left\{R\{u^a,u^a\}(\boldsymbol{x},t;\boldsymbol{\xi},\tau)\right\}, \\ R\{u^a,u^a\} &= \mathcal{F}^-_{\boldsymbol{k}}\mathcal{F}^+_{f}\left\{W\{u^a,u^a\}(\boldsymbol{x},t;\boldsymbol{k},f)\right\}. \end{aligned} \tag{5.80}$$

Hence, the with $\boldsymbol{k} = f\boldsymbol{p}$, we find

$$S\{u^a,u^a\} = (\boldsymbol{x},t;\boldsymbol{p},f) = W\{u^a,u^a\}(\boldsymbol{x},t;f\boldsymbol{p},f). \tag{5.81}$$

The Wigner-Radon representation of the analytic signal can now be expressed as

$$\check{S}\{u^a,u^a\}(\boldsymbol{x},t;\boldsymbol{p},\tau) = \mathcal{F}^+_f\left\{S\{u^a,u^a\}(\boldsymbol{x},t;\boldsymbol{p},f)\right\}. \tag{5.82}$$

Using Eq.(5.80), we see that the Wigner-Radon representation can be expressed in terms of the local space-time auto-correlation function as

$$\check{S}\{u^a,u^a\}(\boldsymbol{x},t;\boldsymbol{p},\tau) = \int_{\boldsymbol{\xi}\in I\!R^3} R\{u^a,u^a\}(\boldsymbol{x},t;\boldsymbol{\xi},\tau+\boldsymbol{p}\cdot\boldsymbol{\xi})\mathrm{d}\boldsymbol{\xi}, \tag{5.83}$$

in which we again recognize a slant stack with respect to the space-time shift variables. Note that in this case $\check{S}$ is complex-valued.

The relation between the local slant-stack power spectrum and ambiguity function can be derived using Eq.(5.7). The ambiguity function is a Fourier transformation of $R\{u,u\}(\boldsymbol{x},t;\boldsymbol{\xi},\tau)\}$ with respect to the space-time coordinates $\boldsymbol{x}$ and t. Because these two variables play no role in the definition of the local slant stack of Eqs.(5.74) and (5.82), we can simply write

$$\breve{S}\{u,u\}(\boldsymbol{x},t;\boldsymbol{p},\tau) = \mathcal{F}_{\boldsymbol{\kappa}}^{-}\mathcal{F}_{\nu}^{+}\left\{\int_{\boldsymbol{\xi}\in I\!R^3} A\{u,u\}(\boldsymbol{\kappa},\nu;\boldsymbol{\xi},\tau+\boldsymbol{p}\cdot\boldsymbol{\xi})\mathrm{d}\boldsymbol{\xi}\right\}, \tag{5.84}$$

where u is either a real-valued function or the analytic function associated with the real-valued u. From here on, we will use the symbol u to denote these signals and the analysis applies also to both real-valued u and analytic u, after taking into consideration the consequences of the positivity of the frequency parameter f (see Appendix B).

Equation (5.84) shows that we can include the local slant stack in the generalized class of local power spectra of Eq.(5.11). The generalized local slant-stack power spectrum of the signal $u(\boldsymbol{x},t)$ is defined as

$$\breve{P}\{u,u\}(\boldsymbol{x},t;\boldsymbol{p},\tau) = \mathcal{F}_{\boldsymbol{\kappa}}^{-}\mathcal{F}_{\nu}^{+}\left\{\int_{\boldsymbol{\xi}\in I\!R^3} M\{u,u\}(\boldsymbol{\kappa},\nu;\boldsymbol{\xi},\tau+\boldsymbol{p}\cdot\boldsymbol{\xi})\mathrm{d}\boldsymbol{\xi}\right\}, \tag{5.85}$$

where $M\{u,u\}(\boldsymbol{\xi},\tau)$ is the characteristic function, defined by Eq.(5.12). We can interpret the generalized local slant-stack power spectrum as a slant stack with respect to the space and time shift variables of a weighted ambiguity function.

5.6.3 Properties of the Wigner-Radon representation

Because of the close relation between the generalized local slant-stack power spectrum and the generalized local wavenumber-frequency power spectrum, the properties of the generalized local slant-stack power spectrum can be easily derived from the properties of the generalized local wavenumber-frequency power spectrum (see section 5.3).

The space-time marginal can be derived from Eq.(5.29) and the definition of the local slowness-frequency power spectrum according to Eqs.(5.74) and

(5.81). We have

$$\begin{aligned} E(\boldsymbol{x},t) =& \int_{\boldsymbol{p}\in I\!R^3}\int_{f\in I\!R^+} S\{u,u\}(\boldsymbol{x},t;\boldsymbol{p},f)\mathrm{d}\boldsymbol{p}\mathrm{d}f \\ =& R\{u,u\}(\boldsymbol{x},t;\boldsymbol{\xi}=\boldsymbol{0},\boldsymbol{\tau}=0) = |u(\boldsymbol{x},t)|^2 . \end{aligned} \tag{5.86}$$

To retain this property in the generalized local slowness-frequency power spectrum the kernel must be constraint according to Eq.(5.30) . Similarly, with Eq.(5.24) and the definitions Eqs.(5.74) and (5.81), we find for the slowness-frequency marginal

$$E(\boldsymbol{p},f) = \int_{\boldsymbol{x}\in I\!R^3}\int_{t\in I\!R} S\{u,u\}(\boldsymbol{x},t;\boldsymbol{p},f)\mathrm{d}\boldsymbol{x}\mathrm{d}t = \left|\breve{\tilde{u}}(\boldsymbol{p},f)\right|^2 . \tag{5.87}$$

This property will be retained in the generalized local slowness-frequency power spectrum if the kernel is constraint according to Eq.(5.26).

The space-time marginal of the Wigner-Radon representation (Eqs.(5.76) and (5.82)) is given by

$$E(\boldsymbol{x},t) = \int_{\boldsymbol{p}\in I\!R^3}\int_{\tau\in I\!R} \breve{S}\{u,u\}(\boldsymbol{x},t;\boldsymbol{p},\tau)\mathrm{d}\boldsymbol{p}\mathrm{d}\tau = |u(\boldsymbol{x},t)|^2 , \tag{5.88}$$

where we have used Eq.(5.87) and applied Parseval's theorem (Eq.(A.8)). The slowness-time shift marginal is given by

$$E(\boldsymbol{p},\tau) = \int_{\boldsymbol{x}\in I\!R^3}\int_{t\in I\!R} \breve{S}\{u,u\}(\boldsymbol{x},t;\boldsymbol{p},\tau)\mathrm{d}\boldsymbol{x}\mathrm{d}t. \tag{5.89}$$

Using Eq.(5.24) with $\boldsymbol{k} = f\boldsymbol{p}$, and the definition of Wigner-Radon representation according to Eqs.(5.76) and (5.82), we arrive at

$$\begin{aligned} E(\boldsymbol{p},\tau) =& \mathcal{F}_f^+ \left\{\chi_{I\!R^+}(f) R\{\tilde{u},\tilde{u}\}(\boldsymbol{\kappa}=0,\nu=0;\boldsymbol{p},f)\right\} \\ =& \mathcal{F}_f^+ \left\{\breve{\tilde{u}}(\boldsymbol{p},f)\breve{\tilde{u}}^*(\boldsymbol{p},f)\right\} . \end{aligned} \tag{5.90}$$

Using the correlation property of the Fourier transformation Eq.(A.5), and taking the inverse Fourier transformation with respect to frequency (cf. Eq.(5.68)), we arrive at

$$E(\boldsymbol{p},\tau) = \int_{\tau'\in I\!R} \breve{u}^*(\boldsymbol{p},\tau')\breve{u}(\boldsymbol{p},\tau+\tau')\mathrm{d}\tau', \tag{5.91}$$

which is the auto-correlation of the global slant stack (see Eq.(5.65)) with respect to the intercept time variable τ.

None of the earlier definitions of the local Radon transform (Milkereit 1987; Copeland et al. 1995) satisfies the marginal properties of Eqs.(5.86)-(5.91). They are all based on the slant stack over a sliding window of data or integration over short line segments. As such, their energetic representation, $|\breve{u}(\boldsymbol{x}, t; \boldsymbol{p}, \tau)|^2$, can be considered as a smoothed version of the Wigner-Radon representation, which can be derived by the following analysis.

If we apply a sliding window $w(\boldsymbol{x}, t)$, centered at $(\boldsymbol{x_0}, t_0)$, we obtain a modified signal, given by

$$u_w(\boldsymbol{x}, t) = u(\boldsymbol{x}, t) w(\boldsymbol{x} - \boldsymbol{x_0}, t - t_0). \tag{5.92}$$

For convenience, we take $\boldsymbol{x_0} = \{0, 0, 0\}$ and $t_0 = 0$ in the following analysis. The local slant stack of the modified signal u_w is given by

$$\breve{u}_w(\boldsymbol{p}, \tau) = \int_{\boldsymbol{x} \in I\!R^3} w(\boldsymbol{x}, \tau + \boldsymbol{p} \cdot \boldsymbol{x}) u(\boldsymbol{x}, \tau + \boldsymbol{p} \cdot \boldsymbol{x}) \, \mathrm{d}\boldsymbol{x}. \tag{5.93}$$

Taking the Fourier transformation with respect to the intercept time τ we find the expression of the sliding-window slant stack in terms of the temporal sliding-window Fourier transformation (cf. Eq.(5.66)),

$$\breve{\hat{u}}_w(\boldsymbol{p}, f) = \int_{\boldsymbol{x} \in I\!R^3} \exp(\mathrm{j}2\pi f \boldsymbol{p} \cdot \boldsymbol{x}) \int_{f' \in I\!R} w(\boldsymbol{x}, f - f') \hat{u}(\boldsymbol{x}, f') \mathrm{d}f' \mathrm{d}\boldsymbol{x}, \; f \in I\!R^+ \tag{5.94}$$

The Fourier transformation over the spatial coordinate $\boldsymbol{x}$ transforms the window operation on $\boldsymbol{x}$ into a convolution in $\boldsymbol{p}$ (cf. Eq.(A.4)) and as a result we find for the sliding-window slowness-frequency spectrum

$$\breve{\hat{u}}_w(\boldsymbol{p}, f) = \int_{\boldsymbol{p'} \in I\!R^3} \int_{f' \in I\!R} \breve{\hat{w}}(\boldsymbol{p'} - \boldsymbol{p}, f' - f) \breve{\hat{u}}(\boldsymbol{p'}, f') \mathrm{d}\boldsymbol{p'} \mathrm{d}f', \; f \in I\!R^+. \tag{5.95}$$

Using the relation, $\boldsymbol{k} = f\boldsymbol{p}$, one sees that the sliding-window slant stack and sliding-window Fourier transformation $\tilde{u}_w(\boldsymbol{k}, f)$ (see Eq.(5.59)) are directly

related through

$$\tilde{u}_w(f\boldsymbol{p}, f) = \breve{\tilde{u}}_w(\boldsymbol{p}, f). \tag{5.96}$$

The last relation also shows that the sliding-window slowness-frequency power spectrum $|\breve{\tilde{u}}_w(\boldsymbol{p}, f)|^2$ can be expressed in terms of a multi-dimensional spectrogram (see section 5.5.2). This brings the sliding-window slant-stack power spectrum into the general class of local Radon representations. The kernel of the sliding-window slant-stack power spectrum is that of the spectrogram, i.e.

$$\Psi(\boldsymbol{\kappa}, \nu; \boldsymbol{\xi}, \tau) = A\{w, w\}(-\boldsymbol{\kappa}, -\nu; \boldsymbol{\xi}, \tau), \tag{5.97}$$

where $A\{w, w\}(\boldsymbol{\kappa}, \nu; \boldsymbol{\xi}, \tau)$ is the ambiguity function of the window. Note that the analysis with respect to the marginal and non-negativity properties of the spectrogram of Chapter 3 also applies to the multi-dimensional spectrogram and the sliding-window slant stack.

5.6.4 Numerical Implementation

The numerical implementation of the local slant-stack power spectrum can be carried out along similar lines as the implementation of the global Radon transformation. Here, we will discuss the implementation for a two-dimensional geometry, i.e. $\boldsymbol{x} = \{x\}$. For the global Radon transformation different approaches have been described (Beylkin 1987; Haneveld en Herman 1990; Vissinga 1992). A comparison of these approaches with regard to accuracy and computational speed has been made by Vercruijsse (1995). The conclusion of Vercruijsse is that the implementation with the method of Vissinga maintains the best balance between accuracy and computational speed in practical applications. In the numerical implementation of the Wigner-Radon representation computational speed is an important factor, as for each point in space-time domain a Radon transformation is carried out. For that reason the method of Vissinga will also be the most effective for the local slant-stack power spectrum. First, a local wavenumber-frequency spectrum from the general class is computed with one of the methods that were outlined in Section 5.5. The local wavenumber-frequency power spectrum is either computed by a 2-D FFT of a modified sliding space-time correlation function or a windowed correlation of a sliding-window Fourier transformation of the data

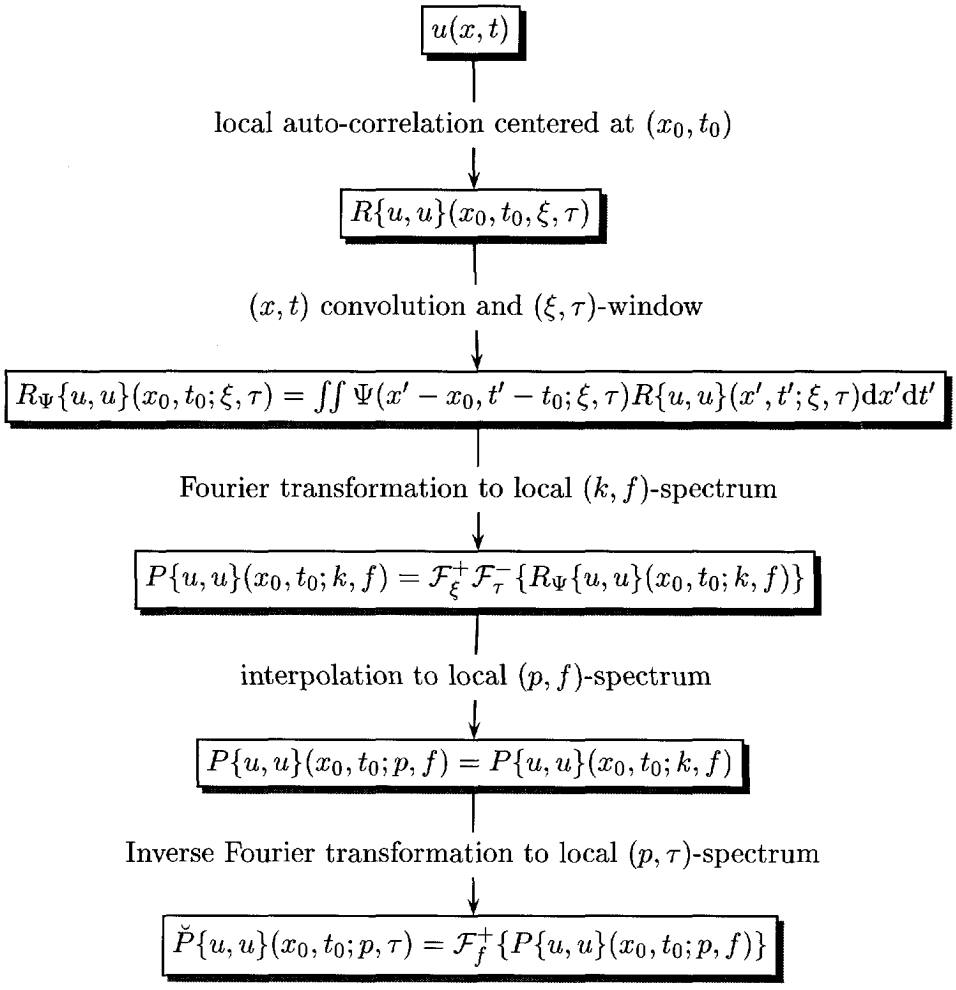

Figure 5.11: *Flow diagram for the computation of the local slant-stack power spectrum via the smoothed pseudo Wigner distribution.*

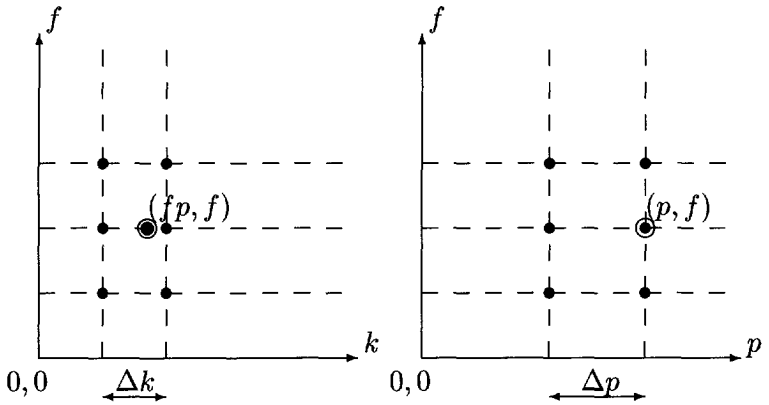

Figure 5.12: *Interpolation from a (k, f)-grid to a (p, f)-grid.*

(see Eqs.(5.44) and (5.45)). We prefer to use the analytic signal in the computation of the local wavenumber-frequency power spectrum. Since there is no energy at negative frequencies in the spectrum of an analytic signal, using the analytic signal rather than a real-valued signal has the advantage that there will be no cross terms between the negative and positive temporal frequencies in the representation. A closer analysis of the cross terms in Wigner-Radon representation will be made at the end of this section.

The next step is to obtain of the local slowness-frequency spectrum from the local wavenumber-frequency spectrum. A rectangular grid of (p, f)-values is obtained through an interpolation in the (k, f)-domain. The interpolation is illustrated in Fig. 5.12. To obtain a value at a point (p, f) (marked with a circle in the figure), the value at the corresponding point (pf, f), has to be computed. Since this point (pf, f) might not coincide with a grid-point in the (k, f)-domain, interpolation is needed in the k direction. In seismic applications a linear - first-order Lagrange - interpolation usually has sufficient accuracy (Vercruijsse 1995).

Finally, the Wigner-Radon representation is obtained by an inverse Fourier transformation of the local slowness-frequency power spectrum (cf. Eq.(5.81)). The computational procedure for the computation of a smoothed pseudo Wigner-Radon representation is outlined in the flow diagram of Fig. 5.11.

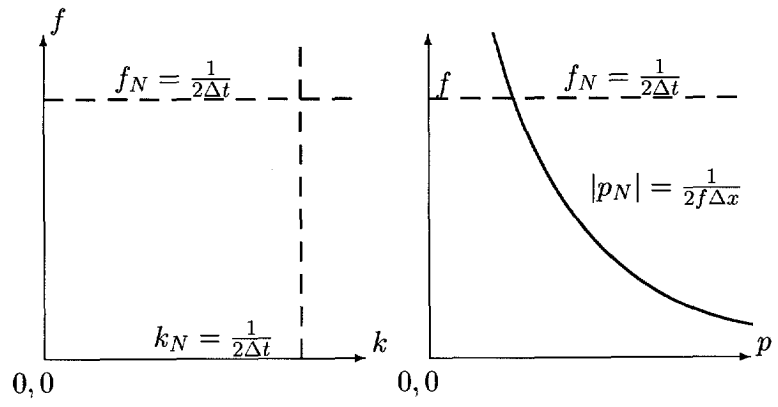

Figure 5.13: *Bounds on the wavenumber-frequency and slowness-frequency domains.*

Aliasing in the slowness-frequency domain

An important aspect in the numerical implementation is that the passing of aliased energy into the representation is to be avoided. In order to fulfill the requirements of the Nyquist sampling theorem, the data must be sampled in time at a sampling interval Δt such that

$$\Delta t \leq \frac{1}{2f_m}, \tag{5.98}$$

where f_m is the highest frequency in the signal. Given a certain a sampling rate, the Nyquist frequency, f_N, is given by

$$f_N = \frac{1}{2\Delta t}. \tag{5.99}$$

The Nyquist frequency gives the upper bound on the frequency spectrum of a sampled signal.

The same requirement has to be met for the spatial sampling interval Δx, i.e.

$$\Delta x \leq \frac{1}{2k_m}. \tag{5.100}$$

In practice, the spatial sampling interval is seldom small enough to prevent spatial aliasing. Usually the spatial sampling interval Δx is chosen such that

the maximum dip p_m that is expected to be present in the data is not aliased, i.e.

$$\Delta x = \frac{1}{2f_m p_m}. \tag{5.101}$$

The Nyquist wavenumber k_N is given by

$$k_N = \frac{1}{2\Delta x}. \tag{5.102}$$

In the Radon domain the limitations k_N and f_N are transformed into a hyperbola by the mapping from (k, f) to (p, f). An expression for this hyperbola in the (p, f)-domain is given by

$$|f p_N| = \frac{1}{2\Delta x}, \tag{5.103}$$

where p_N, is the maximum slowness for which the data are not spatially aliased. In the numerical computation of the local Radon representation the values of points that are mapped outside this hyperbola are set to zero. The bounds on the (k, f)-domain and (p, f)-domain are depicted in Figure 5.13.

Cross terms and resolution

In section 5.3 the cross-term geometry in the two-dimensional Wigner distribution was briefly discussed. The domain allocation of the cross terms in the multi-dimensional Wigner distribution is similar to the time-frequency domain situation that was discussed in Section 2.6.

The cross terms occur at locations that do not correspond to where the energy of a signal is expected to be localized in the local frequency representation. In order to facilitate the interpretation of the local slant-stack power spectrum, suppression of the cross terms is often needed. Similar to the geometry of time-frequency representations, the cross terms in the wavenumber-frequency domain are located midway between the auto terms.

The cross term between two components of a signal is given by the cross-Wigner distribution of the components (see section 2.6). For a two-dimensional signal that is composed of two exponentials,

$$\begin{aligned} u(x,t) =& u_1(x,t) + u_2(x,t) \\ =& \exp(-\mathrm{j}2\pi(k_1 x - f_1 t)) + \exp(-\mathrm{j}2\pi(k_2 x - f_2 t)), \end{aligned} \tag{5.104}$$

the cross-Wigner distribution is given by

$$W\{u_1,u_2\}(x,t;k,f) = 2\cos\left[2\pi((k_2-k_1)x-(f_2-f_1)t)\right] \delta\left(k-\tfrac{1}{2}(k_1+k_2), f-\tfrac{1}{2}(f_1+f_2)\right). \quad (5.105)$$

The cross term is located in the wavenumber-frequency plane at $(k = (k_1 + k_2)/2, f = (f_1 + f_2)/2)$ The mapping from the (k, f)-domain to the (p, f)-domain alters the cross-term geometry and a cross term will no longer always be located midway between two auto terms. In the (p, f)-plane the cross term (Eq.5.105) will be located at $((p_1 f_1 + p_2 f_2)/(f_1 + f_2), (f_1 + f_2)/2)$. The cross terms between two (p, f)-components will now be located on a hyperbola that can be expressed in terms of the auto-term coordinates (p_1, f_1) and (p_2, f_2).

Suppression of cross terms is usually achieved by a smoothing of the representation and as a result the localization of energy in the representation will decrease. However, cross term suppression can in many cases improve the resolution of the representation dramatically. The improvement of resolution through cross term suppression is illustrated with the pseudo Wigner-Radon representation of a signal that is composed of two cosines (Fig. 5.16). The signal is given by

$$u(x,t) = \cos\left[-2\pi(4x-10t)\right] + \cos\left[-2\pi(10x-20t)\right]. \quad (5.106)$$

Ideally, the local Radon representation of this signal would show two peaks at the dips of the two cosine components, $p_1 = 0.4$ [s/m] and $p_2 = 0.5$ [s/m].

The signal of Eq.(5.106) was discretized on a grid of 128 by 128 samples for a length of 1[m] and 1[s]. The local wavenumber-frequency and slowness-frequency representations of the pseudo-Wigner distribution were computed using a sliding window of 64 by 64 samples. Figure 5.14a and 5.14b shows the (k, f)-slice and (p, f)-slice through the representations at the space-time origin, $(x = 0, t = 0)$, respectively.

The Wigner-Radon representation is dominated by two negative-valued cross terms between the positive and negative frequencies of the signal and a cross term midway between the energy of the auto-terms on the upper half plane of the spectrum. In the (p, f)-plane the auto terms and cross terms will be located near the line that connects the two (p, f)-locations of the two

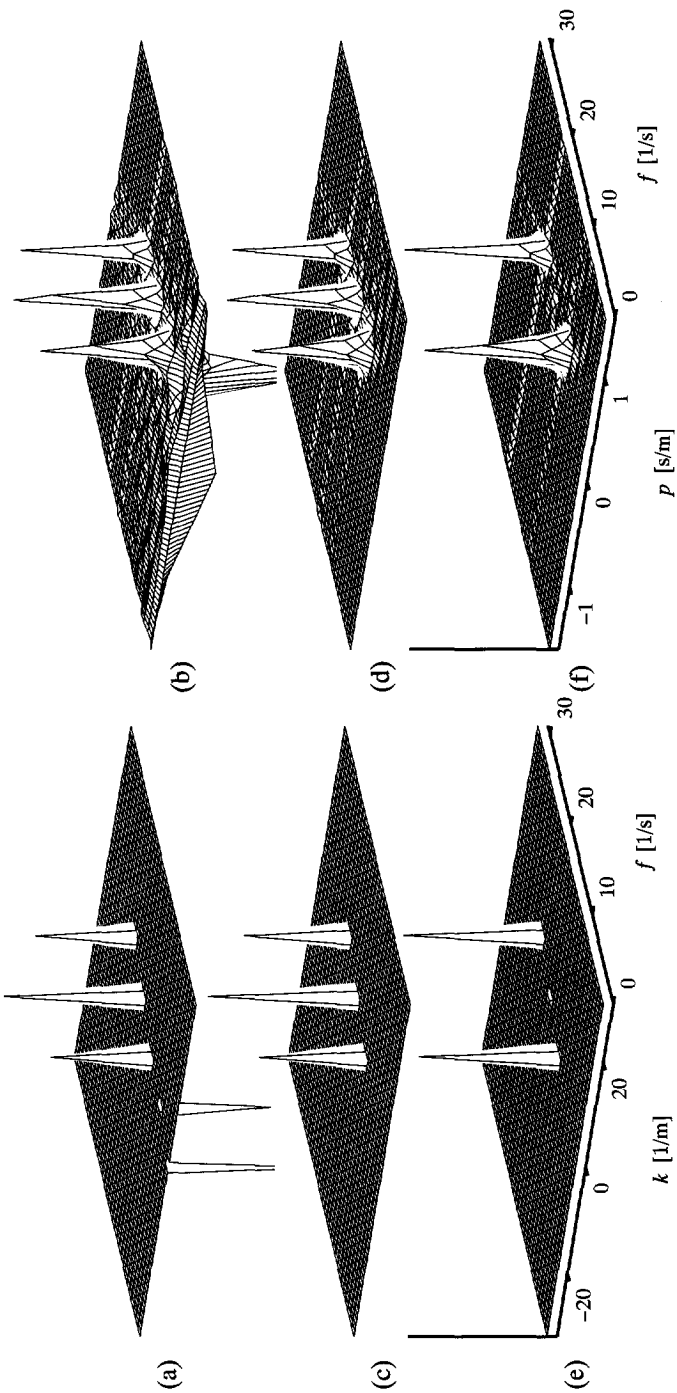

Figure 5.14: *(left) Local power spectra and (right) slowness-frequency spectra for positive temporal frequencies. From top to bottom: pseudo Wigner representations of the real signal, analytic signal, and smoothed Wigner representation of the analytic signal.*

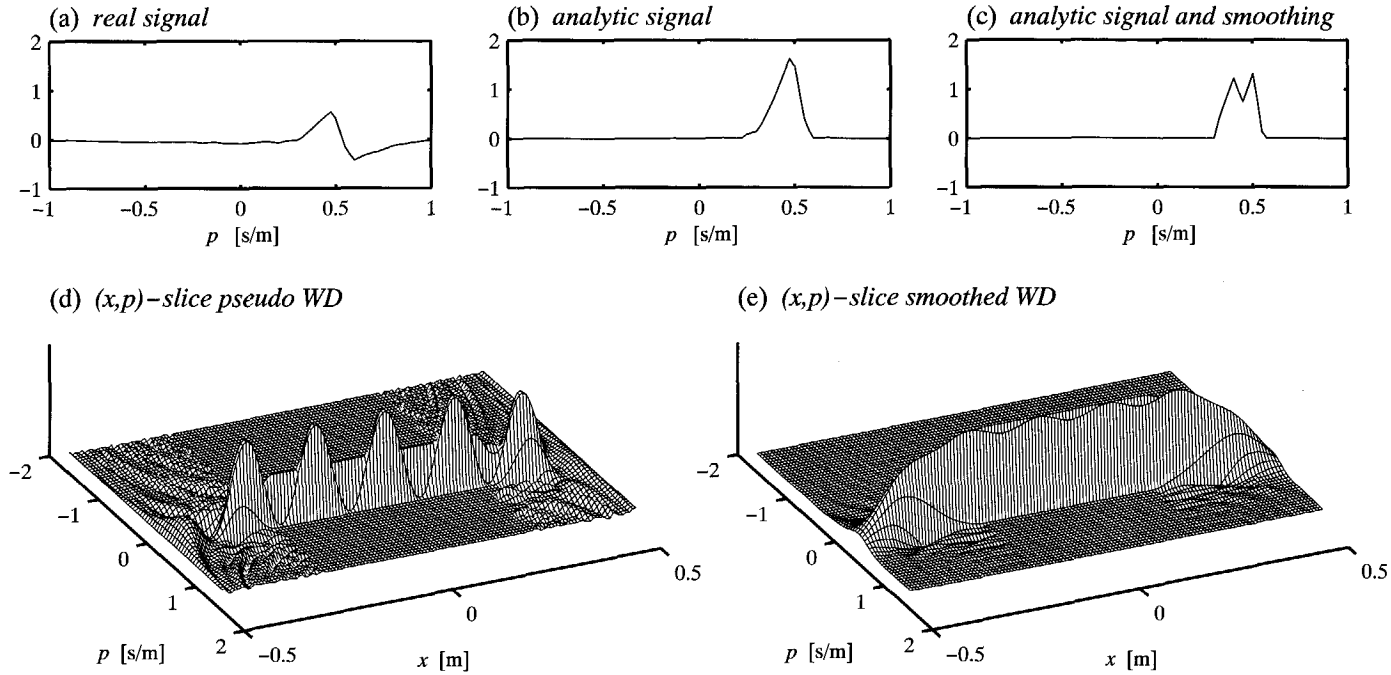

Figure 5.15: *Slowness slices for $\tau = 0$ of the signal of Fig. 5.16. (a)-(c) p-slices (i.e. $S\{u,u\}(0,0;p,0)$): pseudo Wigner distribution of the real-valued signal, pseudo Wigner distribution of the analytic signal, and smoothed pseudo Wigner distribution of the analytic signal. The space vs. slowness slices of the analytic signal through $t = 0$ ($S\{u,u\}(x,0;p,0)$) are shown in (d) and (e). Note that smoothing reduces spatial localization, but suppresses cross terms.*

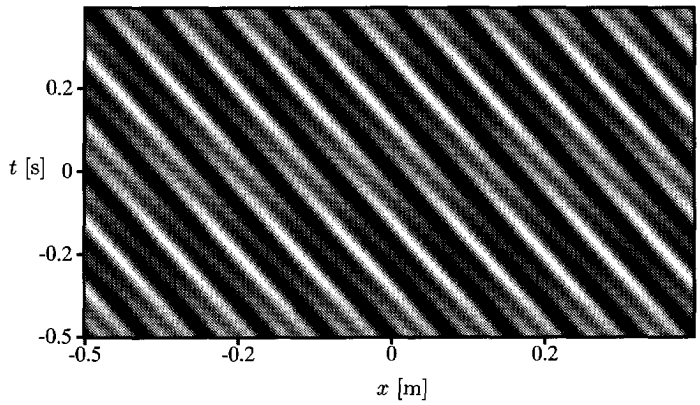

Figure 5.16: *A signal that is the sum of two 2-D cosines (Eq.(5.106)).*

components. In Fig. 5.15 a slice for $\tau = 0$ through the (p, τ)-representation is shown. The slice is obtained by summation over frequency of the slowness-frequency representation of Fig. 5.14a. It is not possible to discern the two separate dips of the signal components.

A first improvement can be made by not using the signal itself, but the analytic signal (see section 2.2.3). The signal is now given by

$$u(x,t) = \exp(\mathrm{j}2\pi 10t)\cos(-2\pi 4x) + \exp(\mathrm{j}2\pi 20t)\cos(-2\pi 10x). \quad (5.107)$$

The analytic signal has no negative temporal frequencies and as a result there will be no cross term between the negative and positive temporal frequencies in the local spectra. The local wavenumber-frequency power spectrum and local slowness-frequency power spectrum of the analytic signal are shown in Fig. 5.14b and Fig. 5.14c, respectively. A slice through the Wigner-Radon representation at $\tau = 0$ is shown in Fig. 5.15b. Due to the cross term between the two components, it is not possible to derive the actual dip content of the signal from the Wigner-Radon representation.

The cross term between the two components can be suppressed by smoothing the pseudo Wigner distribution. Figures 5.14c and 5.14d show the representations that result after a smoothing over 7 by 7 samples over x and t has been included in the computation of the local auto-correlation of the signal. The cross term has now nearly vanished. In the Wigner-Radon representa-

tion (Fig. 5.15c) we now observe two distinct peaks that correspond to the dips of the two components.

The example shows that in many cases a small loss in localization through smoothing results in a much improved resolution. In a smoothed pseudo Wigner representation the degree of smoothing (x,t)-domain and (k,f)-domain can be specified independently. This enables a flexible way for varying the trade off between localization and resolution, depending on the application.

5.6.5 Numerical examples

In this section the representation of a signal by a local slowness-frequency power spectrum and the Wigner-Radon representations is illustrated with three examples. First, we will analyze a signal with a changing dip.

Linearly increasing dip signal

A signal $u(x,t)$ with a single temporal frequency and a linear increase of dip as a function of the spatial coordinate, x, is given by

$$u(x,t) = \exp(\mathrm{j}2\pi f_1(t + \tfrac{1}{2}ax^2)), \tag{5.108}$$

where a is the rate of dip change. The real part of a signal of this type is shown in Figure 5.17. The temporal frequency, f_1 is 30 [s^{-1}]. The rate of dip change af_1 is -2 [s/m], which means that the dip changes linearly from $+1$ [s/m] at the leftmost trace to -1 [s/m] in the far right. The signal was discretized on a grid of 128 by 128 samples. The expression of the signal in the various domains is easily derived. In the following the representation of this signal in the various domain will be derived analytically and illustrated with a numerical computation of the representation of the discretized signal.

The first step in the computation of the local slant stack power spectrum is to correlate the signal over x and t at the (x,t)-coordinate under analysis. The local auto-correlation of the signal is given by

$$R\{u,u\}(x,t;\xi,\tau) = \exp(\mathrm{j}2\pi f_1\tau)\exp(\mathrm{j}2\pi a f_1\xi x). \tag{5.109}$$

The local auto-correlation of the discrete signal was computed over a 64 by 64 Gaussian window. The real part of a slice through the local auto-correlation in the point $(x = -0.25, t = 0)$ is shown in Fig. 5.18a.

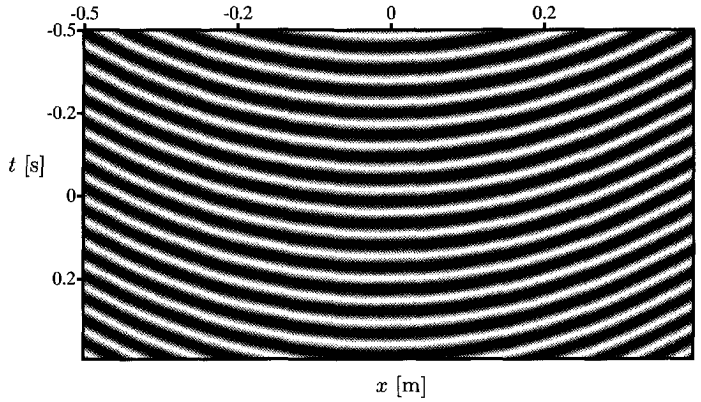

Figure 5.17: *Real part of a signal with a linear change in dip as a function of the spatial coordinate.*

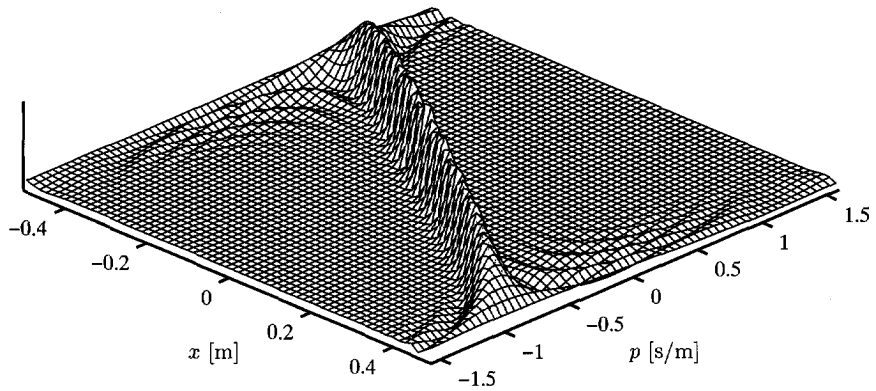

Figure 5.19: $(x, t = 0; p, \tau = 0)$*-slice through the pseudo Wigner-Radon representation of the linearly increasing dip signal.*

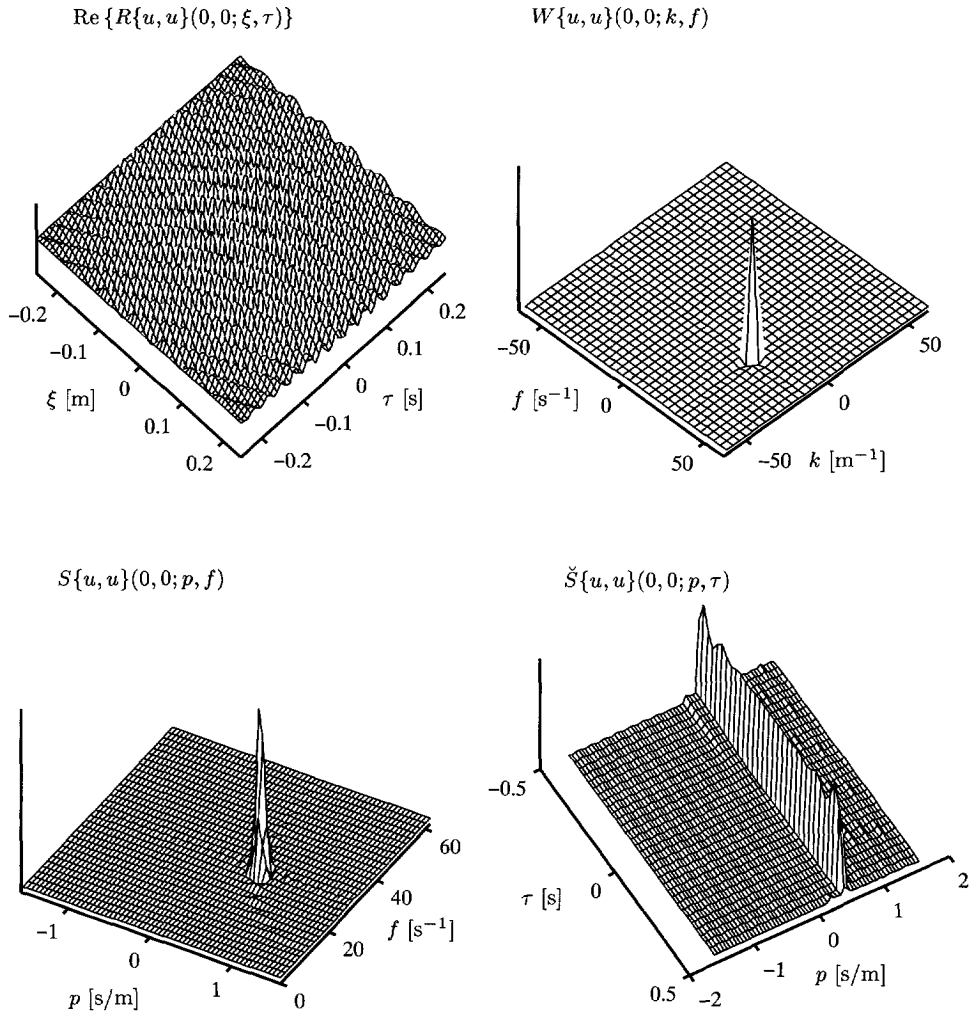

Figure 5.18: *Pseudo Wigner-Radon representation of the linearly increasing dip signal; (a) Real part of the local space-time auto-correlation, (b) local wavenumber-frequency power spectrum, (c) local slowness-frequency power spectrum and (d) pseudo Wigner-Radon representation.*

The Wigner distribution of this signal is found by a Fourier transformation of $R\{u,u\}(x,t;\xi,\tau)$ over the shift variables and is given by

$$W\{u,u\}(x,t;k,f) = \delta(f-f_1)\delta(k+af_1x) \tag{5.110}$$

A slice through the pseudo Wigner distribution at the point $(x=-0.25, t=0)$ is shown in Fig. 5.18b.

The mapping from (k,f)-domain to the (p,f)-domain results in the representation

$$S\{u,u\}(x,t;p,f) = \delta(f-f_1)\delta(p+ax). \tag{5.111}$$

The (p,f)-representation of the discrete signal at $(x=-0.25, t=0)$ is shown in Fig. 5.18c. Finally, after an inverse Fourier transformation over frequency the local slant-stack power spectrum is found as

$$\check{S}\{u,u\}(x,t;p,\tau) = \exp(\mathrm{j}2\pi f_1\tau)\delta(p+ax). \tag{5.112}$$

The real part of the pseudo Wigner-Radon representation at $(x=-0.25, t=0)$ is shown in Fig. 5.18c. It is a cosine signal with a frequency $f_1 = 30[\mathrm{s}^{-1}]$ at $p = 0.5[\mathrm{s/m}]$. If we consider a $(x, t=0, p, \tau=0)$-slice through the Wigner-Radon representation, the representation is given by

$$\check{S}\{u,u\}(x,0;p,0) = \delta(p+ax). \tag{5.113}$$

For the discrete signal this is a linear amplitude ridge ranging from $p=1$ [s/m] in $x=-0.5$ [m] to $p=-1$ [s/m] in $x=0.5$ [m]. The (x,p)-slice is shown in Fig. 5.19. The broadening of the ridge at the end points is an effect of the sharp cut-off of the signal at the edges.

Annular shaped amplitude profile

The local wavenumber-frequency power spectrum of the annular amplitude profile given by Eq.(5.51), was discussed in Section 5.5. The signal is shown in Fig. 5.5a. The signal was discretized on 128 by 128 grid and the (k,f)-spectrum was computed as a pseudo Wigner distribution of a sliding window of data of 64 by 64 samples. Slices through the local wavenumber-frequency power spectrum and Wigner-Radon representations of the signal at three different space-time locations are shown in Fig. 5.20. The wavenumber-frequency representations of the signal at the same locations were shown

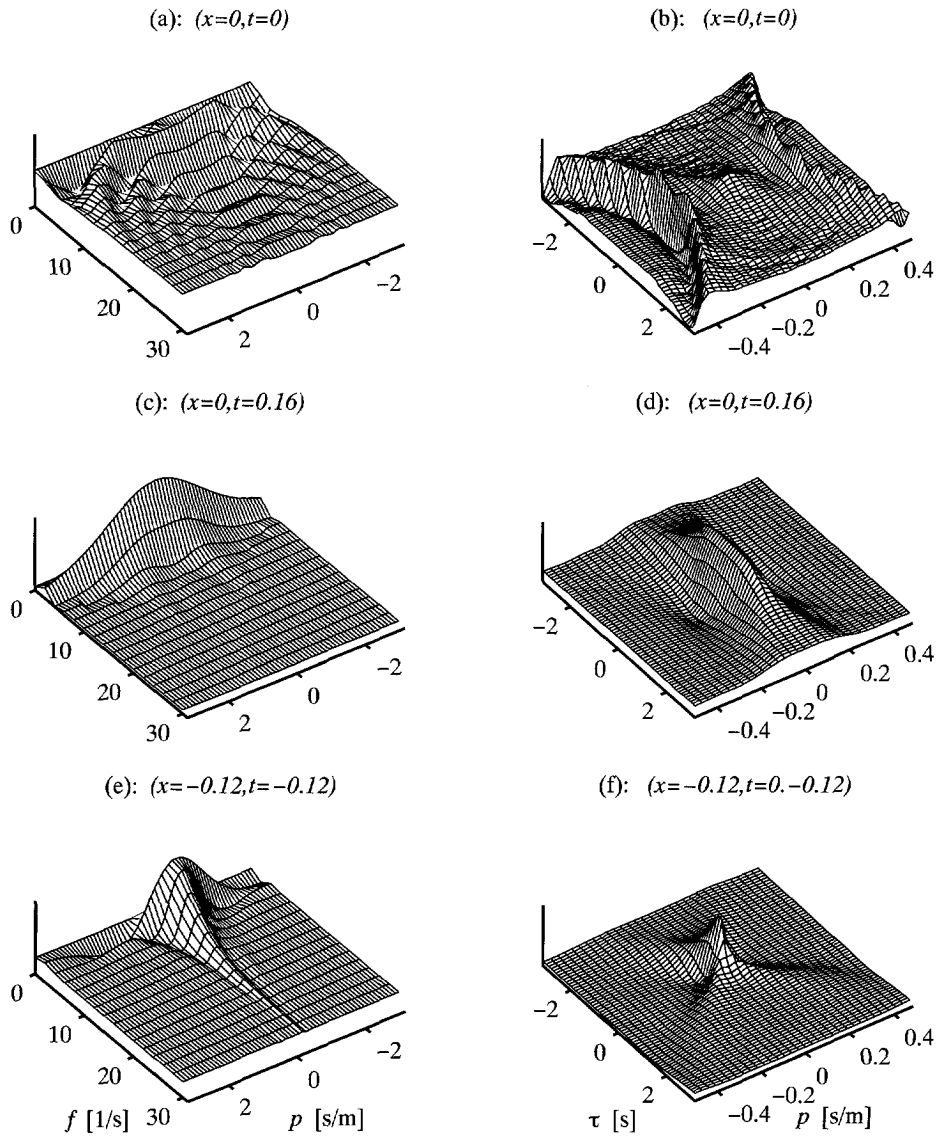

Figure 5.20: *Pseudo Wigner-Radon representation of the annular shaped profile (Eq.(5.51)); (a), (c) and (e) are local slowness-frequency power spectra; (b), (d) and (f) are Wigner-Radon representations.*

in Fig. 5.5. The (p, τ)-slice at $(x = -0.12, t = -0.12)$ shows a peak at $(p = -1, \tau = 0)$. This means that the prevailing dip is -1 [s/m] at this point. For increasing time-shifts, there is also energy at other dips, indicating the change of dip when moving away from the point. The (p, τ)-slice at $(x = 0, t = 0.16)$ shows an energy concentration around $p = 0$. Moving towards increasing time shift, the energy is localized at higher dip-values, reflecting the curvature near the (x, t)-location. The (f, p) and (p, τ)-representations at $(x = 0, t = 0)$ reflect the circular nature of the cross terms.

Chapter 6

Attribute Analysis of three-dimensional Seismic Data

The introduction of dip and azimuth maps of time horizons has greatly improved the structural interpretation of 3-D seismic data (Dalley et al. 1989; Hoetz and Watters 1991). This technique was developed by Shell and is based on a computation of dip and azimuth of a seismic time surface. The input time surface is usually an automatically tracked seismic event. The dip and azimuth maps have been particularly successful for the interpretation of fault patterns in seismic data (see e.g. Jones and Knipe 1996).

In recent years, another novel interpretation technology was developed by Amoco (Bahorich and Farmer 1995). This technique is based on a measurement of the similarity of adjacent traces in a seismic section. It is usually referred to as 'coherence cube technology'. Originally, the coherence attribute was based on similarity measurement between two adjacent traces. However, the extension to volume measurements and the use of more advanced algorithms resulted in much improved results (Gersztenkorn and Marfurt 1996). The coherency technique has been very successfully applied for both structural and stratigraphic seismic interpretation (Bahorich and Farmer 1995; Ortmann and Wood 1995). One of the major advantages of the technique is that the analysis is carried out on a time volume and hence does not require

the picking of horizons first. As a result, the method is less time consuming and interpretational bias that may be introduced by the horizon picking process is avoided. Volume analysis techniques for seismic interpretation are also considered by Hoogenboom et al. (1996), de Jonge et al. (1996), and Dalley et al. (1996), who apply three-dimensional image processing and visualization techniques to seismic data.

In this chapter a combination of both the dip/azimuth and volume analysis techniques is proposed. It is a combination of these two in the sense that we generate dip and azimuth maps of a space-time volume of seismic data. The analysis is an application of the theory that was introduced in the previous chapter to the 3-D migrated seismic data volume.

In order to obtain the dip and azimuth at each subsurface sample point (x, y, t), we compute a generalized Wigner-Radon representation at each (x, y)-location for fixed time t. First, we will discuss the practical aspects of the method. We will then show examples from two field data sets from the Gulf of Mexico and the North Sea.

6.1 Local time-dip and azimuth in 3-D seismic data

The application discussed here is based on a double Radon transformation in a three-dimensional local wavenumber-frequency spectrum. The 3-D local wavenumber-frequency spectrum is obtained by a correlation in the 3-D sliding-window Fourier transformation. The Fourier transformation is carried out with respect to cross-line direction, from here on denoted as x, the in-line direction y and the time variable t. The method is outlined in Section 5.5 for a two-dimensional geometry. The basic equation is Eq.(5.45). Figure (5.4) is the flow chart that illustrates how the equation is implemented in a numerical scheme.

The extension to three dimensions is straightforward. The 2-D Fourier transformations are replaced by 3-D Fourier transformations, with the cross-line direction as the extra dimension. The next step is to obtain the local slowness-frequency representation. The equations involved here, are Eqs.(5.75) and (5.81), which give the local slowness-frequency spectrum in terms of the Wigner distributions for respectively a real and analytic signal.

The interpolation in the wavenumber direction (see section 5.6.4) now becomes a two-dimensional interpolation in both the k_x and k_y directions.

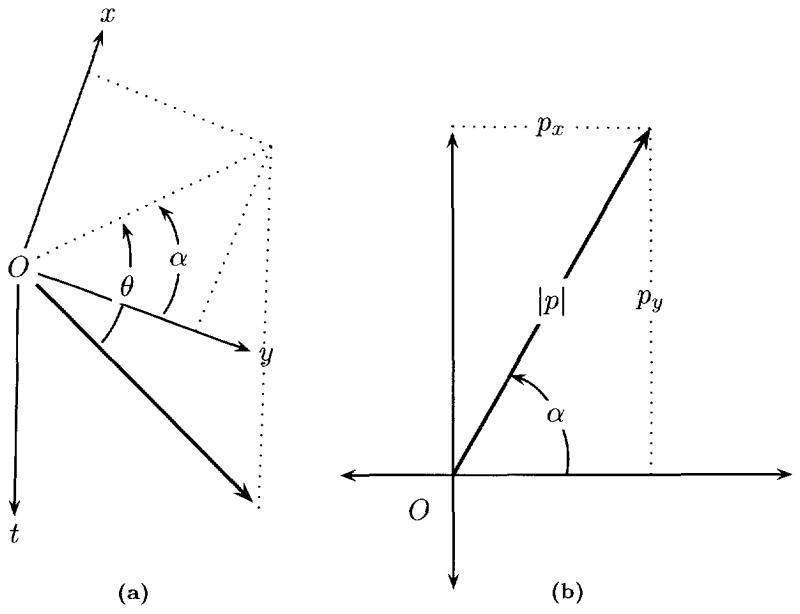

Figure 6.1: *Geometry in the space-time domain and the slowness domain; (a) (x, y, t)-domain, θ is the dip angle and the angle in the (x, y)-plane is the azimuth α; (b) (p_x, p_y)-domain, $|p|$ is the dip modulus and α is the azimuth.*

This two-dimensional interpolation is implemented as a sequence of two one-dimensional interpolations. The implementation of the two-dimensional global Radon transformation is discussed in Vercruijsse (1995). He concludes that in most circumstances a sequence of two one-dimensional linear interpolations is sufficiently accurate. Moreover, in our application where the interpolation is to be carried out for every (x, y, t) analysis point, the extra computation time that is needed for higher order Lagrange or cubic spline interpolation will hardly be justified by the relatively minor gain in accuracy.

Once we have obtained the local slowness-frequency spectrum, we sum over frequency in order to obtain the generalized Wigner-Radon representation, i.e.

$$\check{P}\{u,u\}(x,y,t;p_x,p_y,0) = \int_{f\in I\!R} P\{u,u\}(x,y,t;p_x,p_y,f)\mathrm{d}f. \qquad (6.1)$$

There are two attributes extract from the two-dimensional local slowness power spectrum. The first one is the mean slowness modulus $|p|$, which

represents the time-dip of the signal, relative to the time slice. The dip modulus is given by

$$|p| = (p_x^2 + p_y^2)^{1/2} \geq 0. \tag{6.2}$$

The second attribute is the azimuth angle α, which represents the mean angle of the signal in the (x, y)-plane. The azimuth angle is given in terms of the slownesses as

$$\alpha = \tan^{-1}\left(\frac{p_x}{p_y}\right). \tag{6.3}$$

The geometry relations in the space-time domain and slowness domain are graphically indicated in Fig. 6.1. In order to extract these attributes from the generalized Wigner-Radon representation we first interpolate the spectrum to a polar grid. The generalized Radon representation in polar coordinates is given by

$$\breve{\bar{P}}\{u,u\}(x,y,t;|p|,\alpha,0) = \breve{P}\{u,u\}(x,y,t;|p|\cos(\alpha),|p|\sin(\alpha),0). \tag{6.4}$$

The spectrum in polar coordinates is interpolated from the rectangularly sampled generalized Wigner-Radon representation with a bilinear interpolation. The bilinear interpolation is implemented as a sequence of two linear interpolations. The four rectangular sample points that surround a polar sample point are first used to interpolate in the p_x direction along the sides of the rectangle, followed by interpolation in the p_y direction. The mean time-dip modulus is then obtained from the generalized Wigner-Radon representation in polar coordinates as

$$\langle p\rangle_{x,y,t} = \frac{\int_{-\pi}^{\pi}\int_0^{\infty}|p|\breve{\bar{P}}\{u,u\}(x,y,t;|p|,\alpha,0)\mathrm{d}\alpha\mathrm{d}|p|}{\int_{-\pi}^{\pi}\int_0^{\infty}\breve{\bar{P}}\{u,u\}(x,y,t;|p|,\alpha,0)\mathrm{d}\alpha\mathrm{d}|p|}. \tag{6.5}$$

The mean azimuth is given by

$$\langle\alpha\rangle_{x,y,t} = \frac{\int_0^{\infty}\int_{-\pi}^{\pi}\alpha\breve{\bar{P}}\{u,u\}(x,y,t;|p|,\alpha,0)\mathrm{d}|p|\mathrm{d}\alpha}{\int_0^{\infty}\int_{-\pi}^{\pi}\breve{\bar{P}}\{u,u\}(x,y,t;|p|,\alpha,0)\mathrm{d}|p|\mathrm{d}\alpha}. \tag{6.6}$$

The analysis results in a local time-dip and local azimuth value in each subsurface sample point (x_i, y_i, t_i). Hence, from the input data two attribute

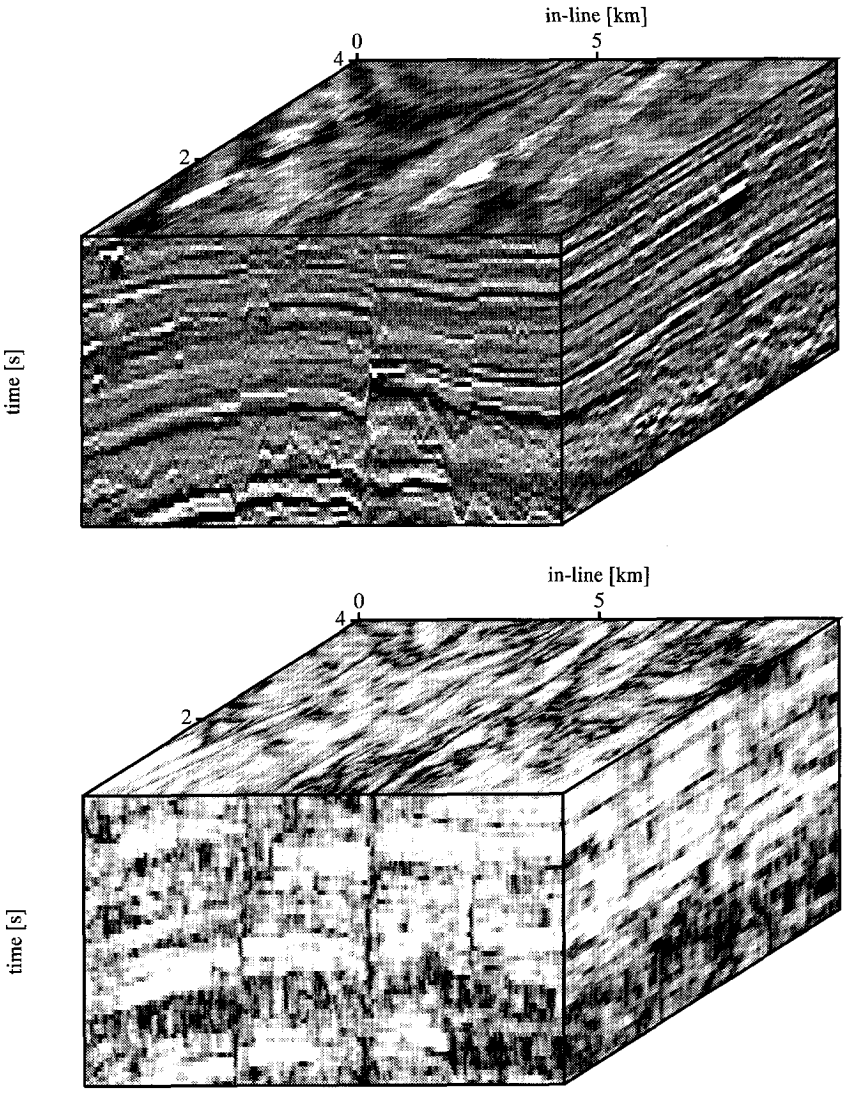

Figure 6.2: *Cube display of seismic data and (bottom) time-dip attribute. The 3-D attribute extraction results in a local time-dip measure in each subsurface sample point.*

data cubes are generated. An example is shown in Fig. 6.2. The discontinuities in the data are delineated by the local time-dip attribute. High time-dip values are shown in black colours. Faults are clearly visible because of their nearly vertical dips. In the upper left corner a channel is visible. Regions with incoherent events show up as dips changing rapidly over a large range of dip values. The data set is discussed in more detail in the next section.

6.2 Gulf of Mexico, South Marsh Island

The South Marsh island area is located in the Gulf of Mexico on the continental shelf, west and adjacent to the present day Mississippi delta. The South Marsh Island data set we discuss here is a part of a larger speculative survey of the area. The data set has also been used for the geological validation of the coherency attribute and some aspects of the interpretation are discussed in Haskell et al. (1995) and Nissen et al. (1995).

The in-line and cross-line trace distances are 25 [m] and 50 [m], respectively. The time sample interval is 8 [msec]. The data were down-sampled from an original post-stack 2-D by 2-D time migrated volume with trace distances of 12.5 [m] by 25 [m] and 4 [msec] sample interval.

In Figs. 6.4 to 6.6, three time slices from the data cube are shown together with their corresponding time-dip attribute display. An in-line section and its corresponding time-dip image is shown in Fig. 6.7. The time-dip and azimuth of the data were computed with the algorithm described in the previous section. The analysis cube used has an area of 4 by 4 traces and height of 4 samples, corresponding to 200 [m] by 100 [m] by 32 [msec]. The correlation in the 3-D sliding window Fourier transformation was performed over a volume of 3x3x3 frequency bins, followed by interpolation to a local slowness-frequency spectrum of 16x16 p values.

The main features of the first slice (Fig. 6.4) are a salt dome and two large channels. The width of the channels is approximately 250 [m]. The present Mississippi River trunk channel varies in width between 1 to 1.3 [km], whereas the smaller distributary channels have a width of the order we observe here (Haskell et al. 1995). In the lower part of the slice some smaller channels are visible between 10 and 15 [km] in-line distance. The lateral migration of the channels we observe in subsequent time slices is relatively small. This corresponds to observations in the modern delta, where most of the channels

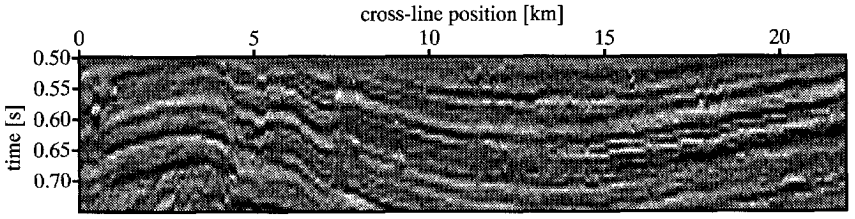

Figure 6.3: *In-line profile at $x = 5$ [km] cross-line position, showing the position of the channels and faults observed in the time-dip slice of Fig. 6.5, in a vertical cross-section.*

are entrenched into the underlying marine clays, preventing their lateral migration (Haskell et al. 1995). The salt dome is surrounded by radial faults extending in all directions away from the salt, perpendicular to the strike. An in-line cross-section, $A - A'$ on the time slice of Fig. 6.4, shows the position of the channels and faults in a cross-section (Fig. 6.3). The lineations in the upper-left corner of the time slices have their origin in what is referred to as the 'acquisition footprint' (Marfurt et al. 1995). This recurring pattern in the reflection strengths is the result of systematic errors introduced by the acquisition geometry or 3-D dip move-out and migration operator biases. The influence of coherent seismic noise on horizon-based dip and azimuth maps is discussed by Hesthammer and Fossen (1997). They observe that in areas with a low signal to noise ratio coherent seismic noise results in features in the horizon dip map that are not related to subsurface structure. Especially in areas with steep dips, these features may strongly resemble fault structure.

The main feature of Fig. 6.5 is a region of strong variable dips. This region coincides with the region of chaotic seismic character in the vertical cross-section of Fig. 6.7. The feature has been interpreted as the head of a submarine canyon, produced by mass wasting (Nissen et al. 1995).

In the time slices below the submarine canyon in-fill, once again a channel-system depositional setting is observed (Fig. 6.6). In the center of the egg-shaped region a channel, that is also clearly visible on the time slice, can be seen. The curved high-dip features surrounding the low with the channel are interpreted as growth faults. In the vertical cross-section (Fig. 6.7) of the time-dip the sub-vertical faults stand out from the rest of the section because they are associated with a steeply dipping discontinuity of the signal.

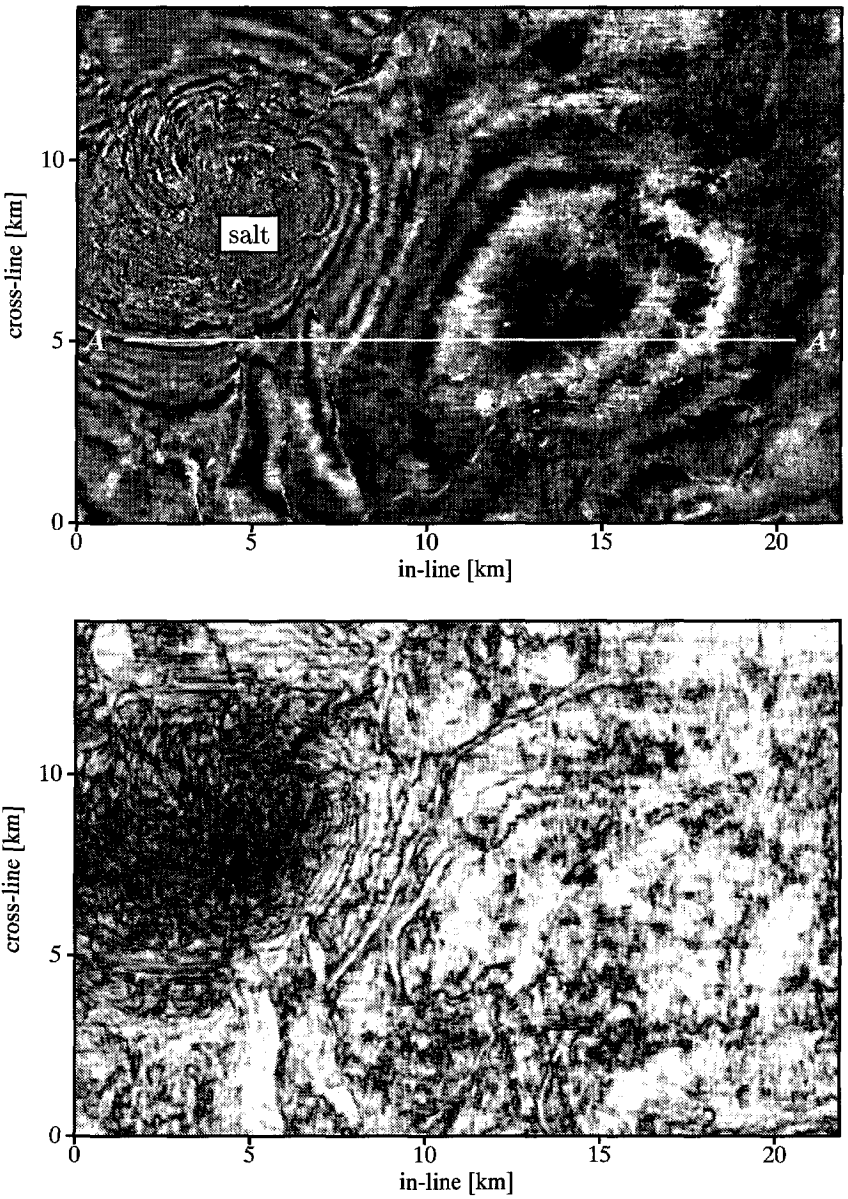

Figure 6.4: *(top) Standard time slice at* $t = 0.644$ [s] *and (bottom) corresponding time-dip slice*

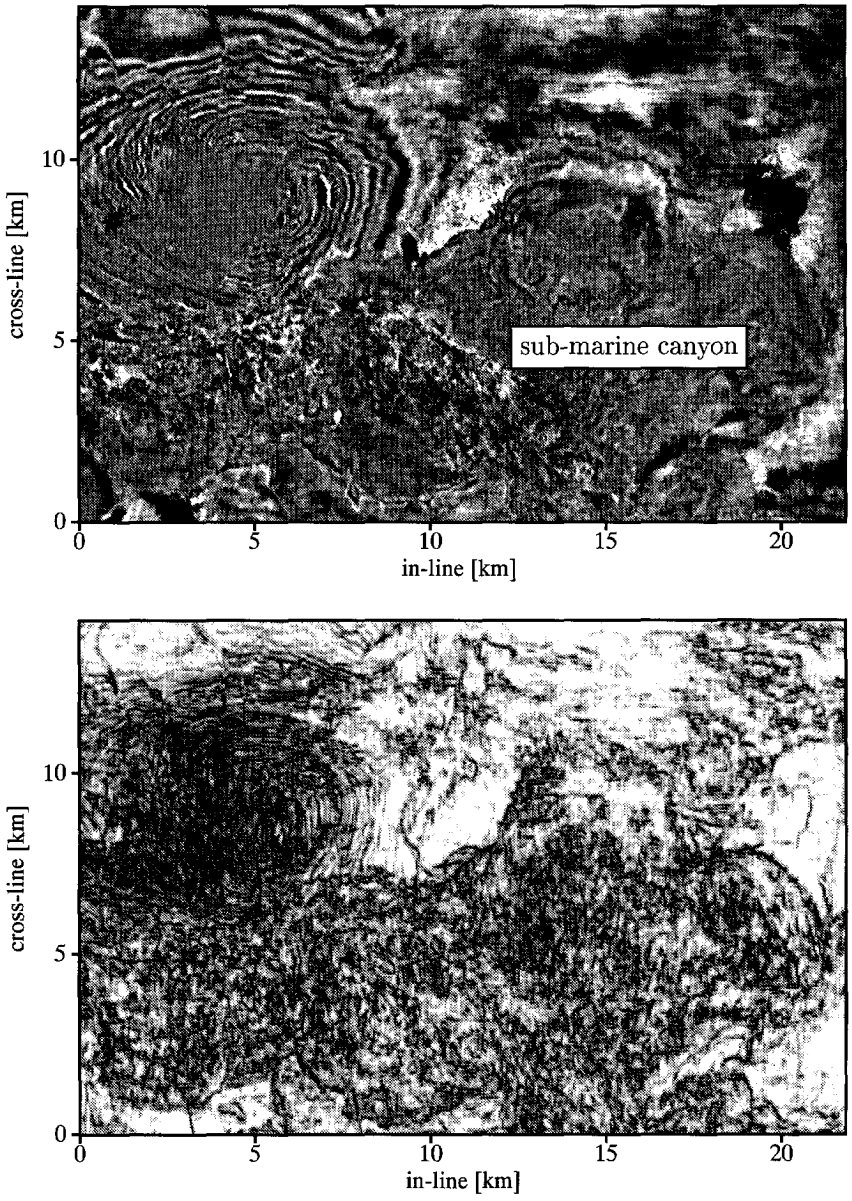

Figure 6.5: *(top) Standard time slice at* $t = 0.980$ [s] *and (bottom) corresponding time-dip slice.*

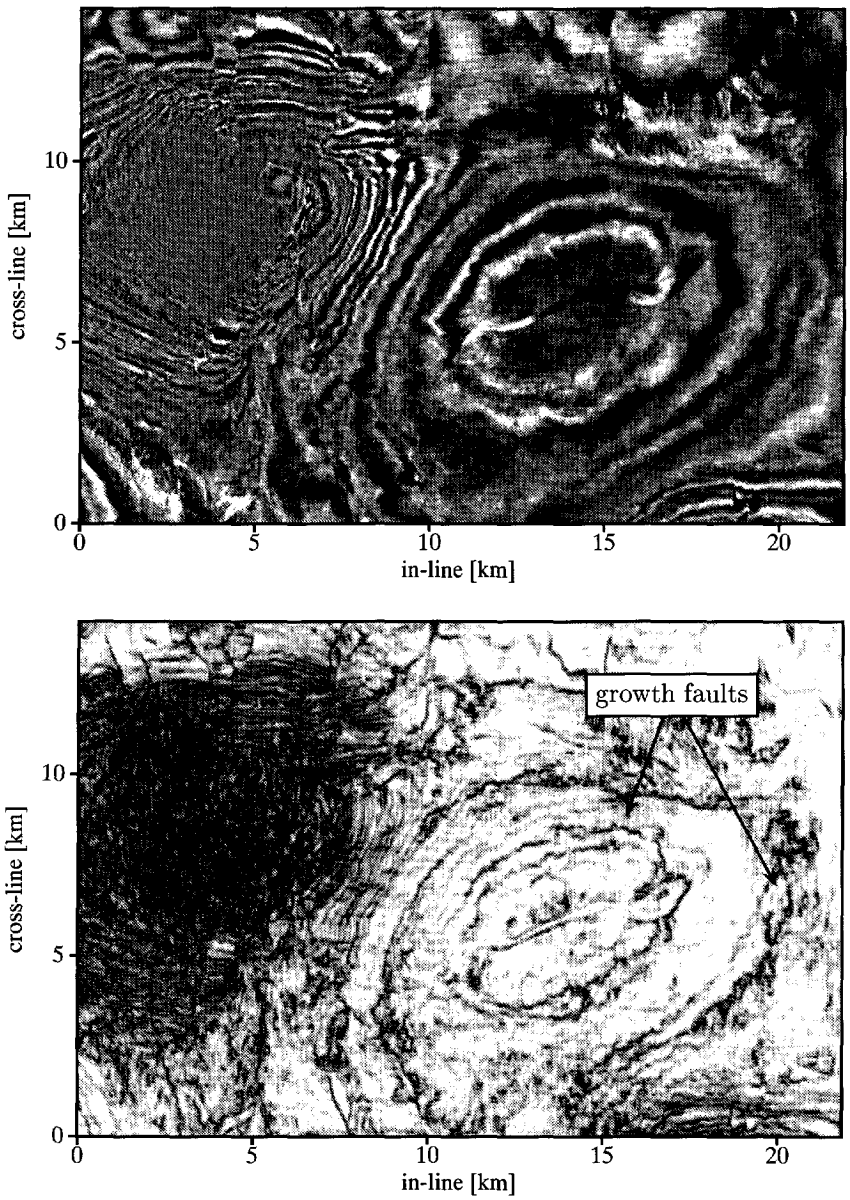

Figure 6.6: *(top) Standard time slice at* $t = 1.340$ [s] *and (bottom) corresponding time-dip slice.*

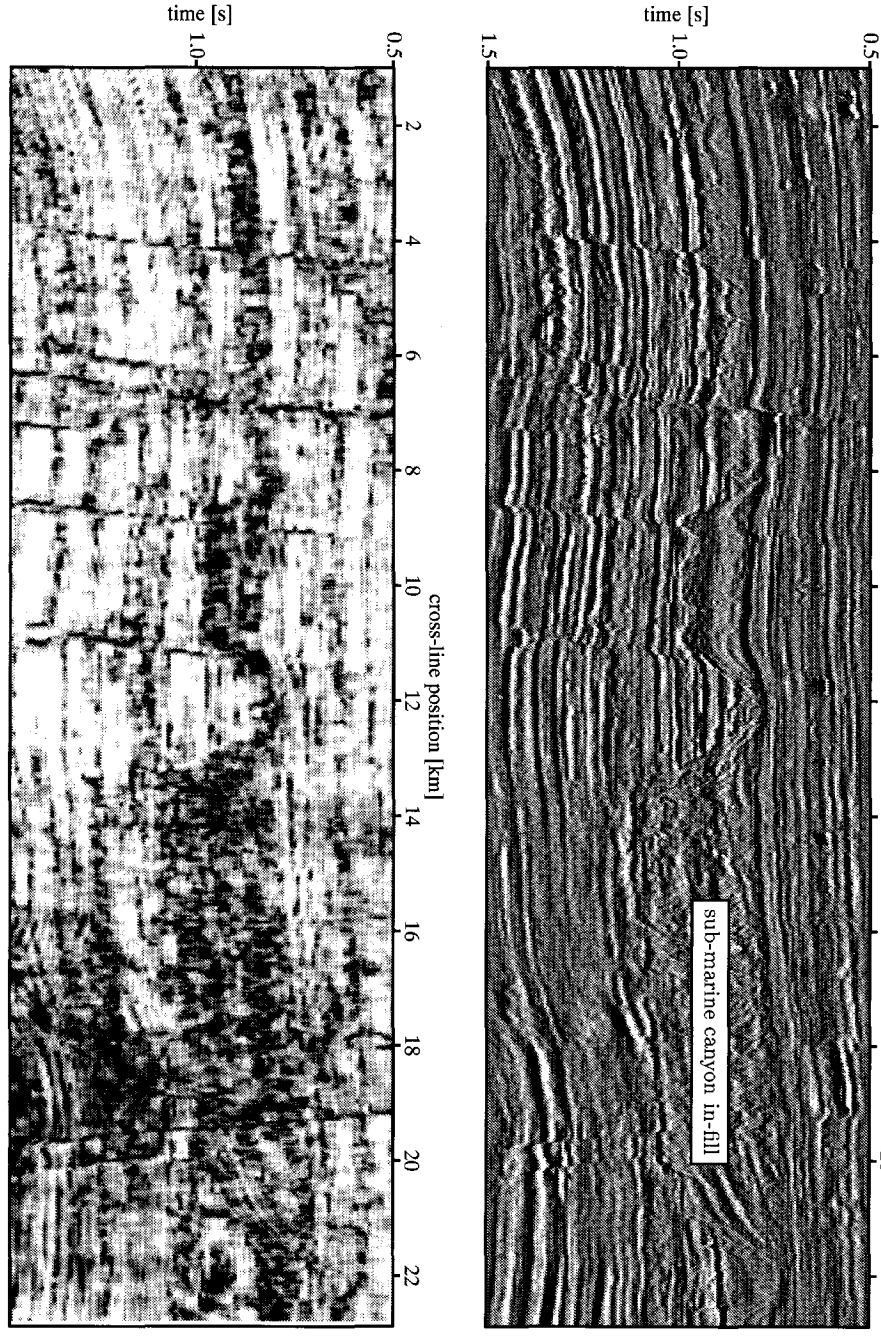

Figure 6.7: *In-line cross-section and time-dip cross-section ; in-line 10, $x = 450$ [m].*

6.3 North Sea data set, Ameland M9 block

The Ameland survey is located in the Dutch sector of the North Sea, north of the island Ameland (block M9).

The in-line and cross-line distances in the seismic data cube are 12.5 [m] and 25 [m], respectively. The time sample interval in the original data set is 4 [msec]. Before attribute extraction, the sampling interval was reduced to 8 [msec] in combination with of a zero phase frequency filter to prevent temporal frequency aliasing. A standard 3-D seismic data-processing sequence has been applied on the data, followed by 2-D by 2-D finite difference time migration.

The analysis cube used has an area of 4 by 4 traces and a height of 4 samples, corresponding to 100 [m] by 50 [m] by 32 [msec]. The correlation in the 3-D sliding window Fourier transformation was performed over a volume of 3x3x3 frequency bins, followed by interpolation to a local slowness-frequency spectrum of 16x16 p values.

Figures 6.8-6.13 show time slices and time-dip slices through the seismic and attribute data cube. Two in-lines and their corresponding time-dip cross-sections are shown in Figs. 6.15 and 6.16. The first time slice at t=0.54 [s] cuts through the upper part of the North Sea Formation (Fig. 6.8). In the time-dip slice we observe a deltaic depositional setting. In the in-line cross-sections of Fig. 6.16, we can also observe the location of this feature in the time-dip cross-section. The depositional environment here differs from the channel system we observed in the previous data example from the Gulf of Mexico. In a sequence of time-dip slices (Fig. 6.9), we observe strong variations in the position of channel segments and an overall more chaotic character of the signal. These two observations suggest a depositional setting in which sediments are transported with relatively high energy and in which the acoustic contrasts between channels and their surroundings is relatively small and discontinuous.

Below 0.6 [s], structural elements dominate the time-dip slices. Since we have much more the structural dip in the lower part of the section, the time slices cut through many horizons and consequently stratigraphic elements, that are usually associated with a single time horizon, are less likely to be observed.

Figures 6.10 and 6.11 show a time slice from near the top of the Chalk

formation. Fault locations and patterns can easily be observed in the time-dip slices. Certain aspects of the reflection character of are intensified by the time-dip display. Differences in continuity of the events, that are also observed in the cross-sections are brought forward in the time-dip map.

The last slice at 1.64 [s] (Figs. 6.12 and 6.13) cuts through Triassic and Zechstein formations. The discontinuity of the seismic events in the lower right corner of the time slice can be very well observed in the time-dip map. These seismic events are associated with an anhydrite layer, below the top of the Zechstein Formation. The positions of lows and highs and the associated faults surrounding them are well delineated in the time-dip map. In Fig. 6.14 the local azimuth of the time slice of Fig. 6.12 is displayed. The azimuth is usually best displayed in a colour map, with a different set of colours for each quadrant of the (x, y)-plane (see e.g. Brown 1997). Since we do not have the possibility to display colours here, we show an illuminated map of the local azimuth. The illumination is chosen as if a light source is located at $(x = 0, y = 0)$, that radiates light in a direction of 45 degrees. The illuminated map shows abrupt changes in the azimuth that can be with associated signal discontinuities, revealing the general structure and the location of faults

The results of the last two time slices show that the time-dip display has the potential to become an effective analysis tool for structural mapping of the subsurface. The creation of fault maps from 3-D seismic data is in most cases a very time consuming process. Generally, it takes the inspection of many cross-sections and time slices before a three-dimensional image of the locations and extent of faults is obtained. The location of faults and their configuration can more easily be recognized in a time-dip slice than on cross-sections or standard seismic time slices. Interpretation of a few time-dip slices may be sufficient for a quick overview of the structural setting of an area in an early stage of an interpretation project. Consequently, an earlier start can be made with the main tasks in an interpretation project: the identification and interpretation of potential hydro-carbon reservoirs.

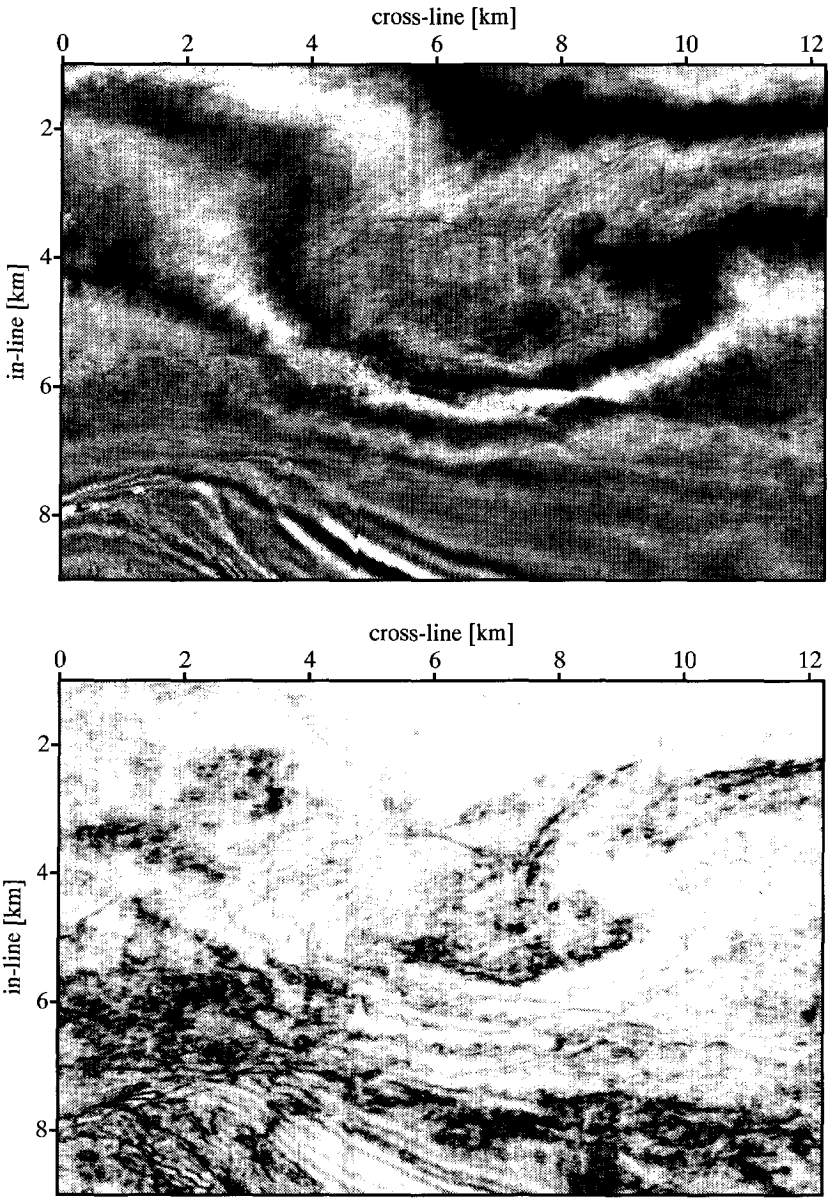

Figure 6.8: *Standard seismic time slice at* $t = 0.424$ [s] *and time-dip slice.*

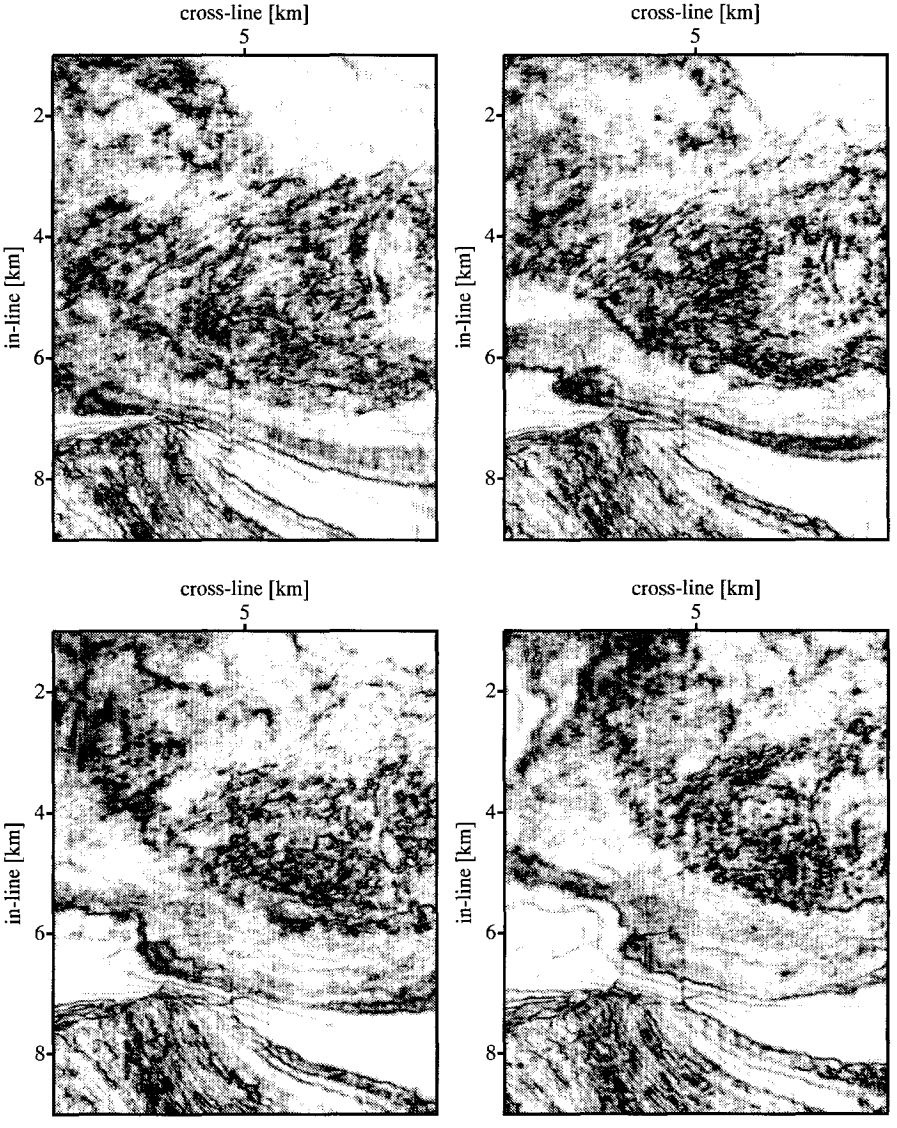

Figure 6.9: *Time-dip slices at (upper left to lower right)* $t = 0.480$[s], $t = 0.494$ [s], $t = 0.502$ [s] *and* $t = 0.510$ [s].

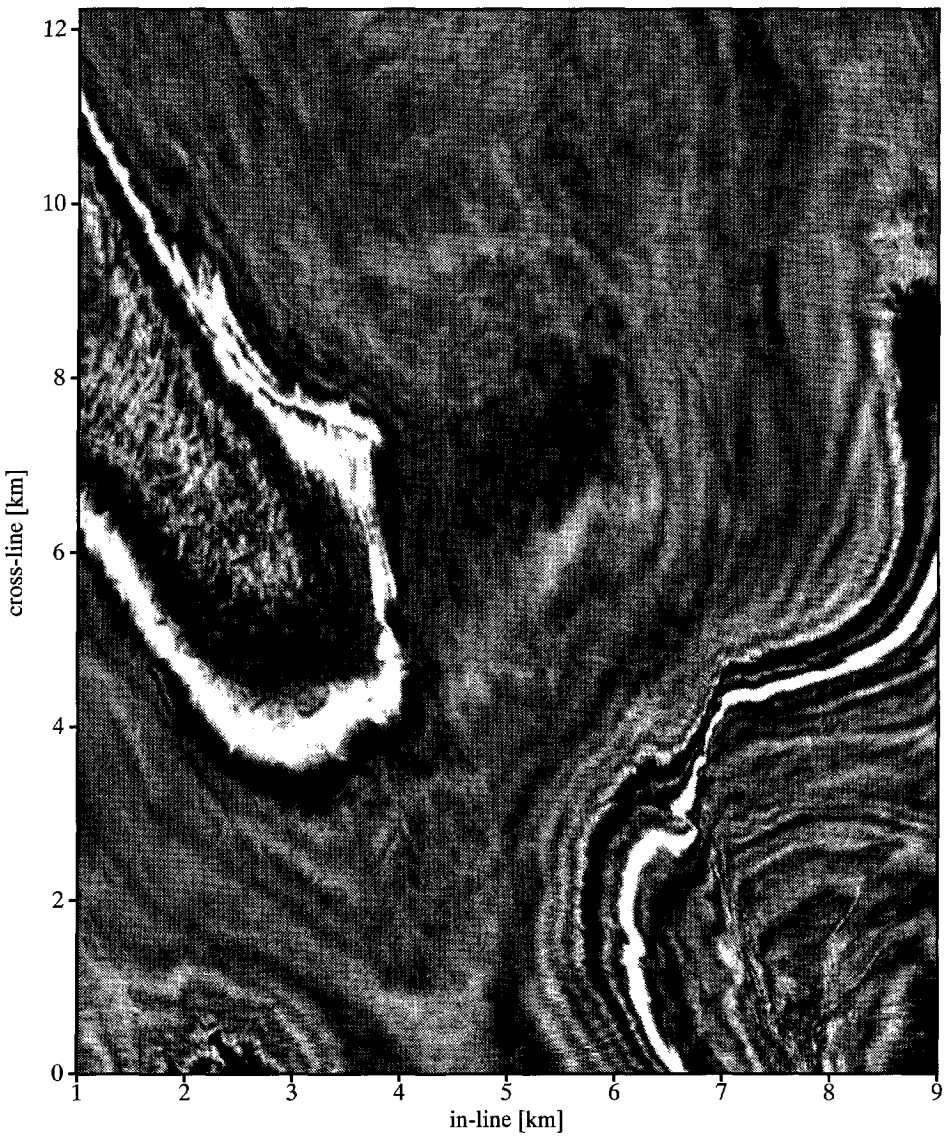

Figure 6.10: *Standard seismic time slice at* $t = 1.0$ [s].

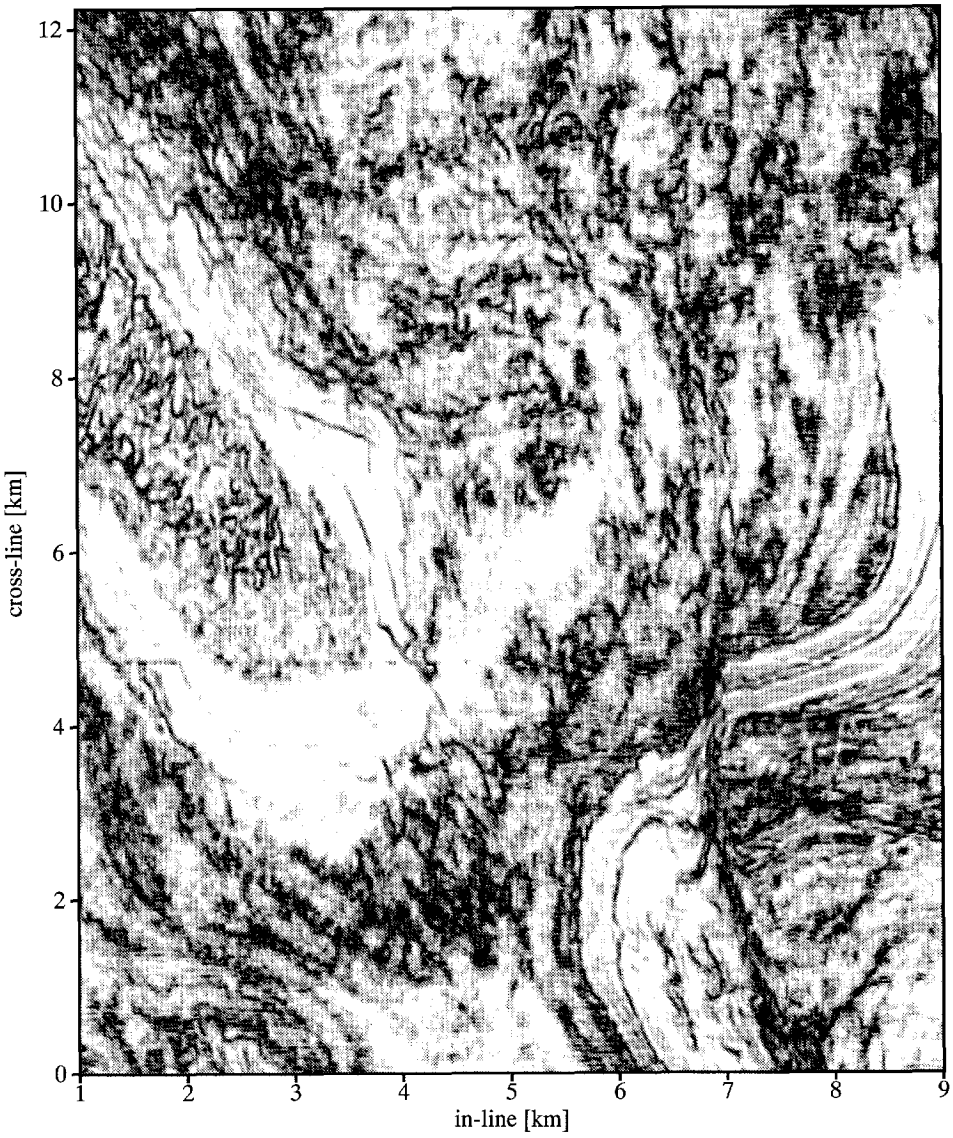

Figure 6.11: *Time-dip slice at* $t = 1.0$ [s].

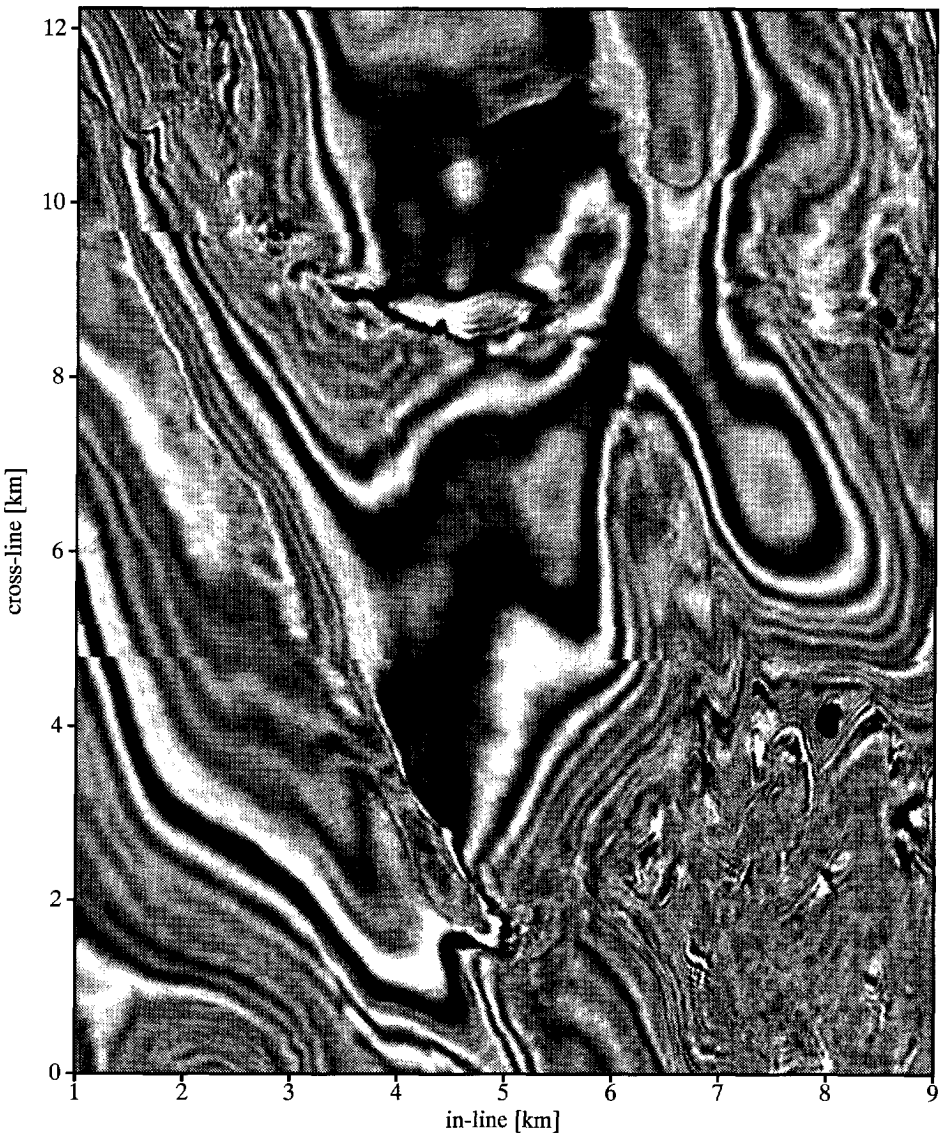

Figure 6.12: *Standard seismic time slice at* $t = 1.64$ [s].

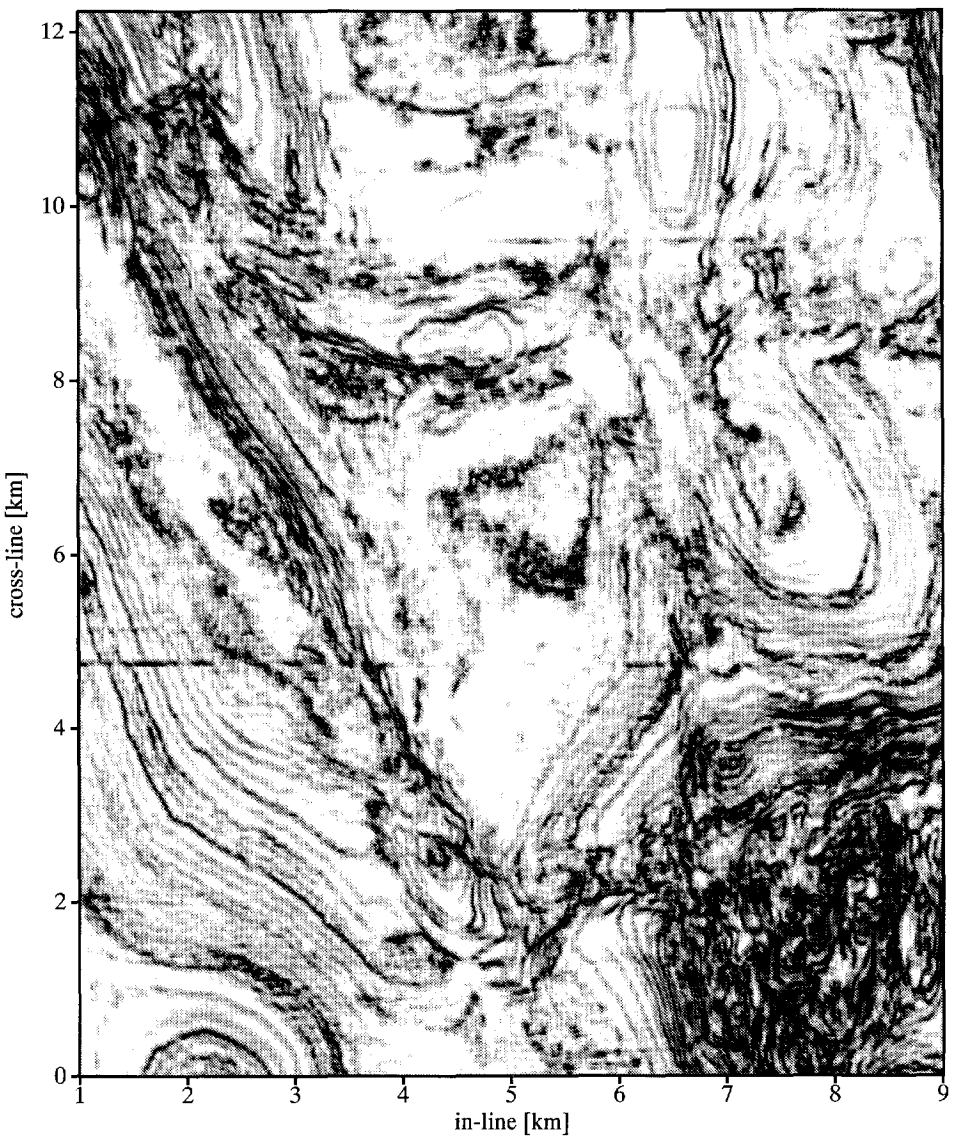

Figure 6.13: *Time-dip slice at* $t = 1.64$ [s].

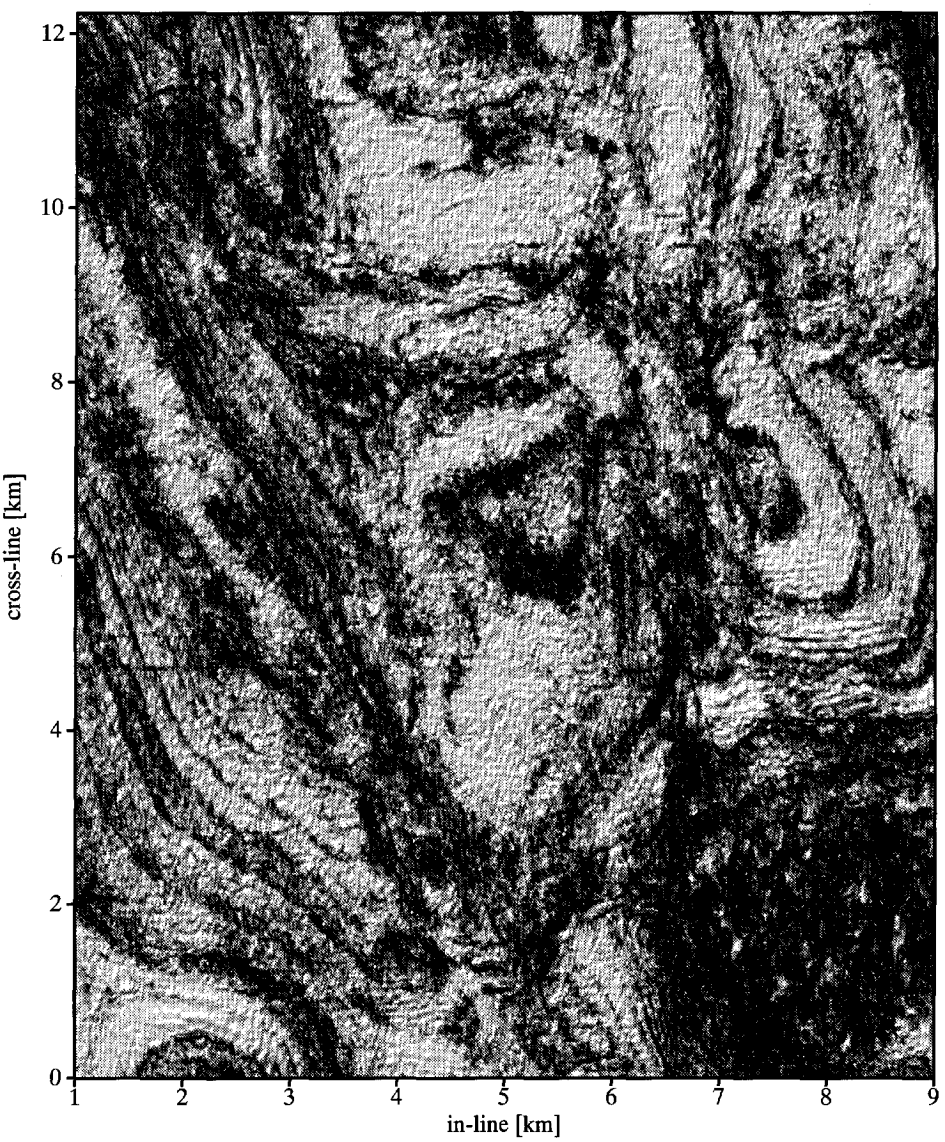

Figure 6.14: *Illuminated map display of the local azimuth slice at* $t = 1.64$ [s].

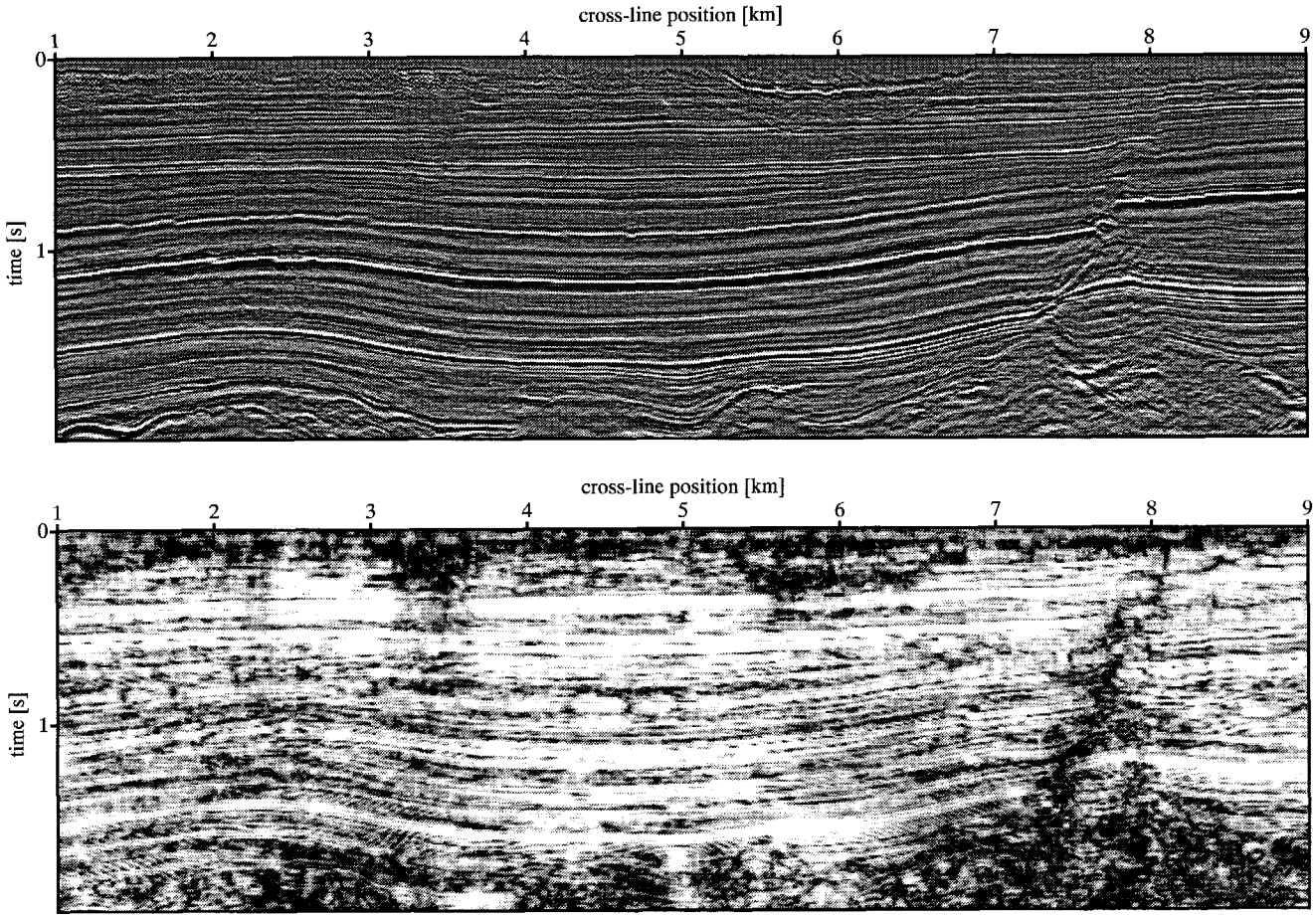

Figure 6.15: *(top) In-line 1 at* $x = 0$ [m] *and corresponding time-dip cross-section.*

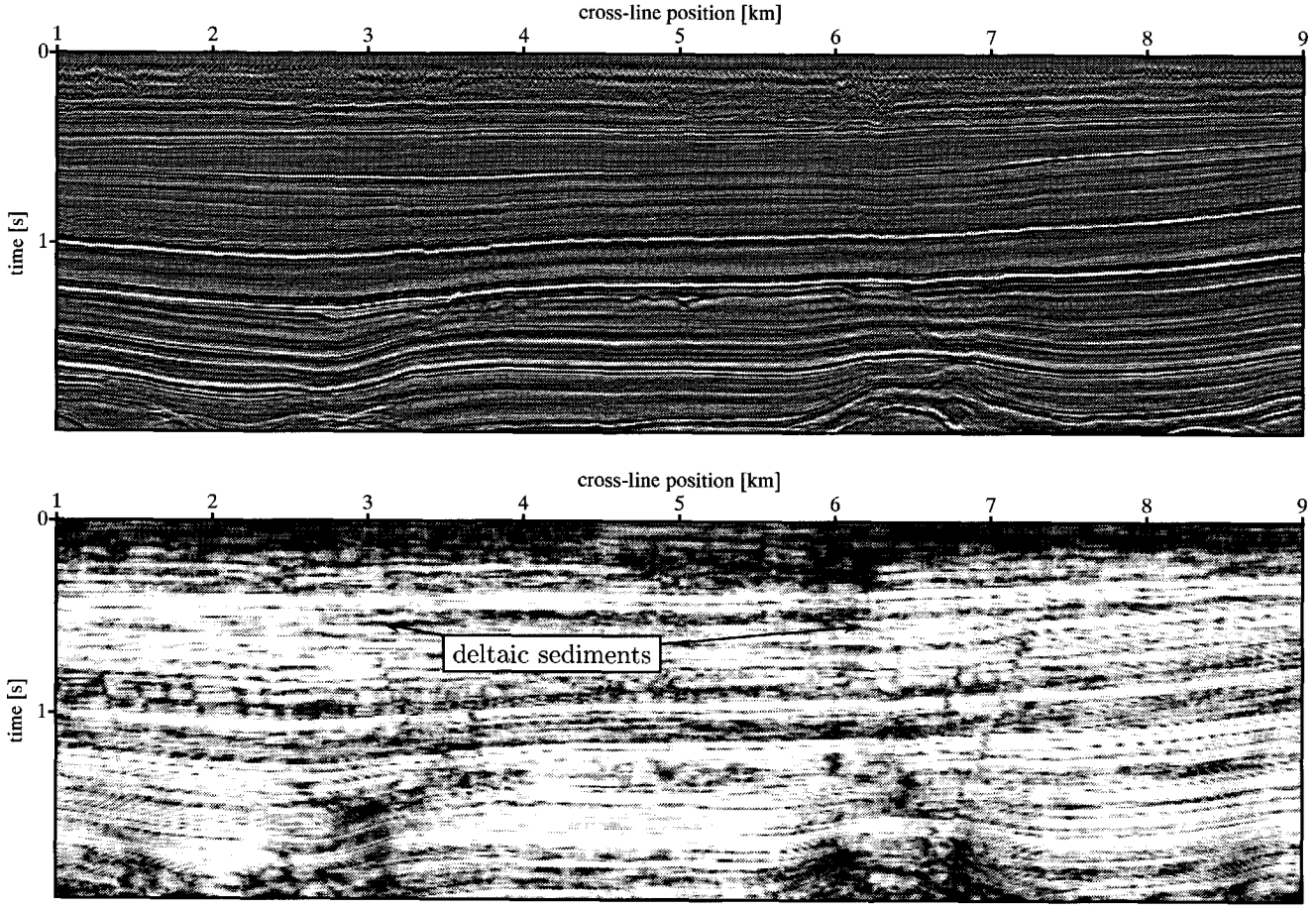

Figure 6.16: *(top) In-line 225 at* $x = 5600$ [m] *and corresponding time-dip cross-section.*

6.4 Discussion and recommendations

In this chapter a method has been proposed for the extraction of the local time-dip and azimuth from a volume of 3-D seismic data. Particularly, the time-dip map effectively reveals the discontinuities that are present in the data. These signal discontinuities can in most cases be related to discontinuities in the subsurface that have a geological significance, such as faults, channels and stratigraphic boundaries.

The attribute extraction was performed on a seismic volume, rather than on stratigraphic surfaces. In the South Marsh Island data example it was shown that in case stratigraphic surfaces and time slices run nearly parallel (i.e. there is little structural dip), stratigraphic features are effectively brought forward in the time-dip display. In case structural dip prevails, for instance in the deeper part of the Ameland data set, time slices cut through many stratigraphic horizons and little stratigraphic information can be extracted from the time-dip slice. To further asses the performance of the method for stratigraphic interpretation, an implementation in which the attributes are extracted in a volume along interpreted horizons is recommended. This extension can be readily made by loading the time-dip data cube onto an interpretation workstation and extract the time-dip value along an interpreted time horizon. This will also enable a better comparison with existing methods, such as horizon based amplitude and dip/azimuth extraction.

The time-dip attribute cube is potentially very useful as an aid in fault interpretation. For instance, the property of the time-dip attribute that it sets the faults apart from the rest of the data volume has a possible application in automated fault recognition and tracking. In such an application, the time-dip data volume could be used to guide the fault tracker through the data volume. The potential result is a 3-D image of the fault plane.

Some aspects of the method proposed in this chapter are illustrated in Fig. 6.17. In Fig. 6.17a we show the result that is obtained with the method that was used to generate the field data examples (see Section 6.1). The analysis was performed on a sliding 4x4x4 space-time cube of data and a correlation over 3x3x3 frequency bins was carried out in the 3-D sliding-window Fourier transformation. Figure 6.17b shows the result of a two-dimensional analysis. In the two-dimensional implementation, the three-dimensional time-dip

is obtained by adding the two time-dip values that are extracted from a two-dimensional sliding-window analysis in the cross-line and in-line directions. Comparing the outcome of the two-dimensional analysis with Fig. 6.17a we observe the dramatic improvement that results from a three-dimensional implementation.

The result that is obtained by extraction of the time-dip attribute from a three-dimensional sliding-window slant-stack power spectrum is shown in Fig. 6.17c. The three-dimensional sliding-window slant-stack power spectrum is obtained by interpolating a three-dimensional spectrogram to a local slowness-frequency representation. The only difference with the generalized Wigner-Radon representation is that no correlation is carried out in the sliding-window Fourier transform of the analysis cube. The result illustrates how the correlation in the wavenumber-frequency spectrum can be used to guide the resolution in the space-time and wavenumber-frequency domains. The correlation accomplishes a sharper localization of the energy in the space-time domain, which in turn results in better resolution in the time-dip map.

Finally, in Fig. 6.17d we show the time-dip map that has been extracted from a generalized Wigner-Radon representation of an analysis cube with a size of 8 by 8 traces by 8 time samples. We observe that with extending the size of the analysis cube, the resolution of the attribute map significantly decreases.

The analysis with a 4x4x4 sliding cube along a single time slice of 800 by 300 traces requires 30 minutes of CPU time on a SUN Sparc 10/40. However, in the present implementation there is still room for a large improvement of the computational efficiency. The algorithm lends itself very well for parallelization, which will be straightforward to implement. Moreover, the use of more efficient data I/O and interpolation routines is also expected to reduce the required CPU time considerably. With these improvements, it may well be possible to come to a more or less real-time implementation.

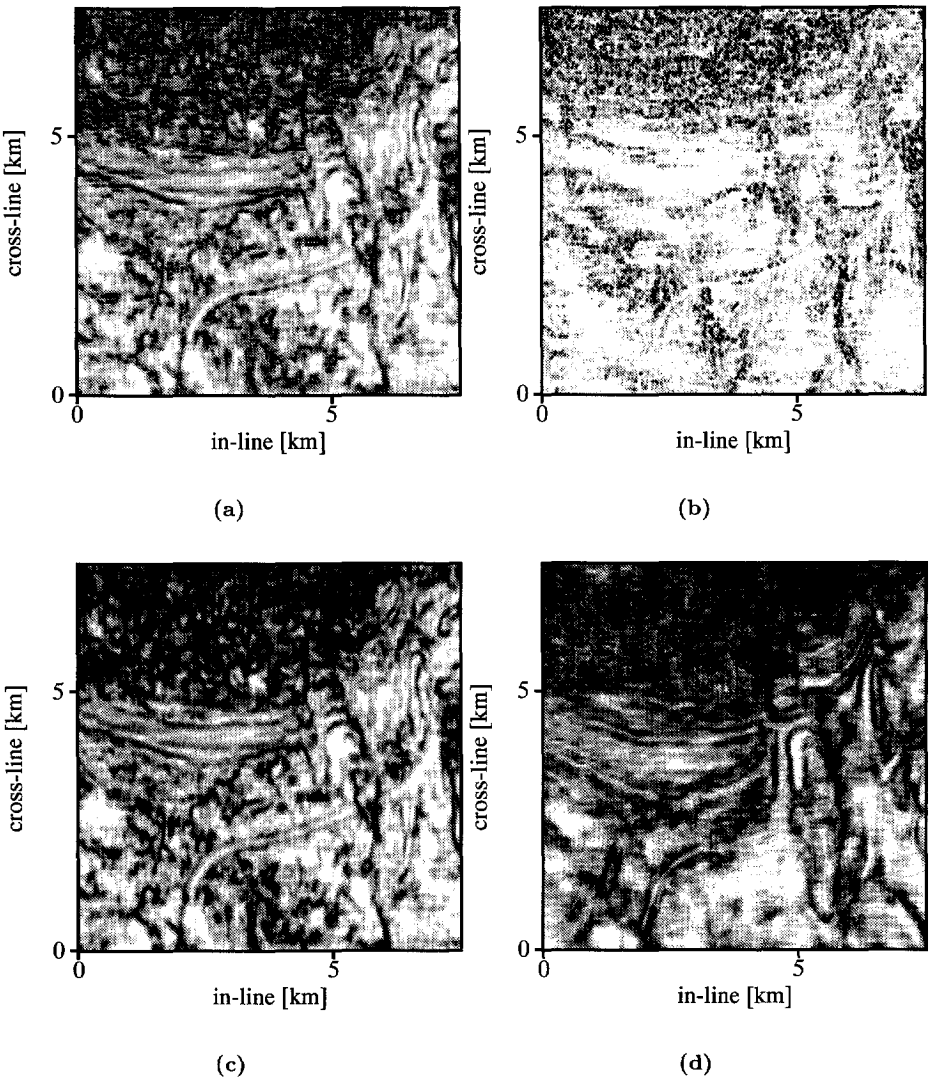

Figure 6.17: *(a) time-dip slice obtained from a 3-D generalized Wigner-Radon representation, (b) time-dip slice obtained by a 2-D by 2-D analysis, (c) time-dip slice obtained from a 3-D sliding-window Fourier transformation, (d) time-dip slice obtained with an 8x8x8 analysis cube.*

Appendix A

Some useful properties of the Fourier transformation

In general $u(t)$ is a complex function of the real variable t. Its Fourier transform pair is defined as

$$\hat{u}(f) = \mathcal{F}_t^- \{u(t)\}(f) = \int_{t \in I\!R} \exp(-\mathrm{j}2\pi f t) u(t) \mathrm{d}t, \tag{A.1}$$

where the subscript t in $\mathcal{F}_t^-$ denotes the transformation variable and the sign denotes the sign in the exponential function, and

$$u(t) = \mathcal{F}_f^+ \{\hat{u}(f)\}(t) = \int_{f \in I\!R} \exp(\mathrm{j}2\pi f t) \hat{u}(f) \mathrm{d}f. \tag{A.2}$$

The hat above a function, as in $\hat{u}(f)$, denotes that it is in its frequency domain representation.

In case the transform variable pair can unambiguously be derived from the variables t and f that are used to denote functions $u(t)$ and $\hat{u}(f)$, we will write $F_t^- \{u(t)\}$ to denote the Fourier transformation and drop the functional dependence in the transformed domain.

The following properties are of importance in this thesis.

Convolution in the time domain

$$\mathcal{F}_t^- \left\{ \int_{\tau \in I\!R} u(\tau) v(t-\tau) \mathrm{d}\tau \right\} = \hat{u}(f)\hat{v}(f), \tag{A.3}$$

where $\hat{v}(f) = \mathcal{F}_t^- \{v(t)\}$.

Convolution in the frequency domain

$$u(t)v(t) = \mathcal{F}_f^+ \left\{ \int_{\nu \in I\!R} \hat{u}(\nu)\hat{v}(f-\nu) \mathrm{d}\nu \right\}. \tag{A.4}$$

Cross-correlation in the time domain

$$\mathcal{F}_t^- \left\{ \int_{\tau \in I\!R} u^*(\tau) v(t+\tau) \mathrm{d}\tau \right\} = \hat{u}^*(f)\hat{v}(f). \tag{A.5}$$

Cross-correlation in frequency domain

$$u^*(t)v(t) = \mathcal{F}_f^+ \left\{ \int_{\nu \in I\!R} \hat{u}^*(\nu)\hat{v}(f+\nu) \mathrm{d}\nu \right\}. \tag{A.6}$$

Auto-correlation in the time domain

$$\mathcal{F}_t^- \left\{ \int_{\tau \in I\!R} u^*(\tau) u(t+\tau) \mathrm{d}\tau \right\} = \hat{u}^*(f)\hat{u}(f) = |\hat{u}(f)|^2, \tag{A.7}$$

where $|\hat{u}(f)|^2$ is known as the spectral energy density function or power spectrum. The fact that the auto-correlation function and the spectral density function are a Fourier transform pair is in random signal theory known as the Wiener-Khinchin theorem.

Applying the inverse operator $\mathcal{F}_f^+$ to the left-hand side of Eq.(A.5) and the operator $\mathcal{F}_t^-$ to the right-hand side of Eq.(A.6), and taking $t = 0$, leads to

$$\int_{\tau \in I\!R} u^*(\tau) v(\tau) \mathrm{d}\tau = \int_{f \in I\!R} \hat{u}^*(f)\hat{v}(f) \mathrm{d}f. \tag{A.8}$$

and

$$\int_{\tau \in I\!R} |u(t)|^2 \mathrm{d}\tau = \int_{f \in I\!R} |\hat{u}(f)|^2 \mathrm{d}f. \tag{A.9}$$

Equations (A.8) and (A.9) are known as Parseval's theorems.

Shift in the time domain

$$\mathcal{F}_t^- \{u(t-\tau)\} = \exp(-\mathrm{j}2\pi f\tau)\hat{u}(f). \tag{A.10}$$

Shift in the frequency domain

$$\exp(\mathrm{j}2\pi\nu t)u(t) = \mathcal{F}_f^+ \{\hat{u}(f-\nu)\}. \tag{A.11}$$

Differentiation in the time domain

$$\mathcal{F}_t^- \{\partial_t u(t)\} = j2\pi f\hat{u}(f). \tag{A.12}$$

Differentiation in the frequency domain

$$-\mathrm{j}2\pi tu(t) = \mathcal{F}_f^+ \{\partial_f \hat{u}(f)\} \tag{A.13}$$

Some additional properties

$$\mathcal{F}_t^- \{u^*(t)\} = \hat{u}^*(-f). \tag{A.14a}$$

$$\mathcal{F}_t^- \{u(-t)\} = \hat{u}(-f). \tag{A.14b}$$

$$\mathcal{F}_t^- \{u^*(-t)\} = \hat{u}^*(f). \tag{A.14c}$$

Appendix B

The Wigner distribution of real-valued and analytic signals

In this appendix the Wigner distribution of a real-valued or analytic signal is discussed. The aim of the discussion is to accommodate the use of a non-negative frequency parameter f in the transform relations of the Wigner distribution, instantaneous auto-correlation, local spectral auto-correlation and ambiguity function. The non-negativity of the frequency is required in the definition of the Wigner-Radon representation. We use the following notation for the Fourier transform operator:

$$\mathcal{F}_a^{\pm}\{g(a)\} = \int_{a\in I\!R} \exp(\pm \mathrm{j}2\pi ab) g(a) \mathrm{d}a. \tag{B.1}$$

The Wigner distribution and its transform equivalents are introduced, starting from

$$R\{u,u\}(t;\tau) = u(t+\tfrac{1}{2}\tau)u^*(t-\tfrac{1}{2}\tau), \tag{B.2}$$

we have

$$\begin{aligned} W\{u,u\}(t;f) &= \mathcal{F}_\tau^{-}\left\{R\{u,u\}(t;\tau)\right\}, \\ R\{u,u\}(t;\tau) &= \mathcal{F}_f^{+}\left\{W\{u,u\}(t;f)\right\}. \end{aligned} \tag{B.3}$$

and in the same way

$$\begin{aligned} A\{u,u\}(\nu;\tau) &= \mathcal{F}_t^- \{R\{u,u\}(t;\tau)\}, \\ R\{u,u\}(t;\tau) &= \mathcal{F}_\nu^+ \{A\{u,u\}(\nu;\tau)\}. \end{aligned} \tag{B.4}$$

One the other hand, when we start from

$$R\{\hat{u};\hat{u}\}(\nu,f) = \hat{u}(f+\tfrac{1}{2}\nu)\hat{u}(f-\tfrac{1}{2}\nu), \tag{B.5}$$

we arrive at

$$\begin{aligned} W\{u,u\}(t;f) &= \mathcal{F}_\nu^+ \{R\{\hat{u},\hat{u}\}(\nu;f)\}, \\ R\{\hat{u},\hat{u}\}(\nu;f) &= \mathcal{F}_t^- \{W\{u,u\}(t;f)\} \end{aligned} \tag{B.6}$$

and

$$\begin{aligned} A\{u,u\}(\nu;\tau) &= \mathcal{F}_f^+ \{R\{\hat{u},\hat{u}\}(\nu;f)\}, \\ R\{\hat{u},\hat{u}\}(\nu;f) &= \mathcal{F}_\tau^- \{A\{u,u\}(\nu;\tau)\}. \end{aligned} \tag{B.7}$$

In all practical cases we consider either that $u(t)$ is real-valued or its associated complex-valued analytic signal. In both cases we can restrict the analysis to positive frequency f. The domain occupied by positive frequencies is introduced as

$$I\!R^+ = \{f \in I\!R\,; f \geq 0\}, \tag{B.8}$$

then the characteristic function $\chi_{I\!R^+}(f)$ of this domain is given by

$$\chi_{I\!R^+}(f) = \left\{0, \frac{1}{2}, 1\right\} \text{ when } \{f>0, f=0, f<0\}. \tag{B.9}$$

Since for real $u(t)$, $R\{u,u\}(t;\tau)$ is also real-valued, we can write

$$\begin{aligned} W\{u,u\}(t;f) &= \mathcal{F}_\tau^- \{R\{u,u\}(t;\tau)\},\ f \in I\!R^+, \\ R\{u,u\}(t;\tau) &= 2\mathrm{Re}\mathcal{F}_f^+ \{\chi_{I\!R^+}(f) W\{u,u\}(t;f)\}, \end{aligned} \tag{B.10}$$

where Re stands for the Real part of . Equation (B.6) is left unchanged and we can write

$$\begin{aligned} W\{u,u\}(t;f) &= \mathcal{F}_\nu^+ \{R\{\hat{u},\hat{u}\}(\nu;f)\},\ f \in I\!R^+, \\ R\{\hat{u},\hat{u}\}(\nu;f) &= \mathcal{F}_t^- \{W\{u,u\}(t;f)\},\ f \in I\!R^+. \end{aligned} \tag{B.11}$$

The analytic function associated with $u(t)$ is most conveniently introduced in frequency domain as

$$\hat{u}^a(f) = 2\chi_{I\!R^+}(f)\hat{u}(f). \tag{B.12}$$

Then it follows that

$$R\{\hat{u}^a, \hat{u}^a\}(\nu; f) = 4\chi_{I\!R^+}(f + \tfrac{1}{2}\nu)\chi_{I\!R^+}(f - \tfrac{1}{2}\nu)R\{\hat{u}, \hat{u}\}(\nu; f) \tag{B.13}$$

Careful analysis reveals that Eq.(B.11) can also be written as

$$R\{\hat{u}^a, \hat{u}^a\}(\nu; f) = 4\chi_{I\!R^+}(f)\Pi(\nu/4|f|)R\{\hat{u}, \hat{u}\}(\nu; f) \tag{B.14}$$

where the rectangular (box-car) function Π is introduced as

$$\Pi(\nu/4|f|) = \left\{1, \frac{1}{2}, 0\right\} \text{ when } \{|\nu| < 2|f|, |\nu| = 2f, |\nu| > 2f\}. \tag{B.15}$$

From Eq.(B.13) it follows that, since

$$R\{\hat{u}^a, \hat{u}^a\}(\nu; f) = 0, \text{ for } f < 0, \tag{B.16}$$

we can restrict the analysis to positive frequencies only. In particular, starting from Eq.(B.13), we can write

$$\begin{aligned} W\{u^a, u^a\}(t; f) &= \mathcal{F}_n u^+ \left\{R\{\hat{u}^a, \hat{u}^a\}(\nu; f)\right\}, \ f \in I\!R^+ \\ R\{\hat{u}^a, \hat{u}^a\}(\nu; f) &= \mathcal{F}_t^+ \left\{W\{u^a, u^a\}(t, f)(t; f)\right\}, \ f \in I\!R^+, \end{aligned} \tag{B.17}$$

and we also have,

$$\begin{aligned} W\{u^a, u^a\}(t; f) &= \mathcal{F}_\tau^- \left\{R\{u^a, u^a\}(t; \tau)\right\}, \ f \in I\!R^+, \\ R\{u^a, u^a\}(t; \tau) &= \mathcal{F}_f^+ \left\{W\{u^a, u^a\}(t; f)\right\}, \ f \in I\!R^+. \end{aligned} \tag{B.18}$$

BIBLIOGRAPHY

Bahorich, M. and Farmer, S., 1995, 3-D seismic discontinuity for faults and stratigraphic features: The coherence cube, *The Leading Edge*, vol. 14, 1053-1058.

Baraniuk, R.G. and Jones, D.L., 1993a, Signal dependent time-frequency analysis using a radially Gaussian kernel, *Signal Processing*, vol. 32, 263-284.

Baraniuk, R.G. and Jones, D.L., 1993b, A signal dependent time-frequency representation: Optimal kernel design, *IEEE Trans. on Signal Processing*, vol. 41, 1589-1602.

Baraniuk, R.G. and Jones, D.L., 1994, A signal dependent time-frequency representation: Fast Algorithm for optimal kernel design, *IEEE Trans. on Signal Processing*, vol. 42, 134-146.

Barnes, A.E., 1993, Instantaneous bandwidth and dominant frequency with applications to seismic reflection data, *Geophysics*, vol. 58, 419-428

Beylkin, G., 1987, Discrete Radon Transform, *IEEE Trans. on Acoustics, Speech and Signal Processing*, vol. 35, 162-172.

Boashash, B., 1992a, Estimating and Interpreting The Instantaneous Frequency of a Signal - Part I: Fundamentals, *Proceedings of the IEEE*, vol. 80, 520-538.

Boashash, B., 1992b, Estimating and Interpreting The Instantaneous Frequency of a Signal - Part II: Algorithms and Applications, *Proceedings of the IEEE*, vol. 80, 540-568.

Boashash, B. and O'Shea, P., 1993, Use of the Cross Wigner-Ville Distribution for Estimation of the Instantaneous Frequency, *IEEE Trans. on Signal Processing*, vol. 41, 1439-1445.

Bodine, J.H., 1986, Waveform analysis with seismic attributes, *Oil & Gas Journal*, June 1986, 59-63.

Boudreaux-Bartels, G.F. and Parks, T.W. , 1986, Time-varying filtering and signal estimation using Wigner distribution synthesis techniques, *IEEE Trans. on Acoustics, Speech and Signal Processing*, vol. 34, 442-451.

Bracewell, R.N., 1978, *The Fourier Transform and Its Applications*, McGraw-Hill Book Company.

Brown, A.R., 1997, *Interpretation of three-dimensional Seismic Data*, AAPG Memoir; 42, American Association of Petroleum Geologists, Tulsa, Oklahoma.

Chapman, C.H., 1978, A new method for the computation of synthetic seismograms, *Geoph. J. R. Astr. Soc.*, vol. 54, 481-518.

Chapman, C.H., 1979, On impulsive wave propagation in a spherically symmetric model, *Geoph. J. R. Astr. Soc.*, vol. 58, 229-234.

Chapman, C.H., 1981, Generalized Radon transforms and slant stacks, *Geoph. J. R. Astr. Soc.*, vol. 66, 445-453

Choi, H.I. and Williams, W.J., 1989, Improved time-frequency representation of multicomponent signals using exponential kernels, *IEEE Trans. on Signal Processing*, vol. 37, 862-871.

Claasen, T.A.C.M. and Mecklenbräuker, W.F.G., 1980a, The Wigner distribution - A tool for time-frequency signal analysis - Part I: Continuous time signals, *Philips Journal of Research*, vol. 35, 217-250.

Claasen, T.A.C.M. and Mecklenbräuker, W.F.G., 1980b, The Wigner distribution - A tool for time-frequency signal analysis - Part II: Discrete time signals, *Philips Journal of Research*, vol. 35, 276-300.

Claasen, T.A.C.M. and Mecklenbräuker, W.F.G., 1980c, The Wigner distribution - A tool for time-frequency signal analysis - Part III: Relations with other time-frequency signal transformations, *Philips Journal of Research*, vol. 35, 372-389.

Cohen, L., 1966, Generalized phase-space distribution functions, *Jour. Math. Phys.*, vol. 7, 781-786.

Cohen, L. and Posch, T.E., 1985, Positive Time-Frequency Distribution Functions, *IEEE Trans. on Acoustics, Speech and Signal Processing*, vol. 33, 31-37.

Cohen, L., 1989 Time-Frequency Distributions - A Review, *Proceedings of the IEEE*, vol. 77 (7), 941-981.

Cohen, L., 1995, *Time-Frequency Analysis*, Prentice Hall Signal Processing Series, Englewood Cliffs, New Jersey.

Cohen, L., 1996a, A General Approach for Obtaining Joint Representations in Signal Analysis - Part I: Characteristic Function Operator Method, *IEEE Trans. on Signal Processing*, 1080-1090.

Cohen, L., 1996b, A General Approach for Obtaining Joint Representations in Signal Analysis - Part II: General Class, Mean and Local Values, and Bandwidth, *IEEE Trans. on Signal Processing*, 1091-1098.

Copeland, A.C., Ravichandran, G., and Trivedi, M.M., 1995, Localized Radon Transform-Based Detection of Ship Wakes in SAR Images, *IEEE Trans. on Geoscience and Remote Sensing*, vol. 33, 35-45.

Dalley, R.M., Gevers, E.C.A., Stampfli, G.M., Davies, D.J., Gastaldi, C.N., Ruijtenberg, P.A., and Vermeer, G.J.O., 1989, Dip and azimuth displays for 3D seismic interpretation, *First Break*, vol. 7(3), 86-95.

Dalley, R.M., Livesey, A.K., Centeno Neelen, R., and Nacken, P.F., 1996, 3D image processing for 3D seismic interpretation, *EAGE 58th Meeting and Technical Exhibition, Amsterdam, the Netherlands, Extended Abstracts of Papers*, X003.

de Jonge, D.Y.C.E.M, Spaargaren, B., and Glass, F.G., 1996, Volume interpretation applications, *EAGE 58th Meeting and Technical Exhibition, Amsterdam, the Netherlands, Extended Abstracts of Papers*, X002.

Flandrin, P., 1993, *Temps-Fréquence*, Hermès, Paris.

Fokkema, J.T. and Ziolkowski, A.M., 1987, The critical reflection theorem, *Geophysics*, vol. 52, 965-972.

Fournier, F. and Derain, J-F., 1996, A statistical methodology for deriving reservoir properties from seismic data, *Geophysics*, vol. 60, 1437-1450.

Fuchs, K. and Müller, G., 1971, Computation of synthetic seismograms with the reflectivity method and comparison with observations, *Geophys. J. R. Astr. Soc.*, vol. 23, 417-433.

Gabor, D., 1946, Theory of Communication, *Journal of the IEE*, vol. 93, 488-497.

Gersztenkorn, A. and Marfurt, K.J., 1996, Eigenstructure based coherence computations, *Sixty-Sixth Annual International SEG Meeting Denver, Expanded Abstracts*, 328-331.

Haneveld, C.J. and Herman, G.C., 1990, A fast algorithm fo the computation of the Radon transform, *Geoph. Prosp.*, vol. 38, 853-860.

Hardage, B.A. (ed.), 1987, Seismic Stratigraphy, in: *Handbook of geophysical exploration, section I. Seismic exploration*, Helbig, K., Treitel, S. eds., vol. 9, Geophysical Press, London-Amsterdam.

Haskell, N.L., Nissen, S.E., Lopez, J.A., and Bahorich. M.S., 1995, 3-D seismic coherency and the imaging of sedimentological features, *Sixty-Fifth Annual International SEG Meeting Houston, Expanded Abstracts*, 1532-1534.

Hesthammer, J. and Fossen, H., 1997, The influence of seismic noise in structural interpretation of seismic attribute maps, *First Break*, vol. 15, 209-219.

Hlawatsch, F. and Boudreaux-Bartels, G.F., 1992, Linear and Quadratic Time-Frequency Signal Representations, *IEEE Signal Processing Magazine*, April 1992, 21-67

Hlawatsch, F. and Krattenthaler, W., 1992, Bilinear signal synthesis, *IEEE Trans. on Signal Processing*, vol. 40, 3321-3334.

Hoetz, H.L.J.G. and Watters, D.G., 1992, Seismic horizon attribute mapping of the Annerveen Gasfield, The Netherlands, *First Break*, vol. 10(2), 41-51.

Hoogenboom, R.C., Dalley, R.M., and Poelen, H.J., 1996, Volume interpretation, a new approach to 3D seismic interpretation, *EAGE 58th Meeting and Technical Exhibition, Amsterdam, the Netherlands, Extended Abstracts of Papers*, X001.

Hudson, R.L., 1974, When is the Wigner quasi-probability density non-negative ?, *Rep. Math. Phys.*, vol. 6, 249-252.

Jacobson, L.D. and Wechsler, H., 1988, Joint spatial/spatial frequency representation, *Signal Processing*, vol. 14, 37-68.

Janse, C.P. and Kaizer, A.J.M., 1983, Time-Frequency Distributions of Loudspeakers: The Application of the Wigner Distribution, *J. Audio Eng. Soc.*, vol. 31, 198-223.

Janssen, A.J.E.M., 1984, Positivity of phase-plane distribution functions, *J. Math. Physics*, vol. 25, 2240-2252.

Jones, D.L. and Baraniuk R.G., 1995, An adaptive optimal-kernel time-frequency representation, *IEEE Trans. on Signal Processing*, vol. 43, 2361-

Jones, G. and Knipe, R.J., 1996, Seismic attribute maps; application to structural and fault seal analysis in the North Sea Basin, *First Break*, vol. 14(12), 449-461.

Jurado, M.J., and Comas, M.C., 1992, Well Log Interpretation and Seismic Character of the Cenozoic Sequence in the Northern Alboran Sea, *Geo-Marine Letters*, vol. 12, 129-136.

Kadambe, S. and Boudreaux-Bartels, G.F., 1992, A Comparsion of the Existence of 'Cross Terms' in the Wigner Disitribution and the Squared Magnitude of the Wavelet Transform and the Short Time Fourier Transfrom, *IEEE Trans. on Signal Processing*, vol. 40, 2498-2571.

Kalkomey, C.T., 1996, Use of seismic attributes as predictors of reservoir properties - potential risks, *Sixty-Sixth Annual International SEG Meeting Denver*, Expanded Abstracts, 1789-1792.

McMechan, G.A. and Ottolini, R., 1980, A direct observation of a $p - \tau$ curve in a slant stacked wavefield, *Bulletin of the Seismological Society of America*, vol. 70, 775-789.

Milkereit, B., 1987, Decomposition and inversion of seismic data - an instantaneous slowness approach, *Geoph. Prosp.*, vol. 35, 875-894.

Mitchum Jr., R.M., Vail, P.R., and Sangree, J.B., 1977, Seismic Stratigraphy and Global Changes of Sea Level, Part 6: Stratigraphic Interpretation of Seismic Reflection Patterns in Depositional Sequences, in: AAPG Memoir; 26, *Seismic Stratigraphy - applications to hydrocarbon exploration*, Payton, C.E. ed., American Association of Petroleum Geologists, Tulsa, Oklahoma.

Marfurt, K.J., Scheet, R.M., Sharp, J.A., Cain, G.J., and Harper, M.G., 1995, Suppression of the acquisition footprint for seismic sequence attribute mapping, *Sixty-Fifth Annual International SEG Meeting Houston, Expanded Abstracts*, 949-952.

Mark, W.D., 1970, Spectral analysis of the convolution and filtering of non-stationary stochastic processes, *J. Sound Vib.*, vol. 11, 19-63.

Morlet, J., Arens, G., Fourgeau, E., and Giard, D., 1982, Wave propagation and sampling theory - Part I: Complex signal and scattering in multilayered media, *Geophysics*, vol. 47, 203-221.

Morlet, J., Arens, G., Fourgeau, E., and Giard, D., 1982, Wave propagation and sampling theory - Part II: Sampling theory and complex waves, *Geophysics*, vol. 47, 222-236.

Nissen, S.E., Haskel., N.L., Lopez, J.A., Donlon, T.J., and Bahorich, M.S., 1995, 3-D seismic coherency techniques applied to the identification and delineation of slump features, *Sixty-Fifth Annual International SEG Meeting Houston, Expanded Abstracts*, 1535-1536.

Oh, S. and Marks II, R.J., 1992, Some Properties of the Generalized time-frequency representation with a cone shaped kernel, *IEEE Trans. on Signal Processing*, vol. 40, 1735-1745.

Ortmann, K.A. and Wood, L.J., 1995, Succesful application of 3-D seismic coherency models to predict stratigraphy, offshore eastern Trinidad, *Sixty-Fifth Annual International SEG Meeting Denver, Expanded Abstracts*, 101-103.

Page, C.H., 1952, Instantaneous power spectra, *Journal of Applied Physics*, vol. 23, 103-106

Phinney, R.A., Chowdhury, K.R., and Frazer, L.N., 1981, Transformation and analysis of record sections, *J. of Geophys. Res.*, vol. 86, 359-377.

Press, W.H., Teukolsky, S.A., Vetterling, W.T., and Flannery, B.P., 1992, *Numerical Recipes in FORTRAN, The Art of Scientific Computing*, Second Edition, Cambridge University press.

Priestley, M.B., 1965, Evolutionary spectra and non-stationary processes, *J. Roy. Statist. Soc. Ser. B*, vol. 27, 1-30.

Priestley, M.B., 1989, *Spectral analysis and time series*, Academic Press, London.

Rihaczeck, A.W., 1968, Signal energy distribution in time and frequency, *IEEE Trans. on Information Theory*, vol. 14, 369-374.

Rioul, O., Vetterli, M., 1991, Wavelets and signal processing, *IEEE Signal Processing Magazine*, vol. 39, 1564-1574

Robertson, J.D. and Nogami, H.H., 1984, Complex seismic trace analysis of thin beds, *Geophysics*, vol. 49 (4), 344-352.

Schlager, W., 1991, Depositional bias and environmental change - important factors in sequence stratigraphy, *Sedimentary Geology*, vol. 70, 109-130.

Sheriff, R.E., 1980, *Seismic Stratigraphy*, IHRDC Publishers, Boston, Massachusetts.

Stankovič, S., Stankovič, L.J., and Uskokovič, Z., 1995, On the Local Frequency, Group Shift, and Cross-Terms in Some Multidimensional Time-Frequency Distributions: A Method for Multidimensional Time-Frequency Analysis, *IEEE Trans. on Signal Processing*, vol. 43, 1719-1724.

Steeghs, T.P.H. and Drijkoningen, G.G., 1994, Joint Time-Frequency Representation of seismic Data, *EAEG 56th Meeting and Technical Exibition, Vienna - Austria, Extended Abstracts of Papers*, P163.

Steeghs, T.P.H., Drijkoningen, G.G., Peet, W.E., and Fokkema, J.T., 1995, A new Method for the Extraction of seismic facies Attributes, *EAGE 57th Meeting and Technical Exhibition, Glasgow - Scotland, Extended Abstracts of Papers*, A029.

Steeghs, T.P.H. and Drijkoningen, G.G., 1995, Time-Frequency Analysis of seismic Sequences, *Sixty-Fifth Annual International SEG Meeting Houston, Expanded Abstracts*, 1528-1531.

Steeghs, T.P.H. and Drijkoningen, G.G., 1996, Time-Frequency Analysis of Seismic Reflection Data, *Proceedings of the 1996 International Conference on Acoustics, Speech and Signal Processing, Atlanta*, vol. 5, 2972-2974.

Steeghs, T.P.H. and Drijkoningen, G.G., 1996, Extraction of Attributes from 3D seismic Data, *EAGE 58th Meeting and Technical Exhibition, Amsterdam, the Netherlands, Extended Abstracts of Papers*, X032.

Stoffa, P.L., Buhl, P., Diebold, J.B., and Wenzel, F., 1981, Direct mapping of seismic data to the domain of intercept time and ray parameter - a plane wave decomposition, *Geophysics*, vol. 46, 255-267.

Sussman, S.M., 1968, Least squares synthesis of radar ambiguity funcions, *Trans. IRE*, vol. IT-8, 246-254.

Taner, T.H. and Sheriff, R.E., 1977, Applications of Amplitude, Frequency and Other Attributes to Stratigraphic and Hydrocarbon Determination, in: AAPG Memoir; 26, *Seismic Stratigraphy - applications to hydrocarbon exploration*, Payton, C.E. ed., American Association of Petroleum Geologists, Tulsa, Oklahoma, 301-328.

Taner, T.H., Koehler, F., and Sheriff, R.E., 1979, Complex seismic trace analysis, Geophysics, vol. 44.

Tobback, T., Steeghs, T.P.H., Drijkoningen, G.G., and Fokkema, J.T., 1996, Decomposition of seismic Signals via Time-Frequency Representations, *Sixty-Sixth Annual International SEG Meeting Denver, Expanded Abstracts*, 1638-1641.

Tobback, T., 1996, *Reconstruction of the signal from its time-frequency representation*, M.Sc. Thesis, K.U. Leuven, Leuven, Belgium.

Treitel, S., Gutowski, P.R., and Wagner, D.E., 1982, Plane-wave decomposition of seismograms, *Geophysics*, vol. 47, 1375-1401.

Vail, P.R., Mitchum Jr., R.M., Todd, R.G., Widmier, J.M., Thompson III, S., Sangree, J.B. Bubb, J.N., and Hatelid, W.G., 1977, Seismic Stratigraphy and Global Changes of Sea Level, Part 1-6, in: AAPG Memoir; 26, *Seismic Stratigraphy - applications to hydrocarbon exploration*, Payton, C.E. ed., American Association of Petroleum Geologists, Tulsa, Oklahoma.

Vercruijsse, P.A., 1995, *Biangular Decomposition of Seismic Data*, Ph.D.-Thesis, K.U. Leuven, Leuven, Belgium.

Ville, J., 1948, Theorie et application de la notion de signal analytique, *Cables et Transmissions*, vol. 2A, 61-74.

Vissinga, M., 1992, *The Radon transform and its application to the interpretation of seismic data*, Ph.D.-Thesis, Delft University of Technology, Delft, the Netherlands.

White, R.E., 1991, Properties of instantaneous seismic attributes, *Geophysics: The Leading Edge of Exploration*, July 1991, 26-32.

Wiggins, J.W., 1985, Entropy-guided deconvolution, *Geophysics*, vol. 40, 2720 - 2726 .

Wigner, E.P., 1932, On the quantum correction for thermo-dynamic equilibrium, *Physical Review*, vol. 40, 749-759.

Wigner, E.P., 1971, Quantum Mechanical Distribution functions Revisited, in: *Perspectives in Quantum Theory: Essays in Honor of Alfred Landé*, Yourgrau and van de Merwe eds., The MIT Press, Cambridge, Massachusetts, 25-36.

Wilcox, R.M., 1967, Exponential Operators and Parameter Differentiation in Quantum Physics, *Jour. of Math. Phys.*, vol. 8, 962-982.

Woodward, P.M., 1953, *Probability and Information Theory with applications to Radar*, Pergamon, London.

Zhao, Y., Atlas, L.E., and Marks, R.J., 1990, The use of cone-shaped kernels for generalized time-frequency representations of nonstationary signals, *IEEE Trans. on Acoustics Speech and Signal Processing*, vol. 38, 1084-1091.

Samenvatting

Lokale Energiespectra en Seismische Interpretatie

In dit proefschrift wordt de analyse van seismische reflectie data door middel van een lokaal spectrum beschreven. De seismische reflectie methode is tot op heden de meest succesvolle techniek voor het in beeld brengen van de ondergrond in het dieptebereik van enige tientallen meters tot een tiental kilometers. Drie-dimensionale seismische beeldvorming van de ondergrond speelt een belangrijke rol bij het zoeken naar en in ontwikkeling brengen van olie- en gasvoorkomens. De veelal zeer grote seismische databestanden vragen om speciale technieken voor dataverwerking, visualisatie en interpretatie. Analyse van de data door middel van een lokaal spectrum kan daarbij een bijzonder nuttig hulpmiddel zijn.

In het één-dimensionale geval kunnen seismische data beschouwd worden als een niet-stationaire tijdreeks. Het lokale spectrum van een niet-stationair signaal is een functie die afhankelijk is van zowel de tijd- als de frequentievariabele. In Hoofdstuk 2 en 3 van dit proefschrift wordt ingegaan op ontwikkelingen in de theorie van de signaalverwerking, waar aanzienlijke vooruitgang is geboekt op het terrein van de lokale (tijd-variante) frequentie analyse. Met name de definitie van een algemene klasse van tijd-frequentie representaties heeft geleid tot een solide basis voor tijd-frequentie analyse.

Een belangrijke tijd-frequentie representatie is de Wigner distributie, die als representatief voor de gegeneraliseerde klasse van tijd-frequentie representaties (Cohen's klasse) beschouwd kan worden.

De meest gangbare methode om andere tijd-frequentie representaties dan de Wigner distributie te verkrijgen is door convolutie van de Wigner distributie met een tijd-frequentie filterfunctie. Door het opleggen van bepaalde voorwaarden aan deze filterfunctie worden de eigenschappen van de bij het filter behorende tijd-frequentie representatie bepaald. In Hoofdstuk 3 wordt eerst in algemene zin op een aantal van deze voorwaarden en eigenschappen ingegaan. Vervolgens worden enige uit de literatuur bekende tijd-frequentie representaties besproken.

De toepassing van de één-dimensionale lokale frequentie analyse op seismische reflectie data wordt behandeld in Hoofdstuk 4. De tijd-frequentie representatie resulteert in een uitermate effectieve weergave van het signaal voor de beschrijving van seismische beelden aan de hand van karakteristieke patronen; de zogenaamde de seismische facies analyse. Een reflectiepatroon is vaak eenvoudiger te interpreteren wanneer het signaal in zijn tijd-frequentie representatie wordt weergegeven dan in het oorspronkelijke beeld. Een andere toepassing van de tijd-frequentie analyse is de kwantitatieve beschrijving van golfvormen aan de hand van de eigenschappen van hun lokale spectrum. De golfvorm-analyse of "seismische attributen" analyse vormt een belangrijke schakel in het vertaalproces van seismische data naar gesteenteeigenschappen. De in dit proefschrift voorgestelde wijze van extractie van signaaleigenschappen via het lokale spectrum is een aanzienlijke verbetering ten opzichte van bestaande technieken, zoals de zogenaamde complex-trace analyse.

De voor de seismische interpretatie belangrijke uitbreiding naar meer-dimensionale analyse-technieken wordt behandeld in Hoofdstuk 5. Bij de seismische interpretatie speelt de hoekafhankelijkheid van het meer-dimensionale signaal een belangrijke rol, omdat de richting van seismische reflecties gerelateerd kan worden aan de structurele opbouw van de ondergrond. De globale Radon transformatie of "slant stack" leidt tot een hoekafhankelijke representatie van het signaal. Een gelijksoortige lokale signaalrepresentatie zou daarom een zeer geschikt hulpmiddel kunnen zijn bij de interpretatie van seismische data. In dit proefschrift wordt een lokale Radon representatie,

de "Wigner-Radon representatie", gedefinieerd en verder uitgewerkt. Deze lokale Radon representatie maakt deel uit van de algemene klasse van lokale spectra.

Het proefschrift wordt afgesloten met een drie-dimensionale analyse van een tweetal veld-data sets, afkomstig uit de Golf van Mexico en de Noordzee. De resultaten laten zien dat met de in dit proefschrift beschreven methode voor seismische data analyse het inzicht in de geologische opbouw van de ondergrond aanzienlijk kan worden vergroot.

Curriculum Vitae

Philippe Steeghs was born in Heerlen, the Netherlands, on May 11 1967. He attended B.C. Schöndeln in Roermond for his secondary education and received the Gymnasium β diploma in 1985. He became a student in geophysics at the University of Utrecht in 1985 and received an MSc (doctorandus) degree in solid earth geophysics in 1992. The subject of his MSc thesis was the acquisition and processing of shallow (land) seismic data. During his studies he worked two summers for NAM Assen and Shell U.K. in London and participated in several marine and land seismic surveys. For a brief period he was an assistant lecturer at the University of Utrecht and in 1993 he became a PhD research assistant (AIO) at the Centre for Technical Geoscience of Delft University of Technology. At the Section of Applied Geophysics of the Faculty of Applied Earth Sciences he conducted research on quantitative seismic interpretation under the supervision of Prof. dr. ir. J.T. Fokkema and Dr. ir. G.G. Drijkoningen. He has published several international conference papers related to the subject of this thesis.